ABSTRACT

Title of dissertation: ION BINDING AND TRANSPORT BY SYNTHETIC

MOLECULAR ASSEMBLIES

Frank William Kotch, Doctor of Philosophy, 2003

Dissertation directed by: Professor Jeffery T. Davis

Department of Chemistry and Biochemistry

Self-assembly of small synthetic molecular building blocks has been applied to generate functional structures capable of binding and transporting cations and anions. Major discoveries from the research include a self-assembled ion pair receptor, ligands capable of K^+-selective transport through membranes, a compound that forms Cl^--selective ion channels in planar and cellular membranes, and a series of efficient chloride transporters.

Calix[4]arene-guanosine conjugates cG **2.26** and cG **2.34** are shown to assemble into Na^+-templated tubular architectures by ^1H NMR, transmission electron microscopy and isothermal titration calorimetry, and to selectively transport K^+ over Na^+ and Cs^+ across

liposome membranes by fluorescent assays. The more lipophilic cG **2.34** forms a water-mediated dimer capable of extracting alkali halide salts from water into organic solution. These conclusions are supported by ^{1}H and ^{23}Na NMR, pulsed-field gradient NMR, ion chromatography and circular dichorism spectroscopy. The (cG **2.34**)$_2$•(H$_2$O)$_n$ dimer is held together by an intermolecular hydrogen-bonded guanosine quartet, based on 1D and 2D NMR experiments, and provides a rare example of a self-assembled ion pair receptor.

Calix[4]arene tetrabutylamide **3.1** forms voltage-dependent chloride-selective ion channels in planar bilayers and cell membranes based on voltage and patch clamp experiments. Compound **3.1** selectively transports Cl$^-$ over HSO$_4^-$ across liposome membranes, is capable of binding and transporting HCl, and can alter the pH inside liposomes experiencing a chloride gradient, based on fluorescent assays and ^{1}H NMR experiments. X-ray crystal structures of calix[4]arene tetramethylamide **2.30**•HCl complexes (**2.30** is an analogue of **3.1**) provides a rationale for how ions are moved across a membrane by **3.1**.

From a series of linear analogues of **3.1**, oligophenoxyacetamide trimer **3.5** was identified as the most potent chloride transporter. Transport of chloride and H$^+$/Cl$^-$ pairs was demonstrated by fluorescent assays and ^{35}Cl NMR. Trimer **3.5** also induces a stable potential into liposomes experiencing a transmembrane anionic gradient, an unprecedented function for a synthetic compound. Compounds capable of transporting chloride or H$^+$/Cl$^-$ pairs have potential as drugs for the treatment of cystic fibrosis and cancer.

ION BINDING AND TRANSPORT BY SYNTHETIC MOLECULAR

ASSEMBLIES

by

Frank William Kotch

Dissertation submitted to the Faculty of the Graduate School of the
University of Maryland, College Park in partial fulfillment
of the requirements for the degree of
Doctor of Philosophy
2003

Advisory Committee:

      Professor Jeffery T. Davis, Chair
      Associate Professor Sergei Sukharev
      Assistant Professor Lyle Isaacs
      Professor Steven E. Rokita
      Professor Philip DeShong

DEDICATION

To Stefanie, Mom, Dad and Jenny for their never-ending love and support.

ACKNOWLEDGMENTS

My deepest thanks and appreciation go to my research supervisor and mentor, Prof. Jeff Davis. I do not think I can overstate the impact Jeff has had on my growth as a scientist. Thank you for teaching me to always ask "how does it work?". The lessons I have learned from Jeff will carry me through my career. Joining Jeff Davis' lab is arguably the best decision I have ever made. And Jeff, you're not rid of me yet, for I'm certain that throughout my life, you will always be my mentor, but also my friend.

For most of my graduate career, Dr. Vladimir Sidorov (Vova) has been my coworker and good friend and has been an "assistant mentor" to me. I am grateful to Vova for every ounce of supramolecular and bioorganic chemistry that I have learned from him. More importantly, Vova has taught me to always seek out the real life applications of the research. Thanks, Vovster! I am undoubtedly a better scientist for having worked with you.

Next, I'd like to acknowledge the four people that got me to graduate school in the first place (in chronological order). I am grateful to Mr. Paul Shandor, my science teacher at Saint Clair Middle School. Mr. Shandor was a true inspiration to me, an excellent teacher, and the reason I became interested in science in the first place. Second, I thank Mr. Albert Portland, my advanced chemistry teacher at Pottsville High School, who prevented me from turning from chemistry altogether. When I all but failed the first semester of Adv. Chem., Mr. Portland's encouragement was the only thing that prevented me from dropping the course. I ended the year with a B, a credit to his excellent teaching. Third, my gratitude goes to Prof. Tom Eberlein at Penn State University, who truly made

me want to be a chemist. Prof. Eberlein talked me out of chemical engineering and into chemistry, which was no small task at that point in my life. Lastly, I thank Dr. Jim Callahan at SmithKline Beecham Pharmaceuticals (now GlaxoSmithKline), who was my supervisor for a year and half of co-op rotations. Jim convinced me to go to graduate school, and for that I am truly grateful. He also taught me synthetic chemistry skills that were invaluable in graduate school.

Working in the Davis group for 5 years has been a pleasure, thanks to the wonderful members of the group. A special thanks to Dr. Xiaodong "Mike" Shi, a classmate, labmate, and friend. Mike was always there to discuss (and sometimes argue) about chemistry, and I learned a lot of science from him and along with him. I express my appreciation to Dr. Allison Marlow who showed me the ropes when I first joined the group. I thank Lenny Williams for many fruitful discussions about synthesis and Valentin Rodionov both for discussions about chemistry and help with computers. Many thanks to Jenny Kuebler and Mark Kaucher; you made my last year in lab fun. Thanks for printing out this thesis, Jenny!!! I have had the pleasure to work with numerous undergraduate students, and I particularly thank Kat Kayser, Hojun Li and Maura Iezzi, who are extremely adept students. I express gratitude to all other past members of the Davis laboratory. You have made my graduate education more rich and enjoyable.

The faculty in the Chemistry and Biochemistry department at the University of Maryland distinguish the department from many departments across the country. The faculty are an interactive group, and are always willing to help each other and graduate students throughout the department. I especially thank the members of my committee; Professors Lyle Isaacs, Steve Rokita and Philip DeShong, who played the largest role in

Dr. Yiu-Fai Lam for NMR experiments, and of course Dr. Vladimir Sidorov for many many experiments and ideas.

I extend much gratitude to Dr. Yiu-Fai Lam for teaching me more than I ever thought I could learn about NMR and for setting up innumerable specialty experiments for me. I cannot imagine graduate school without Yiu-Fai. He certainly facilitated much of my research. Thanks Yiu-Fai!

All analytical support at Maryland is incredible. I thank Dr. Jim Fettinger for crystal structures, and moreso for all the time he spent on my failed crystallization attempts. Dr. Yinde Wang also set up numerous NMR experiments for me over the past five years, and I thank Yinde for all his help. And for mass spectrometry data, I thank Caroline Preyer, Noel Whitaker and Dr. Brian Balgley.

Throughout graduate school, I have had a lot of help from fellow graduate students. I thank Dr. Matt Fasnacht for his continual help with the fluorimeter and fluorimetry experiments, Dr. Patrick Pancras for showing me how to use the IC, Melanie Moses for running EDX experiments, Dr. Trent Volicek for help with UV/Vis experiments, and Esther Chege for providing me with a large stash of calix[4]arene. I thank Bill Walker for many many insightful chemistry discussions and Athi Narayanan for assistance with CD measurements.

I extend my appreciation to my classmates (and friends) Matt Thompson, Chai Engtrakul, Steve Iwanowski, Linda Thompson, Esther Chege, Rueben Correia and Fehmi Damkaci. Here's to our first year… half spent at Cornerstone!

And to friends that made graduate school the fun ride that it was: Jenssen, Melanie, Stephane, Walker, DeGraf, Trent, Sanabia, Bhakti, Banu, Serpil, Suz, Shaundra, Rich,

Anders, Kathleen, Faiza, Sirchio, Jenny, McElroy, McElroy's Mom, Kung, and Brocci (see also previous paragraph)… thanks for the good times!

Yet another attribute of the Chemistry and Biochemistry Department is the staff. I'd like to express my appreciation to all staff that have made my life much easier than it should have been so many times! Especially Diane Canter, Kay Morris, Olivia Noble, Laura Lynch, Sue Pleyo, Sue-Anne Swartz, Carol Diaz, Debbie Iseli, Adrienne Newman, Susan Moritz, and Bill Griffin.

I'd like to raise my glass to my closest friends Jason Christ, Dave Holohan, Duane Shannon, Ed Jurgill, Chris Myro and Dave Troutman….. you might not have been in grad school with me, but your spirit and friendship got me through.

Thanks to A. J. and Doreen Burke at the Pub for friendship, wings, beer and fun times. To D. G. Yuengling & Son… thanks for facilitating so many good times!

And last, but farthest from least, I thank my family. I could not have made it through even one day of the past five years without them. My deepest thanks are to my wife, Stefanie. She has provided me all the support I needed and more, she has been patient beyond patient, and she has tolerated all the pains that go along with having a husband in graduate school. She did it all with a smile. I honestly would have left graduate school three years ago if she had not convinced me otherwise. Thank you, Stef! I love you! I thank my Mom and Dad for helping me every step of the way, and for all the encouragement they have given. I would not have even made it to my freshman year of college had it not been for my Mom saying "try it for a year" (I almost joined the Navy).

Mom and Dad, thanks for all the good food, the financial support, the encouragement, and for teaching me to always live life to the fullest, day by day. Just knowing that you are there for me makes me feel perpetually at home, and that feeling always gets me through. I love you! I thank my sister Jenny (a.k.a. Shorty) for always being my good friend and my brother-in-law Keith for liking science as much as I do. I thank Mom-mom for always making me smile. Thanks to Mom and Dad Brodeur for their love and support and for allowing me to marry their daughter (despite the fact that I was a poor graduate student). I love you all!

TABLE OF CONTENTS

LIST OF FIGURES

xix

LIST OF SCHEMES

LIST OF TABLES

Chapter 1. Synthetic Ion Channels

1.1 Introduction and Thesis Organization

1.1.1 Introduction

"An effective human being is a whole that is greater than the sum of its parts."[1] Indeed, biological systems (human beings included) comprise an extraordinary multitude of smaller parts all working in perfect harmony to achieve the miracle that is life. The complexity of a living cell is manifested by the nucleic acids that form DNA and RNA superstructures, by the amino acids that make up multisubunit proteins, by the lipids that align to form membranes within and around cells, and by the small molecules involved in signaling pathways that transmit information. Of course, a single cell is only the beginning, the basic building block of higher organisms.

From a chemist's point of view, however, the cell is the endpoint, a "whole" to be broken into its constituent parts. It is the ultimate outcome of the chemistry of biological molecules. In order to understand the small parts and interactions that allow a cell to live and function, the entity must be taken apart and viewed at the molecular level. The quest to attain insight into structure-function relationships is a strong driving force in supramolecular chemistry.[2] Indeed, model systems comprising supramolecular complexes have provided simplified, but accurate, views of biomolecular structure and function.[3]

Electrolytes are nearly as ubiquitous as water in Nature, and are essential for cellular processes. The distribution of ions must be regulated among compartments within the cell and in the extracellular matrix.[4-7] Cells do this through the "supramolecular chemistry" of proteins. Ion channels, the focus of this chapter, are comprised of self-assembled protein subunits that form pores to allow ions to pass through the membrane.[4] The K^+ channel and ClC chloride channel structures clearly demonstrate the complexity attainable through the assembly of proteins.[8,9] In addition to transport, the storage of essential ions

(minerals) is also accomplished through protein conglomerates such as the ferritins, iron storage proteins composed of 24 polypeptide subunits.[10]

Synthetic supramolecular assemblies that bind and/or transport ions have provided insight into the factors that affect natural ion channel assembly, selectivity and voltage dependence.[11-14] Model ion channel assemblies have also shown promise as novel antimicrobial agents and in the treatment of disease.[15,16] Indeed, there is value in the application of supramolecular chemistry to the development of ion binding and transport systems. Much of this chapter, a review of synthetic ion channels, and **Chapters 2** and **3**, which focus on detailed studies of synthetic molecular assemblies that bind and transport ions, will demonstrate the accomplishments in this field and further highlight potential applications.

1.1.2 Thesis Organization

This thesis, "Ion Binding and Transport by Synthetic Molecular Assemblies", is organized into four chapters. The initial goal of this research was to develop molecular building blocks that would form ion channels in membranes through self-assembly. This goal was indeed achieved, and thus **Chapter 1** discusses natural ion channels briefly and then reviews both synthetic cation and anion channels in detail. **Chapter 2** focuses on the ion binding and transport properties of assemblies formed from calix[4]arene-guanosine conjugates cG **2.26** and cG **2.34** (**Chart 1.1**). Assembly of calix[4]arene-guanosine conjugates was the initial approach towards cation channels. Both cG **2.26** and cG **2.34** mediate K^+-selective transport across membranes. However, in the study, cG **2.34** was shown to form a water-mediated dimer in organic solvents via intermolecular guanosine quartet formation. This water-mediated assembly is capable of extracting alkali halide salts from water into $CDCl_3$. The (cG **2.34**)$_2\bullet$(H$_2$O)$_n$ dimer is a rare example of a self-assembled ion pair receptor. To put the work into context, **Chapter 2** begins by reviewing both water-mediated supramolecular assemblies and ion pair (ditopic) receptors. Detailed studies of the assembly and ion transport properties cG **2.26** and cG **2.34** are then described. **Chapter 3** is devoted to the chloride transporters calix[4]arene tetrabutylamide **3.1** and trimer **3.5** (**Chart 1.1**). The structure and function of ion

channels formed from calix[4]arene tetrabutylamide **3.1** is first described, followed by functional studies of trimer **3.5**, a more potent chloride transporter than **3.1**. Lastly, **Chapter 4** contains all experimental procedures.

Chart 1.1

cG **2.26**   cG **2.34**   **3.5**
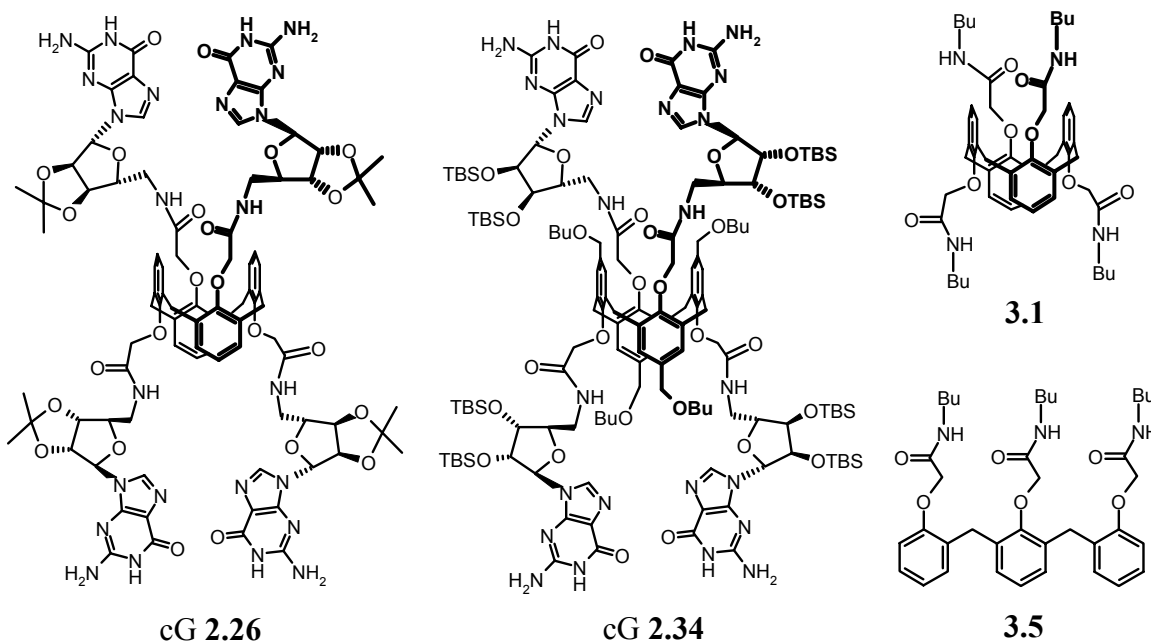
1.2 Ion Channels

1.2.1 Ion Channels in Biological Systems

Ion channels are membrane-bound proteins that allow the regulated diffusion of ions across cell membranes.[4] The channels close and open in response to external stimuli through a process called "gating". Typically, ion channels are voltage-gated, opening and closing with variations in membrane potential, or ligand-gated by other ions (e.g. Ca^{2+}) or small molecules (e.g. neurotransmitters). There are also channels that are gated by temperature and swelling (osmotic pressure changes). Ion channel proteins are found both in the plasma membrane and in intracellular membranes of the mitochondria,

3

endoplasmic reticulum and endosomes. Most ion channels are selective for a specific ion: Na^+, K^+, Ca^{2+}, or Cl^-, leading to their classification as either sodium, potassium, calcium or chloride channels.

The process of ion transport by channels is precisely regulated in and among cells, and its essential role in living systems cannot be overstated. Ion channels generate and relay electrical signals in the nervous system, making them responsible for every movement, sight, sound, taste, feeling and thought. The regulation of cellular ion concentration, pH, volume, and signaling and the transepithelial transport of water and electrolytes are all accomplished by ion channels.[17]

Defects in ion channel function result in a number of diseases, termed "channelopathies".[17-19] Genetic mutations in the cystic fibrosis transmembrane conductance regulator (CFTR), a voltage-dependent Cl^- channel, cause cystic fibrosis. Other Cl^- channel defects have been linked to myotonia (muscle stiffness). Epilepsy can be caused by specific Na^+, K^+, or Cl^- channel defects. K^+ channel mutations in the heart have been implicated in heart arrhythmia. The list of diseases associated with ion channels has grown considerably in recent years, and interest in ion channel structure and function has increased as a result.[17]

Until 5 years ago, channels were studied using three techniques. (1) The investigation of individual channel currents became possible with the development of the patch clamp technique by Neher and Sakmann.[20] This technique is indispensable for measuring channel properties, such as conductance, open state lifetime, and ion selectivity. (2) Site-directed mutagenesis studies have been exploited to determine what sequences are critical for function, and have deduced the pore-forming subunits in many channels. (3) Electron cryomicroscopy has revealed features of channel structures, providing "fuzzy" pictures of the proteins.[21,22]

In 1998, a complete picture of an ion channel was obtained through X-ray crystallography. Roderick MacKinnon and colleagues crystallized the potassium channel from *Streptomyces lividans* and determined its structure.[8] This crystal structure was truly a breakthrough, and took the investigation of ion channel structure to the next level by

providing insight into how channels can both be ion selective and provide high throughput rates. **Section 1.2.2** details the structure of the K$^+$ channel.

1.2.2 The Potassium Channel

The K$^+$ channel crystal structure reported by MacKinnon *et al*. was that of a bacteria, *Streptomyces lividans* (*S. lividans*). By sequence analysis, the *S. lividans* channel (KcsA channel) proved similar to other K$^+$ channels in vertebrates, invertebrates, and plants. The structural features governing ion selectivity and transport in the KcsA channel are therefore almost certainly retained among all potassium channels. Indeed, cloning and mutagenesis studies confirmed that all K$^+$ channels have essentially identical pore constitution, i.e. the amino acid sequence in the pore region is conserved.[23,24] The crystal structure of the KcsA K$^+$ channel has provided tremendous insight into how K$^+$ channels function in cells.

Figure 1.1 shows the structure of the KcsA K$^+$ channel.[8] The channel is a tetrameric self-assembly of four identical proteins, with each subunit comprising an outer, an inner, and a pore helix (**Figure 1.1A**). The inner helices form an "inverted teepee" that points towards the cytosolic membrane surface (**Figure 1.1B**, red). The pore helices are positioned between the inner helices and point toward the center of the channel with their C-termini (**Figure 1.1B**, white). MacKinnon stated that the teepee architecture of the pore "will likely be a general feature" of Na$^+$, K$^+$, and Ca^{2+} channels, based on sequence conservation in this region among the cation channels.[8] **Figure 1.1C** shows a top view of the tetrameric KcsA assembly with a K$^+$ ion (green sphere) in the pore.
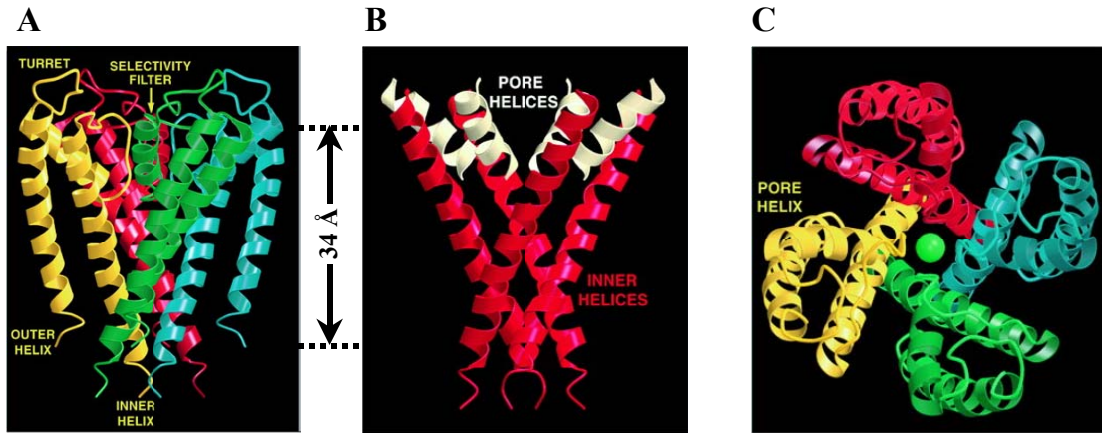
Figure 1.1. Structure of the KcsA K$^+$ channel.[8] (A) Ribbon representation of the KcsA channel tetramer viewed parallel to the plane of the membrane. Subunits are distinguished by color. (B) "Inverted teepee" architecture of the tetramer showing inner (red) and pore helices (white) only. Approximate membrane thickness (34 Å) is indicated between (A) and (B). (C) Ribbon representation of the KcsA channel tetramer viewed from the extracellular side with a K$^+$ cation (green sphere) in the pore. Subunits are distinguished by color. These figures were reprinted with permission from Science and the authors. Copyright 1998 American Association for the Advancement of Science.

The intra- and extracellular openings contain negatively-charged amino acids to attract cations (**Figure 1.2A**, red surface). From the cytosol, the channel begins as a tunnel 18 Å long emptying into a cavity near the center of the membrane. This cavity has a hydrophobic lining and a diameter of ~10 Å (**Figure 1.2B**), large enough to house a hydrated K$^+$ cation. The pore helices contain the "signature" K$^+$ channel sequence, namely TV(I)GYG, and the selectivity filter is constructed of this sequence.[25] The selectivity filter separates the cavity from the extracellular solution, and is 12 Å in length. In the structure, three K$^+$ ions reside in the channel's "conducting pathway", two in the selectivity filter (7.5 Å apart) and one in the hydrophobic cavity (**Figure 1.2A**). This structure solved two mysteries that "tantalized biophysicists for the past quarter century."[8] Namely, how the K$^+$ channel can distinguish between K$^+$ and Na$^+$ and how the

channel can be highly selective and still exhibit throughput rates approaching the diffusion limit.

A

B

Selectivity Filter K$^+$'s

Cavity K$^+$

10 Å cavity
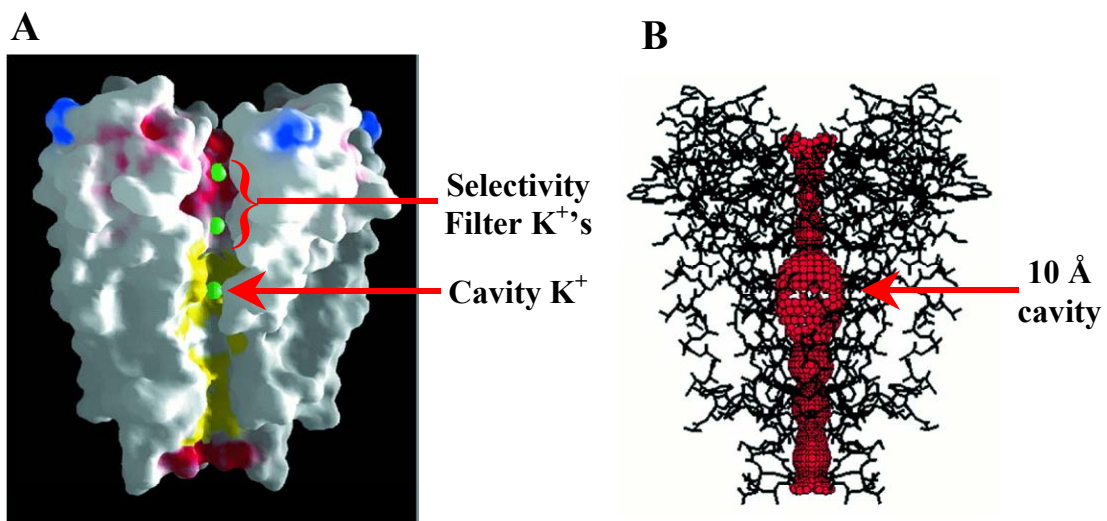
Figure 1.2. (A) Molecular surface of the KcsA channel with three K$^+$ ions in the conduction pathway (green spheres).[8] Colors represent electrostatic potential: blue = positive, white = neutral, red = negative, yellow = hydrophobic residues. (B) The internal pore of the K$^+$ channel (shown in red) within a stick model of the channel structure.[8] These figures were reprinted with permission from Science and the authors. Copyright 1998 American Association for the Advancement of Science.

From inside the cell, K$^+$ ions enter the cavity (near the center of the bilayer) in their hydrated form, thus overcoming the unfavorable hydrophobic environment through water stabilization. The pore helices point into the cavity in an amino-to-carboxyl orientation imposing a negative electrostatic potential via the helix dipole effect (see **Figure 1.1B**).[26] This further stabilizes the cation in the cavity's interior (bilayer center). MacKinnon suggests that the central cavity has a hydrophobic lining to prevent strong interaction of K$^+$ cations with the channel.[8] Such strong cation-channel interactions would most likely prevent high throughput due to tight cation binding. The structure of the cavity and internal pore "ensure a low resistance pathway from the cytoplasm to the selectivity filter."[8]

The selectivity filter consists of a 5-amino acid stretch, TVGYG, that runs 12 Å from the cavity to the extracellular solution. The filter comprises main chain carbonyl oxygens that form a stack of oxygen rings around the pore. The K^+ ions must shed their hydration layer to enter the filter, but are stabilized by oxygen coordination once inside (**Figure 1.3**). The channel discriminates Na^+ by the exact diameter of this oxygen-lined filter. The carbonyl oxygens in the selectivity filter are too far apart to compensate for the dehydration energy of Na^+, thus preventing dehydrated Na^+ from entering.
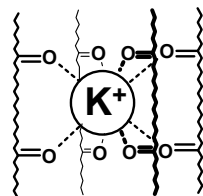
Figure 1.3. Representation of a K^+ cation coordinated in the K^+ channel selectivity filter. Jagged lines represent the protein backbone.

But how can the channel be so selective for K^+ and still provide high transport rates? In the structure, the selectivity filter contained two K^+ ions separated by a single water molecule (K^+-K^+ distance of 7.5 Å). Due to the close proximity of two positive charges, electrostatic repulsion destabilizes the interactions of K^+ with the selectivity filter, thus providing a high K^+ transport rate through the channel.

The two "tantalizing" mysteries have therefore been solved by the KcsA crystal structure. The channel discriminates K^+ (r = 1.33 Å) from Na^+ (r = 0.95 Å) based on their radii by compensating for the dehydration of K^+ upon entering into the filter, but not for that of Na^+. High throughput is accomplished though electrostatic repulsion due to the simultaneous presence of two K^+ ions in the filter.

MacKinnon and colleagues have since solved X-ray crystal structures of a Ca^{2+}-gated K^+ channel and a voltage-dependent K^+ channel.[27,28] The structures have provided a wealth of information concerning the gating mechanisms of these two channels. In 2002, MacKinnon *et al*. solved the X-ray structure of a two ClC chloride channels. The ClC

chloride channel is of particular relevance to the synthetic chloride channel discussed in **Chapter 3** and will be the focus of **Section 1.2.3**.

1.2.3 The ClC Chloride Channel

A report of two ClC chloride channel structures by the MacKinnon laboratory in 2002 was timely.[9] After the detailed K^+ channel structures discussed in **Section 1.2.2**, the features that governed ion selectivity in cation channels (Na^+, K^+, Ca^{2+}) were well understood. Much less was known about ion selectivity in anion channels. ClC chloride channels are responsible for regulating membrane potential and electrical excitability in skeletal muscle. Also, ClC channels are involved in fluid and electrolyte transport in the kidney.[29,30] Several hereditary disorders are associated with genetic defects in human ClC channels.[30]

MacKinnon *et al.* solved the X-ray crystal structures of ClC chloride channels from *Salmonella enterica serovar typhimurium* (StClC) and *Escherichia coli* (EcClC). In this section, all figures show the StClC structure. The EcClC structure is essentially the same. The ClC channel is a dimeric protein with a two-fold symmetry axis perpendicular to the membrane (**Figure 1.4A**, **B**). Each of the two subunits possesses its own pore and Cl^- selectivity filter (Cl^- ions shown as green spheres in **Figure 1.4A** and **B**).
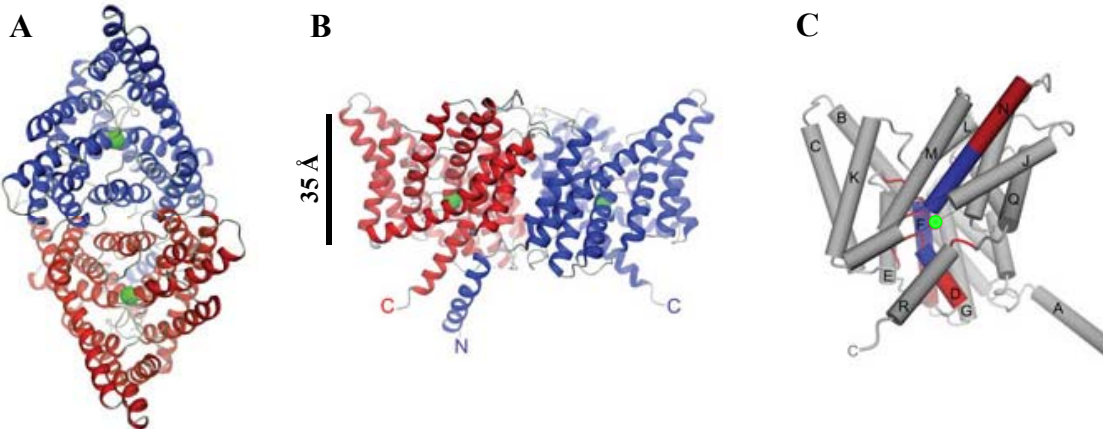
Figure 1.4. Ribbon representation of the StClC chloride channel viewed from (A) the extracellular side and (B) the plane of the membrane.[9] The two identical subunits are blue and red and the Cl⁻ in the selectivity filter is represented as a green sphere. The black line in (B) indicates the approximate 35 Å membrane thickness. (C) Representation of helix dipoles pointing towards the selectivity filter. The N-terminal (positive, blue) and C-terminal (negative, red) ends of the three key helices (labeled D, F and N) are shown. The selectivity filter residues are shown as red cords and the Cl⁻ ion as a green sphere. These figures were reprinted with permission from Nature Publishing Group and the authors. Copyright 2002 Nature.

Within an individual subunit, the selectivity filter is formed by the N-terminal amino acids of three α-helices, shown as red cords in **Figure 1.4C**. The three helices oriented with their N-termini toward the filter generate a positive potential through the helix dipole effect (opposite that of the K⁺ channel).[26] In the selectivity filter, the Cl⁻ is bound through hydrogen bonding to two main chain amide NH groups on one side and hydrogen bonding to a Ser-OH and a Tyr-OH on the other, as depicted in **Figure 1.5**. Like in the selectivity filter of the K⁺ channel (**Figure 1.3**), Cl⁻ ions do not make contact with fully charged residues (Lys or Arg), but instead are coordinated by partially charged atoms (amide and alcohol hydrogen atoms) resulting in weaker binding and thus high throughput rates.
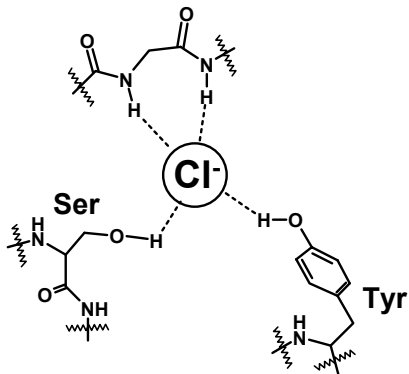
Figure 1.5. Representation of Cl⁻ binding to the ClC channel selectivity filter.

In the ClC channel, the selectivity filter is a narrow 12 Å tunnel in the center of the channel. This is in contrast to the K^+ channel, where the filter is near the extracellular opening. Water-filled cavities are positioned above and below the selectivity filter. In the StClC structure, it was found that the channel was in its "closed" state. A Glu residue was positioned between helices F and N (**Figure 1.4C**), presumably occupying a second anion binding site. It was hypothesized that this Glu residue served as the channel gate, and could be displaced by Cl⁻ at some critical extracellular Cl⁻ concentration.

Indeed, an X-ray crystal structure of a ClC channel with a Glu-to-Ala mutation at that position showed two Cl⁻ ions in the channel, one occupying the same position as in the previous structure and one taking the place of the Glu carboxylate group.[31] The Cl⁻ anions were located only 4 Å apart in the selectivity filter. Once again, as with the K^+ channel, the ClC channel accomplishes high throughput by placing two Cl⁻ ions simultaneously in the filter, thus exploiting electrostatic repulsion to achieve high ionic diffusion rates through the channel.

The amino acids forming the selectivity filter are "quite conserved" among all ClC channels.[9] According to MacKinnon *et al.*, this implies that the anion-selective principles found in the StClC and EcClC channels apply to all channels in the ClC family.

1.2.4 Concluding Remarks

Ion channel X-ray crystal structures will no doubt become more numerous now that the seminal work has been published, X-ray techniques are becoming more sensitive, and methods for high throughput crystallization are being developed.[32] Important to note is that MacKinnon and colleagues *do not* use high throughput technology in their crystallization of channel proteins.[33]

However, the study of ion channels has been ongoing since the first reports by Bertil Hille and Clay Armstrong in the early 1970's.[34,35] Much was learned without the benefits X-ray crystallography, and many predictions made about the potassium and ClC chloride channels were found to be correct. Over three decades of knowledge has been gained concerning ion channel structures and mechanisms.[4] However, since the intended focus of this chapter is synthetic ion channels, natural channels will not be discussed further. But as will become evident throughout this chapter, the impetuses for studying peptide channels (**Section 1.3**) and synthetic channels (**Sections 1.6** and **1.7**) came from Nature, and the information gained has aided in elucidating Nature's ways of transporting ions.

1.3 Peptide Ion Channels

The study of peptide ion channels offers simplicity over that of natural channels. Reasons are: (1) peptides are often easier to obtain than proteins and can be synthesized, (2) peptides are easier to manipulate by methods such as site-directed mutagenesis, and (3) spectroscopic and physiochemical data for peptides can be interpreted to give molecular level details of structure.[36] Peptides have been used as models for protein ion channels. Gramicidin and alamethicin are prime examples of peptide ion channel models for structure and function. This section briefly describes three peptides that form ion channels in membranes: gramicidin, alamethicin and melittin.

Gramicidin. Gramicidin A (GA) is a 15 residue peptide comprising alternating D- and L-amino acids (**Chart 1.2**). Importantly, there are no charged residues in GA, since all residues are neutral, the N-terminus is formylated, and the C-terminus bears an ethanolamine. The Trp (W) residue at position 11 (underlined in **Chart 1.2**) is sometimes

substituted with Phe (F) giving gramicidin B or Tyr (Y) giving gramicidin C, both having properties similar to those of GA.[36]

GA forms ion channels in membranes. The active channel structure is a dimer comprising two $\beta^{6.3}$-helices (6.3 residues/turn).[37] The helices are held together at the center of the bilayer by six hydrogen bonds between their N-termini (**Figure 1.6**). The active GA dimer has been estimated to be 22 Å in length.[38,39] The pore is formed within the $\beta^{6.3}$-helices, wherein the peptide backbone amides line the pore and the sidechains, all of which are uncharged, point outward from the channel into the lipid bilayer. The pore is lined with water molecules.[36] Additional support for a GA dimer structure came from chemical modifications of the peptide. Ion channel activity was maintained when the N-termini of two GA monomers were covalently tethered through either a malonyl or a tartaric acid linker.[40,41] These modified peptides represent early examples of synthetic cation channels.
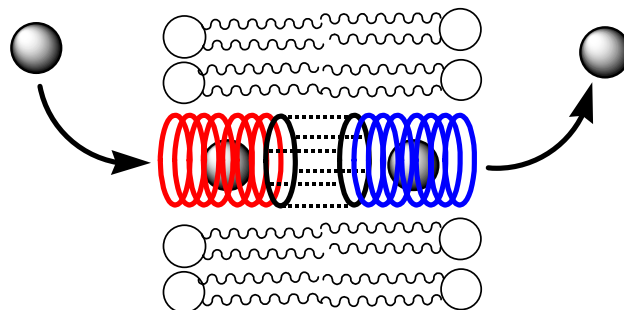
Figure 1.6. Representation of the gramicidin A dimer ion channel. Red and blue are used to distinguish between individual GA peptide monomers, hydrogen bonds are shown as dashed lines, the peptides' N-termini are indicated with black circles, and cations are represented with gray spheres.

GA channels have a single conductance near 5.8 picosiemens (pS), indicative of a single active structure (the GA head-to-head dimer).[42] Open state lifetimes for GA channels average near one second. This is long compared to the millisecond open state lifetimes of many natural channels. The order of selectivity for GA is

$H^+>Cs^+>Rb^+>K^+>Na^+>Li^+$.[43] The proton permeability is attributed to a hopping mechanism through the water-filled pore.

Chart 1.2

$$HCO\text{-}V\text{-}G\text{-}A\text{-}^DL\text{-}A\text{-}^DV\text{-}V\text{-}^DV\text{-}W\text{-}^DL\text{-}\underline{W}\text{-}^DL\text{-}W\text{-}^DL\text{-}W\text{-}NHCH_2CH_2OH$$
Gramicidin A (GA)

Ac-Aib-P-Aib-A-Aib-A-Q-Aib-V-Aib-G-L-Aib-P-V-Aib-Aib-<u>Q</u>-Q-Pheol
Alamethicin (Alm)

$$G\text{-}I\text{-}G\text{-}A\text{-}V\text{-}L\text{-}K\text{-}V\text{-}L\text{-}T\text{-}T\text{-}G\text{-}L\text{-}P\text{-}A\text{-}L\text{-}I\text{-}S\text{-}W\text{-}I\text{-}\underline{K\text{-}R\text{-}K\text{-}R}\text{-}Q\text{-}Q\text{-}NH_2$$
Melittin
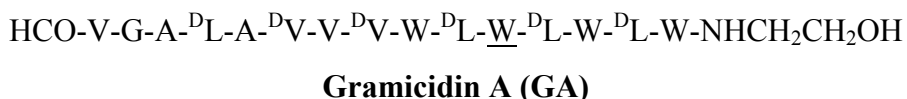
Alamethicin. The antibiotic peptide alamethicin (Alm, **Chart 1.2**) is "the best studied simple model of pores formed by intramembrane aggregation of amphipathic α-helices."[44] This quote from the review by Duclohier and Wroblewski provides a fairly concise summary of the structure and function of Alm. The naturally occurring peptide has some heterogeneity, as position 18 can be Gln (Q, underlined in **Chart 1.2**) or Glu (E). Alm is rich in α-aminoisobutyric acid (Aib), a residue also known as α-methylalanine, and is the source of the peptide's name.[44] Peptides rich in Aib have been termed peptaibols, a classification that includes Alm.[44]

Alm forms ion channels in membranes through aggregation of α-helical monomers. The ion channels are highly voltage–dependent, conducting at negative membrane potentials.[44] This is a signature of Alm and a property that attracted much interest from biophysicists in the late 1960's.[45] The crystal structure of Alm gave insight into the channel's structure and provided a model for the voltage-gating mechanism of protein ion channels.[46]

Channel aggregates can consist of anywhere between 4 and 11 Alm monomers aligned parallel to one another (**Figure 7A**).[47] An increased number of monomers in an aggregate results in an increased pore size, and thus an increased channel conductance.

Alm shows multiple conductance levels ranging from 19 to 4400 pS, as expected for the formation of multiple active structures.[48] The structure of Alm aggregates is described as a "barrel-stave" model, in which the polar faces of the Alm α-helices are oriented toward the center of the aggregate, lining the pore, and the hydrophobic faces of the helices reside on the periphery of the aggregate in contact with the lipid tails of the membrane (**Figure 7B**).[49] Alm channels are selective for monovalent cations over divalent cations and anions.[36]
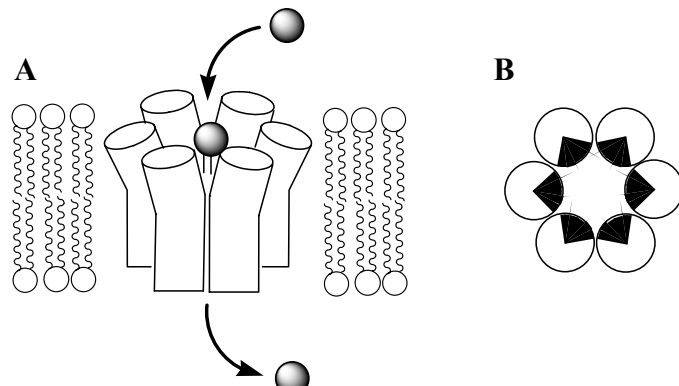
Figure 1.7. (A) Side view representation of a barrel-stave hexameric alamethicin aggregate in a membrane. Alm peptide monomers are shown as bent cylinders and cations as gray spheres. (B) Top view representation of the Alm hexamer shown in A. The polar face of each α-helix points toward the channel pore and is indicated in black.

Melittin. Melittin (**Chart 1.2**) is the major protein in European honey bee venom and is responsible for the "sting".[50] This peptide is unique in that its action on membranes is strongly dependent on the membrane's composition.[51] Melittin bears six positive charges, four on at its C-terminus (K-A-K-A, underlined in **Chart 1.2**) and two at its N-terminus (A and K).[52] Like Alm, melittin forms amphipathic α-helices, with polar residues oriented on one face and hydrophobic residues on the opposite face. In water, melittin is either monomeric or associated in a tetrameric aggregate. A crystal structure of melittin in its tetrameric form showed amphipathic α-helices with two helical regions per monomer, the axes of which are at approximately 120° to each other.[53,54]

Melittin has demonstrated the ability to form voltage-gated ion channels in membranes under specific conditions (i.e. 5 M NaCl), opening at negative

transmembrane voltages.[51] Discrete conductance levels ranging over three orders of magnitude indicate multiple active channel structures. However, the magnitude of conductance shows a fourth power dependence on melittin concentration, suggesting that tetramer association is critical for ion channel formation.[55] Melittin channels exhibit a selectivity for anions over cations, a property attributed to the strongly positive K-A-K-A sequence at the peptide's C-terminus.[55] Anion selectivity is rare among ion channel peptides (all other peptides discussed, or even mentioned, in this section are cation selective). This is also true for synthetic ion channels, as will become apparent in **Sections 1.6** and **1.7**, where the cation channel literature is plentiful and the anion channel literature is sparse.

Melittin is more commonly known for its hemolytic activity, i.e. its ability to induce hemoglobin release from erythrocytes.[50] In model membranes, melittin has shown conductance fluctuations, suggesting membrane disruption and not discrete channel formation.[55,56] In zwitterionic membranes (such as EYPC, used throughout **Chapters 2** and **3**), it has been predicted that melittin will partition into the midpolar region of the bilayer, only partially extending into the hydrophobic membrane center. This gives rise to an increase in bilayer curvature leading to membrane disruption.[57] Lastly, melittin has also been shown to induce micellization and fusion of lipid membranes.[51]

In addition to the peptides discussed, other channel-forming peptides have been identified. Among them are the zervamicins and trichotoxins, peptaibols similar to alamethicin, that exhibit antibacterial activity.[58,59] Magainins, a family of antibiotic peptides, exhibit pore-forming activity and show promise as antitumor agents.[52] The cecropins are insect defensins and function similar to the magainins.[52] Pardaxin, a shark repellent peptide toxin, functions via ion channel formation.[60] All these peptides form channels that are cation-selective. In addition to these known channel-forming peptides, there exist hypotheses that the β-amyloid peptides of Alzheimer's disease and the polyglutamine peptides of Huntington's disease damage or kill cells via formation of ion channels.[61,62] Channel-forming peptides, particularly gramicidin and alamethicin, have inspired the design of synthetic ion channels. In some cases, sequences of the natural

peptides have been incorporated into synthetic channels and in others, the gramicidin and alamethicin structures simply set an example for non-peptide designs. The study of channel-forming peptides is critical for both understanding molecular-level details of natural protein channels and for the design of novel synthetic channel-forming molecules.

1.4 Introduction to Synthetic Ion Channels

It is clear why researchers would want to study ion channels. Since they are found in every cell and are at the core of physiological processes, understanding ion channels has tremendous medical benefit. Also, with the numerous diseases now being linked to ion channel defects, understanding the structure-function relationships of channels could lead to cures or treatments. But why would anyone want to develop and study synthetic ion channels? The impetuses for these studies are similar to those that inspire the investigation of peptide ion channels (**Section 1.3**). The design and synthesis of synthetic channels is intended to: (1) increase the understanding of natural ion channels, (2) provide avenues to novel antimicrobials, and (3) to provide treatments for ion channel diseases. As will be described in **Sections 1.6** and **1.7**, each of the aforementioned goals have been achieved through the development and study of synthetic ion channels. Before reviewing synthetic ion channels, methods used to monitor ion transport across membranes will first be described (**Section 1.5**). Throughout **Sections 1.5**, **1.6** and **1.7**, methods and results that are relevant to the studies described in **Chapters 2** and **3** will be highlighted.

1.5 Methods for Studying Ion Transport across Membranes

1.5.1 Transport Mechanisms

Ions can be transported across a lipid membrane by one of two mechanisms (**Figure 1.8**).[63,64] The ion channel mechanism, being the topic of this chapter, has already been presented. The channel mechanism involves a structured membrane-spanning pore that allows ion flow through the membrane.[63] A second mechanism, the carrier mechanism,

involves the encapsulation of an ion by a membrane-soluble ionophore. The ionophore then "carries" the ion across the lipid bilayer and releases it on the other side.[63]
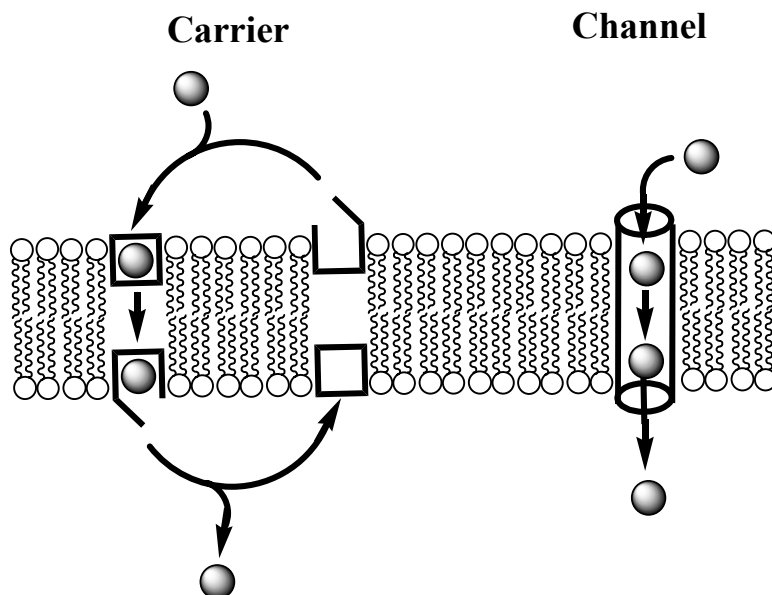
Carrier   **Channel**

Figure 1.8. Carrier and channel mechanisms of ion transport. Ions are represented by gray spheres.

Until the mid 1960's, all transport across membranes was believed to proceed via a carrier mechanism. Bertil Hille was the first to propose the existence of ion channels at meetings of the Biophysical Society starting in 1965, and in a manuscript published in 1970.[34] His ideas were met with much skepticism from scientific peers in the biophysical community.[65] But Hille was correct in his predictions, as has been proven time and time again with the development of the patch clamp technique and more recently through X-ray crystallography.[8,9,20]

In the study of synthetic ion channels, it is important to distinguish between the channel and carrier mechanisms. Transport via both mechanisms results in the same outcome, i.e. net transport of ions from one side of the membrane to the other, so distinguishing the two is not trivial. Convincing evidence of the channel mechanism can be obtained by observation of single-channel currents via the patch clamp or planar bilayer voltage clamp techniques (**Sections 1.5.2** and **1.5.3**). Indirect evidence of a

channel mechanism for synthetic channels has been reported, and will be discussed in **Sections 1.6** and **1.7**.

1.5.2 Patch Clamp Technique

The Patch Clamp technique, developed by Neher and Sakmann, is widely used for studying ion channels in cell membranes.[20] The technique "is an electrophysiological method that allows the recording of macroscopic whole-cell or microscopic single-channel currents flowing across biological membranes through ion channels."[20] The large scientific impact of the patch clamp method was recognized by the 1991 Nobel Prize in Physiology or Medicine awarded to Erwin Neher and Bert Sakmann.[66,67]

For measuring single-channel currents, a small area of a cell membrane is isolated and investigated.[20] This is accomplished using a metal-coated glass pipette electrode containing an electrolyte solution with a tip diameter near 1 μm (open area approximately 1 μm^2). The pipette tip is brought in contact with the surface of the cell membrane and a slight suction is applied. This results in a tight seal between the tip and the membrane. Ion channels within the patch are studied by electrophysiological techniques. By studying an isolated patch, many complications of studying the entire cell membrane, with all of its embedded proteins of various functions, are alleviated.

There are three types of "patches". (1) A "cell-attached" patch exists when the patch remains as part of the cell membrane, isolated only by suction to the pipette. (2) The pipette can be moved away from the cell tearing the patch, which remains over the pipette tip. This is termed an "inside-out" patch, since the cytosolic side of the cell membrane now faces out from the pipette tip, and the extracellular membrane surface faces the electrolyte solution inside of the pipette. (3) The last type of patch is called an "outside-out" patch, which is much like the inside-out patch, but with the membrane flipped. An outside-out patch is formed starting from the cell-attached seal. A small burst of pressure is then forced through the pipette to push the patch open and allow the pipette to penetrate into the cell. Subsequent removal of the pipette tip from the cell results in reforming of the membrane, but with the extracellular membrane surface now facing out from the pipette tip.

An alternative configuration allows for the observation of ion currents for an entire cell. This is termed the "whole-cell" configuration.[20] To achieve the whole-cell configuration, the glass pipette is brought into contact with the cell membrane. Instead of applying a light suction to seal a patch, a pulse of suction is applied creating a hole in the membrane, thus providing access to the interior of the cell. Ion currents can then be measured for the entire cell. This configuration was used to study the synthetic ion channels formed from calix[4]arene tetrabutylamide **3.1** described in **Chapter 3** of this thesis.

The basic ion channel properties measured by the patch clamp technique are conductance, voltage dependence, open probability and ion selectivity. Typical ion channel conductances, from single-channel current measurements, range from 1 to 150 picosiemens (pS).[4] Channel currents are on the order of several picoamperes (pA), with 1.0 pA corresponding to the passage of approximately 6×10^6 monovalent ions per second.[4] Open probability is the fraction of time the channel spends in the open state, and is measured from single-channel currents by dividing the sum of all open times by the duration of recording.[18] A representation of a single-channel current trace is shown in **Figure 1.9.**
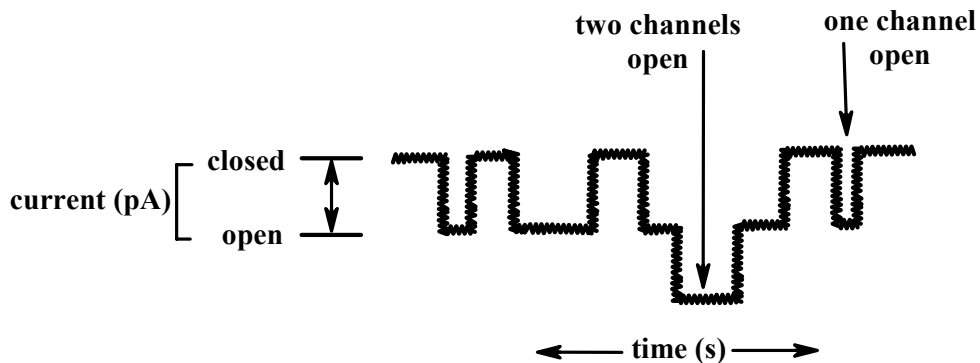
Figure 1.9. Representation of a single-channel current trace.

Ion selectivity can be determined using patch clamp methods, but the details of this procedure will be discussed in the next section on the planar bilayer voltage clamp technique. For a patch, the procedure is the same as for planar bilayers, except a

membrane patch with buffers outside (in the bathing solution) and inside the pipette is used.

1.5.3 Planar Bilayer Voltage Clamp Technique

The study of ion channels in cell membranes via the patch clamp technique provides valuable information concerning the behavior of channels in living biological systems. However, the cell membrane is complicated, comprising many lipids and proteins. First, isolating a single ion channel type (e.g. ligand-gated Na^+ channels) within a patch can be difficult, and the presence of many other membrane-bound proteins, each having a different function, may interfere with channel recordings. Secondly, the membrane lipid content cannot be controlled. And lastly, not all membranes can be reached by a glass pipette.[68]

One method biologists and chemists use to circumvent this problem is by testing proteins or synthetic compounds in planar bilayers. According to Hanke and Schlue: "The most simple membrane model is a planar lipid bilayer composed of one pure lipid, and this is the first system one should construct, investigate and understand."[68] In planar bilayer experiments, the solution composition and membrane lipid composition can be controlled. In this environment, a channel can be isolated in the planar membrane and studied in the absence of other proteins and cellular components.

In the planar bilayer voltage clamp technique, a planar bilayer is formed between two buffer-containing wells. The protein or synthetic compound to be studied is either injected into the buffer on one side of the bilayer or incorporated into the membrane upon formation. Two electrodes, one in each well and both attached to a patch clamp amplifier, generate a potential across the membrane. The grounded electrode typically resides in the well where the protein or compound to be tested is added (often termed the "cis" well). The other electrode (in the "trans" well) is active, i.e. generates the potential. Defining the "cis" and "trans" wells of the set-up is left to the discretion of the researcher, and thus the terms do vary throughout the literature. If the protein or compound of interest functions as an ion channel, single channel current bursts (events) will be observed.

These events are similar to those observed in patch clamp recordings in the single-channel configuration (**Figure 1.9**). **Figure 1.10** diagrams of a voltage clamp setup.
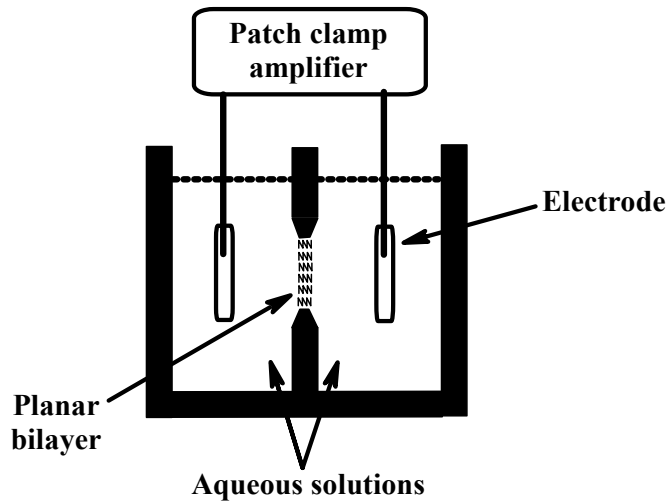
Figure 1.10. Diagram of a planar bilayer voltage clamp setup.

Once the data have been collected, they are analyzed by plotting current *versus* applied voltage (an I/V curve). According to Ohm's law, the slope of this curve is the channel conductance (typically measured in picosiemens, pS). Ion selectivity (i.e. cation-over-anion, or *vice versa*) can be determined through planar bilayer experiments by analysis of I/V curves. To determine ion selectivity, a transmembrane salt gradient is generated, e.g. 500 mM KCl in the cis compartment and 100 mM KCl in the trans compartment. The reversal potential (E_{rev}), i.e. the potential at which the current changes sign, is then measured.[4] A non-zero E_{rev} occurs when the channel in the membrane is selective for a specific ion. For example, a K^+ selective channel, for the case of 500 mM KCl (cis) and 100 mM KCl (trans), will reach an equilibrium state in which $[K^+]_{trans} > [Cl^-]_{trans}$, and $[K^+]_{cis} < [Cl^-]_{cis}$, resulting in a negative E_{rev}. The value of E_{rev} is then introduced into the Goldman-Hodgkin-Katz equation (**Equation 1.1**) to calculate the relative ion permeabilities.[4]

$$E_{rev} = \frac{RT}{F} \ln \frac{P_K[K^+]_t + P_{Cl}[Cl^-]_c}{P_K[K^+]_c + P_{Cl}[Cl^-]_t} \qquad \textbf{Equation 1.1}$$

In **Equation 1.1**, shown for the case described above (KCl on both sides of the membrane), R is the gas constant, T is the absolute temperature, and F is Faraday's constant. P_K and P_{Cl} represent the permeabilities of K^+ and Cl^-, respectively, and subscripts 'c' and 't' indicate concentrations in the cis and trans wells, respectively. After introducing the measured E_{rev} into **Equation 1**, a value for P_K/P_{Cl} is calculated, giving the relative permeabilities of the two ions, and thus the ion selectivity.[4] This same principle can be applied to measure the selectivity within a series of cations or anions. To determine a cation preference between K^+ and Na^+, for example, solutions of equal concentration, but containing different cations, are used. One such experiment would use 100 mM KCl in the cis well and 100 mM NaCl in the trans well. By measuring the E_{rev} and then introducing the value into **Equation 1.1** (but now with three terms: P_K, P_{Na}, and P_{Cl}), a P_K/P_{Na} permeability ratio can be calculated. Throughout **Section 1.6** and **1.7**, ion permeability ratios will be given as reported by the various authors.

Importantly, since the channel being studied in a planar bilayer experiment is isolated, it can be determined whether a single conducting channel structure is formed or conduction is occurring through multiple channel structures. A single conductance level in voltage or patch clamp measurements indicates a single channel structure. However, multiple conductance levels reveal several electrically distinct states. That is, the protein or compound under investigation forms multiple conducting structures in the membrane. A comparison of the ion channel-forming peptides gramicidin and alamethicin demonstrates this point (see also **Section 1.3**).[36] Gramicidin has a single active structure, a membrane-bound dimer, and thus exhibits only one conductance state (5.8 pS) in single-channel measurements. Conversely, alamethicin forms several conducting aggregates, each varying in the number of alamethicin monomers. Indeed, single-channel measurements of alamethicin show multiple conductances. This point is emphasized here because the ion channels formed from calix[4]arene tetrabutylamide **3.1** discussed in

Chapter 3, exhibit multiple conductance states due to the formation of multiple active channel structures.

1.5.4 Liposomes and Liposome Preparation

In addition to planar bilayers, liposomes provide a tunable system for ion transport assays. A liposome is a spherical lipid bilayer that encapsulates an aqueous compartment; it is essentially a cell model. Liposomes are highly versatile and extremely valuable for ion transport experiments for several reasons. (1) The bilayer can comprise any mixture of natural and/or synthetic lipids suitable for the intended assay. (2) The contents of the aqueous intravesicular compartment can be modulated allowing for a wide variety of experiments. Some examples that will be discussed involve entrapment of pH-sensitive fluorescent dyes and NMR shift reagents. (3) The extravesicular solution is also tunable. (4) Liposome experiments can be conducted at various pH and electrolyte concentrations, and allow for pH and ion gradients across the membrane.

Most liposomes discussed in this thesis are composed of egg yolk phosphatidylcholine (EYPC, **Chart 1.3**). EYPC is a neutral lipid, i.e. the phosphate head group has a net charge of zero. Other lipids typically used for liposomes include phosphatidylglycerol (PG) and phosphatidylserine (PS), both of which are negatively charged lipids (net charge = -1 at neutral pH, **Chart 1.3**). Lastly, dipalmitoyl phosphatidylcholine (DPPC) is sometimes used to decipher a carrier or channel transport mechanism by comparison of transport rates in DPPC and EYPC vesicles (described in **Section 1.6.2**).

Chart 1.3
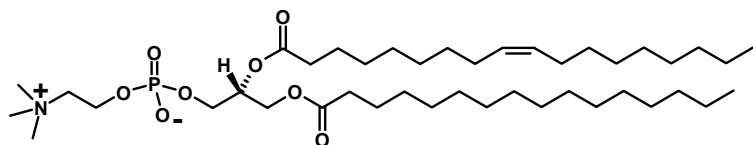
Egg Yolk Phosphatidylcholine (EYPC)
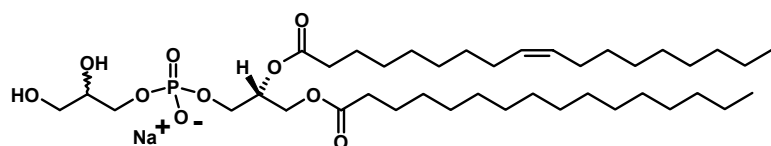
Phosphatidylglycerol (PG)
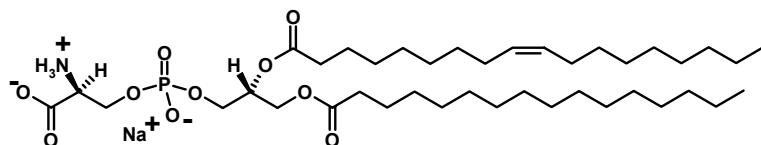
Phosphatidylserine (PS)
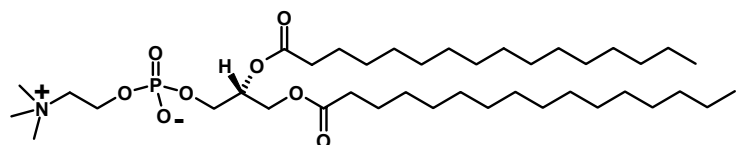
Dipalmitoyl Phosphatidylcholine (DPPC)

In addition to lipid composition, there are two other important properties of liposomes: size and lamellarity. Size is measured by the liposome's diameter, and there are three size categories: small, large and giant. Small vesicles are < 50 nm in diameter. Large vesicles fall in the wide range of > 50 nm to 1000 nm. And lastly, giant vesicles are those with diameters > 1000 nm. In the literature, the term "vesicle" is used interchangeably with "liposome", as will be the case throughout this thesis.

Lamellarity is defined by the number of liposomes within a liposome. Only two possibilities are important: (1) There are no liposomes inside liposomes, i.e. each liposome consists of a single bilayer surrounding an aqueous compartment. Such liposomes are termed "unilamellar" (have one lamellae). (2) There are one or more

liposomes within each liposome, i.e. each liposome is like an onion, with multiple spherical bilayers. "Multilamellar" (having more than one lamellae) is the term used to describe this type of liposomes. Both unilamellar and multilamellar liposomes are depicted in **Figure 1.11**. A test for lamellarity has been devised by McIntyre and Sleight.[69] In their procedure, a NBD-labeled fluorescent lipid is incorporated into liposomes (NBD = 7-nitro-2,1,3-benzoxadiazol-4-yl). Dithionite, when added to the liposomal suspension, reacts only with lipids in the outer leaflet of the membrane (outermost lamellae for multilamellar vesicles), reducing NBD and resulting in quenching of the labeled lipid's fluorescence. The lamellarity can be estimated from the amount by which the fluorescence decreases: approximately 50% for unilamellar vesicles and less for multilamellar vesicles.[69]

Unilamellar   **Multilamellar**
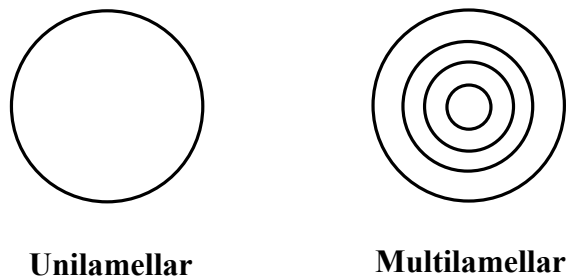
Figure 1.11. Representation of unilamellar and multilamellar liposomes. Each circle represents a spherical bilayer.

Most liposomes used in experiments throughout this thesis are unilamellar vesicles with an average diameter of 120 nm. This classifies them as large unilamellar vesicles, or LUVs. LUVs have the advantage of a large entrapped aqueous compartment. Alternatively, small unilamellar vesicles (SUVs) are often used by researchers. SUVs suffer from a small entrapped aqueous volume. But unlike LUVs, SUVs are not osmotically sensitive.[70] For example, SUVs with a large internal osmotic pressure will not explode when suspended in pure water (zero osmotic pressure), and *vice versa*.

There are a number of methods for the preparation of liposomes of varying size and lamellarity.[70] SUVs are typically prepared by sonication of lipid suspensions.[71] Giant

unilamellar vesicles (GUVs) can be prepared by the rapid evaporation technique.[72] By evaporating a biphasic mixture of a CHCl$_3$:MeOH phospholipid-containing solution and an aqueous buffer under reduced pressure at 40 °C, GUVs with diameters up to 50 μm can be prepared. They can then be separated from larger liposomes by high-speed centrifugation.[73] Since LUVs, and not SUVs or GUVs, are used in experiments in this thesis, all other methods discussed will describe the preparation of LUVs.

The preparation of LUVs can be accomplished using the dialytic detergent method, reverse phase evaporation method, or high pressure extrusion through a polycarbonate membrane with a defined pore size. In the dialytic detergent method, lipids (and components to be entrapped within the vesicles) are solubilized with detergent to form mixed micelles.[74] The detergent is then removed by dialysis, resulting in the formation of large unilamellar liposomes.

Formation of LUVs via reverse phase evaporation is accomplished by introducing an aqueous buffer into a solution of phospholipid dissolved an organic solvent. Subsequent evaporation of the organic solvent under reduced pressure results mostly in the formation of large unilamellar vesicles.[75] The size can be modulated by the lipid or mixture of lipids used.

For extrusion, lipids are first hydrated with an aqueous buffer (containing the desired intravesicular contents) to give a suspension of multilamellar vesicles of varying size. The suspension is then extruded through a polycarbonate membrane having a defined pore size.[76] All liposomes used in the experiments discussed in this thesis were prepared by high pressure extrusion. In most cases, the suspension was extruded through a polycarbonate membrane with a pore size of 100 nm. This gives LUVs with an average diameter of 120 nm.

1.5.5 Base Pulse Assay

The critical element in the base pulse assay is the pH-sensitive fluorescent dye 8-hydroxy-1,3,6-pyrene-trisulfonate (HPTS), commonly called pyranine.[77] **Scheme 1.1** shows the protonation states of pyranine, along with the excitation and emission maxima for each state. Two features of pyranine make this molecule a useful probe for monitoring

ion transport. First, the protonated and deprotonated forms are excited at different wavelengths, but emit at the same wavelength (510 nm). This allows for fluorimetric determination of the protonated:deprotonated ratio, and thus the pH, using a dual excitation configuration. Secondly, pyranine's pK_a is near physiological pH, making it useful for biologically-relevant studies.

Scheme 1.1. Tri-anionic and tetra-anionic pyranine and the excitation and emission maxima for each state.

$\lambda_{ex} = 403$ nm $\lambda_{ex} = 460$ nm

$\lambda_{em} = 510$ nm $\lambda_{em} = 510$ nm
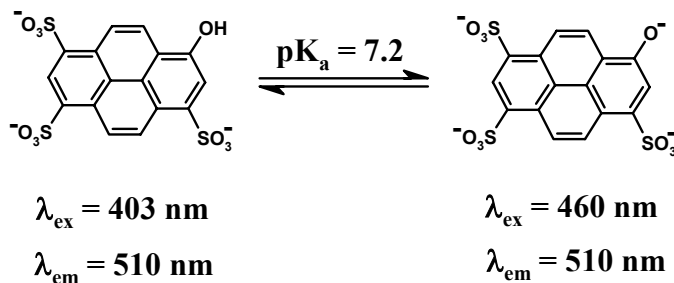
The base pulse experiment was applied in all ion transport studies described in this thesis, and provided valuable insight into ion transport rates and selectivities in all cases. This experiment will therefore be described with the exact conditions imposed for experiments herein. These conditions are similar to those used by other researchers.[78-80]

A base pulse experiment is depicted in **Figure 1.12**. A solution of the compound to be tested (cylinder) is added to a suspension of EYPC LUVs containing entrapped pyranine (green). At this point, the pH of the intra- and extravesicular buffer is equal at 6.4. A NaOH solution is then added to the extravesicular buffer to create a gradient of approximately one pH unit. The pH outside is now 7.4, while it remains at 6.4 inside (situation represented in **Figure 1.12**). The resulting electrostatic potential, caused by proton efflux from the liposomes, can be compensated only by cation influx (blue in) or anion efflux (red out), as mediated by the exogenous ligand (cylinder). If the test compound cannot mediate ion transport, no pyranine fluorescence change will be observed. In other words, protons will not move outward if the electrostatic potential is not compensated. If the compound does mediate ion transport across the membrane, this

will be signaled by the increase in relative pyranine fluorescence that accompanies the rise in intravesicular pH.
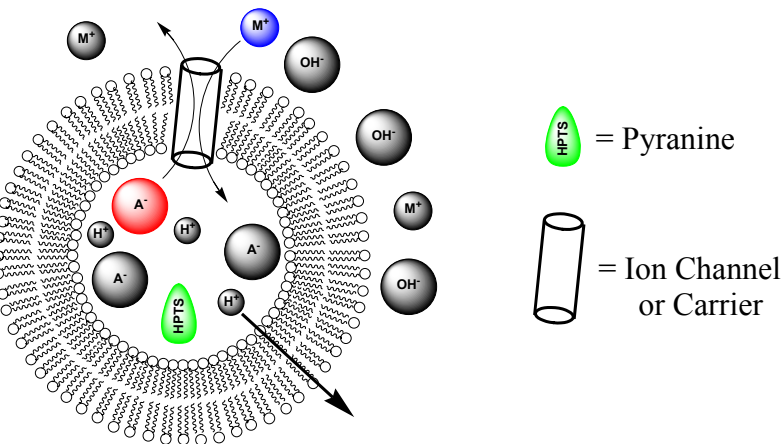
Figure 1.12. A liposome in a base pulse experiment.

In **Chapter 2** of this thesis, cation influx mediated by cG **2.26** or cG **2.34** compensates the electrostatic potential in this experiment. In **Chapter 3**, the reverse situation is occurring, where calix[4]arene tetrabutylamide **3.1** and trimer **3.5** mediate anion efflux, resulting effectively in an outwardly directed H^+/Cl^- cotransport.

1.5.6 pH Stat Assay

In a pH stat assay, the extravesicular solution is held at a constant pH by titration of base in response to mediated proton efflux/cation influx or proton efflux/anion efflux. The rate of addition of base required to maintain the pH reflects the ion transport rate. To describe this experiment in detail, the procedure of Fyles *et al*. will be used as an example.[81]

Large unilamellar vesicles (~150 nm diameter) containing a pH 6.6 buffer were suspended in unbuffered choline sulfate. The extravesicular choline sulfate solution was adjusted to pH 7.6 by addition of choline hydroxide, thus creating a transmembrane pH gradient, followed by addition of the proton ionophore FCCP (carbonyl-*p*-trifluoromethoxyphenylhyrazone). The weak acid FCCP ensures that proton transport

across the membrane can occur rapidly.[82] An alkali metal sulfate solution was then added to the liposome suspension, creating a salt gradient. At this point, cations want to go into the liposomes (down the cation gradient) and protons want to come out (down the pH gradient). However, the two gradients remain, since "the system lacks pathways for cation-proton antiport or anion-proton symport."[81] Addition of a transporter results in inwardly-directed cation transport accompanied by proton efflux. Choline hydroxide titrant is added by the pH stat to maintain pH 7.6, and the rate of this titration reflects the rate of inwardly-directed cation transport. This method can also be used to study anion transporters, either by reversing the pH gradient (acidic outside) or entrapping the salt within the liposomes.
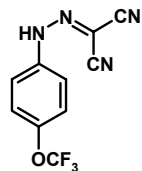
FCCP

1.5.7 NMR Techniques

In the base pulse and pH stat assays, ion transport is measured indirectly by monitoring proton transport (measuring pH). Monitoring the transport of ions directly is possible through the application of NMR spectroscopy. By introducing an NMR shift reagent on one side of the membrane (either inside or outside the liposomes), the ion of interest will have a different NMR resonance inside and outside the liposome. This technique gives the advantage of detecting ion movement by following the ion itself, rather than making assumptions based on pH changes.

NMR methods have been used mainly to follow cation transport, with ^{23}Na$^+$ being the most common. For ^{23}Na, the shift reagent typically used is Dy^{3+} (purchased as DyCl$_3$), although Gd^{3+} is sometimes used.[83-85] The ^{23}Na resonance is shifted upfield by Dy^{3+} (10-20 ppm depending on concentration) and broadened. Thus, taking ^{23}Na NMR spectra at time intervals after addition of a transporter allows Na$^+$ transport to be observed.[86-89] The amount of Na$^+$ transported can be quantified and transport rates can be determined by

30

integration of the ^{23}Na signals at time intervals. Also, the exchange rate of ^{23}Na$^+$ ions across a membrane can be determined from 2D ^{23}Na NMR spectroscopy.[90] Similarly, transport of ^{7}Li$^+$ can be monitored by NMR.[87,88] For ^{7}Li$^+$, Dy^{3+} also causes an upfield shift of the ^{7}Li signal.

NMR has also been applied to monitor Cl$^-$ transport across membranes. A useful shift reagent for ^{35}Cl$^-$ is Co^{2+}, which causes a downfield shift and broadening of the ^{35}Cl$^-$ signal.[91] Phosphatidylcholine vesicles are stable in the presence of Co^{2+} and the shift reagent is impermeable to PC over the course of hours. This system has been applied by Smith *et al.* to monitor the mediated cotransport of NaCl across membranes and in the study of trimer **3.5** described in **Chapter 3** of this thesis.[92,93] The ^{35}Cl$^-$ relaxation agent Mn^{2+} provides an alternative for monitoring Cl$^-$ transport.[94] The ^{35}Cl$^-$ resonance is broadened to *ca.* 1000 Hz in the presence of Mn^{2+}. However, Mn^{2+} can promote fusion or bursting of phospholipid vesicles, and requires specific conditions to prevent such occurrences. With PO$_4$$^{3-}$ as a Mn^{2+} ligand, vesicles are stable for longer periods of time. At an 8:1 PO$_4$$^{3-}$:Mn^{2+} ratio, EYPC vesicles have a half life of several hours, allowing for Cl$^-$ transport to be measured.[94]

1.5.8 Ion-Sensitive Dyes

Like with NMR techniques, ion transport across membranes can be monitored directly using ion-sensitive dyes. Halide-sensitive dyes, such as lucigenin (N,N-dimethyl-9,9-bisacridinium nitrate, shown below) and SPQ (6-methoxy-N-(3-sulfopropyl)quinolinium) are collisionally quenched by halide ions. These membrane-impermeable dyes can be entrapped in liposomes to serve as internal sensors, showing a fluorescence decrease upon halide influx.[95] Similarly, dyes that are sensitive to cations are useful for monitoring Na$^+$ or K$^+$ influx. The Na$^+$-sensitive SBFI (sodium-binding benzofuran isophthalate) and K$^+$-sensitive KBFI (potassium-binding benzofuran isophthalate) both show a fluorescence increase with increasing cation concentration.[96]

λ_{ex} **368 nm**

λ_{em} **506 nm**

Lucigenin
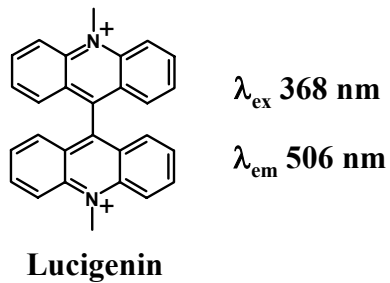
1.5.9 Chloride Selective Electrode

The efflux of Cl⁻ from liposomes has been measured using a chloride-selective electrode.[92,97,98] In a typical experiment, the transporter to be tested is added to Cl⁻-containing liposomes suspended in a non-Cl⁻-containing buffer (e.g. HCO_3^-, NO_3^-). Release of Cl-, mediated by the transporter, is then registered by a response from the electrode. This method provides a relatively inexpensive option for monitoring anion transport.

1.5.10 Membrane Potential

Since all cells maintain transmembrane potentials, the ability to generate and measure membrane potentials in liposomal systems is important to ensure that these cell models more closely resemble the true cellular environment. One such assay involves the highly K⁺-selective ion carrier valinomycin.[99,100] Addition of valinomycin to KCl-containing liposomes suspended in a NaCl buffer results in valinomycin-mediated K⁺ transport out of the liposomes (down the K⁺ gradient).[101] This is accompanied by the generation of a negative transmembrane potential, i.e. negative inside the liposomes, since the efflux of cations is not compensated (valinomycin transports K⁺ and nothing else).[99] Potentials as high as 200 mV can be generated in this system, depending on the magnitude of the K⁺ gradient.

The negative membrane potential can be monitored using the fluorescent dye safranin O.[99,100] The fluorescence of safranin O is higher in a hydrophobic environment (e.g. inside a liposomal membrane) than in a polar environment (e.g. in the extravesicular buffer). Upon generation of a negative membrane potential, the positively charged safranin O moves from the buffer into the membrane, resulting in an increase in fluorescence.[99]

λ_{ex} **522 nm**

λ_{em} **581 nm**

Safranin O
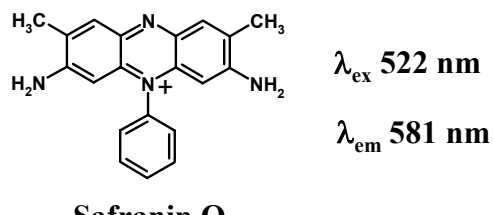
The concentration of valinomycin added is critical in this experiment. Addition of low concentrations (10 µM) results in a potential that is stable for many minutes, where increased concentrations cause a rapid collapse after the initial potential is reached.[99] Secondly, since the dye only accumulates in the membrane in response to negative potentials, positive transmembrane potentials cannot be measured using safranin O.[99]

The valinomycin/safranin O liposome system has been applied to measure the voltage-dependent ion channel formation of alamethicin (see **Section 1.3**).[100] Use of safranin O to monitor the generation of a negative potential by trimer **3.5** in liposomes experiencing a Cl⁻/SO₄²⁻ gradient will be described in **Chapter 3**.

1.5.11 Calcein Release Assay for Detecting Membrane Defects

In deciphering the transport mechanisms of novel ion transporters, it is important to address the possibility that the compound(s) being tested induce large defects in the membrane, through which ions simply spill in or out.[102] A useful liposome assay to test for defect induction involves the dye calcein (a fluorescein derivative).[103]

λ_{ex} **494 nm**

λ_{em} **517 nm**
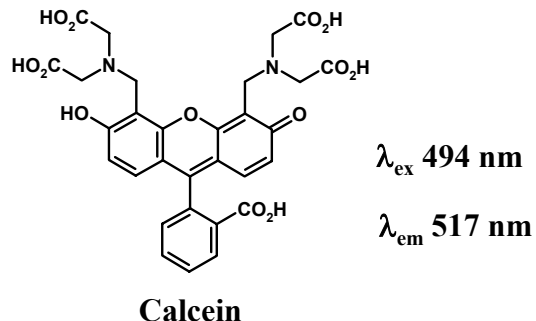
Calcein

At concentrations greater than 100 mM, calcein loses 95% of its fluorescence due to self-quenching.[104] In a typical assay, liposomes containing calcein at >100 mM are suspended in an isoosmotic calcein-free buffer. If the test compound induces large defects, calcein will leak through the pores into the extravesicular buffer. This results in dilution of the dye (to << 100 mM) and thus return of its fluorescence.[103] Conversely, if the compound functions as an ion channel, the pores formed will not be large enough to accommodate molecules of calcein, the dye will remain at high concentration inside the liposomes, and no dequenching will be observed. The same is true for compounds that function as ion carriers. In **Chapters 2** and **3**, the calcein release assay was used to prove that neither cG **2.34** nor calix[4]arene tetrabutylamide **3.1** induce membrane defects.

Carboxyfluorescein, also a fluorescein derivative, displays properties similar to calcein and is sometimes used to identify defect induction.[105] However, the results of carboxyfluorescein assays must be evaluated carefully. In some cases, compounds that mediated carboxyfluorescein release from vesicles also gave single current bursts in planar bilayer measurements.[106,107] Large pores can also be ion channels that show discrete openings and closings.

1.6 Synthetic Cation Channels

1.6.1 Introduction

In 1988, Lear and DeGrado reported the first synthetic peptides to give single-channel currents.[108] One peptide channel studied was H_2N-(Leu-Ser-Ser-Leu-Leu-Ser-Leu)$_3$-$CONH_2$. This peptide forms α-helical structures, four of which come together to form the channel. The single-channel current trace indicated a current of 10 pA and an open state lifetime of 3-8 ms. The lifetime was invariable over transmembrane voltages of 25-175 mV. This was the first report of an undisputable synthetic ion channel.

The preparation of a non-peptide "ion channel" was first reported by Tabushi *et al.* in 1982.[109] This, along with subsequent reports, however, lacked the critical proof of channel formation. In 1992, Kobuke reported the first non-peptide ion channel, as supported by single-channel current measurements (planar bilayer voltage clamp technique).[110] Using a simple design, Kobuke synthesized the amphiphilic ion pairs **1.1** and **1.2**. In this design, the carboxylates bearing a polyether chain were intended to form the ionophoric core of the channel and the ammonium cations would surround the core, due to ion-pairing interactions, to form a hydrophobic outer wall embedded in the membrane. The molecular length estimated from CPK models of the ion pairs as they would exist when anchored in a membrane were 24 and 30 Å for **1.1** and **1.2**, respectively. These lengths were adjusted to fit the lipid monolayer, i.e. one half of the distance through the membrane.

1.1 : n = 2   **1.2** : n = 3
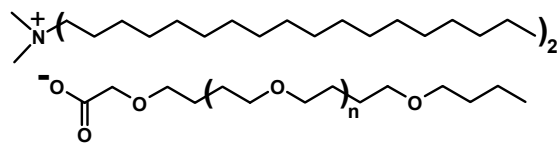
Not only did ion pairs **1.1** and **1.2** form ion channels as confirmed by single-channel current measurements, but the channel structures seemed to be voltage dependent. Channels formed from **1.1** and **1.2** had almost the same channel properties. In the planar bilayer system used, the observation of three different currents at transmembrane

potentials of -80 mV, +47 mV, and +60 mV led to three different conductances of 700 pS, 97 pS, and 13.5 pS, respectively. As described in **Section 1.5.3**, multiple conductances suggest multiple active structures. Lastly, the channel was shown to be cation-selective.

This work by Kobuke demonstrated that the ability to form transmembrane ion channels was not exclusive to proteins and peptides. Here began a slow but sure appearance of publications reporting other artificial ion channels using various structural designs.

The review of synthetic cation channels in **Section 1.6.2** will be organized by author (corresponding author of the research laboratory in which the work was completed). This organization is advantageous since many authors utilize one basic structure for all channels developed in their laboratory (although this not the case with all laboratories discussed). Synthetic cation channels have also been the subject of several reviews.[63,64,102,111-113]

1.6.2 Synthetic Cation Channels

Kobuke. By replacing the carboxylate group in ion pair **1.2** with a dianionic phosphate group to give ion pair **1.3** (**Chart 1.4**), Kobuke *et al.* reported that ion channel activity was maintained.[114] The channel formed was nearly identical to that formed from ion pair **1.2**, except that the phosphate-derived channel had a stronger transmembrane voltage dependence. At +50 mV, the channel was essentially closed, while at +100 mV, the channel remained open.

The reverse case was also investigated. The ammonium species, now bearing the polyether chain, was countered by anions (carboxylate and phosphate-containing species) bearing hydrophobic chains.[115] The "reversed-role" ion pairs proved to form cation-selective ion channels. Despite the positively charged ammonium groups at the opening to the channel, cations were still selectively transported, indicating that the functionality lining the interior of the pore is the deciding feature for transport selectivity.

Chart 1.4

1.3

1.4
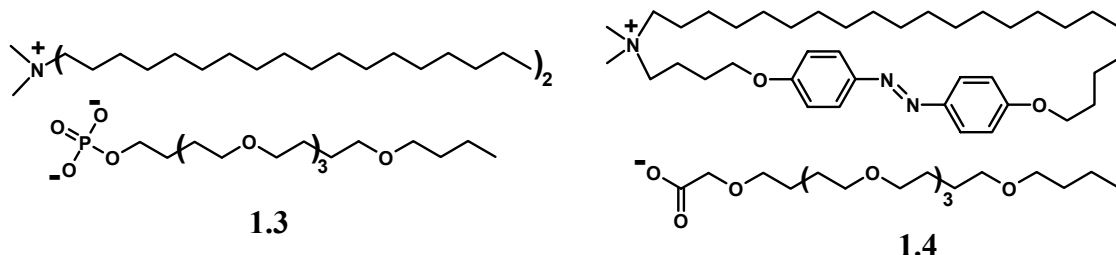
Applying a design similar to ion pair **1.2**, ion pair **1.4** (**Chart 1.4**) was prepared

containing an azobenzene group in one of the ammonium hydrophobic chains.[116] The

azobenzene is photo-isomerizable allowing for photocontrol of ion fluxes. Incorporation

of *trans*-**1.4** (as shown in **Chart 1.4**) resulted in stable ion channels with various

conducting states. These channels were not only cation selective ($P_K/P_{Cl} = 6.1$), but

showed selectivity among the alkali metal cations of $Cs^+ > K^+ > Na^+$ ($P_K/P_{Na} = 6.1$, $P_K/P_{Cs} =$

0.7). When the trans-azobenene bond was isomerized to cis by irradiating the channel at

367 nm, loss of channel activity was observed. Subsequent irradiation at 450 nm to

isomerize back to the trans-azobenzene restored channel activity, demonstrating

photocontrol over ion flow through the channel.[116]

Using a resorcinarene as a scaffold, a second ion channel design was developed.

Resorcinarene **1.5** forms a dimeric assembly in membranes to yield a K^+-selective ion

channel with a single conductance level (**Figure 1.13**).[117] The long alkyl chains reside in

the membrane's interior while the hydrophilic resorcinarene head groups remain at the

membrane surface. The resorcinarene bowl of **1.5** was hypothesized to function as the

channel's selectivity filter. This report in 1995 represented the first example of a K^+-

selective synthetic ion channel.[117]
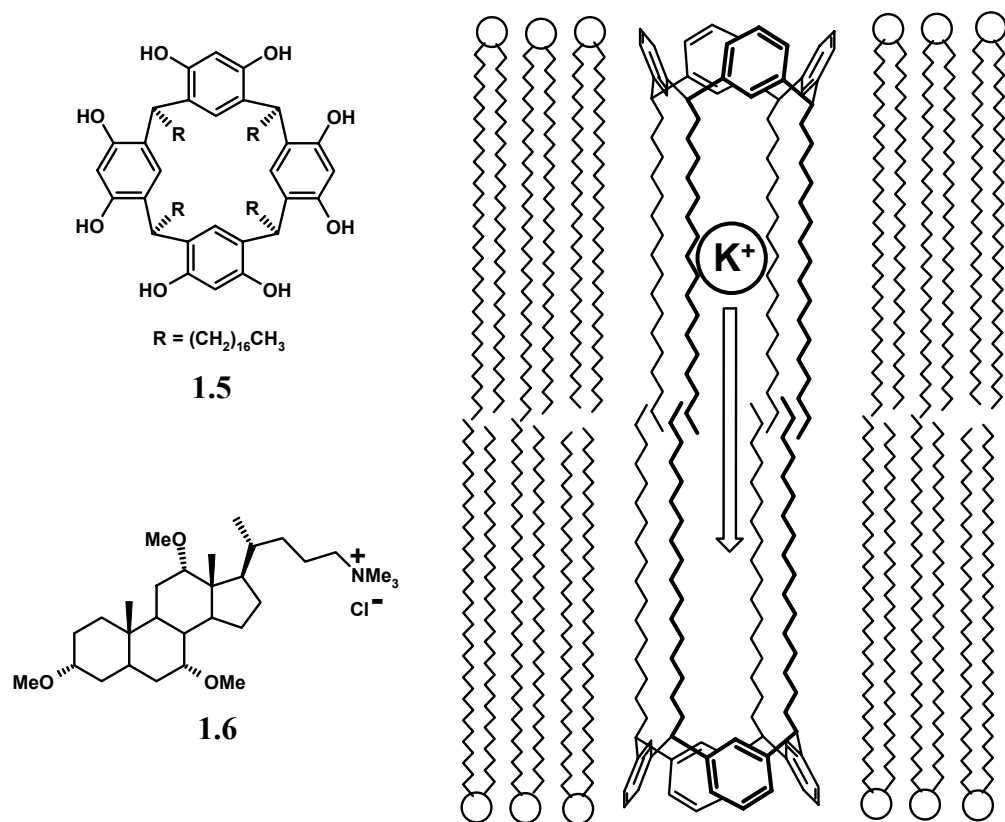
Figure 1.13. Resorcinarene half-channel **1.5** and modified cholic acid derivative **1.6** (left) and the channel structure of (**1.5**)$_2$ in the membrane (right). The resorcinarene OH groups are removed in the (**1.5**)$_2$ channel structure for clarity.[117,118]

Kobuke put forth yet a third ion channel design. Modified cholic acid derivative **1.6** (**Figure 1.13**) formed ion channels with long-lasting open states (~1 s) and various conductance levels.[118] The amphiphilic **1.6** was expected to fit a lipid monolayer, suggesting the channel structure must comprise two of more **1.6** monomers. The pore of the channels is most likely lined with the ether oxygens to provide ion stabilization through the membrane.

This work was extended by covalently linking two cholic acid monomer units. The first cholic acid dimers **1.7** and **1.8** (**Chart 1.5**), linked through a *m*-xylylene dicarbamate unit, were symmetrical, bearing either carboxylate or ammonium moieties as head groups.[119] The dimers formed ion channels, with the active structure comprising dimer

aggregates. Each dimer **1.7** or **1.8** was believed to span the lipid bilayer. The channels were cation-selective, and both discriminated K^+ over Na^+ by approximately 3:1, with no Li^+ current being observed.[119]

Chart 1.5

1.7: $R_1=R_2= CO_2^-$ **1.9**: $R_1= CH_2PO_4^{2-}$, $R_2= CO_2^-$

1.8: $R_1=R_2= CO_2CH_2\overset{+}{N}((CH_3)_3\ Cl^-$ **1.10**: $R_1= CO_2^-$, $R_2= CH_2OH$
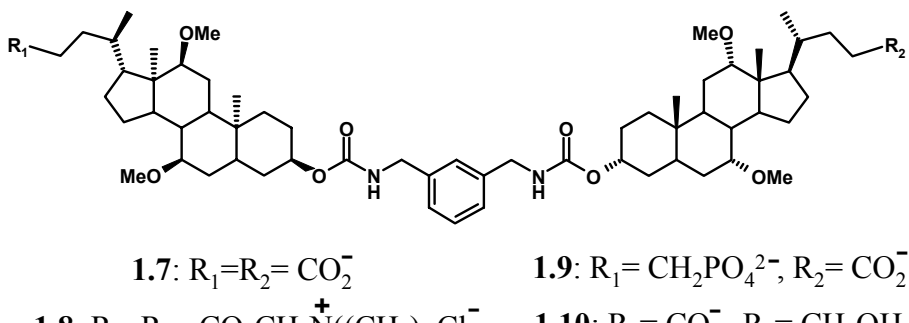
Channel rectification, i.e. favored transport in one direction over the opposite direction, was demonstrated by cholic acid dimers with unequally-charged head groups. By applying a positive membrane potential prior to introducing the compounds, dimers **1.9** (-2/-1) and **1.10** (-1/0) (**Chart 1.5**) inserted into the membrane with the more negative head groups aligned to the positive side.[120] Once the channels were inserted, current values were larger at positive applied voltages than at negative voltages, indicating channel rectification. This was also true for the opposite case, where channels were added at a negative potential and displayed higher current values at negative voltages. After channel formation, the orientation of the channels in the membrane was not reversed, regardless of the potential applied.[120]

With the knowledge that resorcinarene **1.5** (**Figure 1.13**) formed ion channels with a single conductance level (indicating a single active structure) and cholic acid **1.6** (**Figure 1.13**) formed supramolecular channels with long open state lifetimes, but multiple conductance levels, Kobuke combined the two substructures. A resorcinarene derivative bearing four cholic acid moieties (in place of the alkyl chains in **1.5**) was synthesized and investigated. Indeed, the resorcinarene-cholic acid conjugate provided the combined

properties of **1.5** and **1.6**, demonstrating a single conductance level with long-lasting open states.[121] The resulting channel was also selective for K^+ over Na^+ (3:1).

Ghadiri. It was postulated by Ghadiri *et al.* that an even number of alternating D and L amino acids in a cyclic peptide structure would allow the ring to exist in a low-energy flat conformation. In this conformation, all amide functionalities lie perpendicular to the plane of the ring. After synthesizing an alternating D/L peptide ring, it was found that their postulate held true. The peptide rings stacked forming a β-sheet structure.[122]

For the purpose of creating self-assembling ion channels, Ghadiri synthesized cyclic peptide **1.11** (**Figure 1.14**).[123] Leucine was selected to provide a hydrophobic surface to anchor the channel in the membrane and the indole ring of Trp was intended to make up the polar core. The Gln was added only to simplify the peptide synthesis. In an aqueous liposomal suspension, the peptide inserted into the membrane and self-assembled to form ion channels, as demonstrated by pH stat assays, planar bilayer voltage clamp experiments and patch clamp recordings.[123] The channels had a single conductance level (all channels comprised the same number of cyclic peptides) and were weakly K^+-selective. The K^+ throughput rate for channels comprising **1.7** was an impressive $2.2 \times 10^7 \ s^{-1}$, a transport rate greater than that achieved by gramicidin A. The self-assembled nanotube formed from **1.11** is shown in **Figure 1.14** (right). Through polarized attenuated total reflectance spectroscopy measurements, the cyclic peptide assembly was confirmed to align parallel to the lipid hydrocarbon chains when inserted in the membrane.[124]
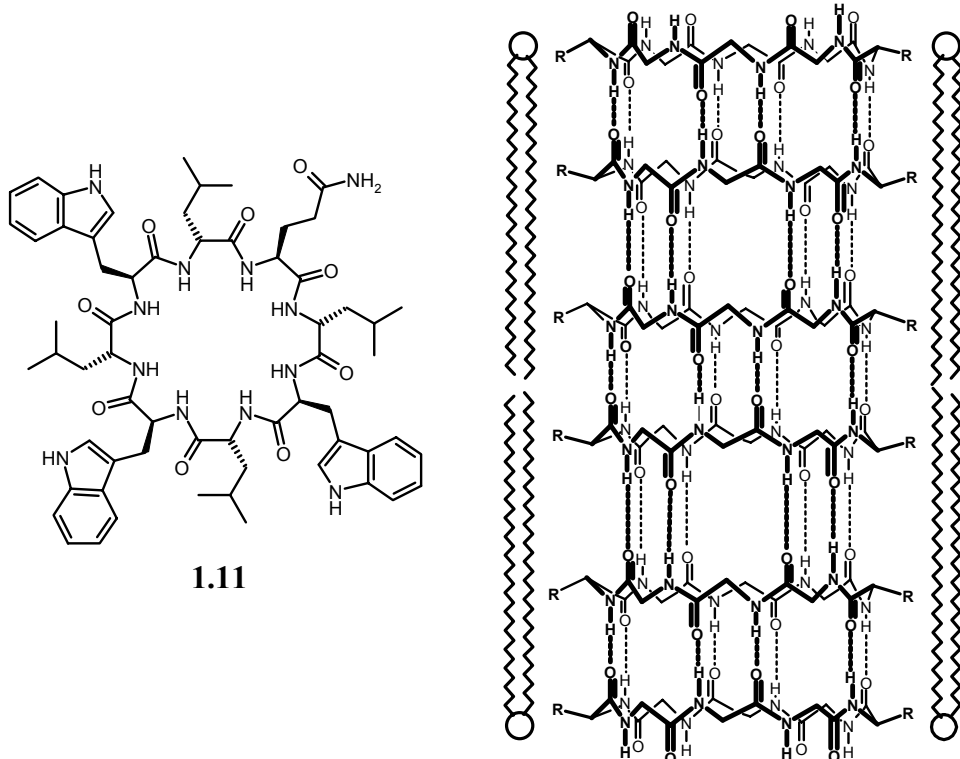
Figure 1.14. Cyclic peptide **1.11** (left) and the membrane spanning self-assembled ion channel formed from **1.11** (right, R = CH(CH$_3$)$_2$, other side chains omitted for clarity).[123]

It was later shown by Ghadiri that cyclic β^3-peptides also allowed for a flat cyclic structure which assembled in the same way as the alternating D/L cyclic peptides. Two such structures investigated by the Ghadiri group were *cyclo*[(-β^3-HTrp)$_4$-] and *cyclo*[(-β^3-HTrp-β^3-HLeu)$_2$-].[125] These compounds formed channels that, like the D/L cyclic peptides, transported K$^+$ ions at a high rate (1.9 x 10^7 ions s^{-1}).

The nanotube structure has awesome potential. Since the channel is formed by self-assembly of identical molecules, the structure will automatically adapt to any membrane thickness. Also, the diameter of the pore can be adjusted by increasing or decreasing the number of peptides in the ring, thus allowing for tuning of the channel selectivity. This was demonstrated by the synthesis of a cyclic decapeptide. The channel formed had an

internal diameter of 10 Å and transported glucose across a lipid bilayer.[126] Nanotubes formed from cyclic peptides have been highlighted in a recent review.[127]

A number of compounds from a series of D,L-α-cyclic peptides was recently shown to act on Gram-positive and Gram-negative bacterial membranes preferentially over mammalian cell membranes.[15] This finding has profound implications for combatting drug-resistant bacteria strains. The cyclic peptides can be readily synthesized in libraries, have a low molecular weight and are stable to enzymatic degradation (due to the D-amino acids), making them optimum drug targets.[15] As was mentioned in **Section 1.4**, the development of novel antimicrobial agents is a goal in the study of artificial ion channels. This goal and has been achieved with D,L-α-cyclic peptides.

Regen. The ion channel designs of Regen *et al.* are based on the polyene macrolide antibiotic Amphotericin B (AmB, **Chart 1.6**) that functions by forming ion channels in fungal membranes.[128] AmB is believed to form a "barrel-stave" structure in the membrane, similar to that described for alamethicin channels (**Section 1.3**).[129] The structure comprises multiple AmB monomers forming a cylindrical tube. In this tube: (1) the hydrophobic polyene segments point out toward the hydrocarbon lipid chains of the bilayer, (2) the hydroxylated faces point inward toward a water-filled pore (the channel), and (3) the sugar groups serve as a polar head group and remain at the membrane surface. Also, cholesterol in the membrane is thought to be intimately involved in stabilization of the AmB channel structure.[130]

In Regen's seminal AmB mimic **1.12** (**Chart 1.6**), a sterol was used as the rigid hydrophobic backbone (in place of the polyene chain of AmB) and polyethyleneoxide chains served as both the hydrophilic face and polar head group (one serving each role replacing the hydroxylated chain and sugar group of AmB, respectively).[86] By adopting a "folded" conformation (shown in **Chart 1.6**), **1.12** displays all three of the AmB regions. Sterol **1.12** demonstrated the ability to transport Na$^+$ across EYPC vesicular membranes as determined by ^{23}Na NMR. The active transport structure was hypothesized to consist of an aggregate (or aggregates) of monomeric **1.12**, since the ion transport activity was

strongly concentration dependent. A barrel-stave-type structure, similar to that formed by AmB, may also be formed by **1.12**.

Chart 1.6

Amphotericin B (AmB)
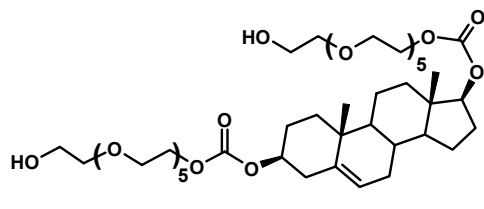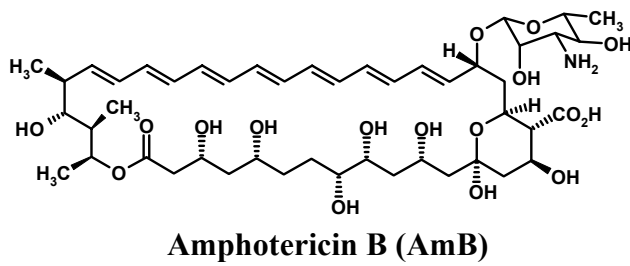
1.12
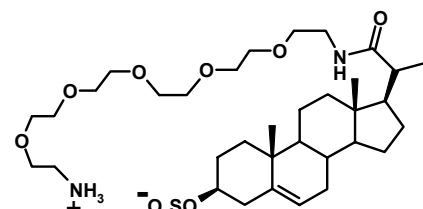
1.13

Although no single-channel current experiments were conducted with **1.12**, comparing the ion transport rates in EYPC and DPPC liposomes at 25 °C provided support for an ion channel mechanism of transport. One property that distinguishes lipid membranes is the gel-to-fluid transition temperature (T_c). Above the T_c, the membrane is in the fluid state, e.g. cell membranes in the body. Below the T_c, however, the membrane exists in the gel or "glass" state, which is much more rigid than the fluid state. At 25 °C, EYPC is in the fluid state. In contrast, DPPC (**Chart 1.3**) exists in the gel state at 25 °C ($T_c = 42$ °C).[70] It is known that transport by an ion carrier shows a reduced rate in the gel state as compared to the fluid state.[131] This is due to slower diffusion through the more rigid membrane. An ion channel, on the other hand, is relatively unaffected by the membrane rigidity, since the channel does not need to diffuse through the membrane in order to transport ions.[131] Therefore, comparing the transport rates at 25 °C in EYPC (fluid state) and DPPC (gel state) can provide insight into the mechanism of transport.

Indeed, **1.12** demonstrated a similar transport rate in EYPC and DPPC liposomes, thus lending support to the ion channel mechanism.[86]

Further investigation into ion conductors based on AmB lead to the construction of a squalamine mimic. Sterol **1.13** (**Chart 1.6**), bearing a polyoxide chain linked through an amide bond to the A ring and a sulfate on the D ring hydroxyl group, was prepared and tested for ion transport and antimicrobial activity.[132] The polyoxide chain is held across the sterol backbone due to electrostatic interactions between the sulfate and the ammonium of the zwitterionic compound. Like sterol **1.12**, the structure of **1.13** resembles that of AmB, with a hydrophobic sterol backbone, a hydrophilic oxygen-containing chain, and a polar (zwitterionic) head group. Transport of Na^+ across an EYPC membrane was shown by ^{23}Na NMR. Since squalamine is itself a strong antimicrobial agent, squalamine mimic **1.13** thus held the potential to demonstrate this property.[133] However, **1.13** showed no antimicrobial activity in bacterial growth inhibition assays.

The active ion-transporting structure formed by **1.13** in membranes was later shown by kinetics experiments to be a membrane-spanning dimer.[134] This is in agreement with the membrane-spanning covalently-linked cholic acid dimers reported by Kobuke (**Chart 1.5**). Ion transport rates in EYPC and DPPC vesicles were similar, supporting transport by an ion channel.[131] An elegant experiment by Otto, Osifchin and Regen, demonstrating that "flip-flop" of **1.13** between the inner and outer leaflets of the membrane was slow, provided further evidence that the active species was an ion channel, and not a carrier.[135] Lastly, **1.13** was shown to favor transport in ergesterol-rich over cholesterol-rich membranes.[136] Such membrane selectivity is promising in the search for novel antimicrobial agents.

A second generation of ion conductors developed by Regen was based on spermine-cholic acid conjugates (four cholic acids linked to one spermine). Like **1.12** and **1.13**, the spermine-cholic acid compounds transported Na^+ across the membrane.[137,138] The active structure was determined to span the membrane, and function as a cation antiport based on Na^+/Li^+ exchange experiments monitored by ^{23}Na and ^7Li NMR. Also, one of these conjugates demonstrated an ability to recognize osmotically-stressed membranes.[139]

Matile. Matile's design, like that of Regen *et al.*, is based on the structure of AmB. In **1.14**, a rigid backbone comprising an oligo(*p*-phenylene) acts as the hydrophobic portion of the channel. The substituents contain polar hydroxyl groups that serve as ion relays. The length of the channel can be varied by changing the number of phenylenes in the backbone. An "octamer" chain was long enough to span the bilayer membrane and provided the backbone for channel-forming structures.[78]

Rigid rod **1.14** functioned via a H^+/K^+ antiport mechanism with a significant H^+ over K^+ selectivity, as determined from base pulse assays.[79] Since the per mole activity of **1.14** was higher at lower concentration (1 µM), i.e. a 20-fold concentration increase led to only a 3.2-fold increase in transport rate, it was suggested that the active structure is monomeric, with a large majority of **1.14** assembled into inactive aggregates at higher concentration. Fluorescence-depth quenching experiments with spin-labeled lipids verified that **1.14** spans the vesicular membrane.[79] Rigid rod **1.14** also accelerated OH^- and/or Cl^- transport across the membrane, as will be discussed in **Section 1.7**.

1.14
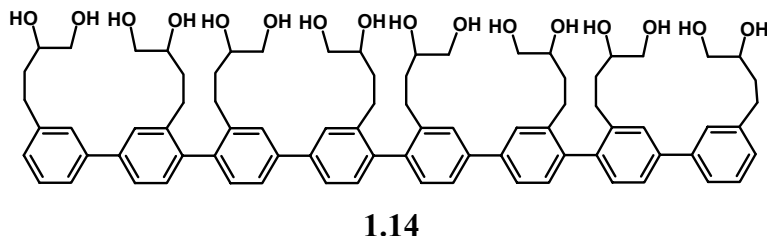
Single channel experiments later showed that **1.14** gave large currents (100-300 pA), but with an extremely short open state lifetime estimated at less than 0.1 ms.[140] Also, the channel activity of **1.14** was voltage-dependent. Since the molecule has no dipole (see push-pull rods described below), this was a surprising observation. At 50 mV, no current was observed, but at 100 mV, large current spikes were apparent. (Voltage dependence in the absence of a molecular dipole was also observed for channels formed from calix[4]arene tetrabutylamide **3.1** described in **Chapter 3** of this thesis.[141]) Based on this finding, the active structure formed by **1.14** was reevaluated to be tetrameric, since large currents most likely result from a large channel pore. A pore diameter of 11 Å was

predicted based on molecular modeling.[140] Smaller currents (2-5 pA) with longer open state lifetimes were observed for derivatives similar to **1.14**.[140] The cation selectivity confirmed via single channel recordings was consistent with H$^+$-selective transport by these derivatives as proposed previously for **1.14**.[79]

The first synthetic ligand-gated channel to be reported was formed from phenylene heptamer **1.15**. The complete channel structure required three elements: n molecules of **1.15**, n Cu^{2+} cations, and one molecule of polyhistidine (pHis).[80] The iminodiacetate head group of **1.15** chelates Cu^{2+}. Subsequent interaction of pHis with the bound Cu^{2+} brings molecules of **1.15** into close proximity, forming a "π -slide" for cations to flow across the membrane via cation-π interactions.[80] The channel spanned the membrane, as shown by fluorescence depth quenching experiments with spin-labeled lipids, and discriminated K$^+$ over Li$^+$, Na$^+$, Rb$^+$ and Cs$^+$ as determined by base pulse assays.

1.15
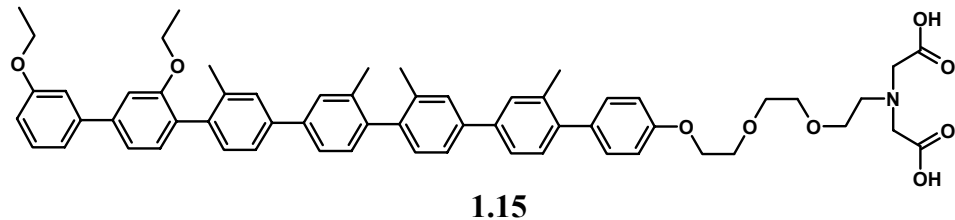
A second approach to assembling rigid rod channels was through the formation of hydrogen bonds between sidechains appended to the oligophenylene backbone. By introducing peptidic sidechains (Leu in **1.16**, **Figure 1.15**), antiparallel β-sheets form between sidechains of neighboring monomers, resulting in the "β-barrel" structure represented in the right panel in **Figure 1.15**.[142] The β-barrel formed from phenylene **1.16** was estimated to be dimeric from ESI-MS data and was held together by β-sheet formation, as suggested by 2D ^{1}H NMR and CD experiments. The (**1.16**)$_2$ β-barrel transported Na$^+$ across EYPC vesicles as measured by base pulse assays.[142]

The β-barrel structure has awesome potential since the diameter and length of the pore can be tuned by varying the peptide sidechain and number of phenylenes in the monomer unit, as will be demonstrated in later examples (**Section 1.7**). This barrel structure is analogous to Ghadiri's peptide stacks discussed previously.[123] The difference

is that β-barrels assemble around the axis parallel to the membrane lipids, where the cyclic peptides stack along that same axis. The two can be deemed orthogonal. That is, the length of peptide stacks is determined by self-assembly and the cavity size can be modified only by synthesis. For β-barrels, the opposite is true. The cavity size is a product of self-assembly, and the length is determined by covalent synthesis.
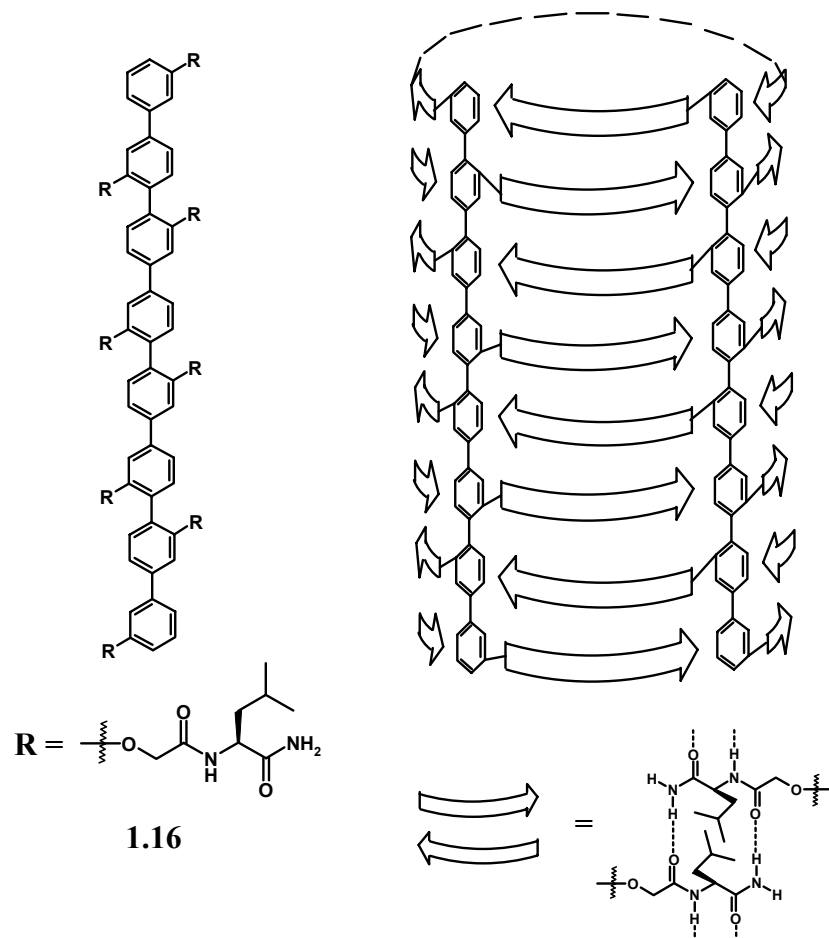
Figure 1.15. The structure of the self-assembling monomer **1.16** (left) and a representation of a β-barrel formed via β-sheet formation between peptide sidechains (right).[142]

In an effort to develop ion channels capable of recognizing polarized bilayers, Matile *et al*. synthesized rigid rod **1.17** (**Figure 1.16**).[14] With an electron-donating group (OMe) on one end of a rigid rod octamer and an electron-withdrawing group (CN) on the

opposite end, phenylene **1.17** has an axial dipole, as shown in **Figure 1.16**. Four aza-18-crown-6 units were appended to the scaffold to function as ion "relays" in the channel. The term given to **1.17**-type molecules, bearing an axial dipole and capable of facilitating ion transport, was "push-pull rods".[14] A negative potential was generated across EYPC-SUVs, as described in **Section 1.5.10**. Base pulse assays showed that **1.17** indeed recognized liposomes with a negative potential, depolarized the vesicles, and subsequently collapsed the pH gradient via ion transport.[14] Simultaneous K^+/Na^+ and H^+/Na^+ antiport mechanisms were proposed. Addition of a symmetric phenylene to polarized vesicles caused no change, showing that the dipole is necessary for recognition of membrane potential.
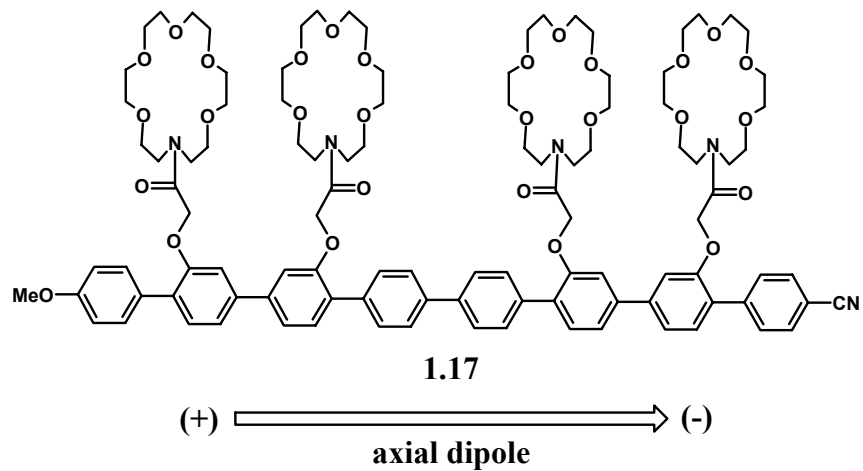
Figure 1.16. Rigid push-pull rod **1.17** indicating the axial dipole.[14]

To ensure an unimolecular ion conducting pathway, push-pull rods bearing six crown units were synthesized.[143] In these rods, $-SCH_3$ and $-SO_2CH_3$ groups served as the electron-donating and electron-withdrawing substituents, respectively. Like **1.17**, Matile's unimolecular push-pull rods demonstrated increased activity over rods lacking an axial dipole in polarized vesicles.[143] The push-pull rods were shown to span the membrane by fluorescence depth quenching experiments.

Lehn. The "bouquet molecules" of Lehn *et al.* are excellent examples of the unimolecular approach to artificial channels. Bouquet molecules consist of a central macrocycle, either 18-crown-6 or a β-cyclodextrin derivative, linked to multiple poly(ethylene oxide) or polymethylene chains.[87,88] One such compound (**1.18**) is shown below. The bouquet molecules were designed to span a lipid membrane forming an unimolecular channel, with the hydrophilic carboxylates remaining at the membrane surface and the crown (or β-cyclodextrin) at the center of the membrane to function as an ion relay. Lehn's report on bouquet molecules was published very near the same time as Kobuke's report on assembled channels supported by single channel current measurements.[110] Although Lehn did not conduct single channel measurements, other support for a channel mechanism was reported, as will be described.

1.18
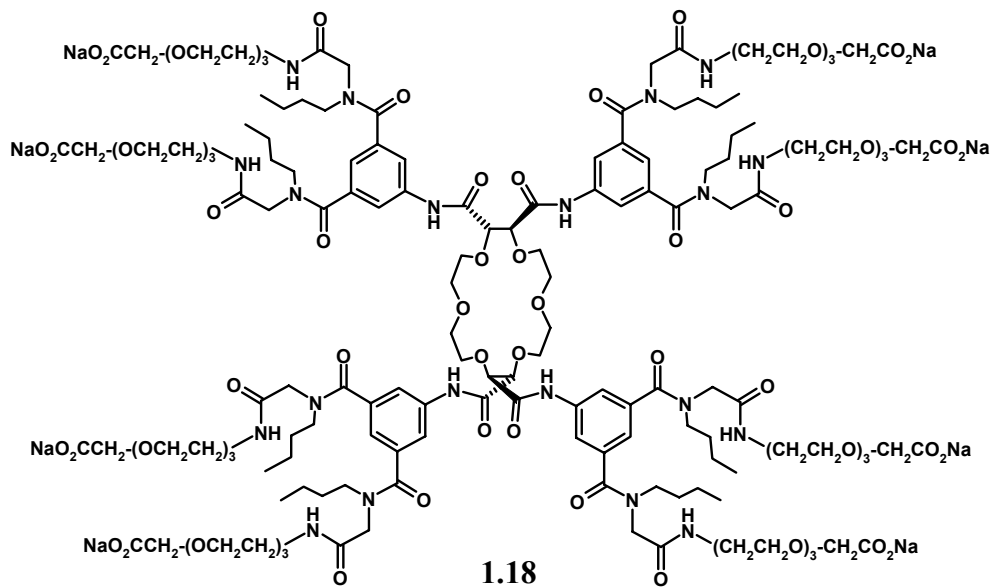
Through the study of ion transport by NMR techniques, both bouquet **1.18** and the β-cyclodextrin derivative were shown to function via a cation antiport. By suspending LiCl-containing liposomes in a NaCl-containing buffer, the rate of Na^+ influx measured by ^{23}Na NMR proved to be equal to Li^+ efflux, as measure by ^{7}Li NMR.[87] That is, the bouquet molecules exchange the cations in a one-for-one manner. Lehn used a comparison of ion transport rates in EYPC and DPPC liposomes to elucidate the transport

mechanism.[131] The bouquet molecules demonstrated a similar transport rate in EYPC and DPPC liposomes, thus lending support to the ion channel mechanism.[87,88]

Importantly, the bouquet compounds bearing polymethylene chains transported ions at very near the same rate as the bouquets bearing poly(ethylene oxide) chains.[87] Lehn commented that this result was interesting and unexpected. The oxygens in the chains were intended to coordinate cations in the channel thus facilitating transport, while the polymethylene chains, lacking the ion-coordinating oxygens, should not facilitate transport.[87] As demonstrated in this case and with other synthetic ion channels, a large number of coordinating groups is not necessarily desirable, since strong ion coordination hinders the transport rate.

Fyles. Much like the approach of Lehn, the initial channel design of Fyles *et al.* was based on an unimolecular channel with an 18-crown-6 core. Fyles constructed a series of two-headed amphiphiles ("bolaamphiphiles") capable of spanning a lipid bilayer.[81,144,145] The basic structure contained a central connector unit (18-crown-6) covalently linked to radiating wall units. Each wall unit bore a polar head group (glucose). The crown ether-wall unit bonds at neighboring methylenes were trans to one another with respect to the crown, so as to orient three wall units in one direction and three wall units in the other. The most effective wall structures had both a hydrophilic and hydrophobic side, the former for ion transport and the latter to face the lipid hydrocarbon tails. Compound **1.19**, shown in **Figure 1.17**, is an example of a bolaamphiphile channel. The predicted membrane structure is represented in the right panel in **Figure 1.17**.

Hexa-substituted **1.19** in addition to a number of tetra-substituted derivatives transported Na^+, K^+, Rb^+ and Cs^+ across vesicular membranes as shown by pH stat experiments.[81] A number of the compounds reported were postulated to function via an ion channel mechanism. The support came from pH stat experiments where a competing cation was added in approximately 20%, e.g. 80% K^+/20% Li^+ to monitor inhibition of K^+ transport by Li^+. Discussing this inhibition assay, Fyles states: "A carrier mechanism could result in rate enhancement but could not give rise to inhibition.[146] The observation of significant inhibition is therefore a strong indication of channel formation."[81]

Compounds (including **1.15**) that showed inhibition by competing cations were therefore hypothesized to form channels.[81] Lastly, the head group has an impact on ion transport rate, as changing the head group from glucosyl to the less polar 3-hydroxypropyl group resulted in a decrease of cation flux.
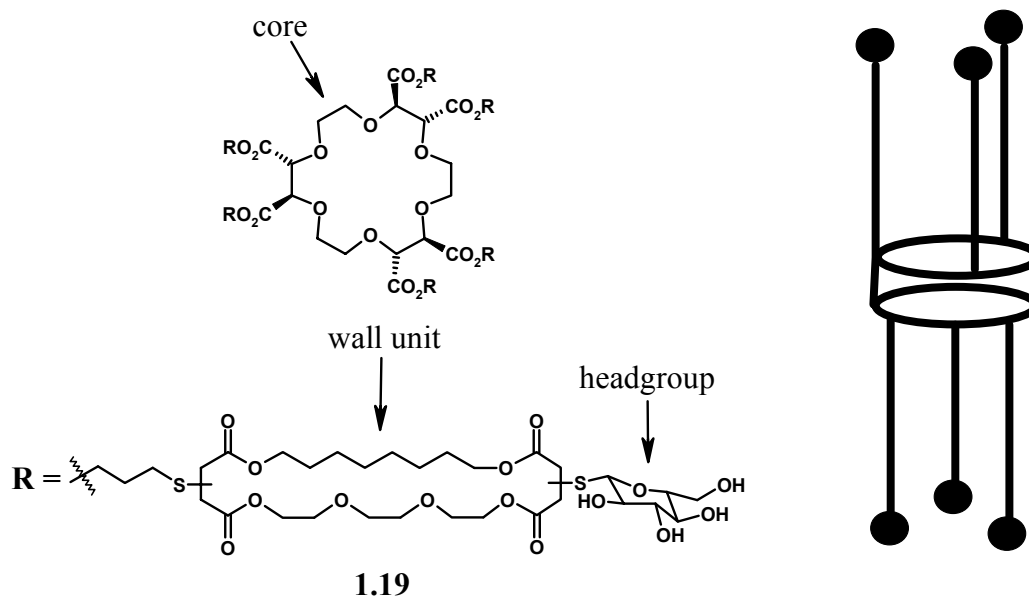
Figure 1.17. Fyles' bolaamphiphile **1.19** with the core, wall unit and head group labeled (left) and a representation of Fyles' unimolecular ion channel structure (right). Cylinder = core, lines = wall units, black circles = head groups.[81,144,145]

Moving away from the bulky 18-crown-6 connector, Fyles developed bolaamphiphile **1.20** (**Chart 1.7**) and other similar compounds with an eye towards a supramolecular channel approach.[147] Basically, the compounds were intended to form a structure similar to that represented on the right in **Figure 1.17**, but through aggregation of monomer units (since the central core is not present to hold the wall units in close proximity).[147] Ion channel activity was observed for these structures as determined by both pH stat and planar bilayer voltage clamp experiments. As judged from pH stat assays, the cation selectivity for **1.20** follows the order $K^+>Rb^+>Cs^+>Na^+>Li^+$. A single conductance level

was observed from the single-channel experiments, indicating a single active structure. From pH stat results at various concentrations, the kinetic order for transport was near 2 for all cations, and an active dimer was thus proposed.[147] The channel structure formed from **1.20** was also believed to comprise a water-filled pore through which ions passed.

Chart 1.7

1.20

1.21

1.22
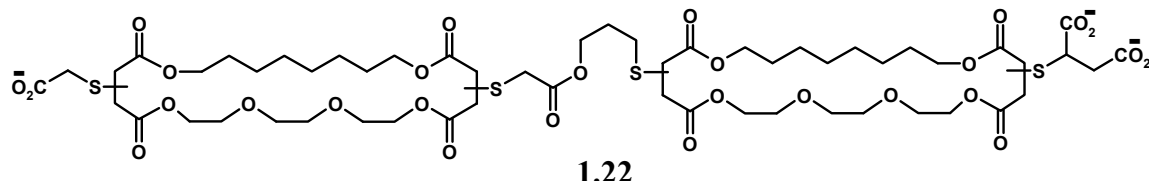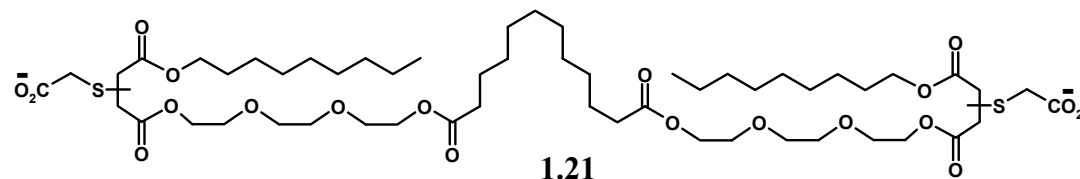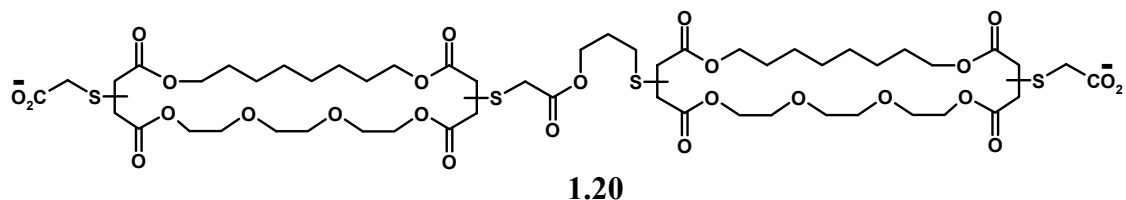
Two structural features of **1.20** (and its derivatives with various head groups) were addressed in subsequent reports. First, the polar oxygen-containing chain of the "wall unit", initially incorporated to serve as an ion relay in the channel, was replaced by a polymethylene chain. The ion transport properties of the more hydrophobic derivatives were "remarkably similar" in pH stat assays.[148] These results are in agreement with the observations made by Lehn upon replacing poly(ethylene oxide) chains with polymethylene chains.[87] The corresponding channels measured in voltage clamp experiments were estimated to consist of larger aggregates than those formed from **1.20**, since the rise times observed were significantly longer (larger aggregates take longer to assemble). The more hydrophobic compounds demonstrated a much higher cation/anion

selectivity. The selectivity was attributed to the inability of channels to support a water-filled pore, thus making the ion dehydration energies a more important factor in ion transport.[148] Anions have a larger dehydration energy than cations, and thus cations penetrate the channel.

More recently, the question of whether or not the bis-macrocycle is a critical element in ion transport was addressed. Acyclic derivative **1.21** (**Chart 1.7**) was investigated, and was shown to retain activity.[149] Although **1.21** showed a 10-fold reduction in activity as compared to **1.20**, voltage clamp experiments showed that the channels formed from **1.20** and **1.21** were similar. The macrocycle seems to assist in membrane insertion, but is not necessary for channel formation.[149]

In an effort to develop a voltage-gated channel, Fyles and colleagues synthesized bolaamphiphile **1.22**, which possesses a molecular dipole moment due to the dianionic succinate group on one side and the monoanionic carboxylate on the opposite side (at pH 6.4).[150] Compound **1.22** exhibited similar behavior as that described for Kobuke's **1.9** and **1.10** (Note: Fyles voltage-gated channel was published 3 years prior to the report by Kobuke).[120] When added at negative membrane potential, **1.22** inserts into the membrane asymmetrically (with the succinate group towards the more positive side). The channel showed "bursts of irregular openings" with currents of 1-10 pA and short open state lifetimes ranging from 0.5-10 ms.[120] Early in the experiment, rectification behavior was observed, with channels only opening at negative potentials. However, after some time (3-4 minutes), the succinate head groups penetrated the membrane, resulting in the presence of both channel orientations. This was observed as a disappearance of channel rectification in later I/V cycles.[150] This result is in contrast to cholic acid dimers **1.9** and **1.10** of Kobuke, which do not reorient in the membrane.[120] The **1.22** channels were proposed to exist as water-filled pores that are larger and less stable than those formed from **1.20**.[150]

At lower pH (5.9), partial protonation of the head groups decreased the electrostatic repulsion between **1.22** monomers leading to longer open states. Addition of Ba^{2+} (1.6 mM, pH 6.4) also stabilized the channels, resulting in discrete single channel openings

with open states as long as 100 ms.[120] From pH stat assays, a cation selectivity of $Rb^+>Cs^+>K^+>Na^+>Li^+$ was observed for channels formed from **1.22**.[150]

The lowest molecular weight channel-forming compound to date was reported by the Fyles laboratory. Isophthalic acid derivative **1.23** (**Chart 1.8**) formed ion channels that were cation selective in the order $Cs^+>K^+>Na^+$.[151] As indicated by planar bilayer experiments, **1.23** clearly forms ion channels. However, **1.23** showed no activity in pH stat vesicle assays. This was an important finding, since a number of authors do not conduct single channel current measurements in their studies of ion channels. Vesicular assays and single-channel current experiments are complementary, and lack of transport activity in one assay does not necessarily indicate that no activity will be observed in the other. The channels exhibited multiple conductance levels, indicative of supramolecular channels with multiple channel structures.[151] Lastly, the channels are under "close structural control", as addition of only one more methylene to the C_{11} chain (i.e. a C_{12} chain) results in a sharp decrease in activity. [151]

Chart 1.8

1.23

1.24
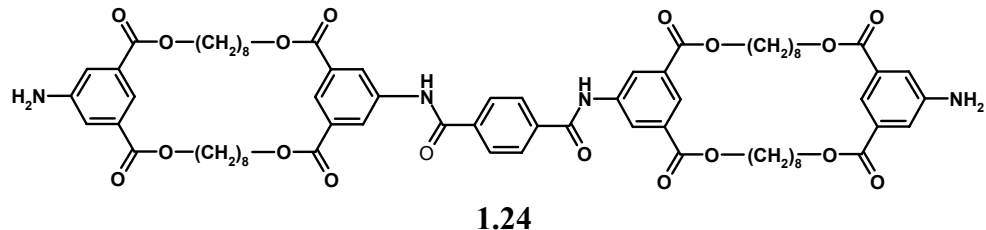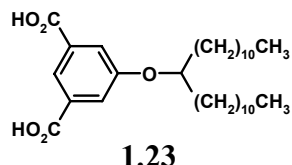
A second class of bolaamphiphile compounds, including **1.24** (**Chart 1.8**), based on isophthalic acid, was developed by the Fyles laboratory in a attempt to achieve more efficient syntheses than the multistep, low-yielding syntheses of **1.20** and **1.21**. Unfortunately, the synthesis of **1.24** and its derivatives proved to be "no improvement

over those leading to compounds" **1.20** and **1.21**.[152] Bolaamphiphile **1.24** did form ion channels. For membrane incorporation, however, it was necessary to mechanically transfer the compound directly to a bilayer from a "clean fine-camel-hair brush" due to its insolubility in the aqueous buffer.[152] Difficult syntheses and low solubility made these bolaamphiphiles poor candidates for optimization.

On the other hand, acyclic analogues of **1.24** showed considerable promise as channel-forming compounds.[153] This de-macrocyclization strategy is the same as was applied in the design of bolaamphiphile **1.21** based on the **1.20** structure.[149] The acyclic derivatives possessed the structure of **1.24**, but with two *p*-aminobenzene groups in place of the "ring-closing" peripheral 5-aminophthalic acid moieties. The acyclic derivatives formed ion channels with a $Cs^+>Na^+>Cl^-$ selectivity as shown by planar bilayer and pH stat experiments.[153]

Gokel. The channel models of Gokel are of the general structure: "sidearm-crown-spacer-crown-spacer-crown-sidearm". The models function as unimolecular ion channels (a single molecule spans the membrane and forms the conducting pore), much like Lehn's bouquet molecules (e.g. **1.18**) and Fyles bolaamphiphile **1.19**. The term "hydraphiles" was coined to refer to this series of channel compounds.[154] Hydraphiles **1.25** and **1.26** (**Chart 1.9**) transport Na^+ across membranes via an ion channel mechanism as shown by base pulse assays, ^{23}Na NMR experiments and planar bilayer voltage clamp measurements.[89,155,156] From the original design, it was predicted that the cation would pass through all three crown ether cavities. However, derivatives lacking the central crown retained ion transport activity. The ions seemingly do not pass through the central crown, and it has been hypothesized that the central crown, when present, functions only as an ion relay at the center of the membrane.[155] Also, water is believed to be intimately involved in Na^+ transport through the channel. Based on the crystal structure of a "model" central relay unit with bound Na^+ and H_2O, taken together with the hypothesis that the central crown functions as a relay, the channel model shown in **Figure 1.18** (for hydraphile **1.26**) was proposed.[155,157] Similarly based on X-ray crystallographic

evidence, the channels formed from calix[4]arene tetrabutylamide **3.1** in **Chapter 3** are proposed to contain water in their active structures (see **Figures 3.7** and **3.8**).[141]

Chart 1.9

1.25 : R = $C_{12}H_{25}$ **1.26** : R = CH_2Ph **1.27** : R = $CH_2(p\text{-}CH_3O\text{-}Ph)$

1.28 R = dansyl   **1.29** R = cholestanyl   **1.30** R = -$(CH_2)_{12}$-(diaza-18-crown-6)-$(CH_2)_{12}$-
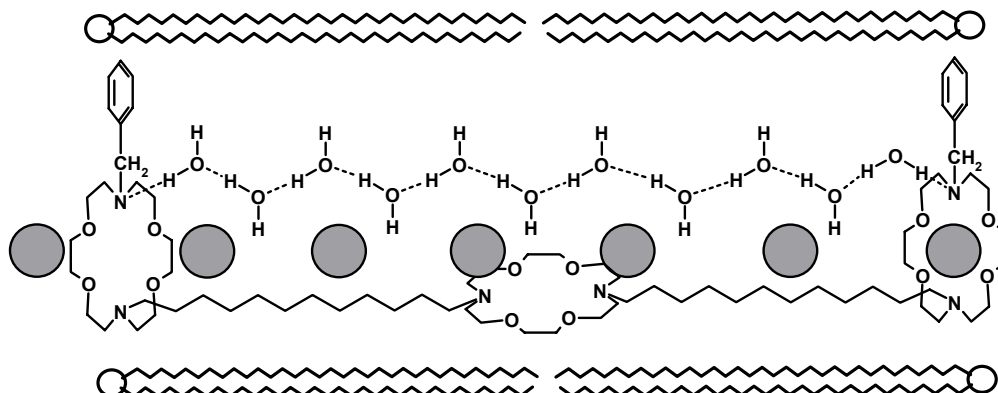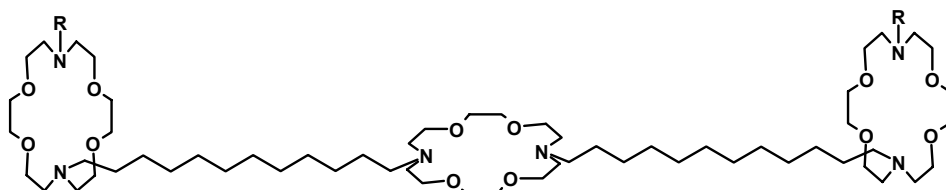
Figure 1.18. Hydraphile **1.26** in the proposed membrane-spanning channel conformation. Na$^+$ is represented by gray spheres. Dashed lines represent hydrogen bonds between water molecules.[155,157]

By replacing the phenyl group in **1.26** with a *p*-OMe group, hydraphile **1.27** (**Chart 1.9**) showed extremely long open state lifetimes in excess of 30 s.[156] Also, cation flux across the bilayer by **1.27** was increased over that mediated by **1.26**, presumably due to more favorable cation-π interactions at the entrance to the channel.[155] Introducing

fluorescent dansyl groups at the same position gave hydraphile **1.28** (**Chart 1.9**). Fluorescent-depth quenching assays with **1.28** showed that the dansyl group (and terminal crown ethers) do indeed reside at the surface of the membrane, in agreement with the prediction that the terminal crowns act as head groups.[156] Lastly, appending cholestanyl groups onto the terminal crown to give **1.29** (**Chart 1.9**) prevents the passage of Na^+ through the channel.[155,158] This finding is in sharp contrast to the cholic acid-resorcinarene conjugate reported by Kobuke.[121] In that case, replacement of alkyl chains with sterol groups resulted in a retention of channel activity and an increase in the open state lifetimes.

The length of the chain connecting the terminal crowns to the central crown is important for activity.[159] Carbon chain lengths of 12 (**1.25-1.29**) and 14 resulted in similar activity. Shortening the chain to 10 or lengthening it to 16 resulted in a two-fold decrease in activity for both cases, while an 8-carbon connector was completely inactive. These data support the proposal that the conducting hydraphile channels span the membrane.[159]

Further exploitation of the hydraphile design lead to compounds with increased transport efficiency and a redox switch. By connecting the 2 dodecyl chains on **1.25** with a fourth diaza-18-crown-6 group, macro-macrocycle **1.30** (a tetramacrocyclic hydraphile) was obtained. Compound **1.30** showed a near 3.5-fold increase in sodium transport rate over **1.25**.[160] A redox-active artificial channel based on the hydraphile design was reported by Hall *et al.*[161] The redox channel consisted of four diaza-18-crown-6 rings, the central two of which were connected through a ferrocene. The compound functioned as a K^+-selective channel and demonstrated rectification, with increased currents at negative membrane potentials as shown by patch clamp recordings.[161]

The most important property of hydraphile channels yet reported is their bactericidal activity. Hydraphile **1.26** was shown to kill *Escherichia coli* with an IC_{50} of 10 μM.[162] This property was attributed to the ion channel activity of **1.26**, with membrane insertion followed by disruption of the osmotic balance as the predicted mechanism of action.[162] In addition to Ghadiri's success with antimicrobial cyclic peptides, Gokel has introduced hydraphiles as novel bactericidal agents.

A collaboration between Gokel and de Mendoza resulted in a novel hydraphile-like channel-forming compound. Calix[4]arene tetracrown 1,3-*alternate* **1.31** formed ion channels that transported Na$^+$ and K$^+$, based on planar bilayer voltage clamp experiments.[163] Channel bursts were observed with large conductances (300 pS in some cases) and open times in the low millisecond range. To answer the question of whether or not the cation passed through the calix[4]arene core, a derivative bearing *tert*-butyl groups on the upper rim was tested. Based in CPK models, the bulky *tert*-butyl groups should prevent cations from entering the calix[4]arene. If the ion passed through the core of **1.31**, the *tert*-butyl derivative would be inactive. But the tert-butyl calix[4]arene-tetracrown was equally active, strongly supporting a transport mechanism that does not involve ion passage through the calix[4]arene 1,3-*alternate* core.[163] Also, the calix[4]arene tetracrown *cone*, a compound incapable of spanning the membrane, was tested. It was shown that the cone conformer functioned through a carrier mechanism.[163]

1.31
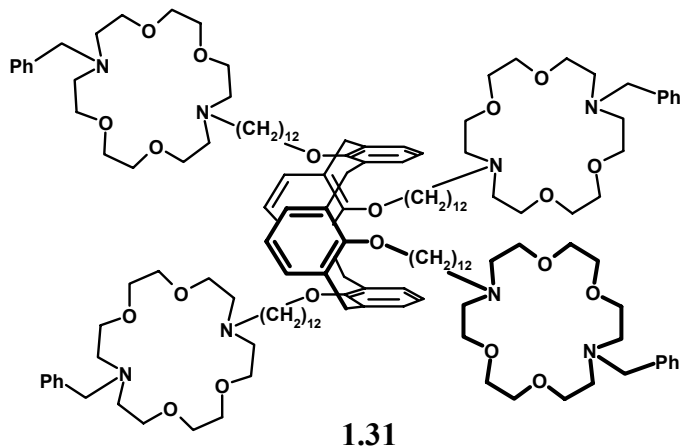
The finding that the ions do not pass through the calix[4]arene 1,3-*alternate* core of **1.31** bears on the findings described in **Chapter 3** of this thesis. Indeed, calix[4]arene-tetrabutylamide **3.1**, a compound that forms chloride channels in membranes, is predicted to form structures that do not involve the calix[4]arene core in ion transport (based on two crystal structures, see **Figures 3.7** and **3.8**).[141] "Opening" the calix[4]arene core to form an analogous linear tetramer resulted in an equally active ion transporter.[93] Like the channels formed from **1.31**, the calix[4]arene core was likely not involved in the active

structures formed from **3.1**. Also, the calix[4]arene 1,3-*alternate*-guanosine conjugates cG **2.26** and cG **2.34** (**Chapter 2**) transport K^+ over Na^+ and Cs^+. In this case, the direct involvement of the calix[4]arene 1,3-*alternate* core in ion transport has yet to be elucidated.

Voyer. The channel designed by Voyer *et al.* was based on α-helix formation of the 21 amino acid peptide **1.32** (**Figure 1.19**).[164] With crown ether residues at positions 2, 6, 9, 13, 16, and 20 of the peptide, folding of the peptide into an α-helix results in a lining up of the crown ethers on one side of the helix (**Figure 1.19**, right). This creates a channel of six stacked crown ether rings through which ions may flow. A 21-crown-7 was chosen since it binds alkali metals weakly. Weak ion binding, as discussed previously, is critical for the high throughput rates associated with channel function.

A.

B.   **α-helix**
                              crown ethers

N-t-BOC-(Leu-X-Leu-Leu-Leu-X-Leu)₃-OMe
1.32

X =
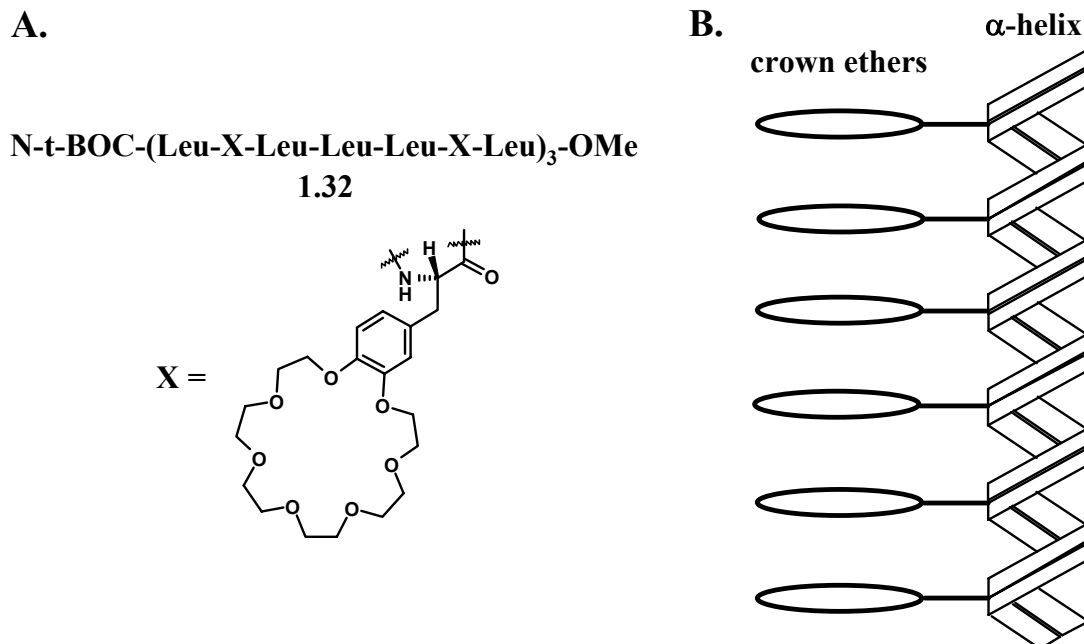
Figure 1.19. 21-crown-7-containing peptide **1.32** (left) and a representation of the unimolecular channel structure resulting from α-helix formation of **1.32**.[164]

The unimolecular channel **1.32** was shown to transport Li^+, Na^+, K^+, Rb^+ and Cs^+ at the same rate, indicating no selectivity among cations.[164] The channel mechanism was supported by single-channel current measurements.[165] Data from circular dichroism and attenuated total reflectance spectroscopy experiments suggest that the α-helical channel functions in a monomeric form and is oriented parallel to the lipid hydrocarbon chains when conduction occurs.[166]

1.6.3. Summary of Synthetic Cation Channels.

Table 1.1 provides a summary of synthetic cation channels listed by principle investigator (as this section was organized). The table lists the compound numbers, whether the channel is monomeric (M) or self-assembled (SA), the cation specificity (if any), whether the channel exhibited single or multiple conductance states (if reported), the voltage dependence (yes or no, if reported), comments specific to the channel(s), and the references. "NR" indicates that the property was not reported.

Table 1.1. Summary of Synthetic Cation Channels.

Principle Investigator	Compounds	M or SA[a]	Cation specificity	Conductance state(s)	Voltage dependence?	Comments	References
Kobuke	**1.1, 1.2, 1.3**	SA	NR[b]	multiple	yes	**1.1, 1.2** 1st non-peptide ion channels	110 114
	1.4	SA	$Cs^+>K^+>Na^+$	multiple	NR	photocontrol	116
	1.5	SA	$K^+>Na^+$	single	NR	1st non-peptide K^+-selective channel, active dimer, cholic acids in place of alkyl chains cause long OSLs[c]	117 121
	1.6	SA	NR	multiple	NR	long OSL[c]	118
	1.7, 1.8	SA	$K^+>Na^+>Li^+$	single	NR	active dimer	119
	1.9, 1.10	SA	NR	multiple	yes	rectification	120
Ghadiri	**1.11**	SA	$K^+>Na^+$	single	NR	antibacterial peptides	123 15
Regen	**1.12**	SA	NR	NR	NR	DPPC/EYPC[d]	86
	1.13	SA	NR	NR	NR	membrane-selective, DPPC/EYPC[d], active dimer	132
Matile	**1.14**	SA	$H^+>K^+$	NR	yes	voltage-dependent but no dipole, active tetramer	78 140

Table 1.1 Cont'd.

Principle Investigator	Compounds	M or SA[a]	Cation specificity	Conductance state(s)	Voltage dependence?	Comments	References
Matile	**1.15**	SA	$K^+ > Li^+$, Na^+, Rb^+ Cs^+	NR	NR	requires Cu^{2+} & pHis, 1st synthetic ligand-gated channel	80
	1.16	SA	NR	NR	NR	dimeric β-barrel	142
	1.17 and derivatives	M	$M^+ > H^+$	NR	NR	push-pull rods, recognize polarized vesicles	14 143
Lehn	**1.18** and cyclo-dextrin derivative	M	NR	NR	NR	bouquet molecules, Na^+/Li^+ antiport, DPPC/EYPC[d]	87 88
Fyles	**1.19**	M	no	NR	NR	bolaamphiphile	81
	1.20, **1.21**	SA	$K^+ > Rb^+ > Cs^+$ $> Na^+ > Li^+$	single	NR	active dimer, macrocycle in **1.20** not critical	147 149
	1.22	SA	$Rb^+ > Cs^+ > K^+$ $> Na^+ > Li^+$	multiple	yes	pH decrease or addition of Ba^{2+} stabilized channels	150
	1.23	SA	$Cs^+ > K^+ > Na^+$	multiple	NR	Smallest channel forming molecule reported to date	151
	1.24 and acyclic derivative	SA	$Cs^+ > Na^+$ (acyclic derivative)	multiple	NR	**1.24** too insoluble, but acyclic derivative promising	152 153

Table 1.1 Cont'd.

Principle Investigator	Compounds	M or SA[a]	Cation specificity	Conductance state(s)	Voltage dependence?	Comments	References
Gokel	**1.25**, **1.26**	M	NR	NR	NR	**1.26** kills E. coli	89 154 155 162
	1.27	M	NR	NR	NR	> 30 s OSLs[c]	156
	1.30	M	NR	NR	NR	Na^+ transport rate 3.5x that for **1.25**	160
Gokel/ de Mendoza	**1.31**	M	NR	multiple	NR	Cations do not pass through calixarene core	163
Voyer	**1.32**	M	no	single	NR	monomeric channel	164 165

a Monomeric (M) or self-assembled (SA) ion channel
b NR = not reported
c OSL = open state lifetime
d Support for channel mechanism from transport rates in DPPC and EYPC liposomes

1.7 Synthetic Anion Channels

1.7.1 Introduction

There are few examples of synthetic anion channels. Most of the work in this area has been done by six research groups (Davis *et al*. included). Different approaches to anion channels use protein fragments, completely synthetic compounds, or a combination of the two. **Section 1.7.2**, like **1.6.2**, will be organized by author and will begin with channels composed of protein fragments and end with the non-natural, synthetic approach.

1.7.2 Synthetic Anion Channels

Glycine Receptor Group. The group responsible for the first synthetic anion channel was "The Glycine Receptor Group" (GlyR Group, this name was given simply for the sake of identification throughout this section). They have subsequently made large contributions to the study of chloride-channel forming peptides, as will described below. The research was done in collaboration between multiple research groups, most from departments at the Kansas State University and the University of Kansas, with a number of corresponding authors on the publications. The multiple collaborations are thus referred to here as a "group", and not an individual senior investigator.

Before describing the first synthetic channel developed by the GlyR group, the inhibitory glycine receptor, upon which this synthetic channel was based, needs to be introduced. The inhibitory glycine receptor (GlyR) is a glycoprotein present in postsynaptic membranes and is responsible for synaptic inhibition.[167] The GlyR is a member of the ligand-gated ion channel receptor superfamily, and is activated by the neurotransmitter glycine (as can be inferred from its name). The subunit structure of GlyR is believed to comprise a large extracellular N-terminal region, four transmembrane domains, M1-M4, and an intracellular loop between M3 and M4.[168] It was believed that the M2 segment, the only sequence that adopts an α-helix in the protein, was responsible for ion transport.[167] Thus, the GlyR group investigated the possibility that a sequence

corresponding to the M2 segment of GlyR could facilitate chloride transport across membranes. This lead to the first synthetic chloride channel, reported in 1993.[12]

The GlyR group showed that the 23-amino acid peptide M2GlyR **1.33** (**Chart 1.10**), a sequence that corresponds to the M2 transmembrane segment of the glycine receptor, formed anion-selective channels in lipid bilayers.[12] The most frequent events observed for channels formed from **1.33** by planar bilayer conductance measurements in KCl buffer had conductances of 26 pS and 49 pS and open state lifetimes near 10 ms. This is "in remarkable agreement" with the conductances of 27 pS and 46 pS and the ≤10 ms open times for GlyR, supporting the hypothesis that M2 is responsible for chloride transport.[12] As shown in **Figure 1.20**, channel events were observed in N-methyl-D-glucamine•HCl, a chloride-containing buffer, but not in the non-chloride-containing sodium gluconate buffer.[12] (A similar experiment was used to confirm Cl⁻ transport by **3.1** in **Chapter 3**.) In addition to this strong evidence for the transport of Cl⁻, measurement of reversal potentials showed that the channel was 85% anion-selective. Notably, a 23-amino acid peptide corresponding to the GlyR M1 domain, a portion of the protein believed not to be involved in ion transport, showed no channel activity.[12]

Chart 1.10

Sequence	Compound	
H₂N-PA<u>R</u>VGLGITTVLTMTTQSSGS<u>R</u>A-COOH	M2GlyR	**1.33**
H₂N-PA<u>R</u>VGLGITTVLTMTTQSSGS<u>R</u>A<u>KKKK</u>-COOH	C-K₄-M2GlyR	**1.34**
H₂N-<u>KKKK</u>PA<u>R</u>VGLGITTVLTMTTQSSGS<u>R</u>A-COOH	N-K₄-M2GlyR	**1.35**

65
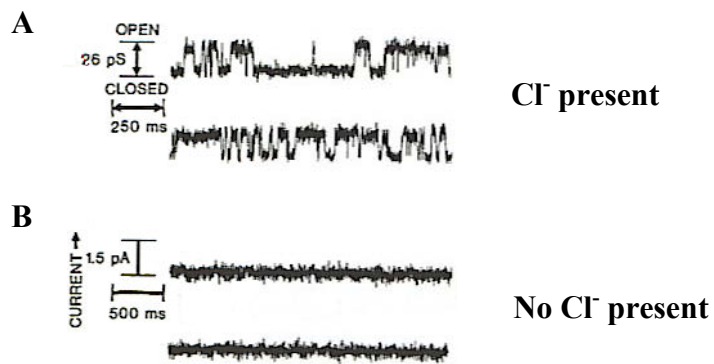
Figure 1.20. Single-channel current recordings from POPE/POPC bilayers containing M2GlyR **1.33** recorded in (A) symmetric 0.5 M N-methyl-D-glucamine•HCl (Cl⁻-containing) buffer and (B) symmetric 0.5 M sodium gluconate (non-Cl⁻-containing) buffer.[12] This figure was reprinted with permission from the *Journal of Biological Chemistry* and the authors. Copyright 1993 The American Society for Biochemistry and Molecular Biology, Inc.

The Arg-3 and Arg-22 residues of **1.33** (underlined in **Chart 1.10**) have been implicated in GlyR's anion selectivity.[169] By replacing these two Arg residues with Glu in **1.33**, a peptide that formed cation-selective channels resulted, confirming the positively-charged arginines' role in affecting anion selectivity.[12]

The oligomeric states of the **1.33** peptide channel assembly were also addressed. GlyR is a pentameric assembly in the membrane.[167] The **1.33** channels exhibit two major conductance states, indicative of two independent active channel aggregates. The conductances of 26 pS and 49 pS were assigned to tetrameric and pentameric aggregates, respectively.[12] To confirm the assignments, four **1.33** sequences were tethered to a 9-amino acid template giving a covalently-linked tetramer. The tetramer formed anion-selective channels with a single conductance of 25 pS, confirming the assignment of the 26 pS **1.33** channel as a tetramer.[12] The dominant conductance level for pentameric GlyR is 45 pS, in agreement with the 46 pS conductance arising from a pentamer.

This initial report by the GlyR group provided support for the following previous predictions about GlyR: (1) GlyR is a pentameric assembly of subunits, (2) the pore is

66

lined by the M2 transmembrane domain, and (3) the Arg-3 and Arg-22 residues are responsible for the channel's anion selectivity.[12]

By adding four lysine (K) residues to the C-terminus, the C-K$_4$-M2GlyR **1.34** peptide's water solubility was greatly increased over that of M2GlyR **1.33**.[170] C-K$_4$-M2GlyR **1.34** (**Chart 1.10**) was shown to induce Cl$^-$ and fluid secretion from model epithelial cell monolayers. The effects of **1.34** were accompanied by an increase in current across the membrane, and removal of Cl$^-$ from the bathing solution inhibited the peptide's effects.[170] The latter finding is consistent with the formation of chloride-selective ion channels by **1.34** as the mechanism of action. C-K$_4$-M2GlyR **1.34** was later found to increase Cl$^-$ currents in a number of other cells, including airway epithelial cells from a human cystic fibrosis patient.[171] This was determined from patch clamp recordings in the whole cell configuration and from planar bilayer conductance measurements. The study also proved that C-K$_4$-M2GlyR **1.34** formed a "distinct conduction pathway", thus eliminating the possibility that **1.34** acted by modulating Cl$^-$ channels already present in the membrane.[171] Induction of transepithelial chloride and fluid secretion is important in the treatment of cystic fibrosis.[172]

An increased current across cell membranes over that observed for **1.34** was achieved by N-K$_4$-M2GlyR **1.35** (**Chart 1.10**), a peptide bearing the four lysine residues at the N-terminus (instead of the C-terminus).[173] N-K$_4$-M2GlyR **1.35** was subsequently shown to restore secretion of the antioxidant glutathione from human cystic fibrosis airway epithelial cells.[174] This result provided further potential for these peptides in cystic fibrosis treatment, as decreased glutathione secretion causes oxidative stress in the airways of cystic fibrosis patients.[175]

A structure-activity analysis of C-K$_4$-M2GlyR **1.34** and N-K$_4$-M2GlyR **1.35** provided insight into the roles of specific peptide regions. Truncating N-terminal residues from **1.34** resulted in a sharp drop in chloride transport activity (lower membrane current).[176] In contrast, deletion of amino acid residues from the C-terminus of **1.35** actually increased the activity for 25 and 22 amino acid sequences 1.5- to 2-fold over the parent 27 amino acid sequence.[176] Activity was retained, albeit greatly reduced, for the 16-amino acid **1.35** analog. From this data, two conclusions were drawn. First, the aqueous

aggregation nucleation site is located near the C-terminus, and its removal results in retention of ion channel activity. Second, the peptide region responsible for assembly of active structures in the membrane resides near the N-terminus, as truncation of N-terminal amino acids results in a loss of activity.[176]

In a separate study, sequences corresponding to transmembrane domains of the Cystic Fibrosis Transmembrane Conductance Regulator (CFTR) were tested for chloride transport activity.[13] This study aimed to corroborate data indicating that the M2 and M6 transmembrane domains are intimately involved in the ion channel pore of CFTR.[177] Peptides M2 **1.36** and M6 **1.37** (**Chart 1.11**) indeed formed anion-selective channels. Ion selectivity was determined by the measurement of reversal potentials in the presence of a salt concentration gradient. Also, like M2GlyR **1.33**, M2 **1.36** and M6 **1.37** were active only in a chloride-containing buffer (results similar as those shown in **Figure 1.20** for M2GlyR **1.33**). Since it was believed that the M2 and M6 CFTR domains together formed the channel, a mixture of M2 **1.36** and M6 **1.37** were tested. Indeed, the M2/M6 mixture formed ion channels that displayed properties distinct from the individual peptides, and the conductance approximated that of CFTR.[13]

Chart 1.11

Sequence	Compound
H_2N-RSIAIYLGIGLCLLFIVRTLLL-COOH	M2 **1.36**
H_2N-KGIILRKIFTTISFCIVLRMAV-COOH	M6 **1.37**

Conversely, peptides with sequences corresponding to the M1, M3, M4 and M5 CFTR domains (domains believed not to be located in the pore) showed no activity. These data strongly suggested that the M2 and M6 transmembrane domains of CFTR are indeed constituents of the pore-forming structure.[13]

The GlyR group has achieved two of the goals for studying synthetic ion channels (**Section 1.4**). Both the GlyR and CFTR peptides have given insight into the natural channel structures by identifying protein domains involved in ion transport. Also, C-K4-

M2GlyR **1.34** and N-K$_4$-M2GlyR **1.35** have demonstrated potential for the treatment of diseases associated with chloride channel malfunction, such as cystic fibrosis.

Woolley. As described in **Section 1.3**, alamethicin (Alm) forms cation-selective channels in membranes. The channel structures comprise various aggregates of Alm monomers, giving rise to multiple conductance levels. In an effort to understand Alm channel structure, Woolley *et al.* synthesized Alm dimers linked at their C-termini through flexible tethers.[178] These Alm dimers formed cation-selective channels, similar to those formed from natural Alm, but exhibited increased open state lifetimes for particular active structures. The longest open state lifetime was attributed to a "6-mer" aggregate, comprising three dimers.[178] In a subsequent study, evidence for the involvement of Glu-18 (Q, see **Chart 1.2**) in interactions with cations at the entrance to the pore suggested its role in the channel's cation selectivity.

In an effort to alter the selectivity of the channel, and thus prove Glu-18's participation in the channel's cation selectivity, Woolley synthesized and investigated Alm dimer **1.38**, with Lys (K) replacing Glu at the 18 position. The hypothesis was that positively-charged Lys residues at the pore entrance would draw anions into the channel. Indeed, **1.38** formed ion channels and demonstrated a switch to anion selectivity.[179] The P_{Cl}/P_K ratio for Alm dimer **1.38** was 4.3 with a 0.01 to 1.3 M KCl gradient and 1.8 with a 0.1 to 1.3 M KCl gradient in planar bilayer measurements. The Lys-18 residues in **1.38** play the same role in anion selectivity as Arg-3 and Arg-22 in M2GlyR **1.33** (**Chart 1.10**). Active channel structures were assigned as "6-mer" (three dimers) and "8-mer" (four dimers) aggregates.[179]

Ac-Aib-P-Aib-A-Aib-A-Q-Aib-V-Aib-G-L-Aib-P-V-Aib-Aib-K^{18}-Q-F-C(O)NH-(CH$_2$)$_4$—

NHAc
O
HN
O
NH
O
H$_2$N

Ac-Aib-P-Aib-A-Aib-A-Q-Aib-V-Aib-G-L-Aib-P-V-Aib-Aib-K^{18}-Q-F-C(O)NH-(CH$_2$)$_4$—

1.38

Aib =
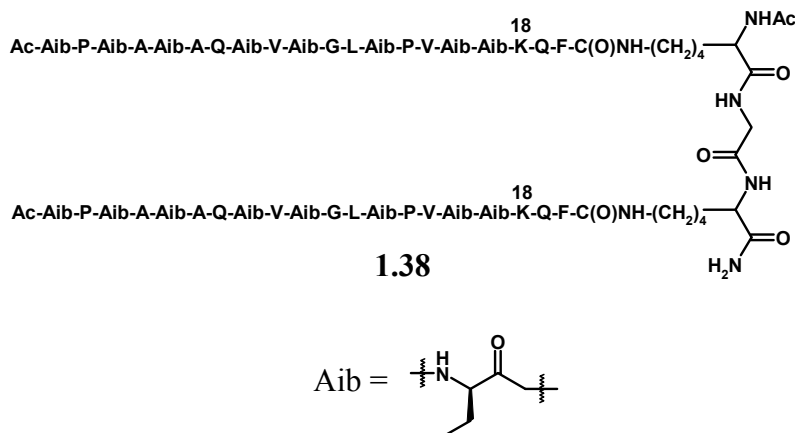
To elucidate the reason for "low" Cl⁻ selectivity and the effect of the ion concentration gradient on channels formed from **1.38**, computer simulations were conducted on the 8-mer aggregate, and two findings were reported.[180] (1) The increased concentration (0.1 M versus 0.01 M) resulted in a shielding of the 8 positive charges of Lys-18 present in the 8-mer channel by 4 Cl⁻ ions. This is likely the cause of the decreased Cl⁻ selectivity (P_{Cl}/P_K 1.8 versus 4.3). (2) The positive charges are present in the entrance to the pore, a wide part of the channel relative to the region near Glu-7. This allows space for counterions to interfere with anion recognition and funneling into the channel. Woolley's prediction is that placing a significant amount of positive charge near (or in place of) Glu-7, in the narrow region of the channel, will increase anion selectivity.[180]

Gokel. Unlike the approaches of the GlyR Group and Woolley, Gokel did not use natural peptide sequences as the template, but hinged the design around a proline-containing peptide sequence attached to a synthetic hydrophobic segment. Proline is known to be critical in the ion selectivity sequences of anion channels.[181] Also, substitution of proline into nicotinic acetylcholine receptors, normally cation selective channels, results in conversion to anion selectivity.[182]

Gokel *et al*. designed the peptide-containing molecule **1.39** (**Chart 1.12**), having a proline flanked by three glycines on each side. The peptide sequence was attached to a

hydrophobic segment intended to anchor the molecule in the membrane.[97,98] Gokel has named the series of chloride channel forming compounds based on this structure SCMTRs (synthetic chloride membrane transporters).[97]

Chart 1.12

1.39: R = $(CH_2)_{17}CH_3$
1.40: R = $(CH_2)_9CH_3$
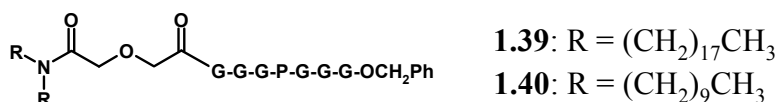
SCMTR **1.39** did indeed transport Cl⁻ across liposome membranes, as determined using a chloride-selective electrode to monitor efflux of Cl⁻ from liposomes.[97,98] Notably, replacement of Pro with Leu in **1.39** resulted in a significant loss of activity, confirming proline's critical role in the anion transport ability of **1.39**.[97,98] Single channel currents were observed in planar bilayer voltage clamp experiments, showing a single conductance at 1300 pS.[97] Measurement of E_{rev} indicated a Cl⁻/K⁺ selectivity of >10:1. The channels were also voltage-dependent, showing long open state lifetimes at +10.5 mV, rapid openings and closings at 0 mV, and no activity at –3.5 mV.[97] These results were interpreted to indicate that **1.39** "forms a large, stable, anion-selective aqueous pore in bilayer membranes."[97] The active structure proposed was a **1.39** dimer.

A second SCMTR derivative, **1.40**, was synthesized to examine the effects of the anchor's aliphatic chain length on chloride transport efficiency.[107] The release of Cl⁻ from liposomes was greater when mediated by **1.40** versus that mediated by **1.39**. SCMTR **1.40** also showed a 15-fold increase in carboxyfluorescein release efficiency over that of **1.39**, and a 17-fold increase in per-mole conductance from single channel measurements.[107] The shorter SCMTR **1.40**, however, was subsequently shown to have no selectivity for Cl⁻ over K⁺, indicating that **1.40** is not an anion channel.[183]

Regen. As discussed in **Section 1.6**, Regen developed squalamine mimic **1.13** (**Chart 1.6**) in a successful effort to identify cation transporters.[132] Sterol **1.41**, a second squalamine mimic, was predicted to behave similarly. Indeed, **1.41** showed ion transport

activity in pH discharge experiments (essentially base pulse experiments) with liposomes.[184] However, further investigation of the transport activity of **1.41** monitored by ^{23}Na and ^{7}Li NMR showed conclusively that no cations were transported by this sterol.[184]

1.41
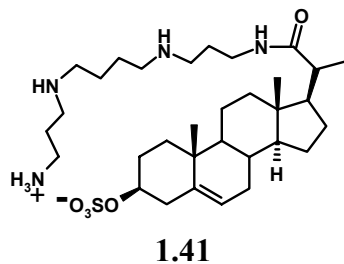
Since **1.41** did not transport Na$^+$ or Li$^+$ in NMR assays, but certainly induced a pH change as shown by pH discharge experiments, only two mechanisms were possible: H$^+$/Cl$^-$ symport or OH$^-$/Cl$^-$ antiport.[184] To distinguish between the two, pH discharge experiments with **1.41** were conducted in the presence and absence of the protonophore FCCP (see **Section 1.5.6**). A 4-fold increase in rate was observed in the presence of FCCP, indicating that H$^+$ transport was "at least partially rate-limiting", thus supporting an H$^+$/Cl$^-$ symport.[185]

An ion channel mechanism of transport was confirmed by a comparison of transport rates between PG and DPPC vesicles.[184] Much like squalamine mimic **1.13**, kinetics experiments supported a **1.41** dimer as the active transporting structure.[185] Interestingly, sterol **1.41** is substantially more active in negatively charged membranes (PG) compared to neutral membranes (PC).[184,185] The ability of **1.41** to recognize negatively charged membranes makes this compound a potential lead for novel antibacterial agents.

Sterol **1.41** most likely forms "proton-ionized channels that permit the passage of only protons and anions."[184] The differences between cation channel-former **1.13** and anion channel-former **1.41** relate to differences in the selectivity filters between the K$^+$ channel and the ClC chloride channel (**Sections 1.2.2** and **1.2.3**). Cation transport by **1.13** is facilitated by oxygens of the polyether chain, much like in the K$^+$ channel, wherein carbonyl oxygens allow for K$^+$ dehydration and transport (see **Figure 1.3**). Conversely, **1.41** bears a polyamine chain, which is likely protonated in the active structure, and

transports Cl⁻ via hydrogen bonding to N-H groups. This resembles the ClC selectivity filter, wherein N-H•••Cl⁻ hydrogen bonds are critical for Cl⁻ selectivity and transport (see **Figure 5**).

A study by Cheng *et al.* later demonstrated that sterol **1.41** mediated Cl⁻ transport across cystic fibrosis airway epithelial cells.[16] This was confirmed through both fluorescence assays with the Cl⁻-selective dye SPQ (see **Section 1.5.8**) and patch clamp recordings in the whole cell configuration.[16] The patch clamp experiments provided further support that **1.41** does indeed function via an ion channel mechanism. The peptide C-K$_4$-M2GlyR **1.34** (**Chart 1.10**) demonstrated similar chloride transport ability in cystic fibrosis cells.[170] The results of this study suggest that **1.41** also has therapeutic potential for cystic fibrosis treatment.[16,172]

Matile. The proton-selective channels formed from oligophenylene **1.14** (see **Section 1.6**) also accelerated OH⁻ and/or Cl⁻ transport across the membrane.[79] Evidence for anion transport came from base pulse assays in which the extravesicular Cl⁻ was replaced with Br⁻ or SO$_4^{2-}$. In both cases, an increase in transport rate was observed, and the researchers stated that "these changes demonstrate polyol-mediated anion transport."[79]

All other anion channels reported by Matile and colleagues comprised β-barrel structures (described in **Section 1.6**). The first of these β-barrel-forming compounds was oligo-*p*-phenylene **1.42** (**Chart 1.13**). Compound **1.42** had the oligo-*p*-phenylene backbone of **1.16** (**Figure 1.15**), except with the extended R = OCH$_2$C(O)Leu-Lys-Leu-NH$_2$ peptide appended to the rod. Compound **1.42** formed β-barrels with large pore diameters due to an increased number of monomers in the barrel (over that observed for **1.16**). Kinetics experiments showed a sixth order dependence on **1.42** concentration, suggesting a **1.42** hexameric barrel (**1.16** barrels consisted of dimers).[106] CD data were consistent with β-sheet formation between monomers and fluorescence depth quenching experiments indicated that **1.42** barrels spanned the bilayer.[106]

The **1.42** β-barrels demonstrated the ability to transport carboxyfluorescein across EYPC bilayers (see **Section 1.5.11**). In the **1.42** barrel, the Lys sidechains are predicted to point toward the channel's pore, wherein the protonated ε-amino groups interact with

73

anions, with the Leu sidechains forming a lipophilic sheath on the outside of the barrel. This hypothesis was supported by the assembly's ability to transport anionic carboxyfluorescein, and certainly represents a plausible structure, since ammonium groups are not likely to protrude into the hydrophobic bilayer. To transport the dye, the necessary pore diameter is estimated at 20 Å.[106] Planar bilayer voltage clamp recordings in an NaCl buffer indicated the formation of channels with open state lifetimes on the order of one second. Seemingly, only a single conducting species, the putative hexamer, is active.

Chart 1.13

1.42: R =

1.43: R =

1.44: R =
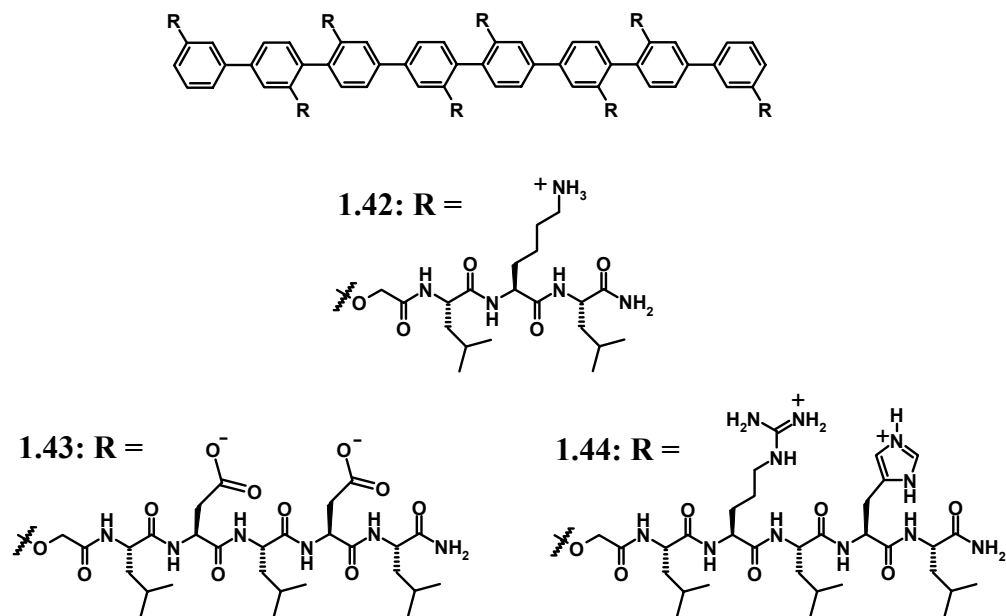
The ion selectivity of β-barrel channels can be modulated based on the peptide sequence incorporated into the rigid rod barrel-forming monomers and by the buffer pH, as demonstrated by compounds **1.43** and **1.44** (**Chart 1.13**).[186] Compound **1.43**, having two anionic Asp residues in the appended peptides, formed ion channels with a cation selectivity (P_K/P_{Cl} = 5.6) as was expected for β-barrels with negative charge lining the pore.[186] Addition of Mg^{2+} to the buffer resulted in a significant decrease in cation selectivity due to chelation of Mg^{2+} by the Asp carboxylates. Compound **1.44**, with an

Arg and a His residue on each peptide, also formed cation-selective channels (P_K/P_{Cl} = 2.1), but only at higher pH (pH 6.0).[186] At pH 4.0, the **1.44** β-barrel channels inverted their selectivity, demonstrating an anion preference of P_{Cl}/P_K = 3.8, a phenomenon attributed to protonation of the Arg and His sidechains (as shown in **Chart 1.13**).[186] All ion selectivities were determined using planar bilayer voltage clamp measurements with a transmembrane salt gradient. This study very elegantly exemplifies the fine balance between ion selectivity in these synthetic channels. Small changes in the environment (pH 6.0 versus 4.0) resulted in an inversion of ion selectivity for **1.44** β-barrels, mimicking the extreme environmental sensitivity of natural systems.

By imparting the molecular dipole characteristic of push-pull rods (see **Section 1.6**) to molecules capable of forming β-barrels, Matile formed "push-pull barrels".[187,188] Octaphenylene **1.45** (**Chart 1.14**) formed tetrameric β-barrels in EYPC membranes, based on kinetic measurements as a function of concentration. The β-barrels recognized polarized membranes, as determined by assays with polarized liposomes, indicating that the molecular dipoles aligned parallel to one another in the active structure.[187] The tetrameric **1.45** β-barrel demonstrated a Cl^-/K^+ selectivity of $2.7 \geq P_{Cl}/P_K \geq 3.7$, and an overall selectivity of $Cl^- \geq F^- \geq OAc^- > K^+$ in planar bilayer voltage clamp measurements.[188] The ion selectivity was supported by base pulse assays on SUVs. As with **1.42**, the anion selectivity of β-barrels formed from **1.45** is attributed to protonated Lys sidechains lining the channel's pore.

Chart 1.14

R =

1.45: R' = SO₂Me

1.46: R' = OMe

75
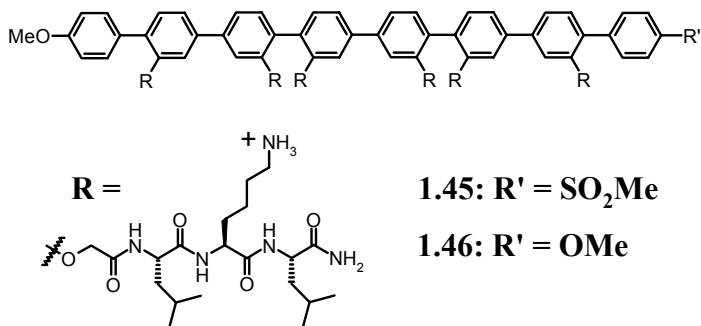
Replacing the methyl sulfoxide group of **1.45** with an OMe group resulted in annihilation of the voltage dependence.[188] In contrast to the push-pull β-barrels formed from **1.45**, β-barrels formed from the symmetrical **1.46** had no dipole, and were therefore insensitive to transmembrane potential. However, **1.46** barrels retained a Cl⁻ selectivity (due to the Lys residues), as determined by base pulse assays.[188] Interestingly, channels comprising **1.46** displayed a significantly longer open state lifetime (approximately 5 seconds) than those formed from **1.45**.

This study yet again underscores the potentially tremendous effects of only slight structural modifications, in this case, the presence and absence of voltage dependence for **1.45** and **1.46**, respectively. The β-barrel ion channels of Matile, as discussed in **Section 1.6**, have awesome potential. This self-assembly approach allows functional tunability from the molecular level. The ability to alter cation/anion selectivity by simply changing the pH (**1.44**) and to impart voltage dependence and/or membrane recognition properties by changing only a few atoms (**1.45** *versus* **1.46**) makes this design an attractive model for cell-specific drugs.

Davis. Throughout the synthetic cation and anion channel reviews, aspects of those studies that relate to the chloride transporters discussed in **Chapter 3** have been highlighted and compared. The Davis laboratory, in which the studies described in **Chapter 3** were conducted, is one of the six research groups to succeed in developing artificial anion channels. Calix[4]arene tetrabutylamide **3.1** and trimer **3.5** (**Chart 1.1**) are efficient transporters of chloride.[93,141] A channel mechanism has been confirmed for the assemblies of **3.1** in both planar bilayers and cells.[141] **Chapter 3** will discuss **3.1** and **3.5** in detail, and can be considered as the completion of this synthetic anion channel review.

1.7.3. Summary of Synthetic Anion Channels.

Table 1.2 provides a summary of synthetic anion channels listed by principle investigator (as this section was organized). The table lists the compound numbers, whether the channel is monomeric (M) or self-assembled (SA), whether the channel exhibited single or multiple conductance states (if reported), the voltage dependence (yes or no, if reported), comments specific to the channel(s), and the references. "NR" indicates that the property was not reported. The channels' anion specificity (e.g. $Cl^->Br^-$) is not indicated, since all but one of the channels described were tested for their ability to transport Cl^- and their selectivities within a series of anions were not reported. The exception is β-barrel **1.45** (see comments in **Table 1.2**).

Table 1.2. Summary of Synthetic Anion Channels.

Principle Investigator	Compounds	M or SA[a]	Conductance state(s)	Voltage dependence?	Comments	References
GlyR Group	M2GlyR **1.33**	SA	multiple	NR[b]	tetrameric and pentameric **1.33** aggregates	12
	C-K$_4$-M2GlyR **1.34**	SA	NR	NR	increased water solubility over **1.33**, induced Cl^- and fluid secretion from cells	170 171
	N-K$_4$-M2GlyR **1.35**	SA	multiple	NR	increased Cl^- currents over **1.34**, induced glutathione efflux from cells	173 174
	M2 **1.36**	SA	multiple	NR	**1.36/1.37** mixtures form hetero-oligomeric channels that mimic CFTR	13
	M6 **1.37**	SA	multiple	NR		13
Woolley	**1.38**	SA	multiple	NR	channels are **1.38** dimers and **1.38** trimers	179
Gokel	**1.39**	SA	single	yes	proposed active dimer	97 98 107

Table 1.2 Cont'd.

Principle Investigator	Compounds	M or SA[a]	Conductance state(s)	Voltage dependence?	Comments	References
Regen	**1.41**	SA	NR	NR	H^+/Cl^- symport, first synthetic Cl^- channel reported, DPPC/PG[c], recognizes negatively charged vesicles, mediates Cl^- transport across cystic fibrosis cells	184 185 16
Matile	**1.14**	SA	NR	yes	accelerates OH^- and/or Cl^- transport, also in **Table 1.1**	79
	1.42	SA	single	NR	β-barrel, proposed active hexamer, transports carboxyfluorescein, conducts in NaCl buffer	106
	1.44	SA	single	NR	β-barrel, cation selective at pH 6.0, anion selective at pH 4.0	186
	1.45	SA	multiple	yes	push-pull barrel, forms tetrameric barrels, anion specificity of $Cl^->F^->OAc^-$, recognizes polarized membranes	187 188
Davis	**3.1**	SA	multiple	yes	voltage dependence but no dipole, water may be involved in channel structure	141
	3.5	NR	NR	NR	~10-fold more potent Cl^- transporter than **3.1**, mechanism of transport unknown	93

a Monomeric (M) or self-assembled (SA) ion channel
b NR = not reported
c Support for channel mechanism from transport rates in DPPC and PG liposomes

1.8 Summary of Synthetic Ion Channels

To appreciate the successes of synthetic ion channel development, the goals stated in **Section 1.4** must be reiterated. Synthetic channels are intended to (1) increase the understanding of natural ion channels, (2) provide avenues to novel antimicrobials, and (3) to provide treatments for ion channel diseases. Each of these goals has been achieved to some extent, as was highlighted throughout this chapter. Synthetic cations channels are numerous, and the factors that affect their formation, selectivity and gating have been elucidated in many cases. The antimicrobial activity of several cation channel-forming compounds has been shown. Synthetic anion channels, however, are at the early stages of development. Despite the relatively few examples of anion channels, potential applications in cystic fibrosis treatment have already been realized. The results described in this thesis show progress in the development of synthetic molecules capable of cation (**Chapter 2**) and anion transport (**Chapter 3**).

Chapter 2. Calix[4]arene-Guanosine Conjugates

2.1 Introduction

The initial research goal of this thesis was to identify compounds that would form ion channels in lipid membranes. Calix[4]arene-guanosine conjugates were designed and prepared for this purpose. Indeed, conjugates cG **2.26** and cG **2.34** transported K^+ over Na^+ and Cs^+ in base pulse assays. Over the course of investigating these compounds, it was discovered that calix[4]arene-guanosine conjugate cG **2.34** formed a water-mediated dimeric assembly in organic solvents. The complex proved capable of extracting alkali halide salts from water into organic solvents. The self-assembled ion pair receptor formed from cG **2.34** is the major finding of research on calix[4]arene-guanosine conjugates presented in this chapter. Also in this study, a compound capable of forming ion channels in membranes, calix[4]arene tetrabutylamide **3.1**, was identified and will be introduced herein and discussed in detail in **Chapter 3**.

cG **2.26**   cG **2.34**
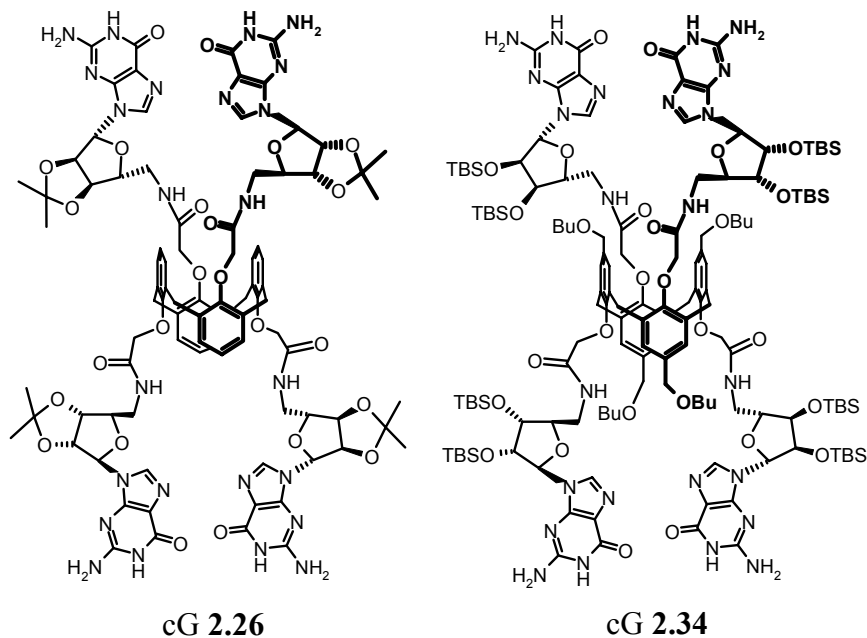
Calix[4]arene-guanosine cG **2.34** forms a water-mediated assembly that functions as an ion pair receptor, and thus water-mediated assembly (**Section 2.2**) and ditopic receptors (**Section 2.3**) will first be reviewed. The rationale for the design of calix[4]arene-guanosine conjugates will then be discussed (**Section 2.4**), followed by the self-assembling and ion transport properties of calix[4]arene-guanosine conjugate cG **2.26** (**Sections 2.5** and **2.6**). Finally, the self-assembled ditopic receptor formed from the more lipophilic conjugate cG **2.34** will be described (**Section 2.7**).

The rationale and results presented in **Sections 2.4.3** and **2.4.4** have been published in the *Journal of the Chemical Society, Chemical Communications*.[189] Much of the results described in **Section 2.7** have been submitted to the *Journal of the American Chemical Society*.[190] Part of the work presented was done in collaboration with Dr. Vladimir Sidorov, along with smaller contributions from other researchers. The contributions of Dr. Sidorov and others are credited in individual sections throughout the chapter.

2.2 Water-Mediated Assembly

2.2.1 Introduction

Calix[4]arene-guanosine conjugate **2.34** forms a water-mediated noncovalent ion pair receptor, and represents the major finding of studies on calix[4]arene-guanosine conjugates (**Section 2.7**). To put this work into the context of what has already been done in this growing area of supramolecular chemistry, **Sections 2.2.2** through **2.2.7** provide a review of water-mediated assemblies.

2.2.2 Water in Biomolecular Assemblies

Water, the solvent of life, constitutes much of the environment of biomolecules. The structure of proteins and nucleic acids is water dependent.[191-193] Not only does water serve to solvate biomolecules, but this ubiquitous solvent participates in specific interactions that modulate biomolecular structure and function.

The hydration of proteins has profound effects on their structure and function.[194,195] In the analysis of 56 protein X-ray crystal structures, including enzymes, antibodies, and

protein assemblies with various physiological functions, Tainer *et al*. found that "…deep grooves in protein surfaces consistently had the width of one water molecule."[196] From this analysis, the researchers concluded that water molecules, bound at specific sites, influence protein stability and activity. An example of water's influence on a structural transition is the oxygenation of hemoglobin. Approximately 60 water molecules bind to hemoglobin during the transition from its deoxygenated to oxygenated state.[197] Water has been shown to play a role in protein substrate recognition. Antigen-antibody association features a network of interfacial water and the recognition of specific DNA sequences by a restriction endonuclease is mediated by one or more water molecules.[198,199] Also, the activity of enzymes in organic solvents is due to retention of bound water by the enzymes.[200]

Water is critical in the stabilization of nucleic acid structure.[201,202] Duplex DNA retains a minor groove spine of hydration to alleviate the destabilizing effects of phosphate-phosphate repulsion.[203,204] A spine of hydration similarly stabilizes triplex and quadruplex DNA.[205,206] Hydration also affects how the major and minor grooves coordinate cations.[207]

In short, biomolecular assemblies are highly water-dependent. Nucleic acid structure and stability and protein structure, stability, activity, and specificity all depend on interactions with water.

2.2.3 Water in Supramolecular Assemblies: Hexameric Resorcinarene Assemblies

In contrast to water's role in biomolecular assemblies, water in synthetic supramolecular assemblies has been less appreciated, and until recently, unexplored. A report by Atwood *et al*. in 1997 spurred an interest in structural water among the molecular recognition community.[208] In this communication, Atwood demonstrated that calix[4]resorcinarene **2.1** (**Chart 2.1**) formed a hexameric capsule in both solution and the solid state (**Figure 2.1**).

Chart 2.1.

R	Resorcinarene
CH_3	**2.1**
$(CH_2)_{10}CH_3$	**2.2**
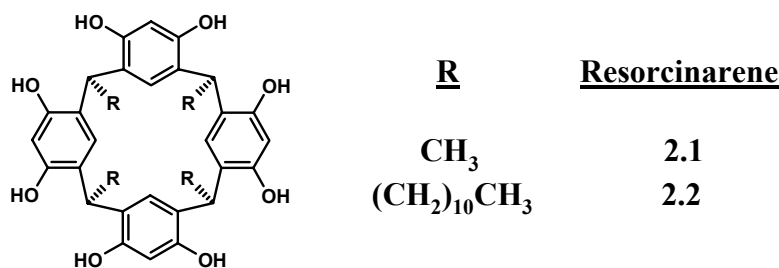
This capsule comprised six resorcinarenes and 8 water molecules. The $(2.1)_6 \cdot (H_2O)_8$ structure was held together by 60 hydrogen bonds between the resorcinarene phenolic OH groups and water, with each resorcinarene making up one face and each water positioned at a corner of a supramolecular cube.[208] The internal volume of the cube was approximately 1375 Å^3. The crystal structure of this assembly along with a simplified representation are shown in **Figure 2.1**.
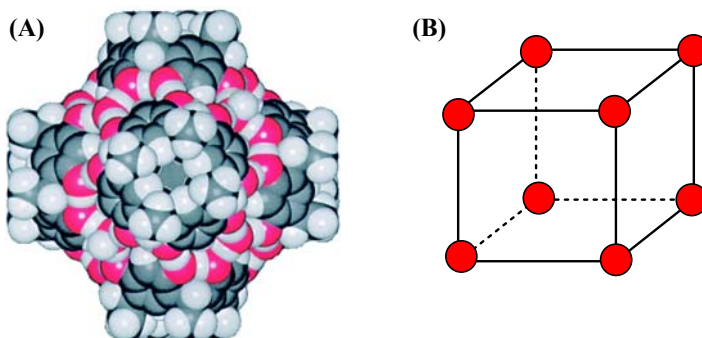
Figure 2.1. (A) X-ray crystal structure of Atwood's hydrogen-bonded cube: $(2.1)_6 \cdot (H_2O)_8$.[208] Colors represent oxygen (red), carbon (gray) and hydrogen (white). This figure was reprinted with permission from Nature Publishing Group. Copyright 1997 Nature. (B) Simplified representation of (A). Each face of the cube is a molecule of **2.1** and at each corner is a water molecule (red sphere).

The solution state structure of resorcinarene **2.2** (**Chart 2.1**), a more lipophilic derivative of **2.1**, has since been studied by a number of researchers. Rebek and coworkers were the first to report assemblies formed from **2.2**. Resorcinarene **2.2** was

insoluble in dry $CDCl_3$. In water-saturated $CDCl_3$, however, **2.2** formed hexameric capsules, similar to those formed by **2.1**, by hydrogen bonding to water molecules and encapsulating tetraalkylammonium, tetraalkylphosphonium, tetrabutylantimonium or tetraphenylantimonium guests.[209,210] For hexamers of **2.2** encapsulating Bu_4SbBr, $(2.2)_6 \cdot (H_2O)_8(Bu_4SbBr)$, other aromatic guests could be co-encapsulated, including benzene, propylbenzene, naphthalene and biphenyl.[210]

Avram and Cohen have studied the assembly of resorcinarene **2.2** by pulsed field gradient NMR (a technique described in **Section 2.7.7**). In contrast to Rebek's report, they showed that in $CDCl_3$, **2.2** assembled in the absence of a lipophilic cation guest, much like Atwood's resorcinarene **2.1**.[211,212] The $(2.2)_6 \cdot (H_2O)_8$ capsule instead contained several chloroform molecules. A later report by Shivanyuk and Rebek confirmed that a guest was not necessary for hexamer formation by **2.2**.[213]

Further investigation of the water- and guest-dependence of resorcinarene **2.2** capsules lead Avram and Cohen to another interesting finding. Unlike in the absence of an ammonium guest, where water is a crucial element of the assembly, a hexameric capsule formed with tetrahexylammonium (Hex_4N^+) as the guest excludes water. Water's participation is not critical with the large Hex_4N^+ in the core of the capsule.

Resorcinarene **2.2** hexameric capsules have also been shown to complex ferrocenium ions **2.3**$^+$. Philip and Kaifer showed that not only was the hexameric capsule $(2.2)_6 \cdot (H_2O)_8$ formed around **2.3**$^+$ upon electrochemical oxidation of ferrocene, but addition of **2.2** to ferrocene lowered its Fe^+/Fe oxidation potential due to the $(2.2)_6 \cdot (H_2O)_8$ assembly's ability to stabilize the cationic **2.3**$^+$.[214] This represents one potential application of resorcinarene water-mediated assemblies. The complex forms from **2.2** molecules and water, but can subsequently bind ferrocenium, and in doing so affect ferrocenium's electrochemical properties. The dimeric water-mediated assemblies formed from cG **2.34** (**Section 2.7**) behave in much the same way, i.e. first the dimers form from **2.34** and water and can then bind ion pairs.

2.3$^+$
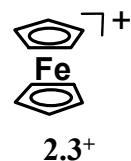
2.2.4 Water in Supramolecular Assemblies: Dimeric Assemblies

Following Atwood's report of the $(2.1)_6 \cdot (H_2O)_8$ hexamer, reports of similar resorcinarenes forming water-mediated dimers began to appear. Murayama and Aoki demonstrated that resorcinarene **2.3** (**Chart 2.2**) formed a dimer structure bridged by water.[215]

Chart 2.2.
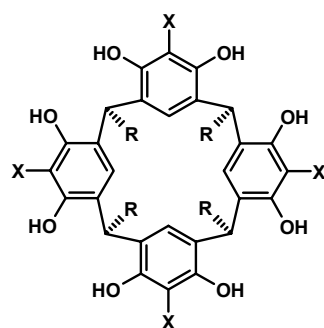
R	X	Resorcinarene
CH_2CH_3	H	2.3
CH_2CH_2Ph	H	2.4
$CH_2CH_2CH_3$	OH	2.5
$(CH_2)_{10}CH_3$	OH	2.6

As represented in **Figure 2.2**, resorcinarene **2.3** hydrogen bonds to 8 water molecules (one for each OH group in **2.3**) and encapsulates Et_4N^+ in a dimer cage in the solid state. Shivanyuk *et al.* showed that both **2.3** and **2.4** formed nearly identical water-bridged dimers in the solid state, but with Et_3NH-H_2O within the capsule.[216]

$\bullet$ = H_2O $\oplus$ = Et_4N^+
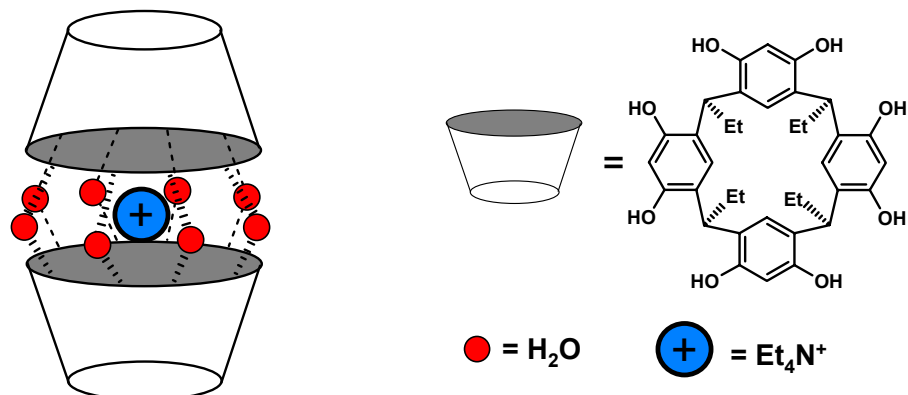
Figure 2.2. Representation of the $(2.3)_2 \cdot (H_2O)_8$ dimer encapsulating Et_4N^+.[215]

Hydroxyresorcinarene derivatives **2.5** and **2.6** (**Chart 2.2**) formed dimeric water-mediated encapsulation complexes with tropylium cations in methanol and 8:2 acetonitrile-water (polar protic media) and in the gas phase.[217] Also, a (**2.5**)$_2$ water-containing dimer was formed in the solid state by incorporating H_2O and CH_3CN solvent molecules.

A rare example of a water-mediated dimeric assembly that did *not* involve a resorcinarene derivative was reported by Habata *et al*. The researchers demonstrated that pyridine-ethylene glycol **2.7** formed dimers, with one water molecule per molecule of **2.7**, as shown in **Figure 2.3**.[218] The structure exists in the gas and solution phases and in the solid state.
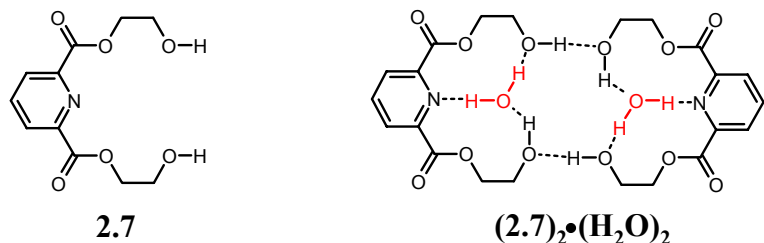
2.7   (**2.7**)$_2$•(H_2O)$_2$

Figure 2.3. Pyridine-ethylene glycol **2.7** (left) and the (**2.7**)$_2$•(H_2O)$_2$ dimer (right).[218]

2.2.5 Water in Unimolecular Receptors

There have been two reports of specific water interactions fixing a productive conformation for unimolecular receptors. Arena *et al*. reported that a single water molecule serves to "clip" the phenolate oxygens, thus fixing the conformation of receptor **2.8**. The fixed conformation enhanced its selectivity for binding the aromatic ring of trimethylanilinium over the -N(CH$_3$)$_3^+$ group (**Figure 2.4**).[219]

2.8•H₂O•TMA
observed

2.8•H₂O•TMA
not observed
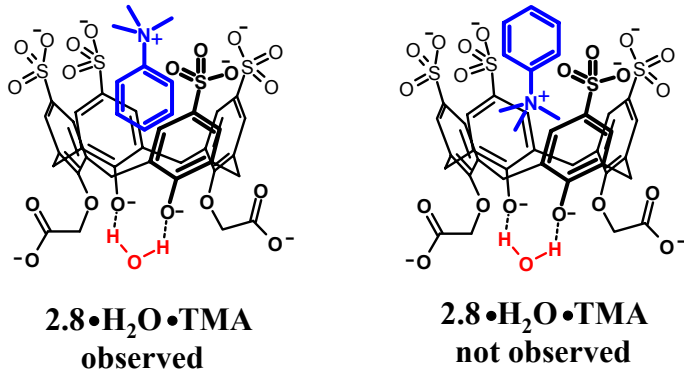
Figure 2.4. Anilinium receptor **2.8•H₂O** with trimethylanilinium (TMA) bound by the aromatic ring (left) and -N(CH$_3$)$_3$$^+$ (right) groups. Only binding of the aromatic ring was observed.[219]

Rebek also demonstrated that water fixes a productive conformation for unimolecular receptor **2.9**.[220] In dry CDCl$_3$, **2.9** was insoluble. In water saturated CDCl$_3$, however, the compound dissolved, with each molecule of **2.9** binding 4 H$_2$O molecules at it's upper rim (**Figure 2.5**). Once formed, the **2.9•(H₂O)₄** receptor was capable of complexing tetramethylphosphonium and triethylammonium cations in its cavity.

2.9
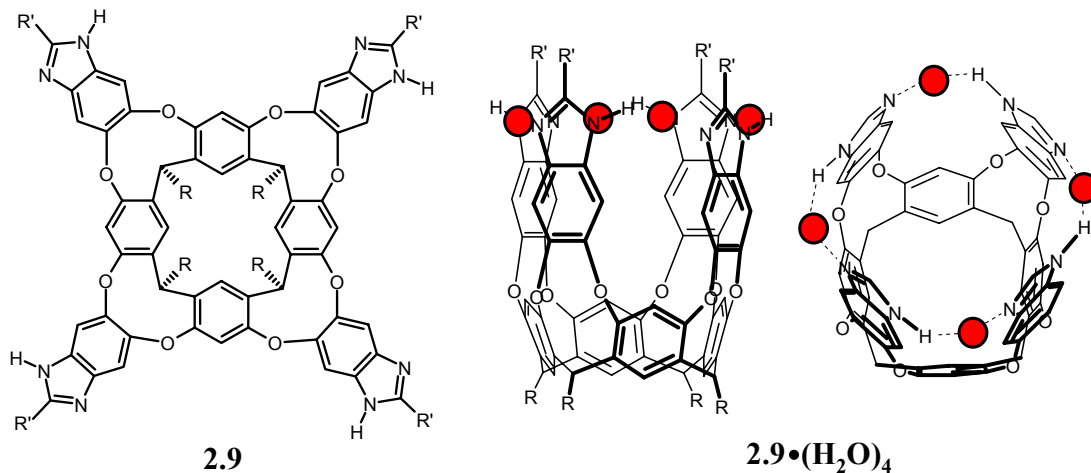
2.9•(H₂O)₄

Figure 2.5. Rebek's resorcinarene **2.9** (left) and representations of receptor **2.9•(H₂O)₄** viewed from the side (middle) and the top (right, R and R' removed).[220] R = (CH$_2$)$_{10}$CH$_3$, R' = H, CH$_3$, or Ph, and red circles represent H$_2$O.

2.2.6 Water-Stabilized Tubular Architectures

Tubular structures stabilized by ligand-water interactions represent elegant examples of potentially functional architectures. The Martin group has demonstrated that **2.10** forms a hexameric ring in the solid state comprising alternating (+)-**2.10** and (-)-**2.10** enantiomers (**Figure 2.6**).[221,222] The (**2.10**)$_6$ hexamer is held together by hydrogen bonding between the alcohol and carboxylate groups (**Figure 2.6**, middle). Hexameric rings further stack through hydrogen bonding to water molecules to form a tubular structure, shown at the right in **Figure 2.6**, with six water molecules per hexamer. Compounds (±)-**2.10** facilitated transport of Na$^+$ across a lipid bilayer as monitored by ^{23}Na NMR.[221] The [(**2.10**)$_6$(H$_2$O)$_6$]$_n$ tube was hypothesized to be the active transporter, functioning as an ion channel.

2.10
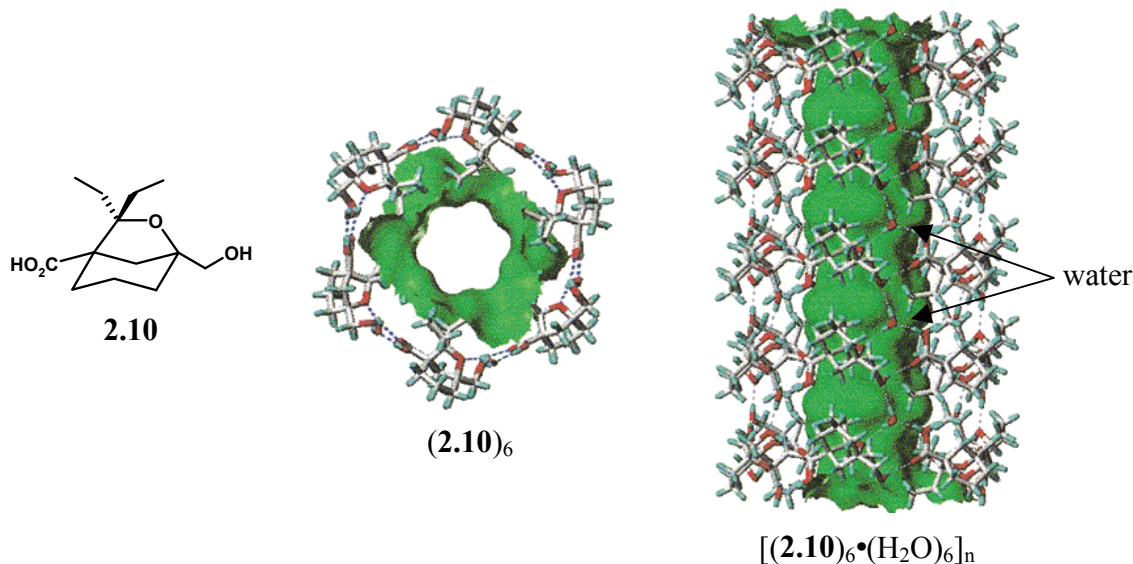
(**2.10**)$_6$

[(**2.10**)$_6$•(H$_2$O)$_6$]$_n$

Figure 2.6. Structure of **2.10** (left), hydrogen-bonded hexamer (**2.10**)$_6$ (middle), and the [(**2.10**)$_6$•(H$_2$O)$_6$]$_n$ tube (right), with water molecules indicated.[221] The channel's internal hydrophobic surface is shown in green. This figure was reprinted with permission from *Organic Letters* and the authors. Copyright 2000 American Chemical Society.

Calix[4]hydroquinone **2.11** formed tubular assemblies with water in the solid state (**Figure 2.7**).[223] Unlike in $[(\mathbf{2.10})_6{\bullet}(H_2O)_6]_n$ where H_2O hydrogen bonded between **2.10** molecules and remained at the periphery of the tube, the $(\mathbf{2.11})_n{\bullet}(H_2O)_m$ tube contained water in the interior. The water-filled channel was proposed as a model for water and ion channels in biological systems.
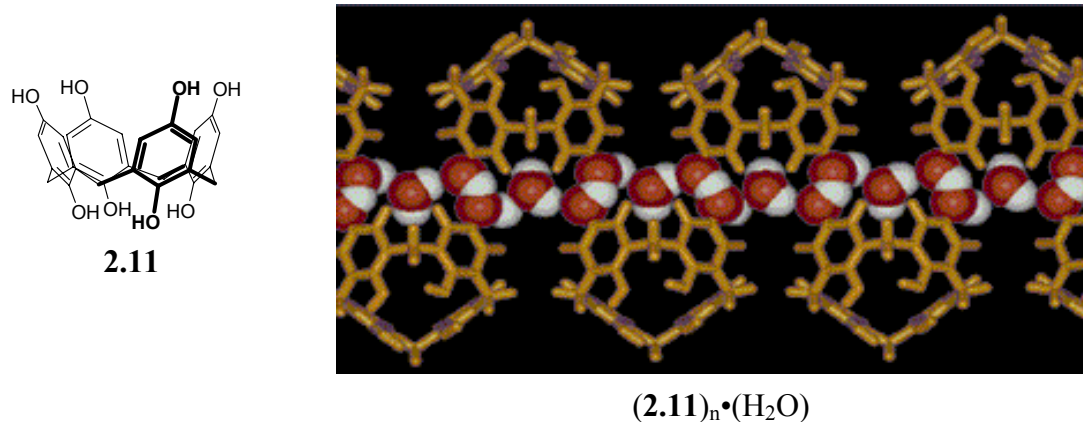
$(\mathbf{2.11})_n{\bullet}(H_2O)$

Figure 2.7. Structure of **2.11** (left) and the $(\mathbf{2.11})_n{\bullet}(H_2O)_m$ tube from the X-ray crystal structure (right).[223] Oxygen and hydrogen atoms of water molecules are shown in red and white, respectively, and molecules of **2.11** are shown in gold. This figure was reprinted with permission from the *Journal of the American Chemical Society* and the authors. Copyright 2001 American Chemical Society.

2.2.7 Summary of Water-Mediated Assembly and Relevance to this Thesis

Examples of water participating directly in supramolecular assemblies are still rare, but the assemblies presented in this section illustrate the potential of this solvent in stabilizing hydrogen-bonded architectures. Atwood's $(\mathbf{2.1})_6{\bullet}(H_2O)_8$ cube was proposed to have applications in catalysis by functioning as a microreactor, in drug delivery and for separations.[208] The $(\mathbf{2.2})_6{\bullet}(H_2O)_8$ cube lowered the redox potential of ferrocene by stabilizing the ferrocenium cation, thus opening the door to electrochemical applications.[214] Water stabilized tubes represent potential water and ion channel structures.[221,223] The $[(\mathbf{2.10})_6{\bullet}(H_2O)_6]_n$ tube has already demonstrated Na^+-transport ability and has shown potential as a porous material for the sorption of N_2 and argon. The

involvement of water in supramolecular systems is likely to become more well recognized and yield new structures with interesting properties.

One key aspect of this thesis is the role of water in mediating functional supramolecular assemblies. In **Section 2.7**, the water-mediated assembly of cG **2.34** leads to a self-assembled ion pair receptor, having both a cation and an anion binding site brought together via formation of the (cG **2.34**)•$(H_2O)_n$ dimer. Evidence for water's direct participation in the structure of ion channels formed from calix[4]arene tetrabutylamide **3.1** will be discussed in **Chapter 3**.

Since the (cG **2.34**)•$(H_2O)_n$ assembly functions as a ion pair (ditopic) receptor, **Section 2.3** is dedicated to reviewing ditopic receptors. In this way, the results of **Section 2.7** can be viewed in the context of previously reported ditopic receptors, particularly those that are formed through self-assembly.

2.3 Synthetic Ditopic Receptors.

2.3.1 Ditopic Receptors: The Basics

Ditopic recognition is the simultaneous complexation of two separate substrates or two separate binding sites on a single substrate by a receptor. Receptors that can accomplish this task contain two binding sites and are termed ditopic receptors. A ditopic receptor may comprise a single molecule or several molecules held together through noncovalent interactions (a self-assembled ditopic receptor). The two binding sites that interact with the substrate(s) can be identical (a homo-ditopic receptor) or different (a hetero-ditopic receptor). Schematic representations of a hetero-ditopic receptor binding two separate substrates and to a single substrate are shown in **Scheme 2.1** (A and B, respectively).

Scheme 2.1. Schematic representation of a ditopic receptor binding (A) two substrates and (B) a single substrate through two interactions.
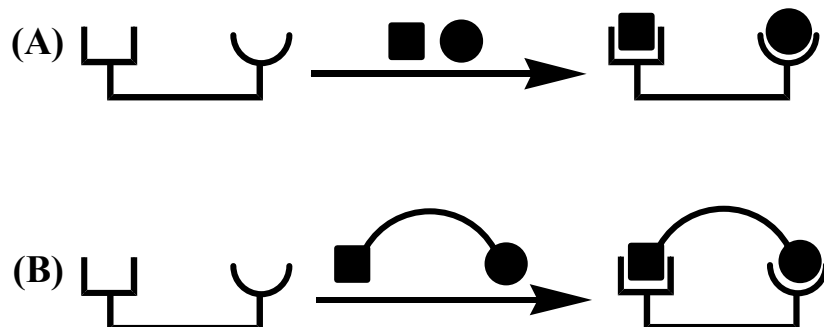
The pioneering efforts of Schmidtchen toward the binding of zwitterionic species will be described to illustrate ditopic recognition.[224] Schmidtchen's receptor **2.12** was capable of binding γ-aminobutyric acid (GABA) in protic solvents. As shown in **Scheme 2.2**, the ammonium and carboxylate groups of GABA complexed to the aza-crown and macrotricyclic quaternary ammonium moieties of **2.12**, respectively. Receptor **2.12** is an example of a hetero-ditopic receptor that binds a single substrate through two interactions (**Scheme 2.1B**). The interactions combined make binding enthalpically favorable even in 9:1 methanol:water, demonstrating one advantage of ditopic recognition; favorable binding energy can be achieved through multiple interactions with the substrate.

Scheme 2.2 Complexation of GABA by Schmidtchen's receptor **2.12**.[224]

2.12

$X = (CH_2)_6$
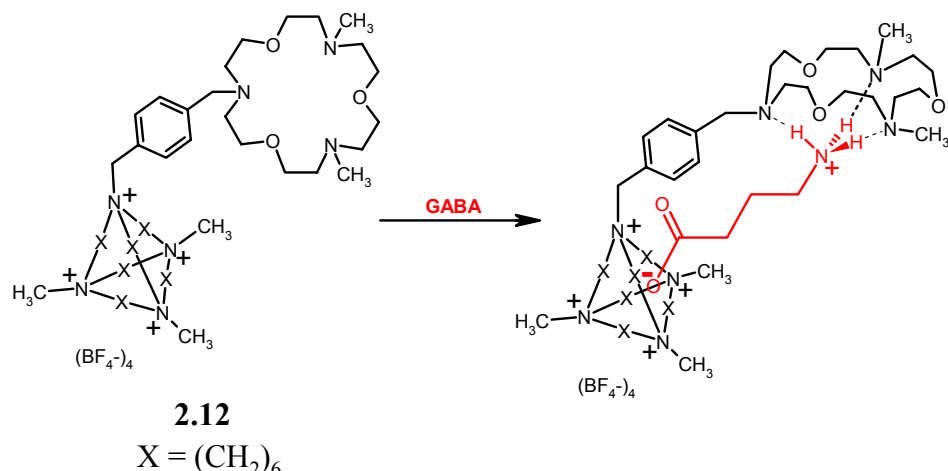
The next two sections will provide an overview of ditopic receptors. **Section 2.3.2** will discuss covalent ditopic receptors, i.e. receptors comprising a single molecule. All receptors in this section are hetero-ditopic receptors designed for zwitterion or ion pair recognition. **Section 2.3.3** will highlight self-assembled ditopic receptors, i.e. receptors held together by noncovalent interactions. Both ion pair receptors and other ditopic receptors will be described. Ultimately, this section is intended to provide an introduction for the self-assembled ditopic receptor formed from calix[4]arene-guanosine cG **2.34** (**Section 2.6**).

2.3.2 Unimolecular Ditopic Receptors

The study of ion recognition began in 1967, with Pedersen's discovery of the crown ethers.[225] Since then, a multitude of receptors for cations has been reported.[226] Over the last 20 years, anion binding has also received significant attention.[227] In contrast to the recognition of single ions by monovalent receptors, ion pair recognition is still in its infancy.[228]

The simultaneous recognition of ion pairs is a burgeoning area of ditopic recognition.[228] There are several practical applications of such salt binding systems. The cotransport of ion pairs across lipophilic membranes by ditopic receptors can mimic biological functions.[92] Complexation of zwitterionic amino acids has shown promise in enantioselective recognition and amino acid transport, demonstrating potential applications to chiral separations and drug delivery.[229,230] Ion pair binding has been exploited for catalysis in organic solvents.[231,232] Furthermore, simultaneous recognition of cation-anion couples has potential in the extraction of toxic metal ions from aqueous into organic media. With potential impact on the fields of medicine, separations and catalysis, ion pair receptors will likely continue to gain the interest of researchers and new receptor designs and applications will be discovered.

As discussed in **Section 2.3.1**, Schmidtchen was responsible for the pioneering efforts in ditopic recognition (**Scheme 2.2**).[224] Work by de Mendoza *et al*. provided receptor **2.13** for the enantioselective recognition of L-tryptophan.[229] In **2.13**, the aza-18-crown-6 moiety serves to bind the ammonium group of L-Trp while the guanidinium group

hydrogen bonds to the carboxylate. Sessler and Andrievsky took an approach similar to that of Schmidtchen and de Mendoza in the development of amino acid transporters.[230]

2.13•(L-Trp)
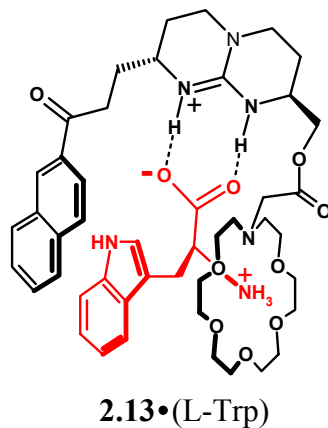
An early example of a ditopic receptor for ion pairs was reported by Reetz *et al.*[233] The researchers synthesized receptor **2.14** (**Chart 2.3**) comprising a crown ether covalently linked to a boron catecholate. Receptor **2.14** complexed KF, binding K^+ with the crown ether through ion-dipole interactions and F^- to its Lewis-acidic boron center via a coordinate bond. A similar receptor, but with Me_3Al in place of the boron catecholate, was selective for LiCl.[234]

Chart 2.3

2.14   **2.15**   **2.16**
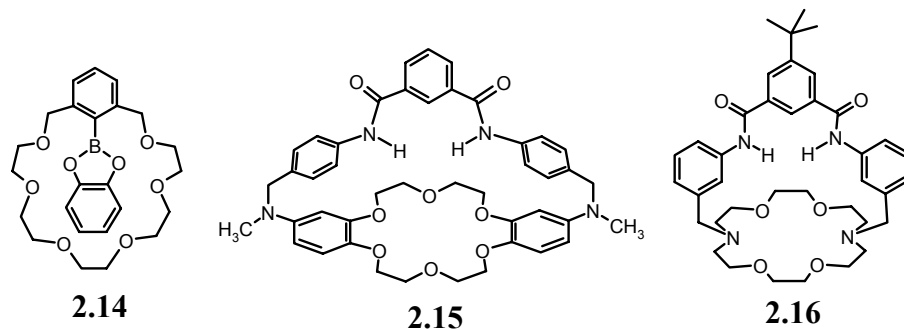
Smith *et al*. developed receptors **2.15** and **2.16** (**Chart 2.3**). Receptor **2.15** bound KCl and NaCl, with Cl^- binding being enhanced by cation complexation to the crown.[235] The salt was bound to **2.15** as a solvent separated ion pair. By reducing the distance between the anion and cation binding sites, receptor **2.16** bound KCl or NaCl as a contact ion

pair.[236] In this case, K$^+$-binding strongly enhanced the Cl$^-$-complexing ability of **2.16**, whereas Na$^+$ had little effect. This is in contrast to **2.15**, where K$^+$ and Na$^+$ had nearly identical cooperative effects on anion binding. **Figure 2.8** shows the X-ray crystal structures for **2.15**•NaCl•CHCl$_3$ and **2.16**•NaCl (A and B, respectively). The structures clearly show that Cl$^-$ is coordinated to the amide NH groups through hydrogen bonding and Na$^+$ to the crown ether through ion-dipole interactions. Receptor **2.15** binds the salt with one molecule of CHCl$_3$ between the ion pair (solvent-separated), while **2.16** binds the salt as a contact ion pair.

(A) 2.15•NaCl•CHCl$_3$ **(B) 2.16•NaCl**
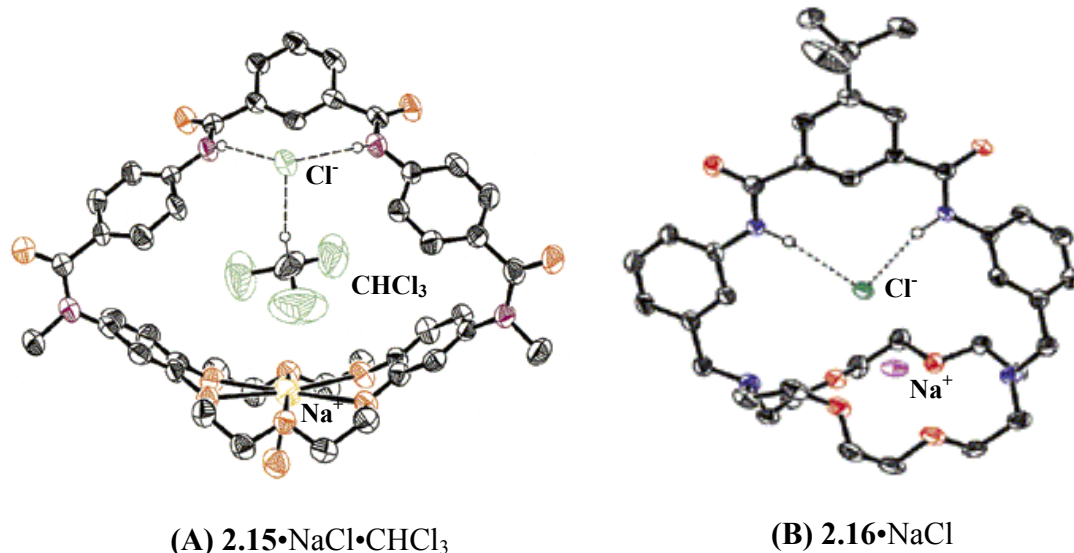
Figure 2.8. X-ray crystal structures of (A) **2.15**•NaCl•CHCl$_3$ and (B) **2.16**•NaCl.[235,236] These figures were reprinted with permission from the *Journal of the American Chemical Society* and the authors. Copyright 2000 American Chemical Society, Copyright 2001 American Chemical Society.

Significant contributions to the area of ditopic recognition have been made by Reinhoudt *et al.* With the combined knowledge that a UO$_2^+$-containing receptor selectively bound H$_2$PO$_4^-$ and benzo-15-crown-5 forms a sandwich complex with K$^+$, the researchers synthesized receptor **2.17**, comprising both anion- and cation-binding

functionalities.[237-239] Indeed, receptor **2.17** (**Chart 2.4**) was selective for KH_2PO_4.
Replacing the two crown ethers with a single Cs^+-selective calix[4]arene-crown ether
provided the CsCl receptor and transporter **2.18** (**Chart 2.4**).[240] A small molecule receptor
reported by Nishizawa *et al.* demonstrated ion pair binding cooperativity.[241] With Na^+
bound to the 15-crown-5 moiety of receptor **2.19**, an increased affinity for NO_3^-, Br^-, and
I^- binding to the thiourea group was observed (**Chart 2.4**, shown with NaBr bound).

Chart 2.4

2.17

2.18
$X = (CH_2)_4$

2.19•NaBr
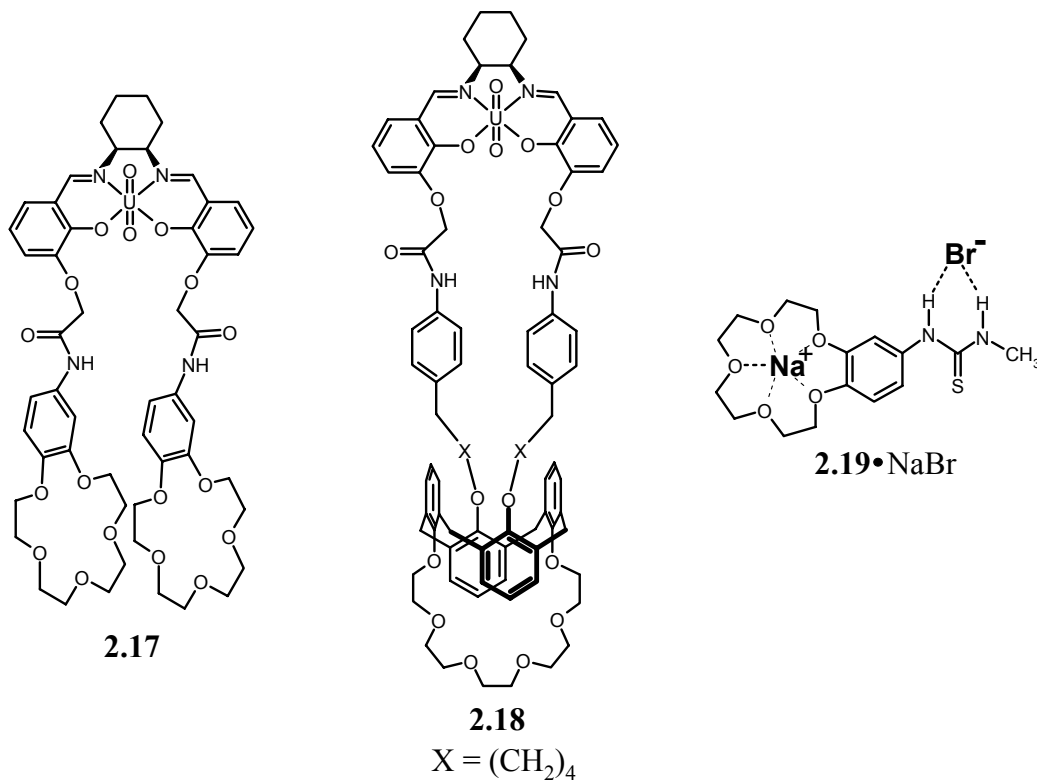
Receptor **2.20**, also reported by the Reinhoudt group, was shown to bind NaX (X =
Cl^-, Br^-). As shown in **Scheme 2.2**, calixarene **2.20** adopted a pinched conformation due
to hydrogen bonding between the urea groups in $CDCl_3$, thus precluding anion binding.[242]
Upon addition of Na^+, cation binding to the lower rim esters causes a conformational
change that breaks the upper rim hydrogen bonds. An anion (Cl^- or Br^-) is then bound to
the urea groups. In the absence of Na^+, no anion binding was observed.

95

Scheme 2.3 Reinhoudt's NaX Receptor.[242]

2.20
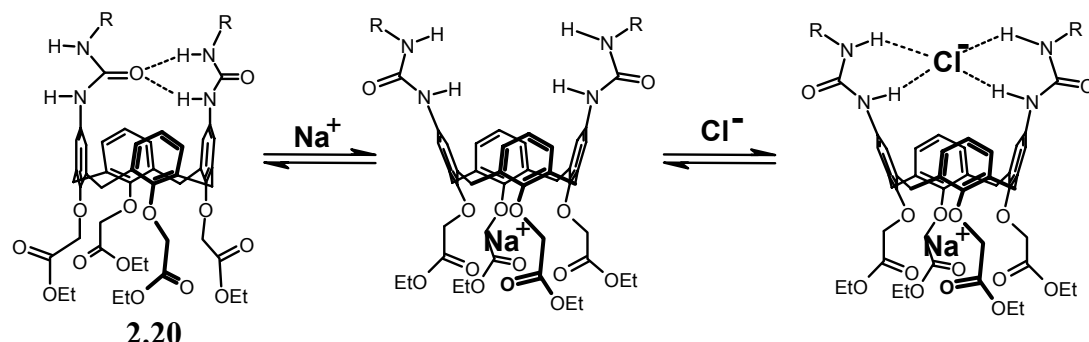
The approach of Beer *et al.* towards ion pair recognition utilized a rhenium-bipyridyl backbone. The bipyridyl moiety in receptor **2.21** extended two arms, each containing two amides and a crown ether for anion and cation binding respectively.[243] Receptor **2.21** displayed a unique property: cation binding to **2.21** altered the anion selectivity. In the absence of a cation, the receptor was selective for $H_2PO_4^-$ over Cl^-. After binding of K^+ as a sandwich complex between the two crown ethers, the selectivity switched to favor Cl^- binding to the now more proximal amides.

2.21•KCl
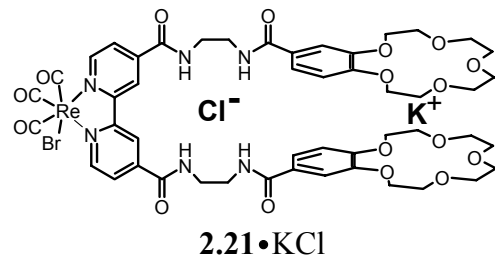
The examples presented in this section were selected to answer one question: What is necessary to bind an ion pair? First, an ion pair receptor must contain both a cation and anion binding site. For the receptors discussed, the two binding sites are connected through covalent bonds (although this is not always the case, as will be described in **Section 2.3.3**). The positioning of the binding sites is critical, and is one of the challenges in ion pair receptor design. Smith stated: "The invention of heteroditopic hosts is a challenging problem in molecular recognition because the binding sites have to be incorporated into a suitably preorganized scaffold that holds them in close proximity, but

not so close that the sites interact."[235] Also, ion binding to one site must not prevent binding at the other site. In some cases, binding at one site can enhance binding or change the selectivity at the other site. For example, the precise positioning of the anion and cation binding sites in receptors **2.15** and **2.16** resulted in binding of solvent-separated and contact ion pairs, respectively.

Cation coordination is mainly accomplished through ion-dipole interactions. The most widely used functionalities are crown ethers that complex cations through coordination of the positively charged center by oxygen lone pairs. By using crown ethers, researchers can modulate the cation selectivity (e.g. Li^+ *versus* Na^+) by simply changing the size of the crown incorporated. The only receptor described that does not contain a crown ether is Reinhoudt's receptor **2.20**, which binds Na^+ through coordination to carbonyl oxygens. Nevertheless, oxygen serves as a universal cation ligand.

Anion binding sites demonstrate more functional variety. Lewis acid groups (B, Al) were exploited by Reetz *et al*. In those receptors, the anion coordinated to the Lewis acidic centers through ion-dipole interactions. Hydrogen bond donor groups are more commonly utilized in anion binding. Four different H-bond donors appeared in the examples presented: (1) guanidinium-receptor **2.13**, (2) amide-receptors **2.15**, **2.16**, **2.21**, (3) urea-receptor **2.20**, and (4) thiourea-receptor **2.19**. In all cases, the anion was bound to the receptor through hydrogen bonding to the donors. Hydrogen bonding is directional, and when the H-bond donors are properly positioned, this directionality can be an advantage. This was the case with Smith's receptor **2.16**, which binds NaCl or KCl as a contact ion pair. Lastly, direct ion-ion interactions serve to bind anions. Schmidtchen's receptor **2.12** contained a tetra-ammonium tricycle that bound the carboxylate of GABA through ion-ion interactions.

This section was intended to provide an overview of ion pair receptors, and not thoroughly review the topic. Excellent reviews on ditopic receptors have been written by Reetz and Sessler *et al*.[228,244] In addition, the topic has been highlighted in reviews by Antonisse and Reinhoudt and by Beer and Gale.[227,245]

97

2.3.3 Self-Assembled Ditopic Receptors

Examples of self-assembled ditopic receptors are rare, and such receptors can indeed be a challenge to develop. The interactions that bind cations and anions to a multisite receptor (e.g. hydrogen bonding, Lewis acid-Lewis base interactions, ion dipole interactions) are the same interactions that hold together self-assembled complexes. This presents a problem, since interactions intended to hold the receptor together may instead be directed toward the ionic guests, and *vice versa*. To overcome this, the assembled receptor must be glued together by interactions that either will not be interfered with by ionic guests or be highly specific toward the intended partner such that the interaction will not be misdirected.

The molecular boxes of Gokel represent an early example of ditopic binding by an assembled receptor.[246] By bringing together two crown ether molecules, one bearing two thymine (T) bases and the other two adenine (A) bases, molecular box **2.22** is formed through Watson-Crick hydrogen bonding. The receptor can bind alkyl-bis-ammonium salts by complexation of the terminal ammonium groups to the crown ethers in **2.22** (**Chart 2.5**). This is an example of a self-assembled homo-ditopic receptor, since the binding sites are identical and complex the same ammonium moiety. Also, **2.22** demonstrates how hydrogen bonding interactions hold the assembly together (A-T pair) and do not interact with the di-ammonium substrate (a strong H-bond donor).

Chart 2.5

2.22•(H$_3$N$^+$-R-NH$_3^+$)
2.23•(Ar-CO$_2^-$)
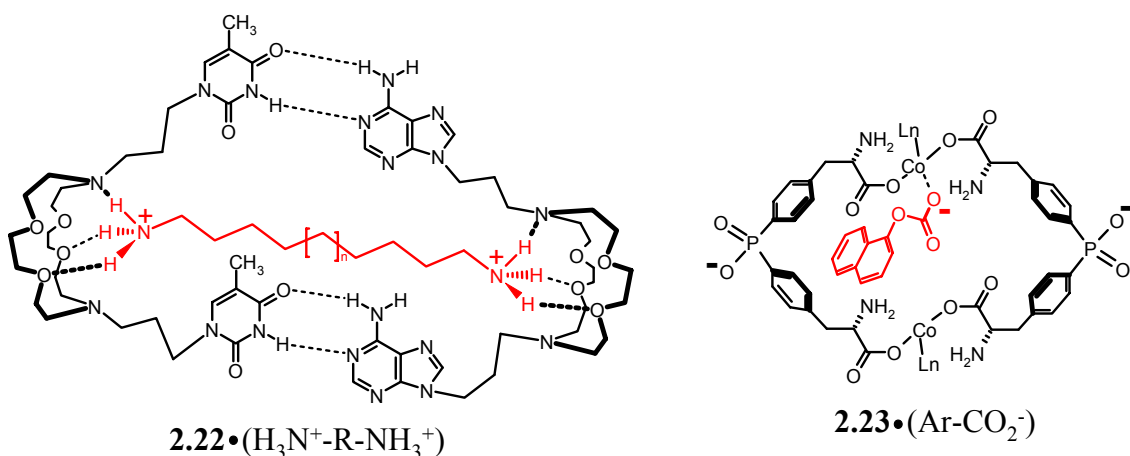
Schwabacher *et al.* reported ditopic receptor **2.23** which is assembled through coordination bonds between amino acid carbonyl groups and Co(II) (**Chart 2.5**). The receptor, once assembled, has a hydrophobic interior, and was shown to transport aromatic hydrocarbons through a bulk aqueous membrane.[247] Receptor **2.23** proved capable of binding indole- and anthracene-containing carboxylates by simultaneous coordination of the anionic oxygen to the metal center and insertion of the aromatic moiety into the hydrophobic pocket.[248]

As for self-assembled ion pair receptors, only two such structures have been reported. The Davis group's efforts in the study of lipophilic guanosine quadruplexes demonstrated such a receptor.[249] As will be described in **Section 2.4.2**, guanosine **2.25** assembles into a hexadecamer in the presence of mono- and divalent cations. The counter anion (typically a phenolate) coordinates to amino NH groups that are brought in close proximity by the nature of the cation-directed assembly (see **Figure 2.10C**). Thus, through self-assembly, the lipophilic G-quadruplex forms both cation and anion binding sites, and binds cations such as Na^+, K^+, Pb^{2+}, and Ba^{2+}, and lipophilic anions, such as picrate. The other example of a self-assembled receptor for ion pairs was reported by Severin *et al.*[250] Severin's approach utilized coordination bonds to form ruthenium metallomacrocycle **2.24** (**Figure 2.9A**), which selectively extracted LiCl from water into CH_2Cl_2 with >1000:1 Li^+:Na^+ selectivity. The **2.24**•LiCl crystal structure (**Figure 2.9B**) shows that the Li^+ coordinates to the three oxygen atoms in the macrocycle's interior, and Cl^- is held in contact with the cation and is also coordinated by three aryl-H⋯Cl^- hydrogen bonds.

(A)

2.24

(B)

Cl⁻

Li⁺
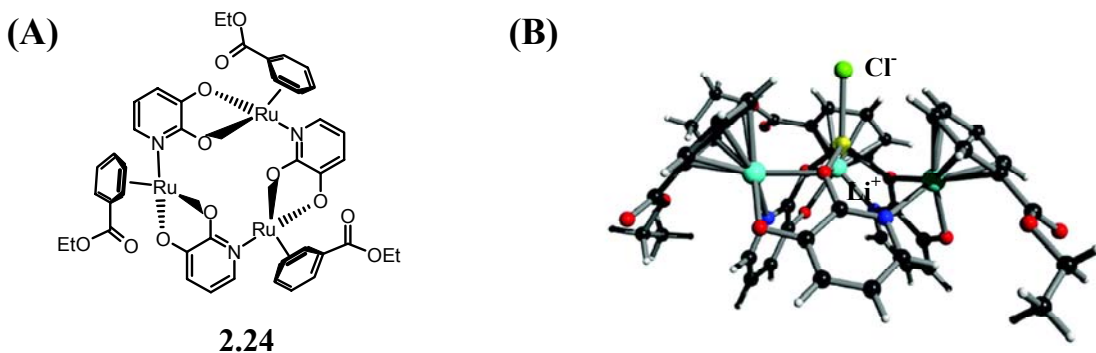
Figure 2.9. (A) Structure of receptor **2.24** and (B) crystal structure of **2.24**•LiCl.[250] This figure was reprinted with permission from Proceedings of the National Academy of Sciences, U. S. A. and the authors. Copyright 2002 National Academy of Sciences, U. S. A.

Self-assembled ditopic receptors have requirements similar to covalent receptors, with the exception that the active receptor's structure is held together by noncovalent interactions. Two binding sites are still necessary, whether they be two crown ether rings (**2.22**), a hydrophobic pocket coupled to a metal anion coordination site (**2.23**), a central ring of oxygens and outwardly directed amino protons (G **2.25** quadruplex), or an oxygen-rich core coincident with electron poor aromatic rings capable of providing Ar-H⋯anion interactions (**2.24**). The self-assembled ion pair receptor formed through water-mediated dimerization of calix[4]arene-guanosine cG **2.34** (**Section 2.7**) contains both cation and anion binding sites. An intermolecular guanosine quartet at the dimer's core provides a central ring of oxygens (as in the G **2.25** quadruplex). Amide NH groups in close proximity to the guanosine quartet coordinate anions. Much like the self-assembled receptors discussed in this section, the binding sites within the (cG **2.34**)$_2$(H$_2$O)$_n$ complex are brought together through noncovalent interactions.

2.4 Calixarene-Guanosine Conjugates: Rationale

2.4.1 Introduction.

From the Davis group's work with lipophilic guanosine quadruplexes came an inspiration to develop artificial ion channels based on this supramolecular structure.[251] This section outlines how the calix[4]arene-guanosine conjugate design was developed, starting with a description of lipophilic guanosine quadruplexes.

2.4.2 Lipophilic G-quadruplexes.

Guanosine has a unique property among the DNA bases as it can form a quartet structure through hydrogen bonding and metal cation coordination.[252] The G-quartet forms because guanosine possesses two hydrogen bond donors (N1-H and N2-H) and two hydrogen bond acceptors (O6 and N7), with the angle between the donors and acceptors being 90°, as shown in **Figure 2.10A**. The G-quartet has four center-pointed carbonyl groups (O6), which endow this assembly with its cation-binding ability.
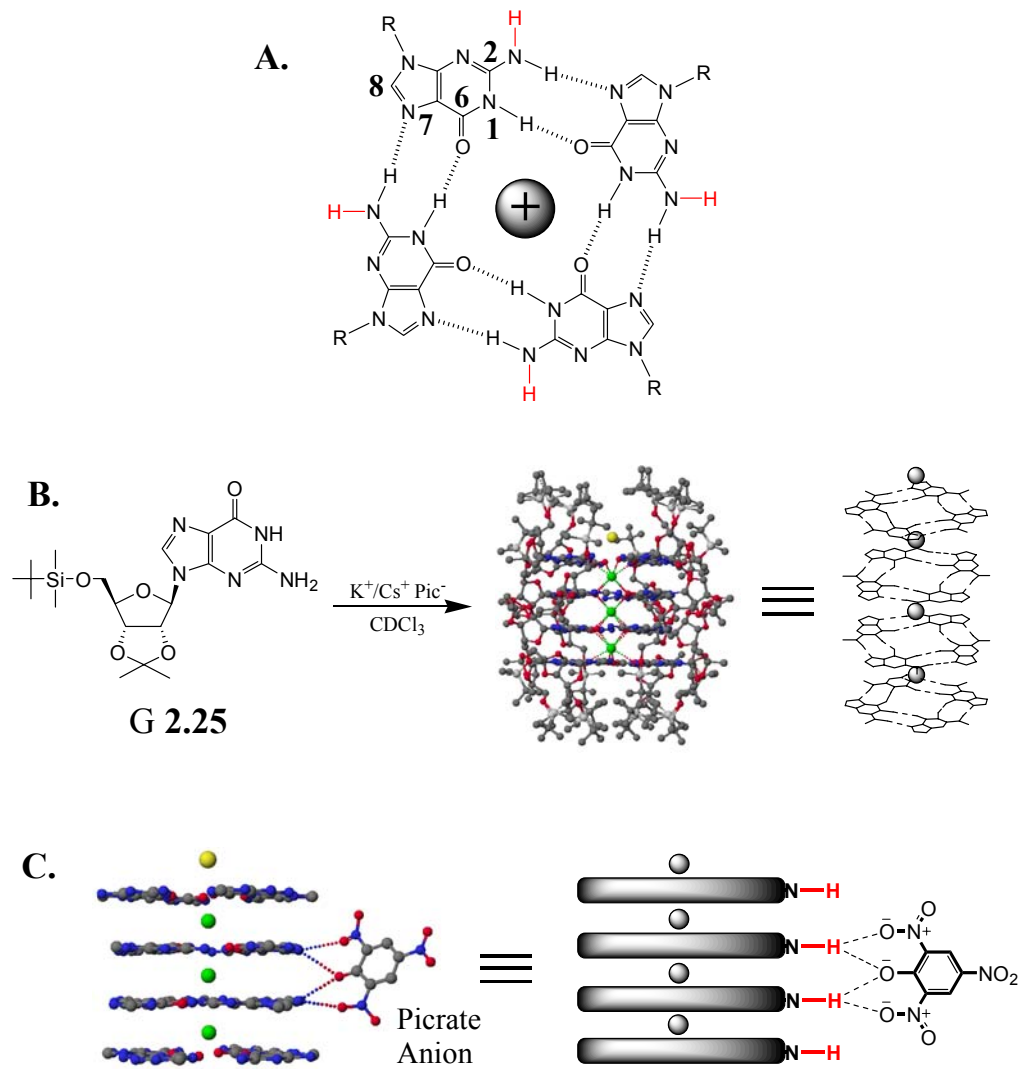
Figure 2.10. (A) The hydrogen-bonded, metal-templated G-quartet (R= ribose). (B) Assembly of lipophilic guanosine quadruplexes from guanosine **2.25**. (C) Crystal structure (left) showing only guanine bases and schematic (right) showing the anion binding site formed through self-assembly. Hydrogens that coordinate the picrate anion upon self-assembly are shown in red in (A) and (C). K^+: green spheres, Cs^+: yellow spheres, C: gray, N: blue, O: red.[251]

The lipophilic guanosine **2.25** forms a quadruplex structure in the presence of monovalent or divalent cation salts in organic solvents and in the solid state.[249,251,253,254] As shown in **Figure 2.10B**, the K^+/Cs^+ structure comprises four stacked G-quartets (in π-stacking distance) with cations residing in between the quartet layers, coordinating to the guanosine carbonyl oxygens.[251] The counter anions coordinate to the central quartets through hydrogen bonding to N2-amino protons, thus holding the two "octamers" together (**Figure 2.10C**).

2.4.3 Nucleoside Numbering Conventions.

The accepted numbering conventions of the guanosine and adenosine nucleosides will be used often in **Sections 2.5-2.7**. **Figure 2.11** shows these conventions. In the formation of the G-quartet, guanosine's N1-H and N2-H hydrogen bond to the O6 and N7 of the adjacent base (see **Figure 2.10A**). The ribose ring is numbered independently by placing a prime (') after the number. For example, the calix[4]arene-guanosine conjugates described in this chapter were synthesized by converting the 5'-OH to a $5'-NH_2$, and then linking the nucleoside to the calix[4]arene through the $5'-NH_2$.
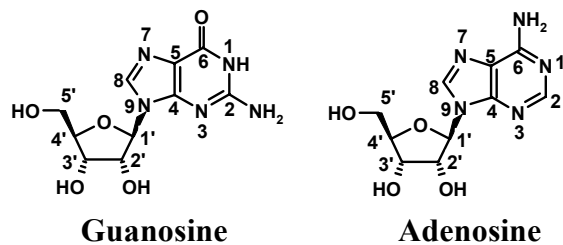
Figure 2.11. Numbering conventions for guanosine and adenosine.

2.4.4 Rationale for the Design of Calix[4]arene-Guanosine Conjugates.

The impetus for synthesizing the first calix[4]arene-guanosine conjugate cG **2.26** was to find a molecule capable of forming self-assembled ion channels. From work in the Davis group on lipophilic G-quadruplexes, much experience in studying assemblies based on the cation-templated G-quartet had been gained. The lipophilic G-quadruplexes, like the K^+/Cs^+ quadruplex shown in **Figure 2.10**, have a cation "channel" through the

core, and seemed at first glance to be prime candidates for artificial ion channel structures. In fact, the Davis group's first report describing such a G-quadruplex was entitled "Toward Artificial Ion Channels: A Lipophilic G-Quadruplex".[251] The quadruplex, however, comprises 24 components; sixteen guanosines, four cations, and four anions. An ion channel should be active in a lipid membrane. As such, 24 components would need to come together within the membrane resulting in a tremendous entropic penalty. Indeed, ion transport experiments provided evidence that G **2.25** was inactive in liposomal membranes.

Keeping the G-quartet as a central motif, the goal was to append guanosine to a scaffold from which it could form quartet structures by hydrogen bonding with neighboring monomers. By placing two guanosines on one side of the scaffold and two on the other, the G-bases would be well positioned to form intermolecular quartets. The chosen scaffold was the calix[4]arene 1,3-*alternate*, and calix[4]arene-guanosine conjugate cG **2.26** became the target for initial study.[255,256]
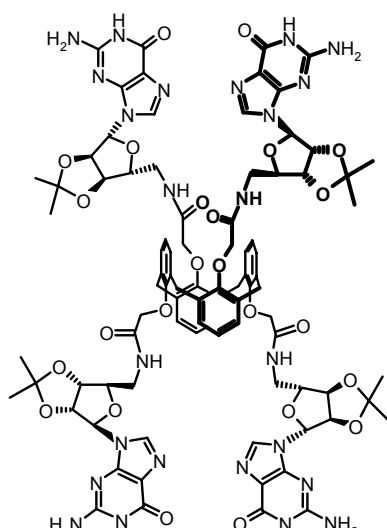
cG **2.26**

As shown in **Scheme 2.4,** addition of a cation to cG **2.26** was expected to induce the formation of cation-templated intermolecular G-quartets between molecules of **2.26**, resulting in an infinite one dimensional nanotube. The self-assembled cG **2.26** nanotube might assemble in membranes to provide active ion channels. This design had two advantages: (1) Appending guanosine to a scaffold would preorganize the bases for intermolecular hydrogen bonding and thus alleviate some of the entropic cost of association in the membrane. Once assembled, only 2-4 molecules of **2.26** are expected to span a lipid bilayer (compared to 16 in the quadruplex). (2) The 1D-assembly could, in theory, adjust to any bilayer thickness due to the reversible nature of the 1D self-assembly.

Scheme 2.4. Representation of nanotube formation by cG **2.26** upon cation-templated self-assembly. Gray spheres represent Na^+ cations. Blue and red are used to distinguish between individual cG **2.26** molecules.

cG **2.26**   (cG **2.26**)$_n$•(Na^+)$_n$
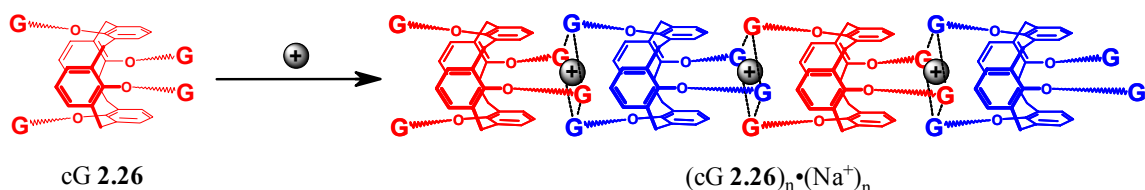
2.5 Calix[4]arene-Guanosine cG 2.26 forms 1D Supramolecular Polymers.

2.5.1 Introduction

This section describes the synthesis and self-assembling properties of calix[4]arene-guanosine conjugate cG **2.26**. The results presented strongly suggest that the cG **2.26** design was effective. Conjugate cG **2.26** indeed formed cation-templated nanotubular architectures, as depicted in **Scheme 2.4**. The work described herein was done as a collaboration with Dr. Vladimir Sidorov. My contribution to this work was the synthesis of 5'-amino-5'-deoxy-2',3'-isopropylideneguanosine **2.27**, the key intermediate that was linked to the calix[4]arene core to give cG **2.26**. All other synthesis and experiments were

directed by Dr. Sidorov. This section on the first generation calix[4]arene-guanosine conjugate cG **2.26** has been included for completeness, as the results presented here directly relate to the self-assembled ditopic receptor formed from cG **2.34** discussed subsequently in **Section 2.7**.

2.5.2 Synthesis of Calix[4]arene-Guanosine Conjugate cG 2.26 and Control Compounds.

Compound cG **2.26** was synthesized as shown in **Scheme 2.5**. Calix[4]arene tetraester **2.28** was prepared according to the procedure of Iwamoto and Shinkai.[257] The key intermediate 5'-amino-5'-deoxy-2',3'-isopropylideneguanosine **2.27** was prepared following the procedure of Robins *et al.*[258] Hydrolysis of tetraester **2.28** gave tetraacid **2.29**. EDCI-promoted coupling of **2.29** with guanosine **2.27** afforded calix[4]arene-guanosine conjugate cG **2.26** in 55 % yield (**Scheme 2.5**). Conjugate cG **2.26** was characterized by ^{1}H NMR and fast atom bombardment mass spectrometry (FAB-MS), and the data are shown in **Figure 2.12**.

Scheme 2.5. Synthesis of calix[4]arene-guanosine cG **2.26**.

(A)

(B)
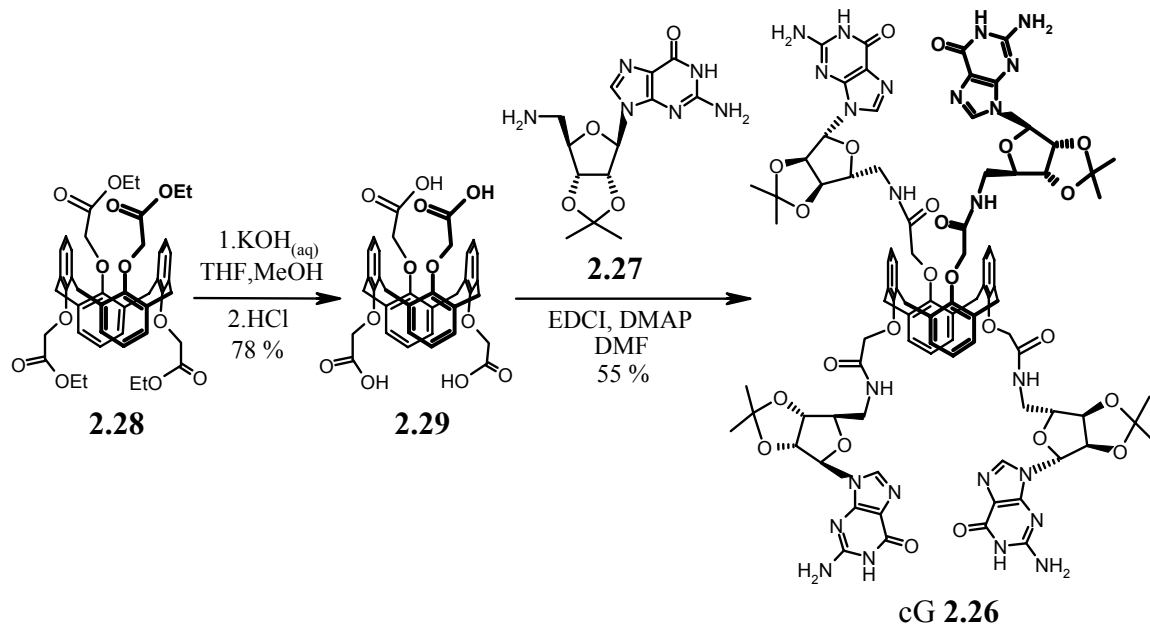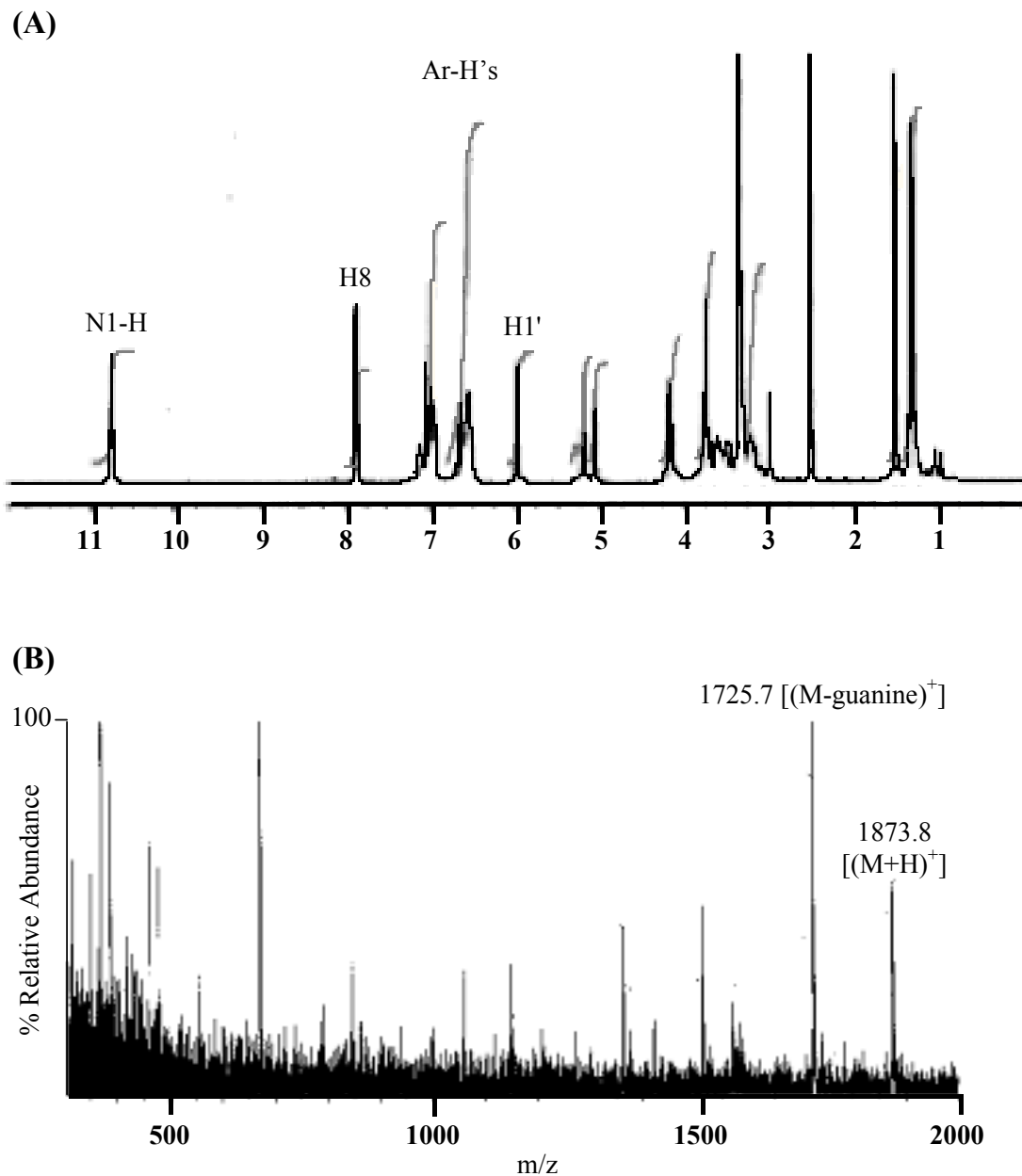
Figure 2.12. ^{1}H NMR at 400 MHz in DMSO-d$_6$ (A) and FAB-MS spectra (B) of cG **2.26**.

Calix[4]arene **2.30** (**Scheme 2.6**) was also synthesized as a control compound. Calix[4]arene tetramethylamide **2.30** was prepared by treatment of tetraacid **2.29** with SOCl$_2$ to give tetraacid chloride **2.31**. Subsequent coupling of **2.31** with CH$_3$NH$_2$ afforded calix[4]arene tetramethylamide **2.30** in 60 % yield (**Scheme 2.6**).

Scheme 2.6. Synthesis of calix[4]arene tetramethylamide **2.30**.
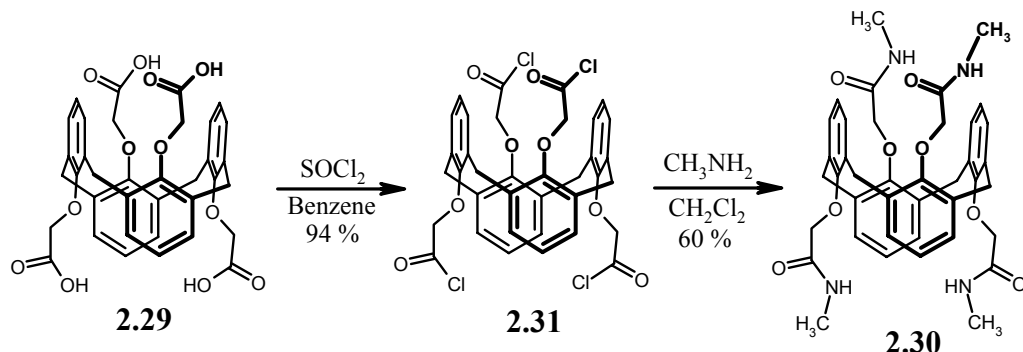
2.5.3 Evidence for Supramolecular Polymer Formation from Calix[4]arene-Guanosine cG 2.26.

Conjugate cG **2.26** was insoluble in most solvents, but did dissolve in 1:1 CH$_3$CN:H$_2$O. To test the ability of cG **2.26** to undergo cation-templated self-association, NaBPh$_4$ was chosen as the salt since NaBPh$_4$ is highly soluble in 1:1 CH$_3$CN:H$_2$O and BPh$_4^-$ is a non-coordinating anion, and should thus not interfere by interaction with the ligand or by ion pairing with Na$^+$.

Addition of NaBPh$_4$ to a solution of cG **2.26** in 1:1 CH$_3$CN:H$_2$O resulted in instantaneous and quantitative formation of a (cG **2.26**•Na$^+$)$_n$•(BPh$_4^-$)$_n$ polymer. The ^{1}H NMR spectrum of this material in DMSO-d$_6$ confirmed that it was a mixture of cG **2.26** and the BPh$_4^-$ anion. Further evidence for formation of this polymer is described below.

Transmission electron microscope (TEM) images show the precipitate formed upon addition of NaBPh$_4$ to cG **2.26** to consist of micrometer-long strands, visible as either single tubes or as bundles of tubes ranging from approximately 3 nm to 50 nm in thickness (**Figure 2.13**). The strands are relatively straight, without much bending. The thickness of the individual tubes was near the microscope's limit of resolution, namely *ca.*

3 nm. Since our recent X-ray structure of a lipophilic G-quadruplex had a 2.65 nm diameter, the individual rods formed from Na$^+$ templated aggregation of cG **2.26** have dimensions expected for a G-quartet.[251] These electron micrographs of insoluble aggregates, showing such defined structure, are entirely consistent with nanotube formation by cG **2.26** upon Na$^+$ coordination.
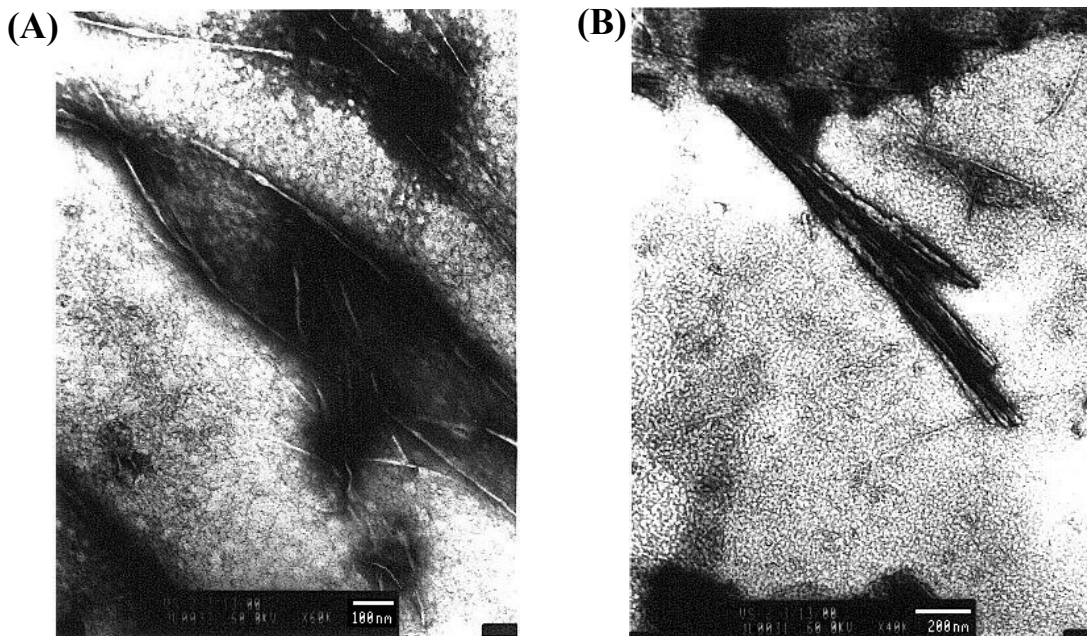
Figure 2.13. Representative TEM images of the precipitate formed from cG **2.26** and NaBPh$_4$ in 1:1 CH$_3$CN:H$_2$O solution. Objects have thicknesses between *ca.* 3 nm (many objects in A) and *ca.* 50 nm (most objects in B) and lengths of 80 nm through 1.5 μm. The unit scale is 100 nm in (A) and 200 nm in (B). TEM images were taken by Mahnaz El-Kouedi at Georgetown University.

The stoichiometry of the insoluble aggregates formed between cG **2.26** and NaBPh$_4$ was quantitatively determined using isothermal titration calorimetry (ITC). Titration of a solution of cG **2.26** in 1:1 CH$_3$CN-H$_2$O with NaBPh$_4$ resulted in significant generation of heat until a 1:1 ratio of cG **2.26** to NaBPh$_4$ had been reached (**Figure 2.14 A** and **B**). The total enthalpy of Na$^+$ binding by cG **2.26** was -9 kcal/mol, and this exothermic reaction

coincided with precipitation of (cG **2.26**•Na$^+$)$_n$•(BPh$_4^-$)$_n$ aggregates from solution. The absence of other inflection points in the ITC experiment, besides that for the prominent 1:1 cG **2.26**-NaBPh$_4$ stoichiometry, suggests that nanotube formation by cG **2.26** does not pass through shorter, intermediate structures. That is, Na$^+$-templated formation of (cG **2.26**•Na$^+$)$_n$•(BPh$_4^-$)$_n$ is highly cooperative. Control ITC experiments showed that 2',3'-isopropylidene guanosine G **2.33**, a compound lacking the calixarene framework, does not bind to NaBPh$_4$ in 1:1 CH$_3$CN-H$_2$O (**Figure 2.14 C** and **D**). The heat evolved upon addition of NaBPh$_4$ to 1:1 CH$_3$CN-H$_2$O is the same both in the presence and absence of G **2.33** in the solution. These control experiments clearly illustrate the entropic advantage of attaching the guanosine nucleobase to the 1,3-*alt*-calixarene scaffold.
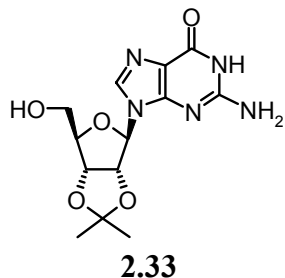
2.33
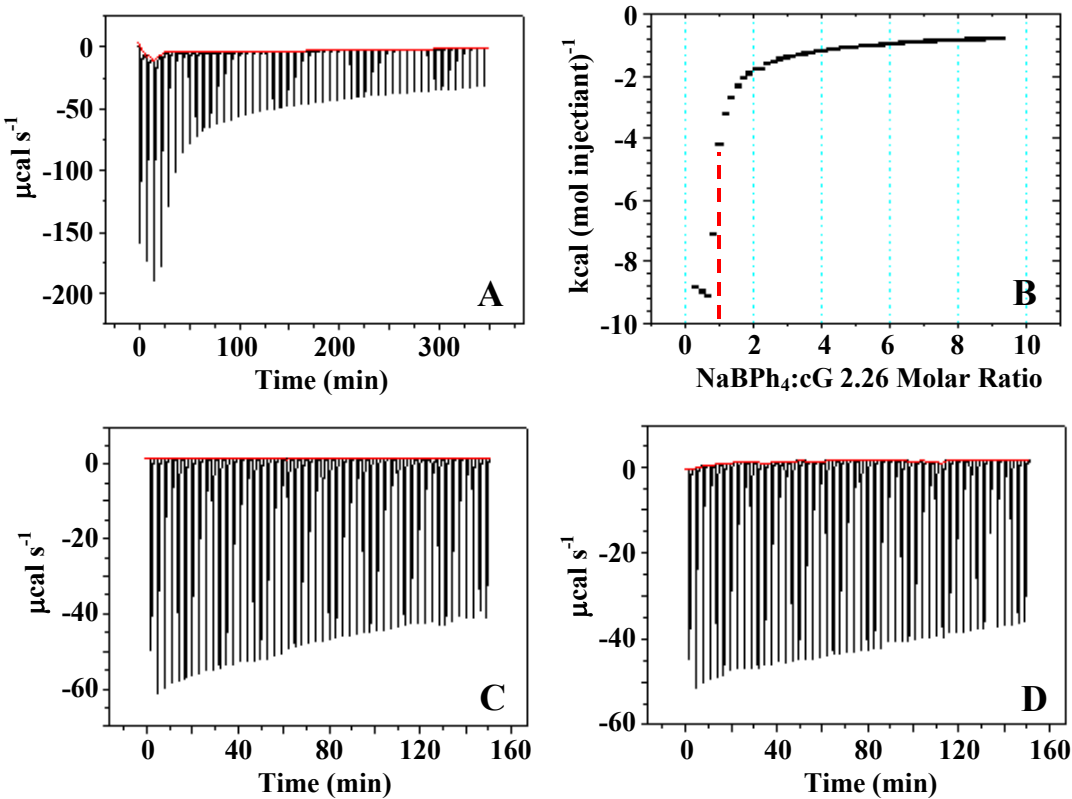
Figure 2.14. Isothermal Titration Calorimetry: (A) Titration of $NaBPh_4$ into 1:1 CH_3CN-H_2O solution containing cG **2.26**. (B) Integration curve of raw data from titration (A). The inflection point (indicated by the dashed red line) corresponds to a 1:1 $NaBPh_4$:cG **2.26** ratio. Total enthalpy of interaction is -9 kcal/mole. (C) Titration of $NaBPh_4$ into 1:1 CH_3CN-H_2O solution. (D) Titration of $NaBPh_4$ into 1:1 CH_3CN-H_2O solution containing G **2.33**. Data were collected by Dr. Vladimir Sidorov in the laboratory of Prof. Robert Flowers at the University of Toledo.

The guanosine nucleobases are indeed instrumental for the cation-templated self-association of cG **2.26**. Thus, addition of NaBPh$_4$ to calix[4]arene tetramethylamide **2.30** resulted in no change in the ^{1}H NMR spectrum of **2.30** in 1:1 CD$_3$CN-D$_2$O (**Figure 2.15**). Also, **2.30** remained in solution upon addition of NaBPh$_4$, unlike in the case of cG **2.26** where precipitation of (cG **2.26**-Na$^+$)$_n$(BPh$_4^-$)$_n$ aggregates was observed.
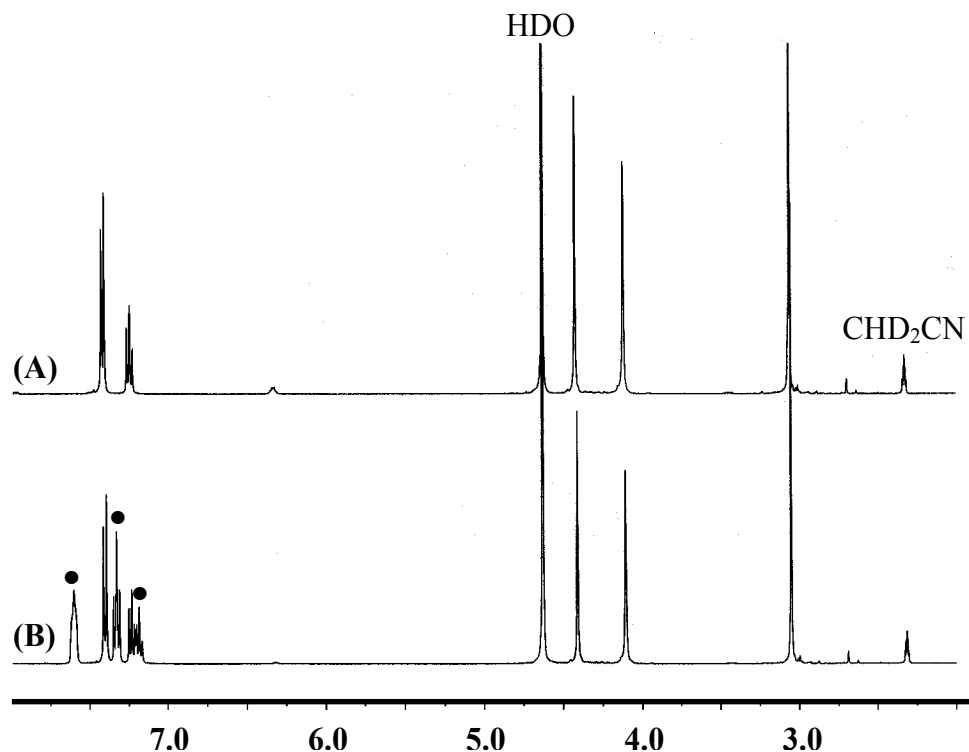
Figure 2.15. ^{1}H NMR spectra of (A) **2.30** and (B) a 1:1 mixture of **2.30**-NaBPh$_4$ in 1:1 CD$_3$CN-D$_2$O. The BPh$_4^-$ signals in (B) are indicated with dots (•).

2.5.4 Reversibility of cG 2.26 Polymerization.

The Na$^+$-mediated polymerization of cG **2.26** was reversible. Increasing the temperature above approximately 40 °C resulted in redissolving of the precipitate. Upon cooling back to 25 °C, (cG **2.26**•Na$^+$)$_n$•(BPh$_4^-$)$_n$ again precipitated out of solution. In addition to temperature, pH also had a dramatic effect on the solubility, and presumably the aggregation state, of cG **2.26**. The insoluble (cG **2.26**•Na$^+$)$_n$•(BPh$_4^-$)$_n$ dissolved upon decreasing the pH from 7 to 2. Protonation of guanosine's N2 or N7 (see **Figure 2.10A**)

112

should disrupt the hydrogen bonded structure, providing further evidence for a G-quartet. Bringing the pH up to 9 by addition of triethylamine caused reprecipitation of (cG **2.26**•Na$^+$)$_n$•(BPh$_4$$^-$)$_n$. The thermal lability and acid sensitivity of hydrogen-bonded nanotubes formed from cG **2.26** are consistent with the reversible nature of self-assembly.

2.5.5 Summary and Potential Applications of cG 2.26 Assemblies.

This section presented strong evidence for Na$^+$-templated nanotube formation from cG **2.26**. Three features of this design are worth emphasizing: (1) long-range structure can be controlled by cation templation, which triggers formation of an extensive hydrogen-bonded assembly; (2) aggregation is enabled by covalent attachment of guanosine units to a calixarene 1,3-*alt* scaffold, and (3) self-association of cG **2.26** occurs in highly polar solvents. The reversible formation of these structures in aqueous solution at temperatures near 40 ºC makes cG **2.26** and its analogs interesting as materials for biomedical applications. The pH-mediated assembly-disassembly of (cG **2.26**•Na$^+$)$_n$•(BPh$_4$$^-$)$_n$ can also be exploited to similar ends. For example, this system is attractive for drug delivery systems that rely on pH-dependent release.

Although supramolecular polymerization in biological systems has been understood for decades, synthetic supramolecular polymers have only recently attracted chemists and polymer scientists alike.[259,260] Excellent reviews by Meijer *et al*., ten Cate and Sijbesma, and Moore highlight the future prospects of this burgeoning field.[260-262] The (cG **2.26**•Na$^+$)$_n$•(BPh$_4$$^-$)$_n$ system described in this section has already been cited for its potential to form artificial ion channels in membranes.[261] Ion channel formation was the intended application for this system, as discussed in **Sections 2.1** and **2.4.4**, and the ion transport properties of cG **2.26** are described in **Section 2.6**.

2.6 Calix[4]arene-Guanosine Conjugate cG 2.26 Transports K$^+$ over Na$^+$ and Cs$^+$ Across a Lipid Membrane.

2.6.1 Introduction: Restating the Hypothesis.

Conjugate cG **2.26** was synthesized with the goal of developing a self-assembled ion channel. The Na$^+$-templated formation of nanotubes from cG **2.26** was a positive step towards this goal, since a cation-filled tube was envisioned as a potential channel structure, and prompted the investigation of the ion transport properties of cG **2.26**. A pictorial demonstration of the hypothesized (cG **2.26**)$_n$ channel transporting ions across a membrane is shown in **Figure 2.16**.
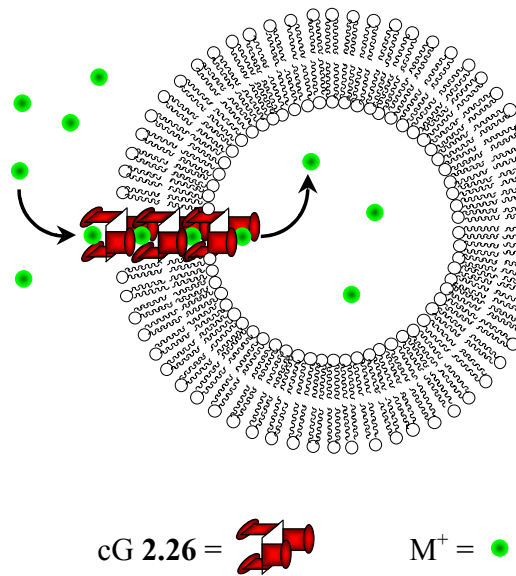
cG **2.26** =   M$^+$ = ●

Figure 2.16. Schematic representation of an ion channel formed from cG **2.26** within a lipid membrane. Molecules of cG **2.26** are depicted in red and metal cations are shown as green spheres.

2.6.2 Ion Transport Experiments with cG 2.26.

The ion transport properties of cG **2.26** were investigated using the base pulse assay described in **Section 1.5.5**. Large unilamellar vesicles (LUVs) composed of egg yolk phosphatidylcholine (EYPC) were used. In all cases, the vesicles contained a 10 mM

phosphate buffer at pH 6.4, 100 mM NaCl, and 10 μM of the pH-sensitive dye pyranine. The extravesicular solutions contained 10 mM phosphate buffer at pH 6.4 (initially) and 100 mM MCl (M = Na$^+$, K$^+$, or Cs$^+$). The fluorescence traces for base pulse experiments with three different MCl-containing extravesicular buffers upon application of cG **2.26** (final concentration of 2.5 μM, 1:200 ligand: lipid ratio) are shown in **Figure 2.17A**.

After addition of NaOH solution to the extravesicular buffer, thus creating a transmembrane pH gradient of approximately unity (base pulse), the growth of electrostatic potential caused by proton efflux from the liposomes can be compensated by either the influx of cations or efflux of anions mediated by the exogenous ligand (cG **2.26**, in this case). For the case of cation transport, proton efflux is compensated by influx of M$^+$ from the extravesicular solution, until the vesicles are lysed with detergent (Triton-X100). Lysis releases all contents and thus introduces the formerly entrapped pyranine dye to the extravesicular pH. The fluorescence after the Triton pulse is taken to be equivalent to 100 % of transport.

As shown in **Figure 2.17A**, the initial rate of transport in the presence of cG **2.26** with the three MCl buffers follows the order K$^+$>Cs$^+$>Na$^+$. This result strongly suggests transport of cations by cG **2.26**. If cG **2.26** was an anion transporter, changing the extravesicular solution from NaCl- to KCl- to CsCl-containing buffer, keeping the anion constant (Cl$^-$), should result in no change in transport rate upon changing the identity of the cation. Also, a selectivity for K$^+$ over Na$^+$ and Cs$^+$ was observed. Since G-quartets are known to preferentially bind K$^+$, this result might be expected if the active transport structure contains one or more G-quartets.[263] The (cG **2.26**•Na$^+$)$_n$•(BPh$_4^-$)$_n$ nanotubes visualized by TEM (**Section 2.5.3**) had diameters consistent with a G-quartet, providing evidence for the presence of this motif. It is predicted that the active M$^+$-transporter has a similar tubular structure, with G-quartets coordinating and transporting K$^+$. In the absence of cG **2.26**, i.e. injection of DMSO only, no transport was observed (black trace, **Figure 2.17A**). Blanks in all three buffers gave overlaying traces.
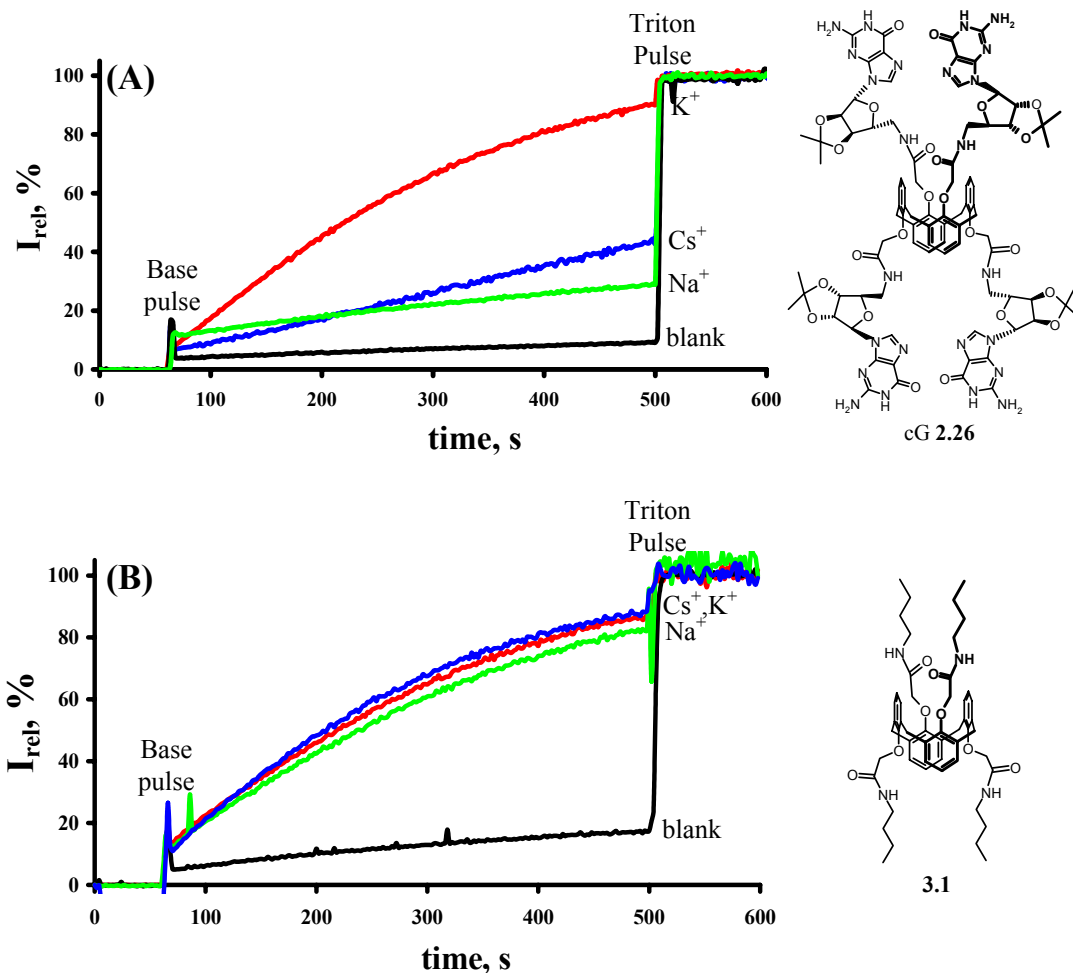
Figure 2.17. Liposome transport assays with (A) cG **2.26** and (B) calix[4]arene-tetrabutylamide **3.1**. In all experiments, suspensions of EYPC LUVs containing the pH-sensitive dye pyranine in a phosphate buffer were used. The intravesicular solution contained 10 mM sodium phosphate, pH 6.4, 100 mM NaCl and the extravesicular solution contained 10 mM sodium phosphate, pH 6.4, 100 mM MCl (M = Na^+, K^+, Cs^+). Time events: *0 sec:* 20 μl of (A) 0.25 mM solution of cG **2.26** in DMSO added (red, blue and green curves, 1:200 ligand:lipid ratio) or 20 μl of DMSO added (black curve, blanks), (B) 0.5 mM solution of **3.1** in THF added (red, blue and green curves, 100:1 ligand:lipid ratio) or 20 μl of THF added (black curve, blanks), *60 sec:* (A,B) 21 μl of 0.5 M NaOH added (Base Pulse), *500 sec:* (A,B) 40 μl of 50 % aqueous Triton X-100 added (Triton Pulse). Extravesicular buffers contained 100 mM NaCl (—), KCl (—), or CsCl (—).

Calix[4]arene-tetrabutylamide **3.1** was intended as a control compound for cG **2.26**, as it possessed the 1,3-*alternate* calixarene frame, but lacked the guanosine bases thought to be necessary for nanotube formation and cation transport. The expectation was that calix[4]arene-tetrabutylamide **3.1** would show no activity in ion transport assays. As shown in **Figure 2.17B**, this was not the case. In the presence of **3.1**, nearly identical ion transport rates were observed with all three extravesicular buffers (NaCl, KCl, and CsCl). Chloride was present in all three buffers, suggesting that **3.1** functioned as an anion transporter. Indeed, **3.1** forms chloride-selective ion channels in lipid membranes. **Chapter 3** will discuss the anion transport properties of **3.1** and similar secondary amide compounds.

3.1
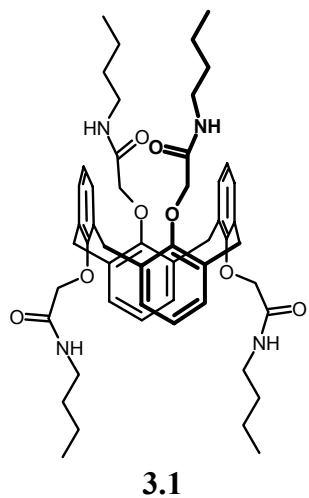
The data in **Figure 2.17A** suggest that cG **2.26** does indeed function as a cation transporter, with a selectivity for K^+ over Na^+ and Cs^+. The mechanism of transport and the active structure are still unknown. The prediction that the guanosine bases are critical for cation transport holds some validity, as removal of the guanosines results in anion transporter **3.1**. Further evidence for guanosine's participation in K^+ transport and selectivity by calix[4]arene-guanosine conjugates came from transport assays with the more lipophilic cG **2.34**, described in **Section 2.7.14**.

117

2.6.3. Summary and New Directions

Calix[4]arene-guanosine cG **2.26** transports K^+ selectively over Na^+ and Cs^+ across EYPC liposomal membranes. In the course of investigating calix[4]arene-guanosine cG **2.26**, a self-assembled chloride-selective ion channel formed from calix[4]arene-tetrabutylamide **3.1** was discovered, and will be described in **Chapter 3**. For the dual purpose of investigating the mechanism of cG **2.26** Na^+-templated polymerization and developing more lipid soluble derivatives, the more lipophilic calix[4]arene-guanosine cG **2.34** was synthesized. As the properties of cG **2.34** were elucidated, attention was focused on ion binding, in addition to ion transport, as cG **2.34** demonstrated the ability to form a noncovalent ion pair receptor. This ion pair receptor will be the main focus of **Section 2.7**.

2.7 Water Mediated Assembly Provides a Noncovalent Ion Pair Receptor.

2.7.1 Introduction.

In this section, the formation and properties of a water-stabilized dimer comprising calix[4]arene-guanosine conjugate cG **2.34** are described. As with cG **2.26**, the 1,3-*alt* conformation of cG **2.34** orients orthogonal pairs of nucleobases to facilitate formation of intermolecular hydrogen-bonded G-quartets. The more lipophilic cG **2.34**, however, is soluble in organic solvents, and enables further investigation of calixarene-guanosine assemblies over those conducted with cG **2.26**. Like its predecessor cG **2.26**, cG **2.34** forms noncovalent polymers with $NaBPh_4$. But with water alone, cG **2.34** forms a discrete dimer structure in organic solvents. The resulting (cG **2.34**)$_2$•$(H_2O)_n$ dimer, formed in wet $CDCl_3$, has a unique property: it extracts alkali halide salts from water into organic solution. As depicted in **Figure 2.18**, the dimer is held together by an intermolecular G-quartet, formed from two guanosines of one molecule and two guanosines of another. The "internal" (i) and "external" (e) guanosine bases are labeled in **Figure 2.18**, and this notation will be used throughout this section.

118
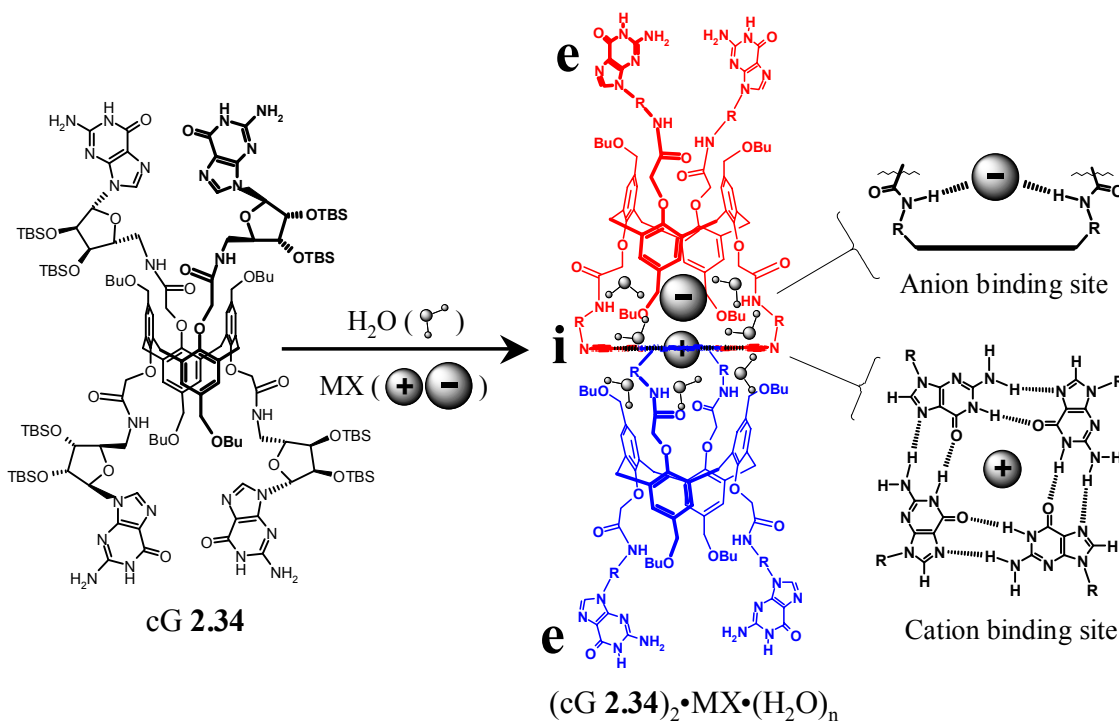
Figure 2.18. Representation of the dimeric complex (cG **2.34**)$_2$·MX·(H$_2$O)$_n$ indicating the anion and self-assembled cation binding site. Abbreviations are: R = ribose, Bu = butyl, TBS = *tert*-butyldimethylsilyl, i = "internal" guanosines, e = "external" guanosines.

In (cG **2.34**)$_2$·(H$_2$O)$_n$, the G-quartet, formed through self-assembly, serves as the cation binding site. The 2° amides, through which the guanosine bases are linked to the calix[4]arene core, serve as the anion binding site. As with most ditopic receptors discussed in **Section 2.3**, (cG **2.34**)$_2$·(H$_2$O)$_n$ coordinates cations via ion-dipole interactions with oxygen ligands (four O6 atoms of the G-quartet) and anions through amide NH hydrogen bonds. The ion pair, once bound, stabilizes the (cG **2.34**)$_2$ dimer. This complex provides a rare example of a self-assembled ditopic receptor, especially for such hydrophilic salts as NaCl.

The three compounds discussed in this section are shown in **Chart 2.6**. Two control compounds, cA **2.35** and G **2.36**, were used to probe the roles of the guanine base and the calix[4]arene core, respectively, in cG **2.34** self-assembly and salt binding. Calix[4]arene-adenosine cA **2.35** is identical to cG **2.34**, except with adenine replacing guanine as the

nucleobase. Adenine does not have the same hydrogen bonding properties as guanine and typically adenine does not self-associate. An adenosine tetrad has been reported, but the A$_4$ structure was observed only when π-stacked on a telomeric G-quadruplex.[264] Most importantly, cation-templated quartet structures of adenine have not been reported, making cA **2.35** an ideal control for proving guanine to be a critical element of cG **2.34**. G **2.36** is a "monomeric" analog of cG **2.34**, as it is essentially one quarter of cG **2.34**'s structure. Monomer G **2.36** was used to confirm the calixarene core's role in cG **2.34** association, since it contains both the guanine base and the 2° amides needed for cation and anion binding, but lacks the cyclic core that preorganizes the guanosines in cG **2.34**.

Chart 2.6

cG **2.34**   cA **2.35**   G **2.36**

G =   A =   Bu = butyl
                         TBS = *tert*-butyldimethylsilyl
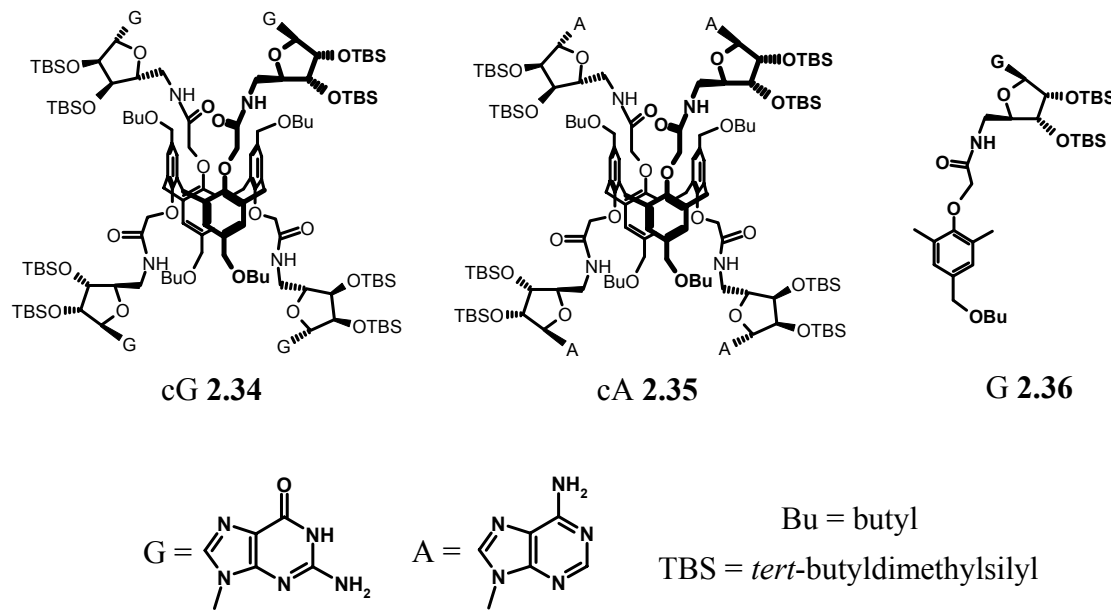
2.7.2 Synthesis of cG 2.34, cA 2.35, and G 2.36.

Calixarene-guanosine conjugate cG **2.34** was synthesized by coupling of calixarene acid chloride **2.41** with 5'-aminoguanosine **2.47**. Calix[4]arene-1,3-*alt*-tetraacid chloride **2.41** was prepared from calix[4]arene as shown in **Scheme 2.7**.

Scheme 2.7. Synthesis of calix[4]arene-1,3-*alt*-tetraacid chloride **2.41**.
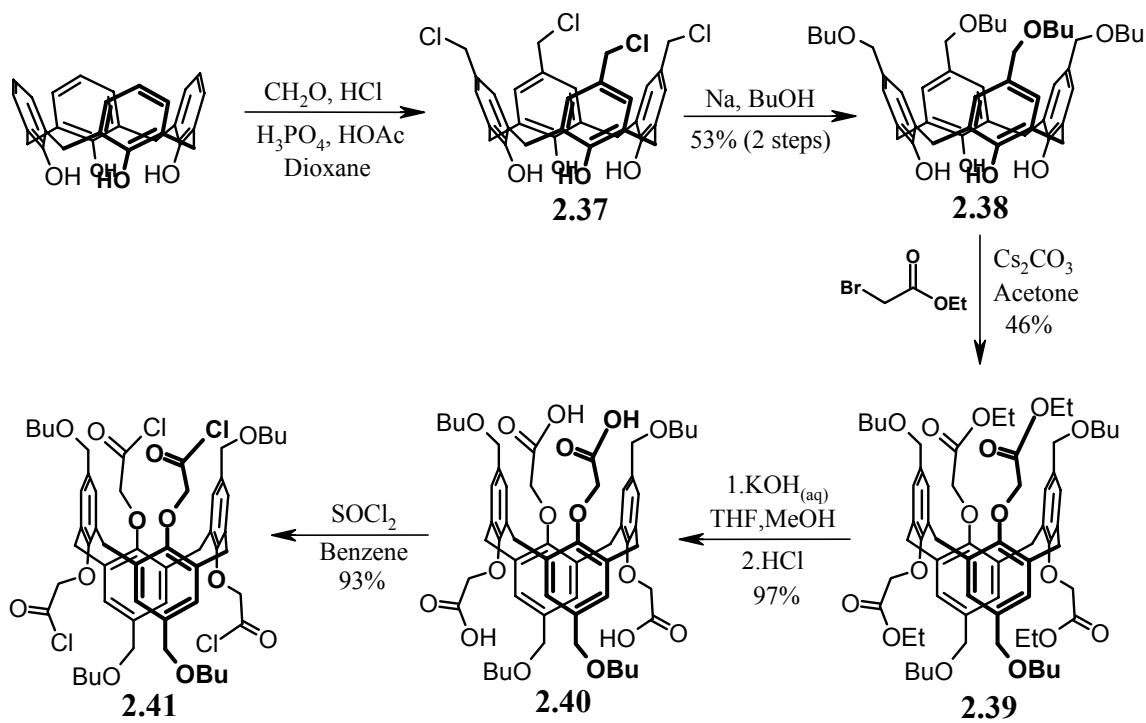
Calix[4]arene was chloromethylated at the upper rim,[265] followed by nucleophilic substitution with NaOBu in BuOH to give **2.38**. Subsequent alkylation of the lower rim with ethyl bromoacetate afforded calixarene-1,3-*alt* **2.39**. Alkylation of the lower rim is a critical step, as it locks the conformation of the calixarene core.[257] Typically, a mixture of calixarene conformers is obtained, but the base used, e.g. Na_2CO_3 *versus* Cs_2CO_3, can favor the formation of one conformer over others. Thus, by choosing the correct base for the alkylation, one can preferentially form one conformer, and then separate it from the mixture by either crystallization or column chromatography. Cesium carbonate (Cs_2CO_3) has been used for formation of the desired 1,3-*alternate* conformation, and was used in the synthesis of **2.39**.[257] Base hydrolysis to give **2.40** followed by reaction with $SOCl_2$ in benzene afforded calix[4]arene-1,3-*alternate*-tetraacid chloride **2.41**.

Scheme 2.8. Synthesis of 5'-aminoguanosine **2.47**.
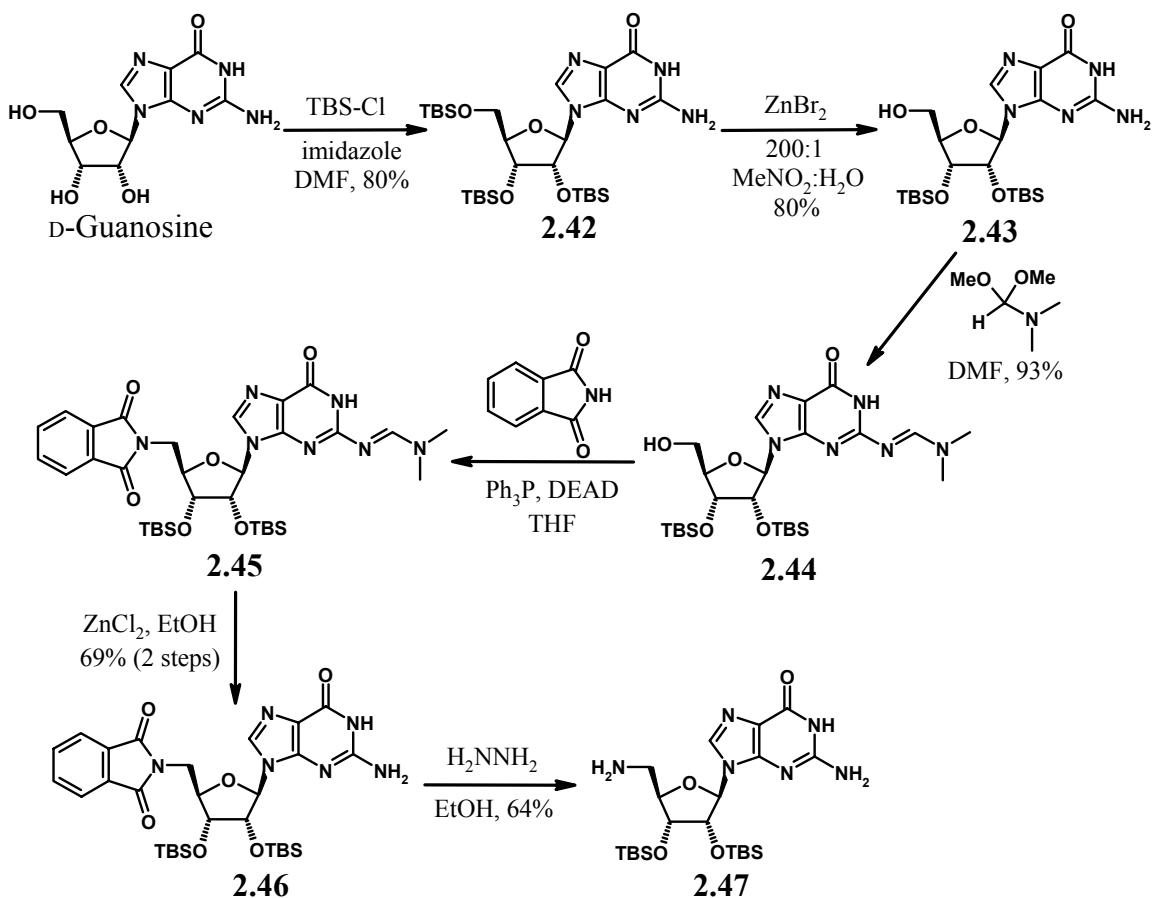
5'-Amino-5'-deoxy-2',3'-*O*-di-*tert*-butyldimethylsilylguanosine **2.47** was prepared from D-guanosine as shown in **Scheme 2.8**. Trisilylation of the ribose was accomplished following the procedure of Li and Miller to give **2.42**.[266] The 5'-silyl group was selectively removed with ZnBr$_2$ in aqueous nitromethane, as described by Seela, to give **2.43**.[267] Protection of the N2 with an amidine group followed by Mitsunobu coupling of phthalimide to the 5'-carbon afforded guanosine **2.45**. Removal of the N2-amidine with ZnCl$_2$ in EtOH to give **2.46** and subsequent hydrazinolysis gave 5'-amino-5'-deoxy-2',3'-*O*-di-*tert*-butyldimethylsilylguanosine **2.47**.

Importantly, protection of the N2 to give **2.44** is necessary, as failure to do so results in iminophosphorane formation at that position under Mitsunobu conditions.[268] Thus,

reaction of guanosine **2.43** under Mitsunobu conditions resulted in formation of iminophosphorane **2.48** as shown in **Scheme 2.9**. A parallel result was observed by Li and Miller.[266]

Scheme 2.9. Iminophosphorane formation at N2 of guanosine **2.43** under Mitsunobu conditions.
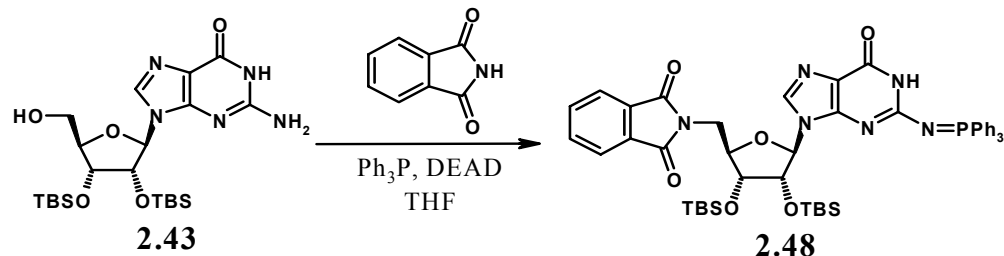
In working out the synthesis of guanosine **2.47**, another interesting result concerning the Mitsunobu coupling was observed. As shown in **Scheme 2.8**, the coupling of phthalimide to **2.44** to give **2.45** proceeded smoothly. In contrast, with compound **2.49** (**Scheme 2.10**), in which the 2'-OH and 3'-OH are protected by an isopropylidene group, cyclonucleoside **2.50** was formed. This is the result of intramolecular nucleophilic attack on the 5'-OPPh$_3^+$ by N3 in the Mitsunobu intermediate (**Scheme 2.10**). Having two TBS groups on the 2'-OH and 3'-OH in **2.44** prevents this intramolecular attack, presumably by altering the sugar pucker in such a way that the 5' carbon is too far from N3 for cyclization to occur. Similarly, Li and Miller observed cyclization of unprotected guanosine under Mitsunobu conditions.[266] In that report, cyclonucleoside formation was circumvented by protecting the guanine O6 with a benzyl group. As shown here, protecting the 2'-OH and 3'-OH with TBS is an alternate approach to preventing cyclonucleoside formation under Mitsunobu conditions.

Scheme 2.10. Cyclization of **2.49** under Mitsunobu Conditions.

2.49   **2.50**
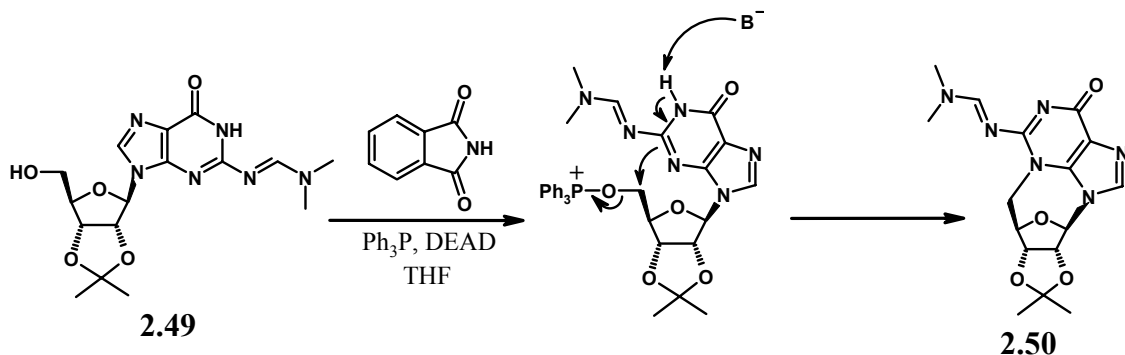
Conjugate cG **2.34** was obtained in 49% isolated yield by coupling of calix[4]arene acid chloride **2.41** with guanosine **2.47** as shown in **Scheme 2.11**. The ^{1}H NMR, ^{13}C NMR and ESI-MS spectra of cG **2.34** are shown in **Figure 2.19**.

Scheme 2.11. Final coupling to give calix[4]arene-guanosine cG **2.34**.

2.41   **2.47**

Et$_3$N
CH$_2$Cl$_2$
49 %

cG **2.34**

(A)

H8 +
5'-amide
NH

N2-H₂

Ar-H's

H1'

N1-H

H2'

Integral

(B)
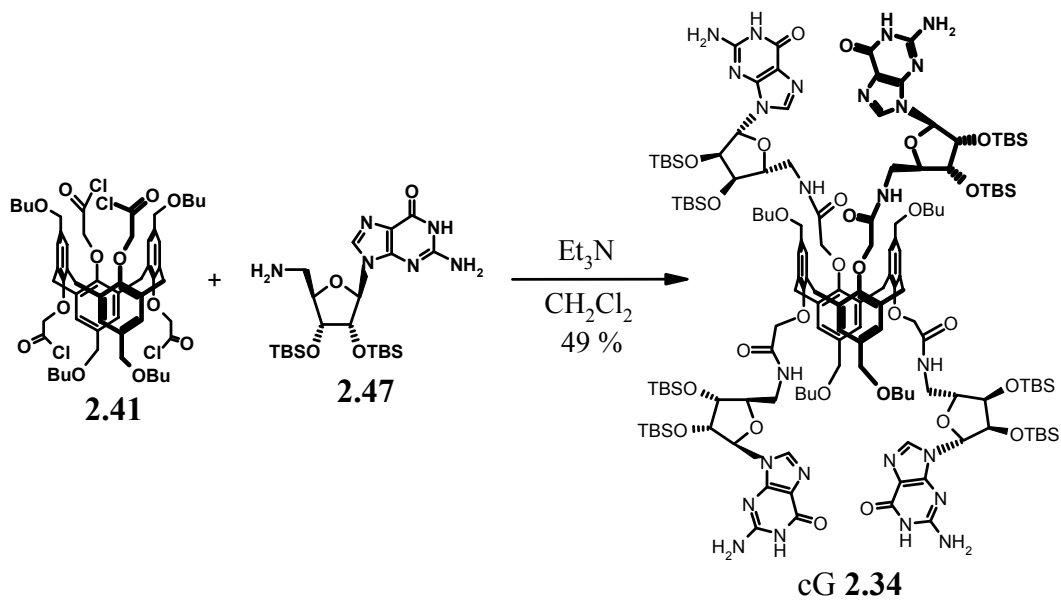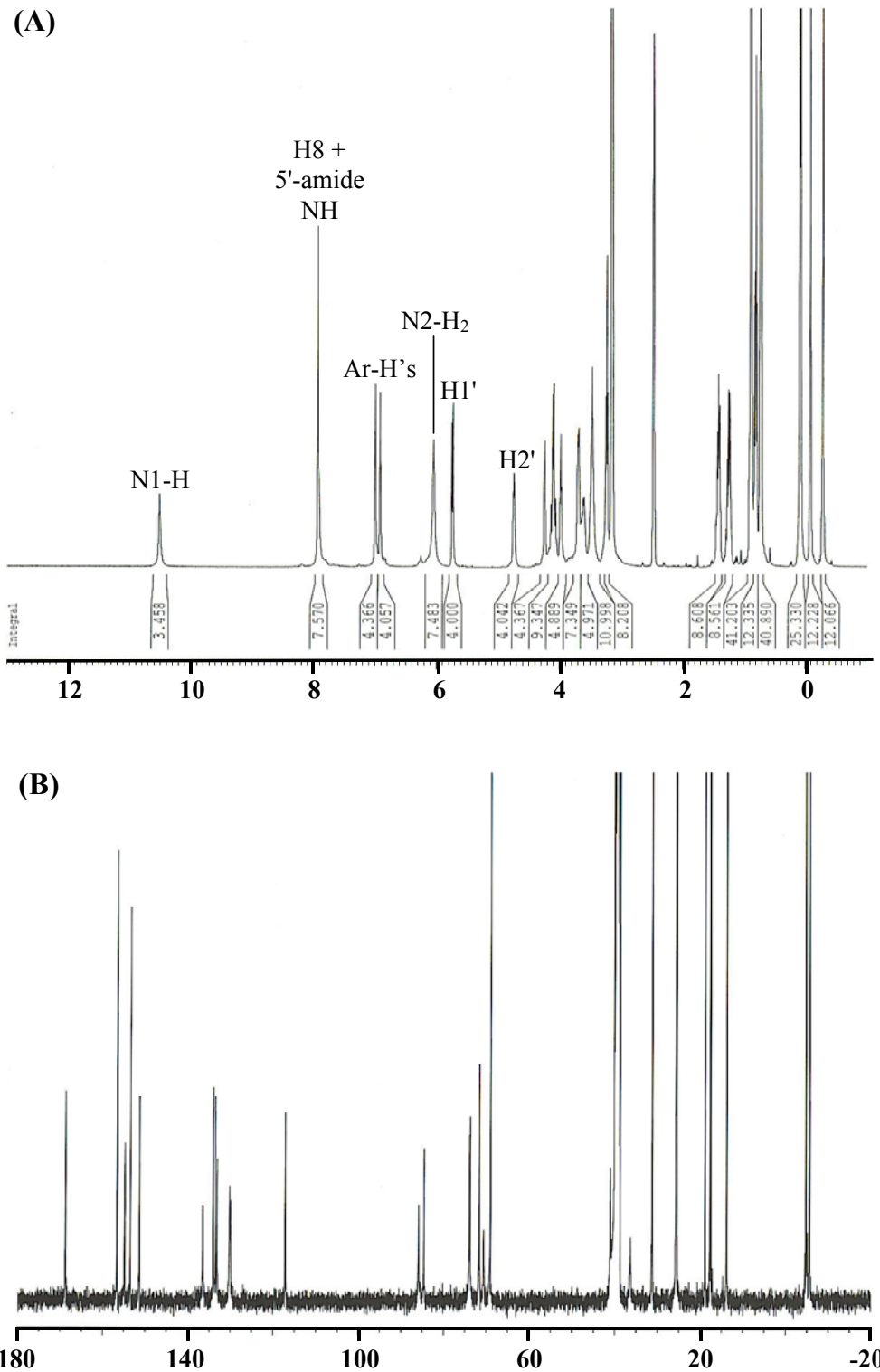
Figure 2.19 (A,B). ^{1}H NMR (A) and ^{13}C NMR (B) spectra of cG **2.34** in DMSO-d$_6$.

125
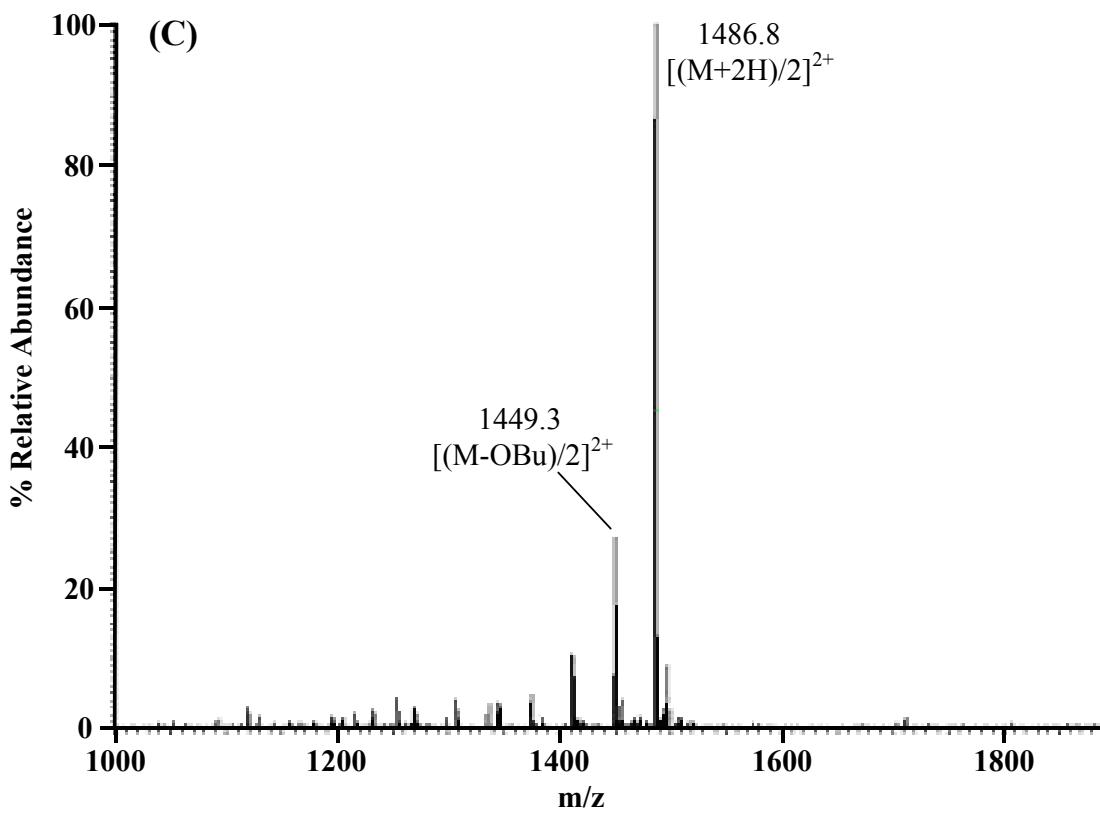
Figure 2.19 (C). ESI-MS spectrum of cG **2.34**.

5'-Amino-5'-deoxy-2',3'-*O*-di-*tert*-butyldimethylsilyladenosine **2.56** was prepared from D-adenosine as shown in **Scheme 2.12** following the same synthetic sequence as described for guanosine **2.47.** As in the case of guanosine, the adenine N6 must be protected to prevent iminophosphorane formation under Mitsunobu conditions.[268]

Scheme 2.12. Synthesis of 5'-aminoadenosine **2.56**.
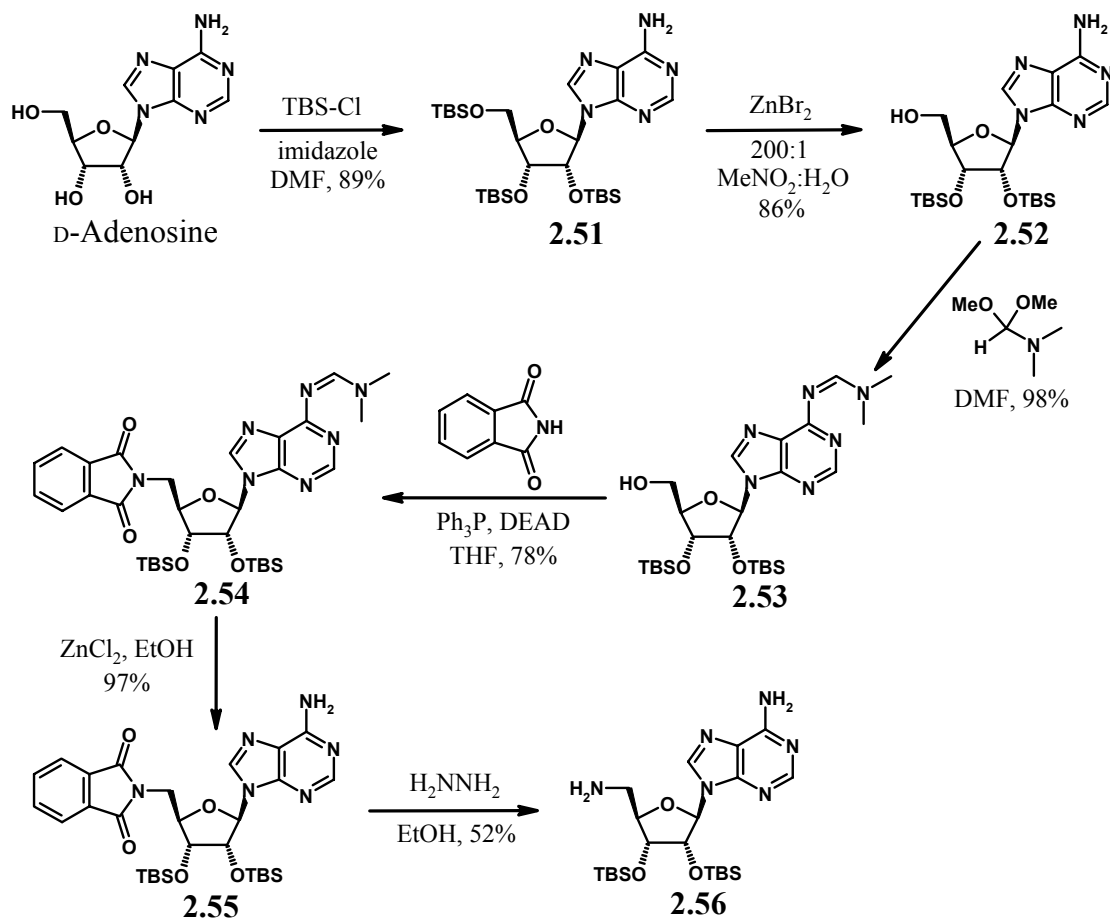
Control compound cA **2.35** was synthesized in 41% yield by coupling of acid chloride **2.41** with 5'-aminoadenosine **2.56**, as shown in **Scheme 2.13.**

Scheme 2.13. Final coupling to give calix[4]arene-adenosine cG **2.35**.

cA **2.35**
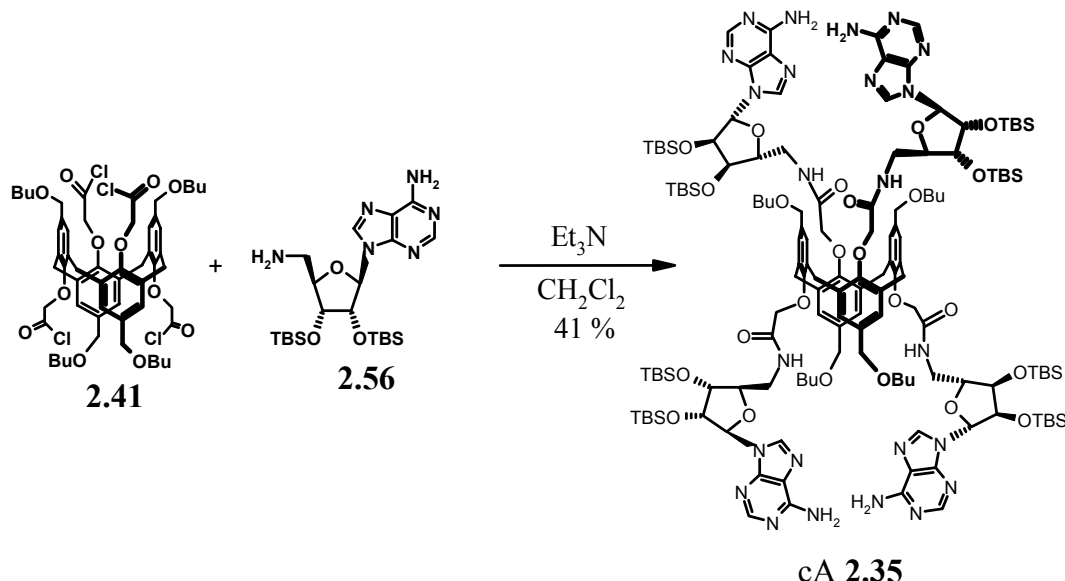
Control G **2.36** was prepared by the coupling of guanosine **2.47** with (4-butoxymethyl-2,6-dimethylphenoxy)-acetyl chloride **2.61**. Compound **2.60** was synthesized from 2,6-dimethylphenol as shown in **Scheme 2.14**. Compound **2.60** was then reacted with SOCl₂ to give acid chloride **2.61**, followed by coupling with 5'-aminoguanosine **2.47** to afford control compound G **2.36** in 66 % yield. The synthesis of compound **2.60**, conversion to acid chloride **2.61** and final coupling to give G **2.36** was completed by Katherine J. Kayser, an undergraduate student under my supervision.

Scheme 2.14. Synthesis of control compound G **2.36**.
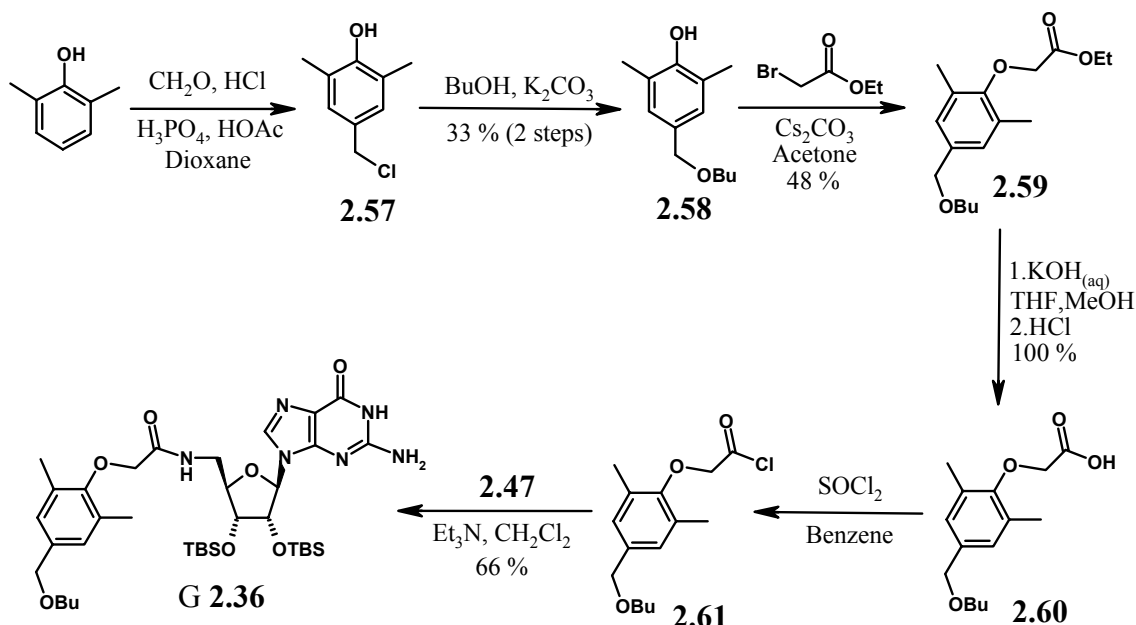
2.7.3 Conjugate cG 2.34 Forms a Discrete Species in Water-Saturated CDCl₃.

The NMR spectra in **Figure 2.20** show that water enables discrete self-assembly of cG **2.34** in CDCl₃. As expected for a monomer, cG **2.34** gave one set of sharp ¹H NMR signals in DMSO-d₆ (**Figure 2.20A**). In contrast, cG **2.34** was poorly soluble in CDCl₃, giving a noisy NMR spectrum with broad signals for NH protons (**Figure 2.20B**). This was attributed to nonspecific aggregation in the solid state.[209,210,220] Washing a CDCl₃ suspension of cG **2.34** with water completely dissolved the compound and improved spectral resolution, consistent with transformation from an aggregate to a discrete species. The two sets of resolved ¹H NMR signals (**Figure 2.20C**) provided the first hint that cG **2.34** dimerizes in water-saturated CDCl₃. Two sets of signals, an "inner" and "outer" set, are consistent with the breaking of cG **2.34**'s symmetry upon dimerization via G-quartet formation. As will be described, this discrete species is a dimer, with the formula (cG **2.34**)₂·(H₂O)ₙ.
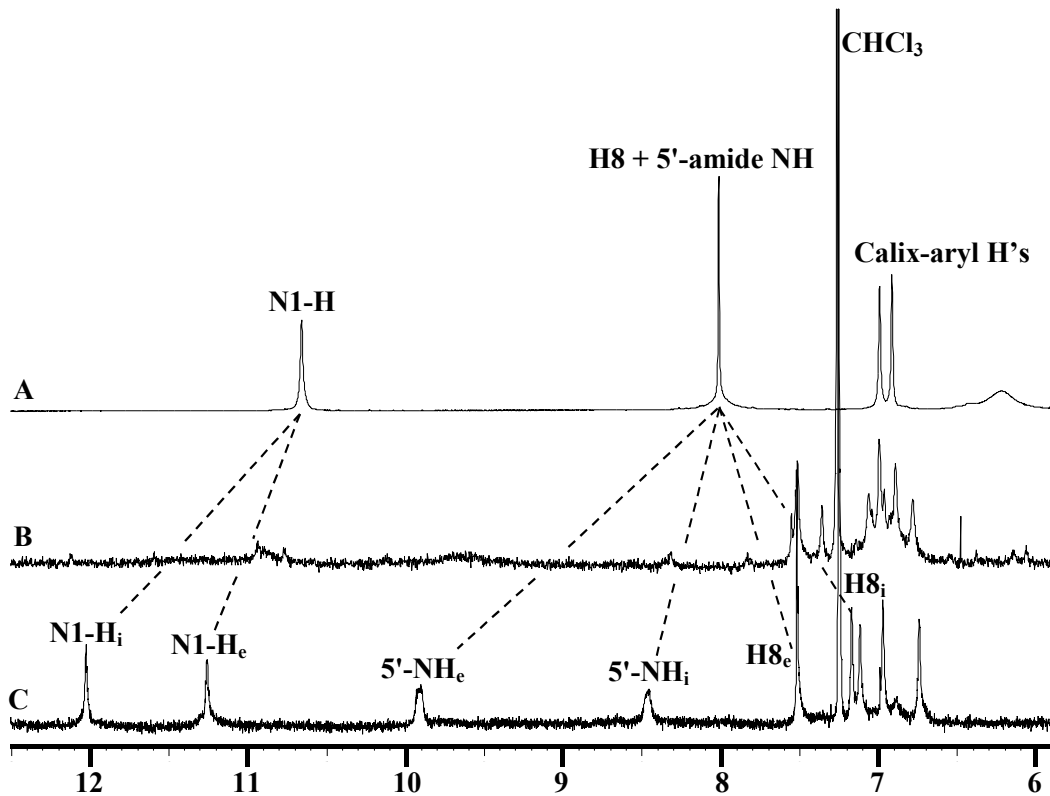
Figure 2.20. ^{1}H NMR spectra of cG **2.34** in DMSO-d$_6$ (A), CDCl$_3$ (B), and (cG **2.34**)$_2$•(H$_2$O)$_n$ in water-saturated CDCl$_3$ (C). Dashed lines indicate the splitting of cG **2.34** signals. *Note*: H8 and 5'-amide NH signals overlap in DMSO-d$_6$ at room temperature.

2.7.4 (cG 2.34)$_2$•(H$_2$O)$_n$ Functions as an Ion Pair Receptor.

The (cG **2.34**)$_2$•(H$_2$O)$_n$ complex is an ion pair receptor, capable of extracting alkali halides from water into CDCl$_3$. Washing a CDCl$_3$ solution of (cG **2.34**)$_2$•(H$_2$O)$_n$ with aqueous 1.0 M NaCl, 1.0 M NaBr, or 1.0 M KCl (**Figure 2.21A**,**C**, and **E**, respectively) gave similar, but distinct, spectra for the different (cG **2.34**)$_2$•MX•(H$_2$O)$_n$ complexes. The 5'-NH amide proton near δ 8.6 showed different ion-induced chemical shifts for the NaCl and NaBr complexes (**Figure 2.21C** and **A**), implicating this NH group in anion binding. In comparing the ^{1}H NMR spectra of the NaCl and KCl complexes, it was the N1-H signal near δ 12.2 that shifted the most (**Figure 2.21C** and **E**), identifying this "inner" guanosine as the cation binding site.

130
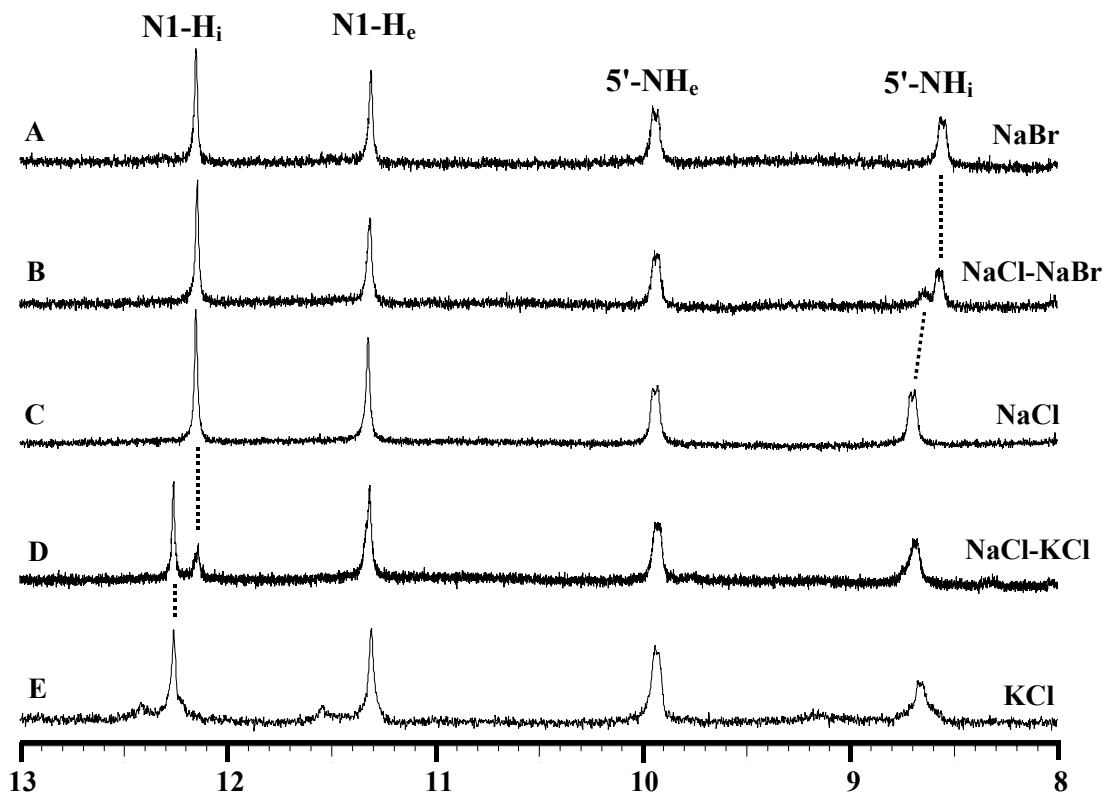
Figure 2.21. Low field region of the ^{1}H NMR spectra of (cG **2.34**)$_2$•(H$_2$O)$_n$ in water-saturated CDCl$_3$ after washing with aqueous (A) 1.0 M NaBr, (B) 0.5 M NaBr/0.5 M NaCl, (C) 1.0 M NaCl, (D) 0.5 M NaCl/0.5 M KCl, and (E) 1.0 M KCl. Dashed lines highlight the individual complexes in the mixtures.

Competition experiments revealed that the (cG **2.34**)$_2$•(H$_2$O)$_n$ has modest cation and anion extraction selectivities. A K$^+$:Na$^+$ selectivity of 2:1 was determined from integration of the separate N1-H signals near δ 12.2 after extraction of a 1:1 NaCl:KCl solution (**Figure 2.21D**). The K$^+$:Na$^+$ selectivity was the same whether using the Cl$^-$ or Br$^-$ salts, indicating little cooperativity in the extraction of alkali halide ion pairs by cG **2.34**. To measure anion extraction selectivity, an aqueous solution containing 1:1 NaCl:NaBr (0.5 M each) was extracted using cG **2.34**. Integration of the separate 5'-NH signals near δ 8.6 revealed a 2:1 Br$^-$:Cl$^-$ extraction selectivity (**Figure 2.21B**). Again, no cooperativity in alkali halide extraction was observed, as the anion selectivity was the same for the Na$^+$ and K$^+$ salts.

Direct evidence for Na^+ extraction by cG **2.34** into $CDCl_3$ was obtained by ^{23}Na NMR. A 20 mM solution of (cG **2.34**)$_2$•NaCl•$(H_2O)_n$ in $CDCl_3$ gave a ^{23}Na NMR signal at δ -5.23 (**Figure 2.22**).
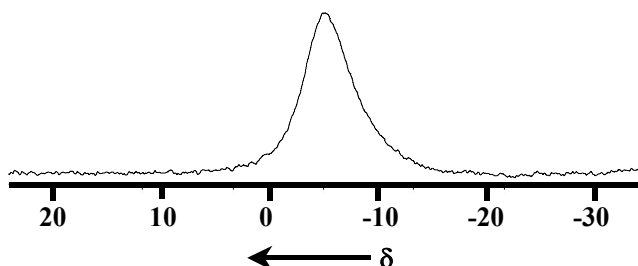
Figure 2.22. ^{23}Na NMR of (cG **2.34**)$_2$•NaCl•$(H_2O)_n$ in $CDCl_3$ (20 mM in cG **2.34**).

Ion pair extraction by cG **2.34** was confirmed and quantified by ion chromatography (IC). Complexes of (cG **2.34**)$_2$•MX•$(H_2O)_n$ in CD_2Cl_2 were preformed. The salt was then back-extracted into H_2O, as depicted in **Scheme 2.15**. The aqueous layer's ion content was measured by IC, and the values obtained are shown in **Table 2.1**. The salts investigated were NaCl, NaBr, KCl, and KBr. Back-extraction of KBr gave a cG **2.34**:salt ratio of ~2:1, while ratios somewhat greater than 2:1 were obtained with NaCl, NaBr and KCl. ^1H NMR spectra before and after back-extraction confirmed conversion from (cG **2.34**)$_2$•MX•$(H_2O)_n$ to (cG **2.34**)$_2$•$(H_2O)_n$. Importantly, the cation and anion concentrations were always close to 1:1, confirming ion pair binding by cG **2.34**. This direct evidence for ion pair extraction by (cG **2.34**)$_2$•$(H_2O)_n$ proves this complex to be a self-assembled ion pair receptor.

Also, a competition experiment was performed. A 1:1 aqueous mixture of NaBr and KCl (giving 1:1:1:1 Na^+:K^+:Cl^-:Br^-) was extracted by cG **2.34**, then back-extracted and measured. The selectivities were approximately 2:1 K^+:Na^+ and 3:1 Br^-:Cl^- (**Table 2.1**), in reasonable agreement with the ion selectivities measured by ^1H NMR integration. One factor that may affect the selectivity is the lower desolvation energies of K^+ (70.5 kcal/mol) *versus* Na^+ (87.2 kcal/mol) and Br^- (75.3 kcal/mol) *versus* Cl^- (81.3 kcal/mol).[269] However, the energy differences are large, namely 16.7 and 6.0 kcal/mol for

cations and anions, respectively. If desolvation energy was the only factor influencing extraction selectivity, cG **2.34** would extract KBr exclusively. It is likely that the ions bound in the dimer are not completely dehydrated due to residence in a water-filled cavity at the dimer's core. There are clearly other factors that must enhance the Na^+ and Cl^- binding affinities of the (cG **2.34**)$_2$ dimer. The thermodynamic stabilities of the final (cG **2.34**)$_2$·MX·$(H_2O)_n$ complexes are clearly important.

Scheme 2.15. Representation of salt back-extraction from (cG **2.34**)$_2$·MX·$(H_2O)_n$ in CD_2Cl_2 into H_2O.
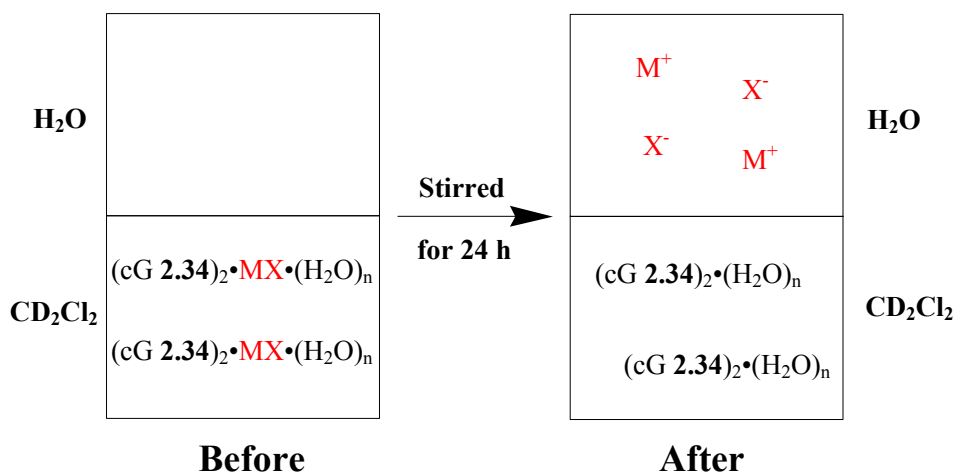
Table 2.1. Ion concentration from the back-extraction of salt from (cG **2.34**)$_2$·MX·$(H_2O)_n$ in CD_2Cl_2 into H_2O measured by ion chromatography. The concentration of cG **2.34** was 2 mM in all experiments.

Salt Extracted	Cation (Conc., mM)	Anion (Conc., mM)
NaCl	Na^+ (0.72 ± 0.14)	Cl^- (0.60 ± 0.07)
NaBr	Na^+ (0.80 ± 0.06)	Br^- (0.65 ± 0.03)
KCl	K^+ (0.81 ± 0.08)	Cl^- (0.85 ± 0.08)
KBr	K^+ (0.95 ± 0.09)	Br^- (0.96 ± 0.04)
1:1:1:1 Na^+:K^+:Cl^-:Br^-	Na^+ (0.37 ± 0.07) K^+ (0.71 ± 0.06)	Cl^- (0.19 ± 0.02) Br^- (0.69 ± 0.07)

2.7.5 Control Compounds Demonstrate that both Guanine and the Calix[4]arene are Critical in cG 2.34 Self-Association and Ion Binding.

In contrast to cG **2.34**'s self-assembly and ionophoric properties, control compounds cA **2.35** and G **2.36** demonstrated none of these properties. Both compounds were soluble in CDCl₃, gave single sets of ^{1}H NMR resonances, and showed only minor NMR spectral changes upon washing with water or aqueous salt solutions. ^{1}H NMR spectra before and after water and NaCl₍aq₎ washes are shown in **Figures 2.23** and **2.24** for cA **2.35** and G **2.36**, respectively. The downfield shift and sharpening of the H8 resonance of G **2.36** in CDCl₃ *versus* water-saturated CDCl₃ may be due to a change in conformation resulting from hydration of the nucleobase. Also, both cA **2.35** and G **2.36** extracted little salt (< 10 %) in the back-extractions monitored by IC, and showed no ^{23}Na NMR signal upon washing 20 mM solutions of the control compounds with 1.0 M NaCl₍aq₎. These data indicate that cG **2.34** requires both the guanosine nucleobase and the calix[4]arene core for dimerization and ion pair extraction.
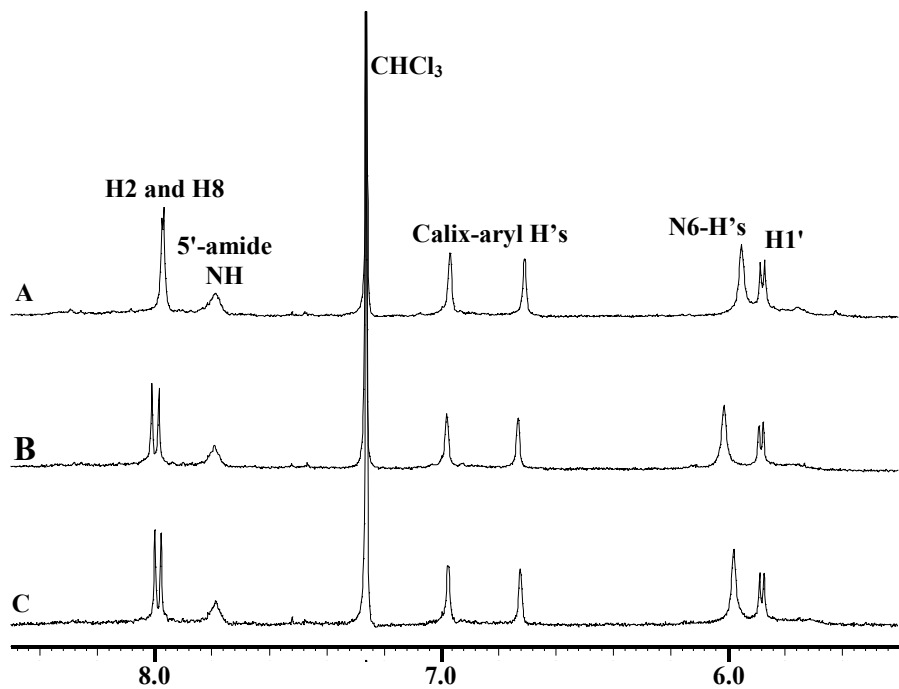
Figure 2.23. ^{1}H NMR spectra of control compound cA **2.35** in CDCl₃ (A) and in CDCl₃ after washing with water (B) and 1.0 M NaCl₍aq₎ (C).
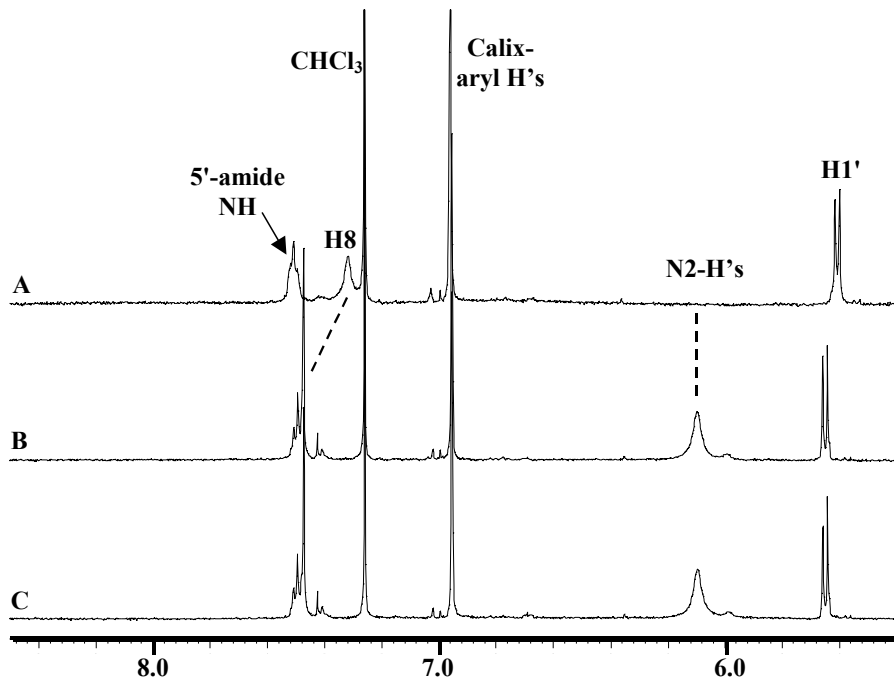
Figure 2.24. ^{1}H NMR spectra of control compound G **2.36** in CDCl$_3$ (A) and in CDCl$_3$ after washing with water (B) and 1.0 M NaCl$_{(aq)}$ (C). Dashed lines indicate the appearance of the N2-H signal and the shifting of the H8 signal upon washing with water.

2.7.6 Determination of a (cG 2.34)$_2$ Dimer: Techniques that Failed to Give Proof

Techniques typically used for determining supramolecular size include fast atom bombardment and electrospray ionization mass spectrometry (FAB-MS and ESI-MS) and X-ray crystallography. Both FAB-MS and ESI-MS of (cG **2.34**)$_2$·(H$_2$O)$_n$ and (cG **2.34**)$_2$·NaCl·(H$_2$O)$_n$ from various solvents and under various conditions gave only cG **2.34** molecular ion peaks ([cG **2.34** + Cs]$^+$ in FAB-MS, [(cG **2.34** + 2H)/2]$^{2+}$ and [(cG **2.34** + Na + H)/2]$^{2+}$ in ESI-MS), indicating that only the monomer is stable under the ionization conditions. Conjugate cG **2.34** failed to yield X-ray quality crystals, thus precluding X-ray crystallographic analysis. However, mass spectrometry measures ions in the gas phase and X-ray crystallography shows molecules or complexes as they exist in the solid state. The question at hand was whether or not cG **2.34** formed a dimer in solution.

With the lack of proof for a (cG **2.34**)$_2$·NaCl·(H$_2$O)$_n$ dimer from other techniques, attention was shifted to pulsed-field gradient NMR spectroscopy. Ultimately, it was this technique that provided evidence for a solution phase dimer. **Section 2.7.7** gives an introduction to pulsed-field gradient NMR spectroscopy, and **Section 2.7.8** describes the use of this technique to prove cG **2.34** dimerization.

2.7.7 Introduction to Pulsed Field Gradient NMR Spectroscopy.

2.7.7.1 The Pulsed-Field Gradient NMR Experiment.

Pulsed Field Gradient (PFG) NMR spectroscopy was used to confirm a cG **2.34** solution phase dimer, as will be described in **Section 2.7.8**. PFG-NMR is a valuable method for determining the self-diffusion coefficients (D$_s$) of molecules and assemblies in solution. According to the pulsed gradient spin echo technique introduced by Stejskal and Tanner,[270] the ratio between the echo intensity in the presence (I) and absence (I$_o$) of a pulsed gradient is given by:

$$\ln(I/I_o) = -\gamma^2 g^2 \delta^2 (\Delta - \delta/3) D_s \quad (\textbf{Equation 2.1})$$

In **Equation 2.1**, γ is the gyromagnetic ratio (26,752 rad·gauss^{-1}·s^{-1} for ^{1}H), g is the pulsed gradient strength (gauss·cm^{-1}), δ and Δ are the duration and separation of the two gradient pulses, respectively, and D$_s$ is the self-diffusion coefficient. The pulse sequence for the original experiment is shown in **Figure 2.25**.[271]
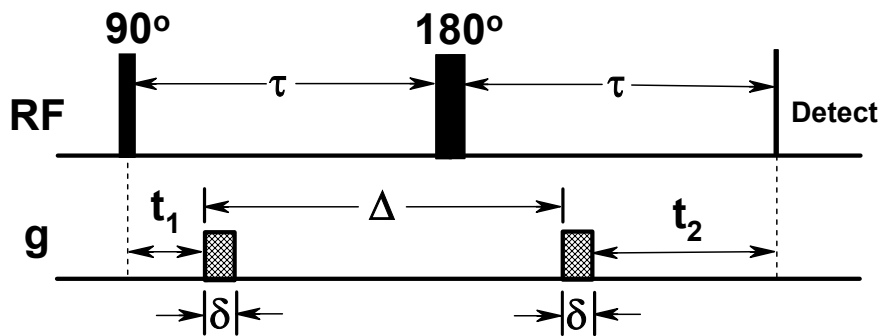
Figure 2.25. Pulse sequence for measurement of diffusion coefficients by the pulsed gradient spin echo technique.[271] RF = radio frequency, g = gradient.

Stejskal and Tanner describe the PFG-NMR experiment in their seminal paper as follows: "Following the 90° (RF) pulse there is a negligible loss of phase coherence until the first gradient pulse (δ). This pulse produces an almost instantaneous phase shift depending on the position of each nucleus in the direction of the field gradient at that time. Following the gradient pulse the loss of phase coherence is again negligible; but the nuclei, as they diffuse, change position. The 180° (RF) pulse inverts the phase shifts, and then the second gradient pulse (δ) produces phase shifts equal to the those produced by the first gradient pulse. In the absence of diffusion, the second gradient pulse, aided by the 180° pulse, would exactly undo the effect of the first. Diffusion causes this refocusing to be incomplete. Note that in this experiment the nuclear positions are recorded by the first gradient pulse, and any change at the time of the second is noted by the incompleteness of the refocusing."[270]
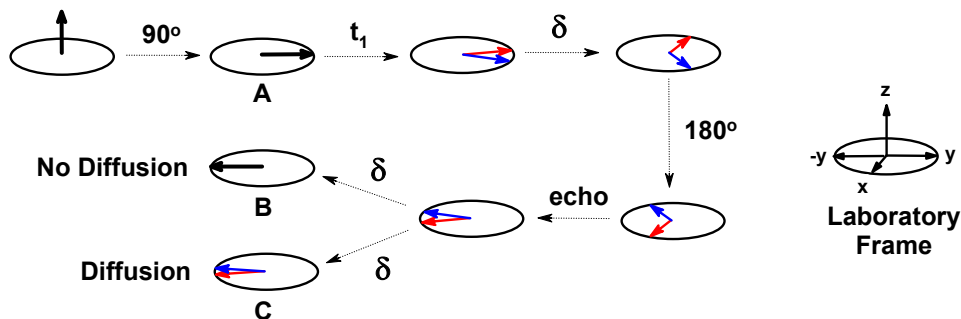
Figure 2.26. Pictorial representation for a PFG-NMR experiment. Black vectors represent red and blue vectors aligned together.

The Stejskal-Tanner explanation is shown pictorially in **Figure 2.26**. At the beginning of the experiment, all nuclei are aligned in the z-direction. After a 90° RF pulse, the nuclei are aligned in the y-direction. After time t_1, the nuclei have begun to relax in the x-y plane (spin-spin relaxation). The first gradient pulse (δ) causes what Stejskal and Tanner refer to as an "almost instantaneous phase shift." Basically, the nuclei's magnetization vectors (red and blue) move further apart. The 180° pulse then flips the vectors in the exact opposite direction. Next comes the "echo". That is, the magnetization vectors continue toward the -y direction (the same direction as before the 180° pulse). This is where diffusion affects the final outcome. In the absence of diffusion, the second gradient pulse (δ) will exactly undo the first because the pulsed-field strength will be the same (the nuclei are at the same point on the gradient). This results in **B**, where the resultant magnetization vector has the same magnitude but opposite direction of that immediately after the 90° pulse (**A**). If diffusion *does* occur, the second gradient pulse (δ) will deliver a different pulsed-field strength than that which the nuclei felt from the first δ (the nuclei changed position and are now at a different point on the gradient). This results in incomplete refocusing to give **C**. The absolute magnitude of the red and blue vectors in **C** on the -y axis is less than that of the vector in **B**. Thus, diffusion causes an attenuation of the NMR signal. Increasing the gradient strength causes an increased signal attenuation. Information about the molecular diffusion is acquired by running a series of PFG-NMR experiments with the gradient strength increasing incrementally in

138

each experiment. The signal attenuation is monitored over the course of all experiments and fitted using **Equation 2.1** to give the self diffusion coefficient (D_s) for that species.

2.7.7.2 Applications of PFG-NMR Spectroscopy in Supramolecular Chemistry

While PFG-NMR has proven to be an invaluable tool for the study of proteins,[272,273] the technique has more recently been applied to characterize the aggregation state of hydrogen bonded assemblies in $CDCl_3$. Using complexes of known molecular weight and structure as standards, Timmerman *et al.* characterized three new hydrogen-bonded complexes having molecular weights from 3600-5000.[274] Utilizing PFG-NMR, Cohen *et al.* demonstrated that resorcinarene **2.2** (**Chart 2.1**) forms a hexameric capsule both in the presence and absence of a tetraalkylammonium guest (see **Section 2.2.3**).[211,275]

Hupp and Larive *et al.* applied PFG-NMR to metal coordination complexes, and characterized molecular square **2.62** through diffusion measurements.[276] In this report, the researchers comment on the importance of appropriate standards for comparison in these experiments: "Excluding strictly spherical species, evaluation of molecular weights via diffusion parameters requires diffusion standards because diffusion coefficients are not directly related to molecular weight. Instead, they reflect effective hydrodynamic radii. Therefore, not only the size, but also the shape, of the molecule will determine the value of D_s."[276] In their experiments, Hupp and Larive used other known molecular square complexes, and also "corners" of molecular squares, to elucidate the size of **2.62**. In **Section 2.7.8**, the dimeric nature of (cG **2.34**)$_2$·NaCl·(H_2O)$_n$ was confirmed using an appropriate standard.

2.62

L =
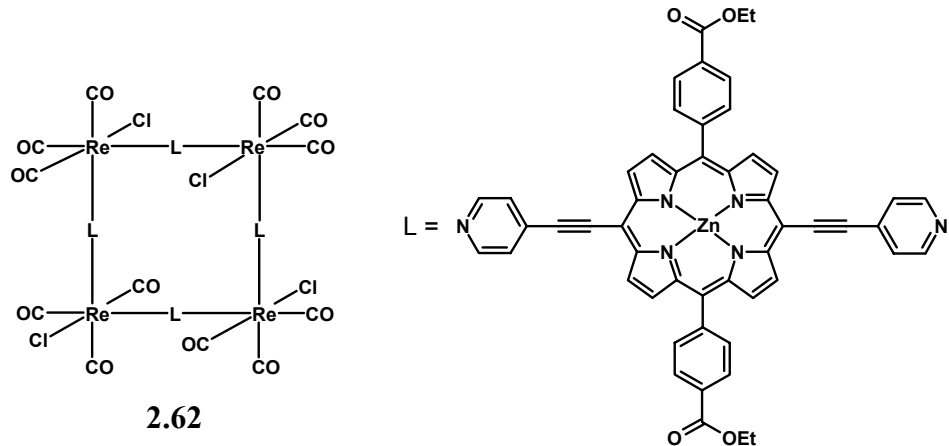
PFG-NMR has been exploited to confirm solution phase dimerization for various systems. A number of studies have predicted a dimer to have a self-diffusion coefficient that is 72-75% that of a monomer (D_s dimer/D_s monomer = 0.72-0.75).[272,273,277,278] Dimeric protein assemblies supported by PFG-NMR have been reported in these studies. PFG-NMR has more recently been applied to characterize solution phase dimerization of small molecules. Led *et al.* demonstrated the dimerization of a helical peptide.[279] Meijer *et al.* employed PFG-NMR to support the solution phase enantioselective dimerization of **2.63** (**Scheme 2.16**).[280] In a system similar to that used to characterize the (cG **2.34**)$_2$ dimer in **Section 2.7.8**, Walker *et al.* confirmed that the antibiotic ramoplanin (mw 2554) forms a dimer in CD$_3$OD via PFG-NMR.[281] At concentrations near 1 mM in CD$_3$OD, ^{1}H NMR suggested a ramoplanin dimer-monomer mixture. Using the monomer as the internal standard, having a known molecular weight, the researchers confirmed a ramoplanin dimer by comparison of the dimer and monomer diffusion rates.

Scheme 2.16. Enantioselective dimerization of **2.63**.[280]
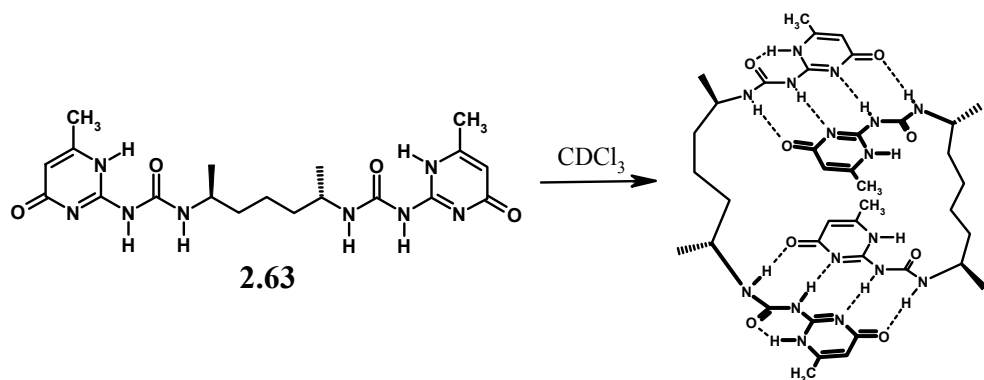
In summary, PFG-NMR is a useful technique for determining the size of supramolecular complexes, provided a suitable standard is used. This technique has been exploited to determine the aggregation state of the cG **2.34** complex in CDCl$_3$ solution, as described in the next section.

2.7.8 Confirmation of a (cG 2.34)$_2$ Dimer by PFG-NMR Spectroscopy.

As discussed in **Section 2.7.7.2**, evaluating the size of an assembly using diffusion coefficients requires a standard with similar structure and molecular weight. Accordingly, D$_s$ values were measured for samples containing both cG **2.34** (mw 2972) and cA **2.35** (mw 2908) in the same NMR tube. Monomeric cA **2.35** served as the internal standard for determining the aggregation state of cG **2.34**. The D$_s$ values for 1:1 mixtures of (cG **2.34**)$_2$·NaCl·(H$_2$O)$_n$ and cA **2.35** (each 6.7 mM in monomer) were determined in CDCl$_3$ and DMSO-d$_6$, and are shown in **Table 2.2**. The D$_s$ values were determined based on the attenuation of the H1' signal for cG **2.34** and cA **2.35** in both solvents (for a depiction of the "external" H1' of the (cG **2.34**)$_2$·NaCl·(H$_2$O)$_n$ complex in CDCl$_3$, see **Figure 2.18**). Also, the Stejskal-Tanner plots (ln(I/I$_o$) *versus* $\gamma^2 g^2 \delta^2 (\Delta-\delta/3)$) are shown in **Figures 2.27** and **2.28** for experiments in CDCl$_3$ and DMSO-d$_6$, respectively. The necessary hardware set-up and the software protocols for all PFG-NMR experiments were prepared by Dr. Yiu-Fai Lam.

Table 2.2. Self-diffusion coefficients (D_s) for (cG **2.34**)$_2$•NaCl•(H_2O)$_n$ and cA **2.35** measured by PFG-NMR in both $CDCl_3$ and DMSO-d_6.

Solvent	D_s ((cG **2.34**)$_2$•NaCl•(H_2O)$_n$) 10^{-10} m^2/s	D_s (cA **2.35**) 10^{-10} m^2/s	Ratio D_s(**2.34**):D_s(**2.35**)
$CDCl_3$	3.82 ± 0.10	5.37 ± 0.10	0.71 ± 0.01
DMSO-d_6	0.91 ± 0.02	0.94 ± 0.01	0.97 ± 0.01
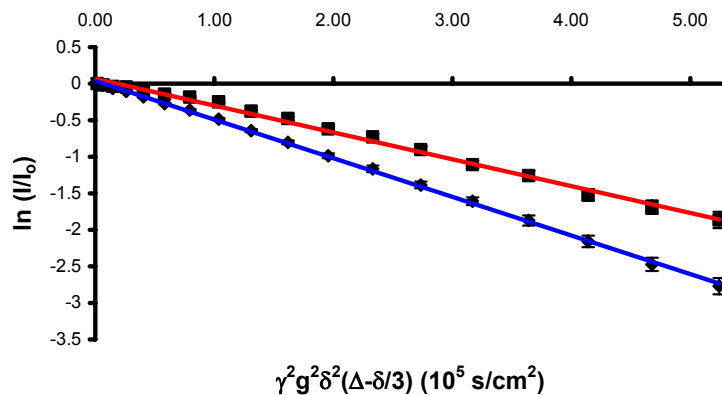
Figure 2.27. Stejskal-Tanner plot of the normalized intensity as a function of $\gamma^2 g^2 \delta^2 (\Delta - \delta/3)$ for dimeric (cG **2.34**)$_2$•NaCl•(H_2O)$_n$ (red) and monomeric cA **2.35** (blue) in $CDCl_3$ at 26 °C. Data are derived from the attenuation of one H1' signal for (cG **2.34**)$_2$•NaCl•(H_2O)$_n$ (H1' of G's *not* involved in G-quartet) and the H1' signal for cA **2.35**. The slope of each line is equal to -D_s for that species.
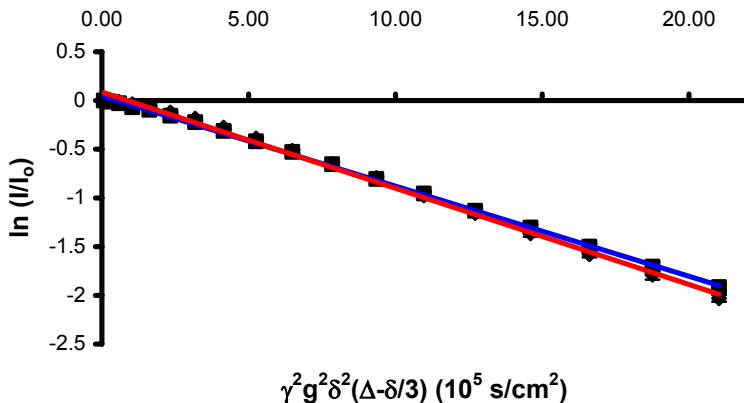
Figure 2.28. Stejskal-Tanner plot of the normalized intensity as a function of $\gamma^2 g^2 \delta^2 (\Delta - \delta/3)$ for monomeric cG **2.34** (red) and cA **2.35** (blue) in DMSO-d_6 at 26 °C. Data are derived from the attenuation of the H1' signals of both compounds. The slope of each line is equal to $-D_s$ for that species.

In CDCl$_3$, the intact (cG **2.34**)$_2$·NaCl·(H$_2$O)$_n$ dimer diffuses slower than cA **2.35** and the ratio of D$_s$(**2.34**):D$_s$(**2.35**) = 0.71 (**Table 2.2**) agrees well with the theoretical dimer:monomer range of 0.72-0.75.[272,273,277,278] The Stejskal-Tanner plot (**Figure 2.27**) shows clearly that the signal for (cG **2.34**)$_2$·NaCl·(H$_2$O)$_n$ attenuates slower than the signal for cA **2.35**, indicating that (cG **2.34**)$_2$·NaCl·(H$_2$O)$_n$ is diffusing slower than cA **2.35**. In the competitive solvent DMSO-d_6, where cG **2.34** undoubtedly exists as a monomer, the D$_s$(**2.34**):D$_s$(**2.35**) ratio was 0.97 (**Table 2.2**). The nearly equal diffusion coefficients are expected for two monomeric species of similar size and molecular weight. The nearly overlaying trendlines in the Stejskal-Tanner plot (**Figure 2.28**) emphasize that cG **2.34** and cA **2.35** are diffusing at the same rate in DMSO-d_6. This result, indicating a dimer in CDCl$_3$, is consistent with the two sets of ^{1}H NMR signals and with the near 2:1 cG **2.34**:salt stoichiometry obtained from the IC experiments (**Sections 2.7.3** and **2.7.4**). It is therefore concluded that the (cG **2.34**)$_2$•(H$_2$O)$_n$ dimer binds one ion pair.

2.7.9 Salt Binding Imparts Stability to the (cG 2.34)$_2$·(H$_2$O)$_n$ Dimer.

The ion pair, once bound, stabilizes the (cG **2.34**)$_2$ dimer to increasing temperature. Above 35 ºC in CDCl$_3$, (cG **2.34**)$_2$·(H$_2$O)$_n$ decomposed into nonspecific aggregates, as indicated by ^{1}H NMR (**Figure 2.29A**). After increasing the temperature to 50 ºC and returning to 25 ºC, the structural integrity of the complex was mostly regained. Since the CDCl$_3$ remained saturated with water, cG **2.34** was still exposed to the conditions under which the complex forms (or reforms) near room temperature. In contrast, NMR spectra showed that (cG **2.34**)$_2$·NaCl·(H$_2$O)$_n$ remained intact up to 55 ºC (**Figure 2.29B**, spectra at 50 ºC and 55 ºC were nearly identical). Complex stabilization by salt is likely due to Cl$^-$ binding by the 5'-amide NH groups and Na$^+$ coordination to the dimer's G-quartet.

A. (cG **2.34**)$_2$•(H$_2$O)$_n$ **B.** (cG **2.34**)$_2$•NaCl•(H$_2$O)$_n$
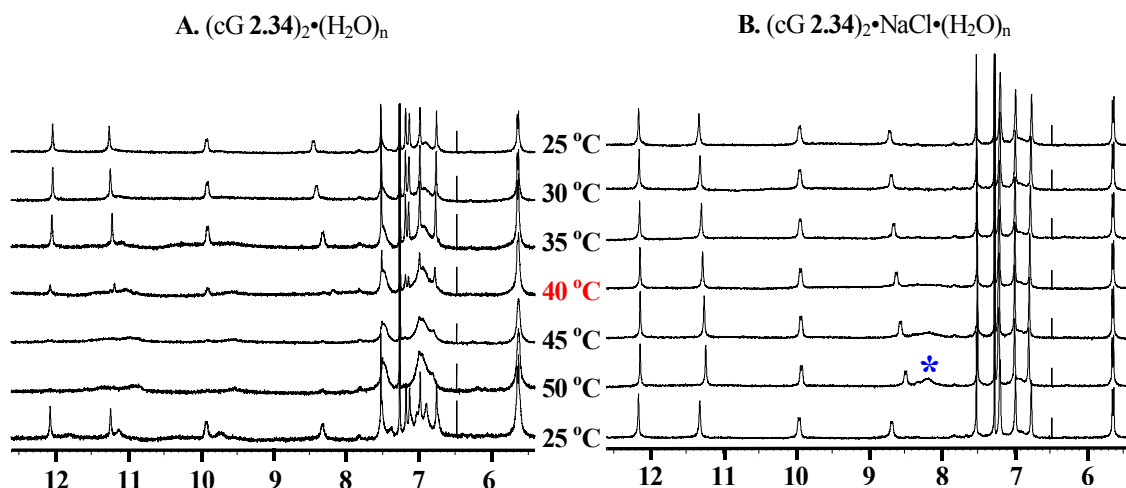
Figure 2.29. ^{1}H NMR spectra in CDCl$_3$ from 25 up to 50 °C, then back to 25 °C for: (A) (cG **2.34**)$_2$•(H$_2$O)$_n$ and (B) (cG **2.34**)$_2$•NaCl•(H$_2$O)$_n$. Samples were 2 mM in cG **2.34**. Blue asterisk indicates the N2-H$_2$ signal at 50 °C.

2.7.10 Evidence for a G-Quartet in (cG 2.34)$_2$•NaCl•(H$_2$O)$_n$ from Low Temperature ^{1}H NMR and ^{1}H-^{1}H NOESY.

Evidence for an intermolecular G-quartet in (cG **2.34**)$_2$•NaCl•(H$_2$O)$_n$ came from low temperature 1D ^{1}H NMR and a ^{1}H-^{1}H NOESY experiment. At low temperature (0 ^{o}C to -20 ^{o}C), new signals appear at δ 9.9 and δ 6.6 (**Figure 2.30**). As will be described, these signals were assigned to one of the guanosine exocyclic N2 amino groups, based on NOE data.
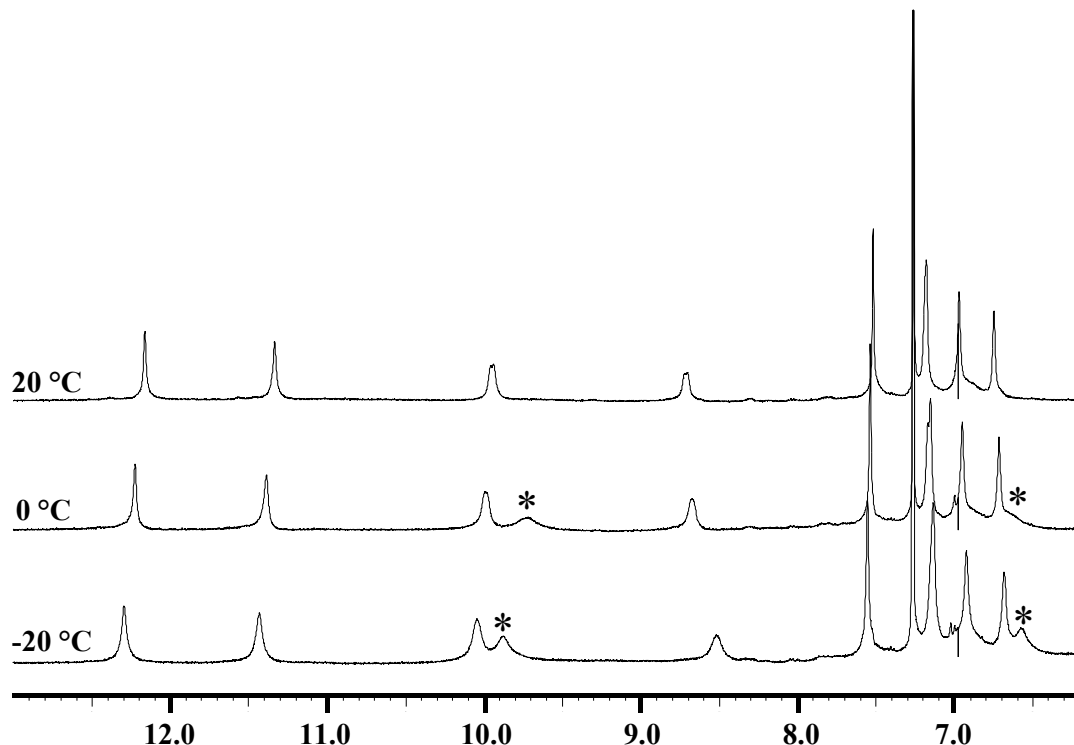
Figure 2.30. ^{1}H NMR spectra of (cG **2.34**)$_2$•NaCl•(H$_2$O)$_n$ at 20 ^{o}C, 0 ^{o}C, and -20 ^{o}C. New signals for the exocyclic amino N2-H$_a$ and N2-H$_b$ protons are indicated with asterisks.

145
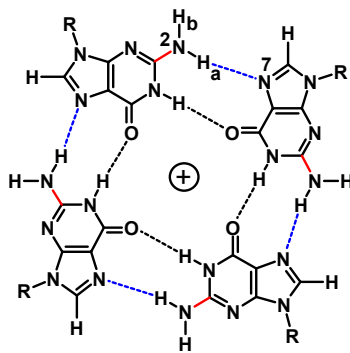
Figure 2.31. G-quartet showing the C2-N2 bond (red) and the N2-H···N7 hydrogen bond (blue).

Due to the N2-H···N7 hydrogen bond formed in the G-quartet, there is a significant barrier to rotation about the C2-N2 bond (red in **Figure 2.31**). At low temperature, the rotation slows and two signals are observed in the ^{1}H NMR spectrum, one hydrogen bonded at δ 9.9 and one "free" proton at δ 6.6 (labeled **a** and **b** in **Figure 2.31**, respectively). At room temperature, these two signals are broadened into the baseline due to moderate rotation about the C2-N2 bond. At 50 °C, however, rotation is fast enough that the two N2-H protons become equivalent (coalesce) on the chemical shift time scale, and a single broad resonance begins to grow in at δ 8.25 (blue asterisk in **Figure 2.30B**), exactly half way between the δ 9.9 and δ 6.6 resonances observed at -20 °C.

This behavior has been observed for other G-quartet systems. Collaborative work by the Davis and Gottarelli labs demonstrated that G-quartet formation from G **2.64** showed separate N2-H$_a$ and N2-H$_b$ signals near δ 9.4 and δ 5.0, respectively.[282] These signals were only observed below -10 °C. Above -10 °C, the signals were broadened into the baseline. Also, Sessler *et al*. reported a G-quartet formed from guanosine G **2.65** in the absence of a cation (see **Figure 2.36A**). Sessler's G-quartet also showed separate N2-H$_a$ and N2-H$_b$ signals that were, again, only observed at low temperature.[283]

G **2.64**
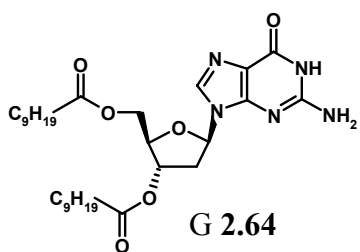
Before providing further evidence for a G-quartet, it is necessary to describe how the H1' and H8 resonances of the two sets of signals were assigned in (cG **2.34**)$_2$•NaCl•(H$_2$O)$_n$. Assignments were made based on ^{1}H-^{1}H COSY, ^{1}H-^{1}H NOESY, and ^{1}H-^{13}C HMQC data for (cG **2.34**)$_2$•NaCl•(H$_2$O)$_n$ recorded at -20 ^{o}C. The two sets of ^{1}H NMR signals are labeled as internal (i), near the G-quartet bridge, and external (e), near the periphery of the dimer, as shown in **Figure 2.18** (page 119).

From the COSY spectrum, the ribose signals were assigned based on their 3-bond correlations within the sugar ring. The H1' resonance is typically the furthest downfield of the sugar protons. **Figure 2.32** shows correlations for the internal signals (i) in blue, near the G-quartet, from 1'$_i$-4'$_i$ and the external signals (e) in red, on the periphery of the dimer, from 1'$_e$-3'$_e$. To further support the assignment of the resonances at δ 5.63 and 5.00 as H1' protons, the ^{1}H-^{13}C HMQC experiment determined that the carbons to which H1'$_i$ and H1'$_e$ are attached (C1'$_i$ and C1'$_e$) have similar chemical shifts, namely δ 90.9 and 89.9, respectively. These ^{13}C chemical shifts are near the value of δ 88.7 reported for C1' of guanosine **2.42** (see **Scheme 2.8**).[284]
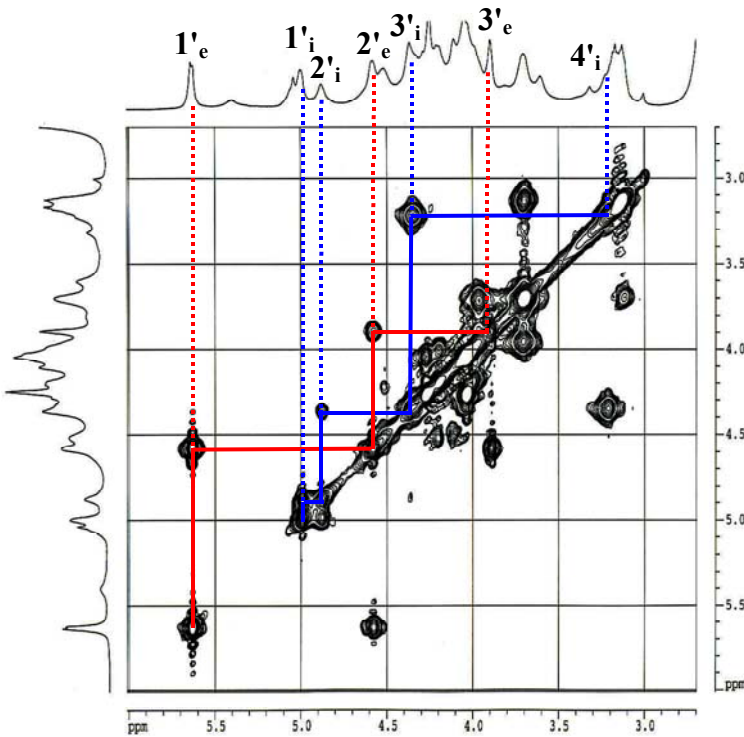
Figure 2.32. ^{1}H-^{1}H COSY spectrum of (cG **2.34**)$_2$•NaCl•(H$_2$O)$_n$ at -20 $^\circ$C. Red lines indicate external (e) signal correlations and blue lines indicate internal (i) signal correlations.

The H8 resonances were then assigned based on a NOESY experiment. In guanosine, NOEs are often observed between the H8 and H1' protons (**Figure 2.33B**).[253,282] In the NOESY spectrum in **Figure 2.33A**, H1'$_e$···H8$_e$ and H1'$_i$···H8$_i$ NOEs are indicated by red and blue lines, respectively. The H8$_i$ resonance is overlapped with a calix[4]arene aromatic resonance (ArH) near δ 7.15. **Figure 2.33C**, an expansion of the correlations along the F1 (vertical) axis, shows that there are indeed two signals. The H8$_i$ signal at δ 7.14 shows NOEs to N2-H$_i$ and H1'$_i$ (blue lines). The other signal at δ 7.13, the calix[4]arene ArH, shows an NOE to a second ArH (green lines).

148
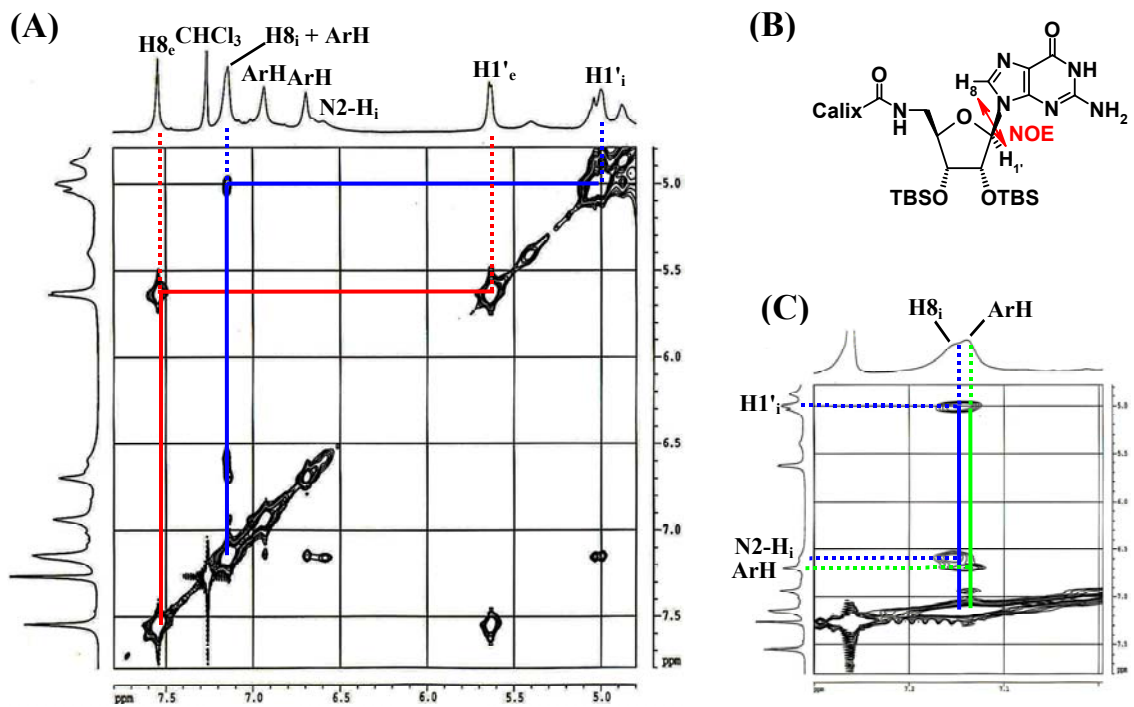
Figure 2.33. (A) ^{1}H-^{1}H NOESY spectrum of (cG **2.34**)$_2$•NaCl•(H$_2$O)$_n$ at -20 ^{o}C. Red lines indicate external H1'$_e$···H8$_e$ signal correlations and blue lines indicate internal H1'$_i$···H8$_i$ signal correlations. (B) Guanosine structure indicating the H1'···H8 NOE. (C) Expansion of the F1 (vertical) axis correlations near δ 7.15. Blue lines indicate H1'$_i$···H8$_i$ and N2-H$_i$···H8$_i$ NOEs and green lines indicate ArH···ArH NOEs.

With the H1'$_e$, H1'$_i$, H8$_e$, and H8$_i$ signals assigned, evidence for a G-quartet came from the ^{1}H-^{1}H NOESY experiment at -20 ^{o}C. As shown in **Figure 2.34**, both the hydrogen bonded N2-H$_{a,i}$ (δ 9.9) and the non-hydrogen bonded N2-H$_{b,i}$ (δ 6.6) showed NOEs to a single G N1-H$_i$ proton (δ 12.3). Moreover, both N2-H$_i$ signals correlated to the guanosine H8$_i$ proton (δ 7.2), a hallmark of a G-quartet.[282] This characteristic NOE pattern, taken together with the similarity of the low temperature 1D ^{1}H NMR results to other G-quartet systems, confirms a G-quartet bridge in the (cG **2.34**)$_2$ dimer.
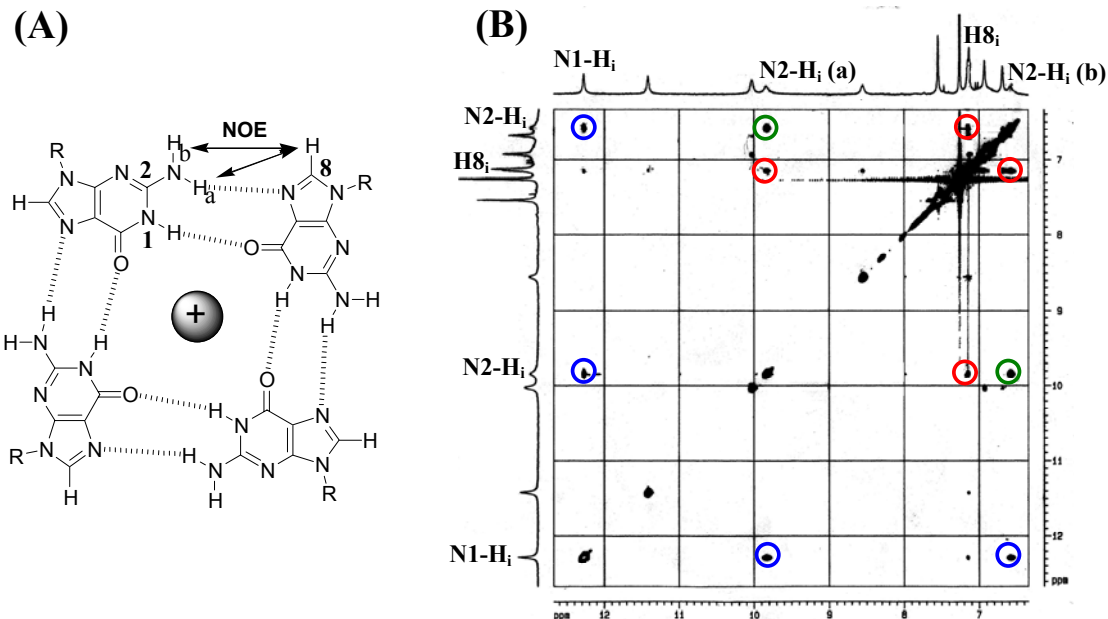
Figure 2.34. (A) G-Quartet indicating characteristic N2-H⋯H8 NOEs. (B) ^{1}H-^{1}H NOESY spectrum of (cG **2.34**)$_2$•NaCl•(H$_2$O)$_n$ at -20 $^{\circ}$C. Red: N2-H$_i$⋯H8$_i$ NOEs, Green: N2-H$_{a,i}$⋯N2-H$_{b,i}$ NOEs, Blue: N1-H$_i$⋯N2-H$_i$ NOEs.

Although evidence for both dimerization and a G-quartet came from the NaCl-containing complex, (cG **2.34**)$_2$•(H$_2$O)$_n$ is also likely to be a dimer complex held together by a G-quartet. To reiterate, both the (cG **2.34**)$_2$•(H$_2$O)$_n$ and (cG **2.34**)$_2$•NaCl•(H$_2$O)$_n$ complexes have very similar ^{1}H NMR spectra in water-saturated CDCl$_3$ (**Figure 2.35**), suggesting similar structure.
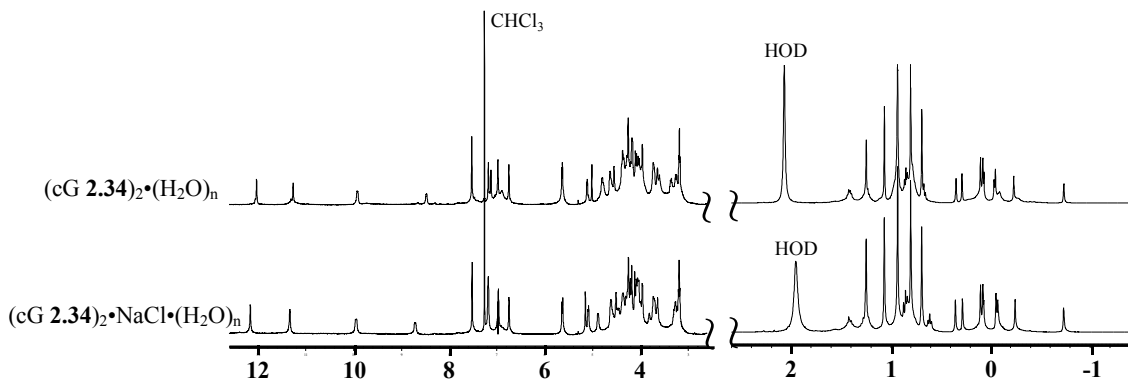
Figure 2.35. ^{1}H NMR spectra of (cG **2.34**)$_2$•(H$_2$O)$_n$ and (cG **2.34**)$_2$•NaCl•(H$_2$O)$_n$ in CDCl$_3$ at 23 °C. Samples were 2 mM in cG **2.34**.

The G-quartet holding the (cG **2.34**)$_2$•(H$_2$O)$_n$ dimer together would lack the templating cation. G-quartet formation in the absence of a cation does, in fact, have precedence. Sessler *et al*. demonstrated that guanosine derivative G **2.65** forms G-quartets both in solution and the solid state in the absence of a cation.[283] In that report, Sessler highlighted the critical role of the relative base-to-sugar conformation in G-quartet formation. Compound G **2.65** (**Figure 2.36A**), due to the bulky *N,N*-dimethylaniline attached to C8, adopts a *syn* conformation. That is, the base is positioned directly over the sugar, as shown in the structure. (The *anti* conformation would have the base pointing away from the sugar, or to the right in the structure, where the aniline group now resides). It had been thought that a cation was critical for G-quartet formation, since without a cation, other lipophilic guanosine derivatives formed hydrogen bonded ribbons and not quartets.[285,286] However, the formation of ribbons involves H-bonding to N3 (numbered in **Figure 2.36A**). In the *syn* conformation, the N3 is blocked thus preventing ribbon formation, and driving the formation of a G-quartet.

A G-quartet in (cG **2.34**)$_2$•(H$_2$O)$_n$ may very well hydrogen bond to water through the O6 carbonyl groups, with water taking the place of a cation. In fact, in the original G-quartet report, it was stated that a G-quartet "…would contain a hole in the middle in which it might be possible to place one water molecule per tetramer."[287] There have been numerous reports on crown ether-water complexes in which the water binds to the crown by hydrogen bonding to two oxygen atoms across the macrocycle.[288-290] A report by

151

Young and Sykes detailed the crystal structure of **2.66**·HNO$_3$·3H$_2$O, in which one water molecule was hydrogen bonded both to the quinone carbonyl and to an ether oxygen on the opposite side of the macrocycle (**Figure 2.36B**, H-bonded oxygens in blue).[291] The O···O distance was 4.65 Å. The O···O distance across the G-quartet in the K$^+$/Cs$^+$ G-quadruplex crystal structure (see **Figure 2.10**) was 4.58 ± 0.06 Å.[251] Based on the similar distances between O···O in **2.66** and O···O in the G-quartet, it is reasonable to predict that a water molecule can hydrogen bond across the quartet, as shown in **Figure 2.36C**.
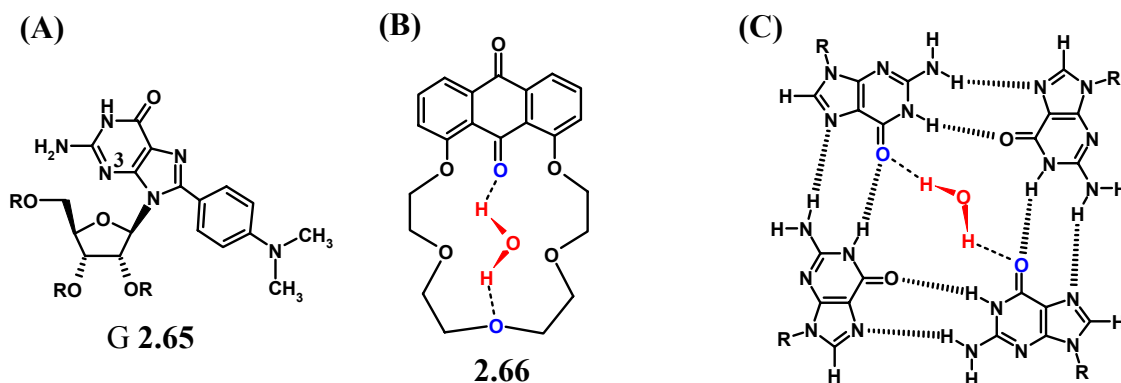
Figure 2.36. (A) Sessler's *N,N*-dimethylaniline-G **2.65** (R = C(O)CH(CH$_3$)$_2$) in the *syn* conformation.[283] (B) Representation of H$_2$O hydrogen bonding across crown ether **2.66** (O···O distance is 4.65 Å[291]). (C) Representation of H$_2$O hydrogen bonding across a G-quartet (G-quartet O···O distance when coordinating K$^+$ is 4.58 Å[251]).

2.7.11 Location of the Water in the Complex by ^{1}H-^{1}H NOESY.

NOE measurements have proven valuable for locating water in the interior of biomolecules.[292] The site-specific solvation of organic species has also been elucidated using NOE data.[293,294] In the case of (cG **2.34**)$_2$•NaCl•(H$_2$O)$_n$, information from the NOESY experiment (**Figures 2.33** and **2.34**) provided valuable information by locating the complex-bound water near the putative G-quartet.

The HDO signal (δ 2.8 at -20 °C) showed crosspeaks with N1-H$_i$ (δ 12.3), 5'-amide NH$_i$ (δ 8.6), N2-H$_i$ (δ 9.9, 6.6) and H8$_i$ (δ 7.2), the same internal resonances previously determined to be involved in (or located near) the G-quartet (**Figure 2.37**). Protons that

show NOEs with HDO are located close in space (within 5 Å) to the HDO molecules.[292] Water-nucleobase crosspeaks were not observed for the dimer's external set of signals. The G N1-H_i and 5'-NH_i amide protons that correlate with HDO are the same protons implicated to be in the dimer's cation and anion binding sites, respectively (see **Section 2.7.4**). This indicates that the ion pair and water are bound in the core of the dimer complex (**Figure 2.37**, left), although it is not yet clear whether the salt is bound as a contact ion pair or a solvent-separated ion pair.
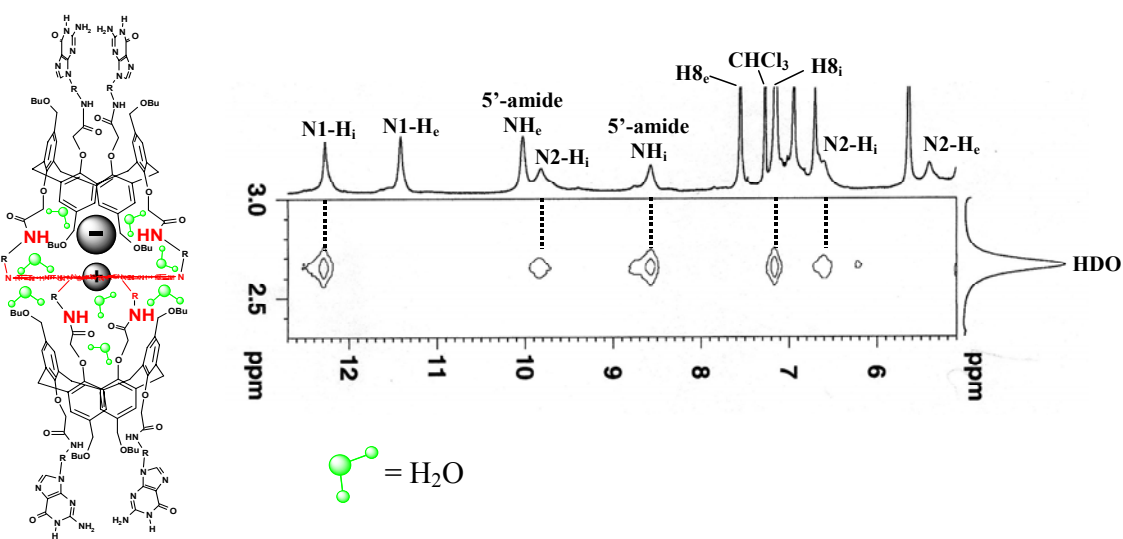
Figure 2.37. Representation of (cG **2.34**)$_2$•NaCl•(H_2O)$_n$ (left) showing water in green and ^{1}H-^{1}H NOESY (right) showing (cG **2.34**)$_2$•NaCl•(H_2O)$_n$ crosspeaks with HDO at -20 °C. Only the internal (i) set of signals shows crosspeaks.

2.7.12 Circular Dichroism Spectra of cG 2.34 Depend on the Solvent and Conditions.

Circular dichroism (CD) has previously been used to study the structure of chiral calixarenes and of G-quartet based assemblies.[251,295-298] CD spectroscopy also provided qualitative insight into self-association of cG **2.34** (**Figure 2.38**). The CD spectra of cG **2.34** (1.0 mM) were recorded using a 0.1 mm cell to ensure that the same concentrations were used for CD and NMR measurements. As shown in **Figure 2.38**, the spectra vary

with solvent and ionic conditions, reflecting a significant conformational change by cG **2.34**. The CD spectrum in CD_3OD, a solvent in which cG **2.34** is monomeric, has a symmetrical exciton coupling, with a positive band centered at 282 nm and a negative band centered at 250 nm. The spectrum of (cG **2.34**)$_2 \cdot$(H$_2$O)$_n$ in wet CDCl$_3$ is quite different from the spectrum in CD_3OD, as it shows an asymmetric and positive Cotton band. This difference indicates a change in conformation and/or secondary structure for cG **2.34** upon moving from CD_3OD to water-saturated CDCl$_3$. All of the salt complexes, (cG **2.34**)$_2 \cdot$MX$\cdot$(H$_2$O)$_n$, gave similar spectra, featuring an enhanced positive Cotton band at 284 nm for the K$^+$ salts and at 286 nm for the Na$^+$ salts. That the CD spectra of cG **2.34** change so markedly under conditions that favor self-association and salt binding is consistent with other studies on the association-dissociation of calixarene dimers.[297] The CD bands can not yet be unequivocally assigned to specific chromophores in cG **2.34**, since both the calixarene aromatic rings and the guanine base have UV absorption shoulders in the 270-280 nm region. Nonetheless, these preliminary experiments open the door for further and more detailed CD investigation of the structure and thermodynamics of these chiral assemblies.
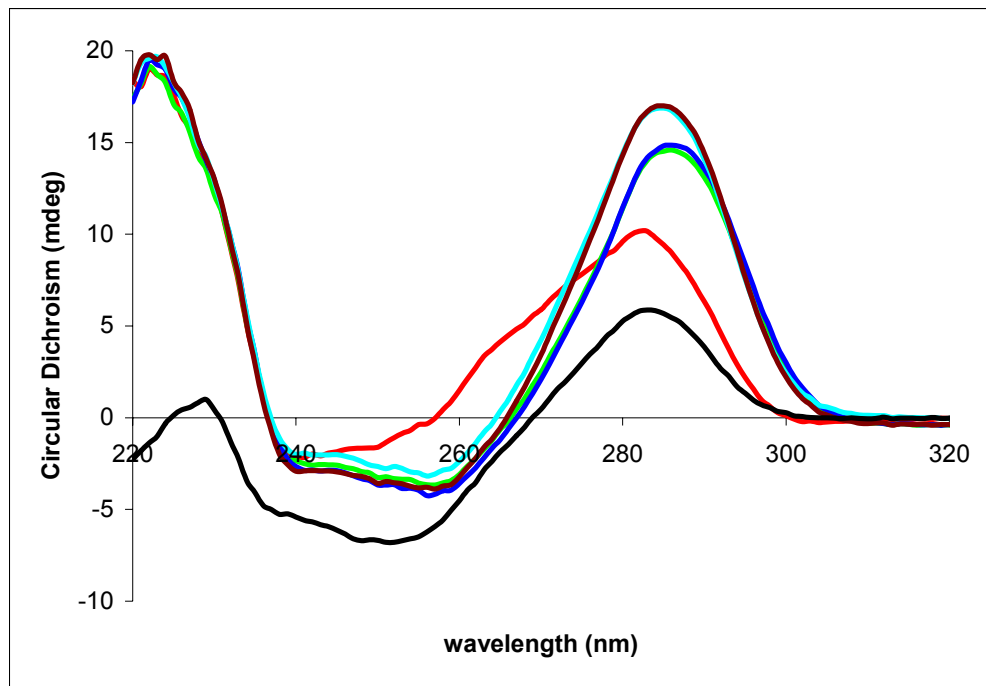
Figure 2.38. Circular dichroism spectra of cG **2.34** in CD_3OD (—), (cG **2.34**)$_2$•$(H_2O)_n$ in water-saturated $CDCl_3$ (—), and (cG **2.34**)$_2$•MX•$(H_2O)_n$ in water-saturated $CDCl_3$, where MX is: NaCl (—), NaBr(—), KCl (—) and KBr (—). All samples were 1.0 mM in cG **2.34**.

2.7.13 Supramolecular Polymer Formation from cG 2.34: The Anion Controls the Aggregation State.

In previous studies, we found that the first-generation compound, cG **2.26,** reversibly precipitated from solution in the presence of NaBPh$_4$, indicating formation of a noncovalent aggregate (**Section 2.5**). Sodium tetraphenylborate, with its non-coordinating anion, also triggers a similar aggregation of cG **2.34**. As represented in **Scheme 2.17**, introduction of NaBPh$_4$ to a $CDCl_3$ solution of either (cG **2.34**)$_2$•$(H_2O)_n$ or (cG **2.34**)$_2$•MX•$(H_2O)_n$ results in formation of a noncovalent polymer.

Scheme 2.17. Schematic representation of the reversible polymerization of cG **2.34**. Blue and red are used to distinguish between individual molecules.

$$(cG\ \mathbf{2.34})_2 \bullet (H_2O)_n$$

$$MX_{(aq)}$$

$$H_2O$$

$$(H_2O = \ )$$

$$(cG\ \mathbf{2.34})_2 \bullet MX \bullet (H_2O)_n$$

$$NaBPh_{4(aq)}$$

$$H_2O$$

$$NaBPh_{4(aq)}$$

$$MX_{(aq)}$$

$$(cG\ \mathbf{2.34} \bullet Na^+)_n \bullet (BPh_4^-)_n$$
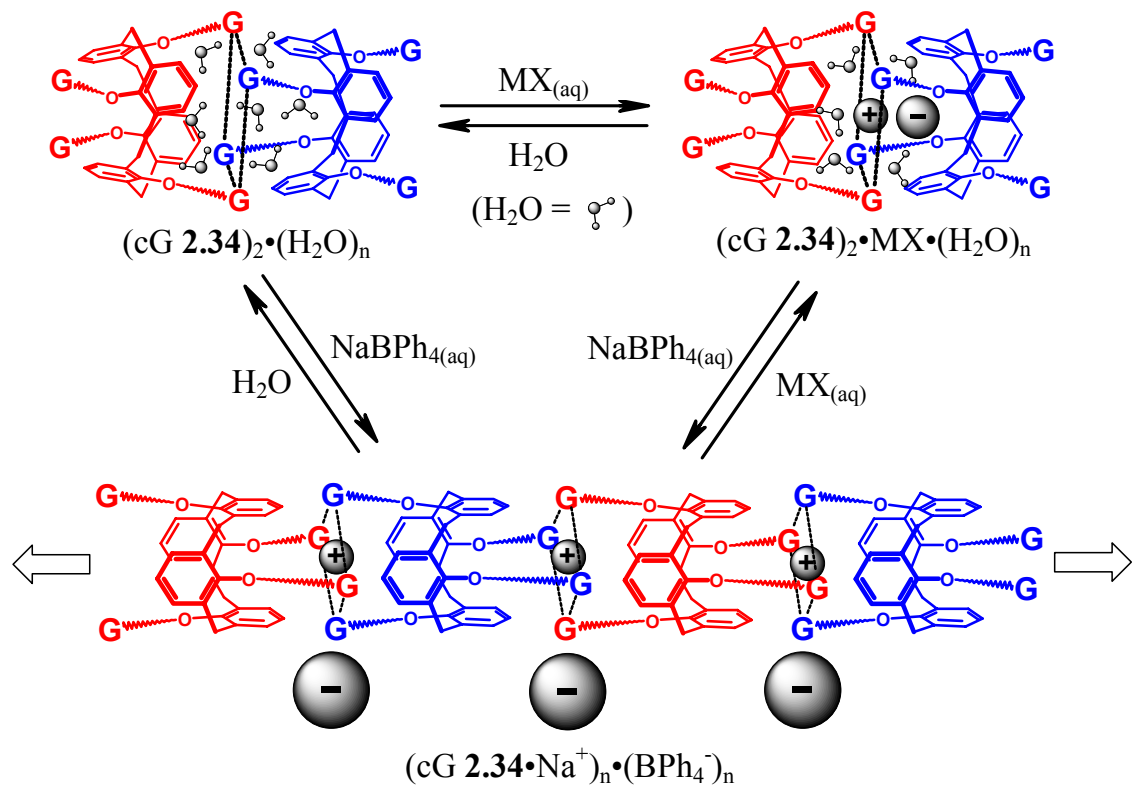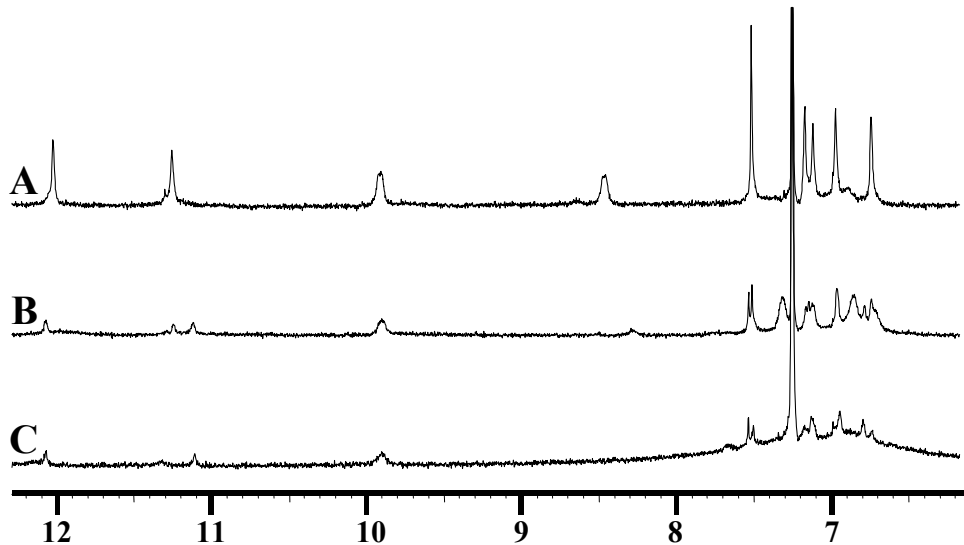
Figure 2.39. Titration of (cG **2.34**)$_2$•(H$_2$O)$_n$ in CDCl$_3$ (6.7 mM in cG **2.34**) with 0.15 M NaBPh$_4$ in 1:1 CDCl$_3$:CD$_3$CN as followed by NMR: (A) 0 *equiv*. (B) 0.5 *equiv*., and (C) 1.0 *equiv*.

Titration of (cG **2.34**)$_2$•(H$_2$O)$_n$ (**Figure 2.39A**) with a solution of NaBPh$_4$ in 1:1 CDCl$_3$:CD$_3$CN resulted in formation of a (cG **2.34**•Na$^+$)$_n$•(BPh$_4^-$)$_n$ polymer, as indicated by ^{1}H NMR. Thus, addition of 0.5 *equiv* of NaBPh$_4$ to (cG **2.34**)$_2$•(H$_2$O)$_n$ in CDCl$_3$ caused increased NMR noise and signal broadening due to aggregation (**Figure 2.39B**). Further addition of NaBPh$_4$ to a 1:1 ratio of cG **2.34**:NaBPh$_4$ resulted in a further increase in noise (**Figure 2.39C**) accompanied by precipitation of the polymer. The broad signals and the increased signal-to-noise ratio in the ^{1}H NMR spectrum in **Figure 2.39C** are characteristic of a noncovalent polymer.[261]

Washing a CDCl$_3$ solution of (cG **2.34**)$_2$•(H$_2$O)$_n$ with 1.0 M NaBPh$_{4(aq)}$ led to complete precipitation of cG **2.34**. The Si:Na ratio, and thus the cG **2.34**:Na$^+$ ratio, was obtained by semi-quantitative energy dispersive X-ray (EDX) analysis. EDX analysis provides information on elemental composition by energizing the sample with an electron beam and measuring the energies of the X-rays emitted from the sample.[299] Semi-quantitative EDX analysis of the precipitate gave a Si:Na ratio of 10.3:1 (± 15%) indicating a 1:1 cG **2.34**:NaBPh$_4$ ratio, in agreement with a polymer comprising

157

intermolecular Na$^+$-G-quartets.[189] A representative EDX spectrum is shown in Figure **2.40**. The expected Si:Na value for a 1:1 cG **2.34**:Na ratio is 8:1, as each cG **2.34** contains 8 silicon atoms.

This (cG **2.34**•Na$^+$)$_n$•(BPh$_4^-$)$_n$ precipitate could be converted back to the soluble (cG **2.34**)$_2$•(H$_2$O)$_n$ or (cG **2.34**)$_2$•MX•(H$_2$O)$_n$ dimers by washing with H$_2$O or an aqueous salt solution (**Scheme 2.17**), demonstrating the assembly's reversibility. The structural tunability of cG **2.34** assemblies is an attractive feature for building various supramolecular architectures from one instrumental molecular platform by varying a single component. In this case, that single component is the anion. It remains an open question as to why (cG **2.34**)$_2$•(H$_2$O)$_n$ and (cG **2.34**)$_2$•NaCl•(H$_2$O)$_n$ form discrete dimers instead of polymerizing. One possible explanation for the lack of polymerization is that the water or salt that binds in the dimer's interior induces a conformational change disfavoring the external guanosine nucleobases from also forming intermolecular G-quartets. Such ion-induced conformational changes are well known for 1,3-*alternate* calixarenes.[242,300]
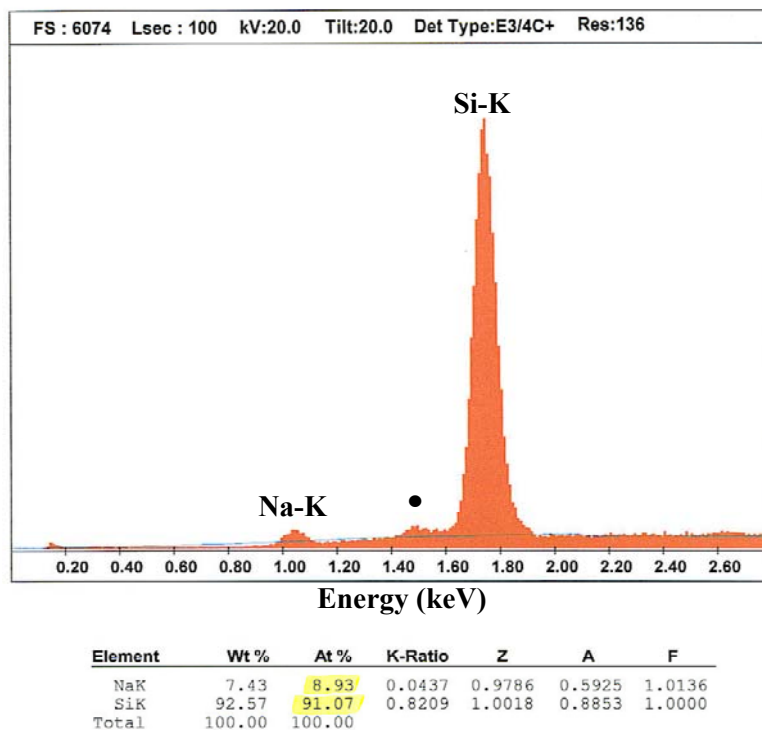
Figure 2.40. Energy Dispersive X-ray (EDX) analysis recorded for a solid sample of (cG **2.34**•Na⁺)ₙ•(BPh₄⁻)ₙ. The signal marked with a dot (•) originates from the aluminum in the sample tray. K indicates a K-shell electron. EDX analysis was run by Melanie Moses.

The evidence provided for a G-quartet in (cG **2.34**)$_2$•NaCl•(H$_2$O)$_n$ in **Section 2.7.10** further supports the hypothesis that it is also a Na⁺-G-quartet holding together both the (cG **2.34**•Na⁺)ₙ•(BPh₄⁻)ₙ and (cG **2.26**•Na⁺)ₙ•(BPh₄⁻)ₙ noncovalent polymers. In essence, the (cG **2.34**)$_2$•NaCl•(H$_2$O)$_n$ dimer is a "model system" for the polymer, isolating the G-quartet within a discrete structure so it can be studied.

2.7.14 Ion Transport by cG 2.34 and cA 2.35.

The ion transport properties of cG **2.34** and control compound cA **2.35** were investigated using the base pulse assay (**Section 1.5.5**) under the conditions described in **Section 2.6.2** (for transport assays with cG **2.26**). As shown in **Figure 2.41A** and **Table 2.3**, cG **2.34** transports K^+ selectively over Cs^+ and Na^+ ($K^+ > Cs^+ > Na^+$). The transport properties of cG **2.34** are similar to those of the more polar cG **2.26** (see **Figure 2.17A** in **Section 2.6.2**). The control compound cA **2.35** demonstrated a transport selectivity of $K^+ \approx Cs^+ > Na^+$(**Figure 2.41B**, **Table 2.3**). The initial pseudo-first order rate constant for cG **2.34**-mediated transport of K^+ was 1.7-fold greater than that of K^+ or Cs^+ transport mediated by cA **2.35** (**Table 2.3**).
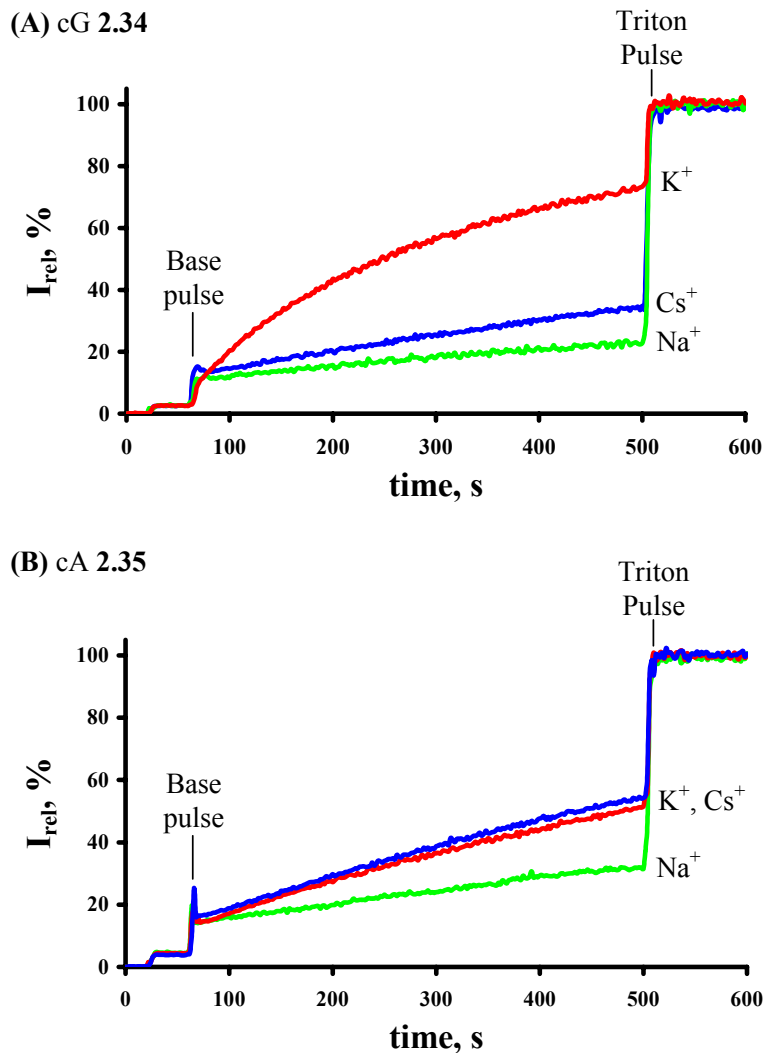
Figure 2.41. Liposome transport assays with (A) cG **2.34** and (B) cA **2.35**. In all experiments, suspensions of EYPC LUVs containing the pH-sensitive dye pyranine in a phosphate buffer were used. The intravesicular solution contained 10 mM sodium phosphate, pH 6.4, 100 mM NaCl and the extravesicular solution contained 10 mM sodium phosphate, pH 6.4, 100 mM MCl (M = Na^+, K^+, Cs^+). Time events: *0 sec:* 20 µl of (A) 1 mM cG **2.34** solution in DMSO added or (B) 1 mM cA **2.35** solution in DMSO added (final concentration: 10 µM, 1:50 ligand:lipid ratio), *60 sec:* (A,B) 21 µl of 0.5 M NaOH added (Base Pulse), *500 sec:* (A,B) 40 µl of 50 % aqueous Triton X-100 added (Triton Pulse). Extravesicular buffers contained 100 mM NaCl (—), KCl (—), or CsCl (—).

161

Table 2.3. Initial Pseudo-First Order Rate Constants (x 10^{-3} s^{-1}) for Intravesicular/Extravesicular Electrolyte Exchange in the Presence of 10 μM cG **2.34** or cA **2.35** with NaCl-, KCl-, and CsCl-containing Extravesicular Buffers.

Ion Transporter	NaCl	KCl	CsCl
cG **2.34**	1.5	7.8	2.5
cA **2.35**	1.7	4.6	4.3

Calcein release assays, described in **Section 1.5.11**, were used to test if cG **2.34** or cA **2.35** induce large defects in the bilayer, through which ions may pass. At a final concentration of 25 μM (1:20 ligand:lipid ratio), no release of the self-quenching dye calcein from liposomes was observed (**Figure 2.42**, blue and red traces). The concentration used here (25 μM) is 2.5-fold higher than that used in the base pulse assays (**Figure 2.41**). Also, no release was observed at lower ligand concentrations. These data indicate that cG **2.34** and cA **2.35** do not induce defects in the lipid bilayer, but transport ions through either a channel or a carrier mechanism. For comparison, injection of melittin, a peptide known to induce defects in EYPC membranes (see **Section 1.3**), results in a rapid release of the liposome-entrapped calcein, seen as a sharp increase in fluorescence (**Figure 2.42**, green trace).
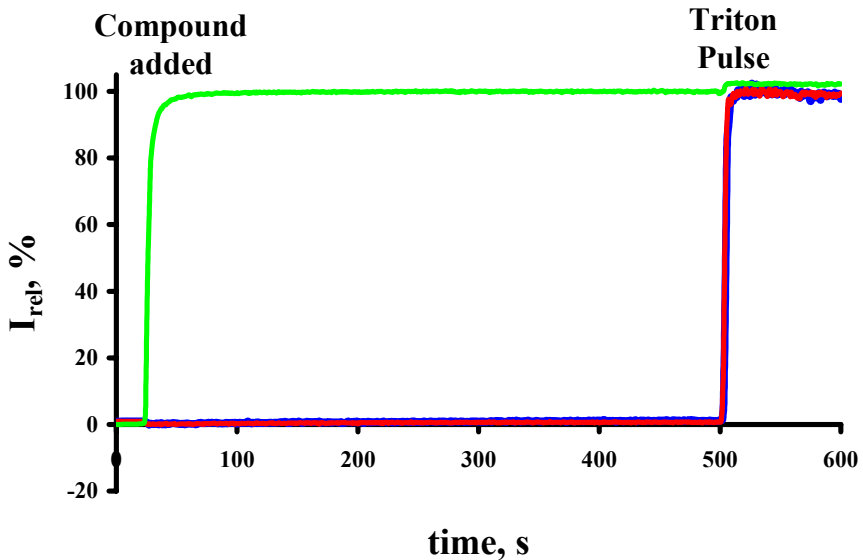
Figure 2.42. Calcein release assays with cG **2.34**, cA **3.35**, and the defect-inducing peptide melittin. In all experiments, suspensions of EYPC LUVs were used. The intravesicular solution contained 10 mM sodium phosphate, pH 6.4, and 120 mM calcein. The extravesicular solution contained 10 mM sodium phosphate, pH 6.4, and 200 mM NaCl (isoosmolar). Time events: *20 sec:* 20 μl of 2.5 mM cG **2.34** solution in DMSO added (—), 2.5 mM cA **2.35** solution in DMSO added (—) or 100 μM melittin in phosphate buffer added (—), *500 sec:* 40 μl of 50 % aqueous Triton X-100 added (Triton Pulse).

The mechanism of transport (i.e. carrier or channel) and the active cG **2.34** and cG **2.26** structures responsible for ion transport (i.e. monomer, dimer, or multimer) remain to be elucidated. However, by bringing the results of base pulse assays with cG **2.34** and cA **2.35** (**Figure 2.41**) together with the cG **2.26** base pulse assays (**Figure 2.17A**) and the ion binding properties of cG **2.34** discussed throughout this section, several predictions can be made:

(1) Calix[4]arene-guanosine conjugates cG **2.26** and cG **2.34** demonstrated similar ion transport properties, suggesting that a calix[4]arene core (with or without

163

butoxymethylene chains) bearing four guanosine bases (with either an isopropylidene or silyl protecting groups) is the basic structure required for K^+-selective transport.

(2) Control compound cA **2.35** showed transport properties different than those exhibited by cG **2.34**, with cA **2.35** transporting K^+ and Cs^+ at nearly half the rate of K^+ transport mediated by cG **2.34**. Most importantly, cA **2.35** is not K^+-selective. Since cA **2.35** possesses a structure nearly identical to cG **2.34**, but with adenine in place of guanine on the bases, the transport data implicate the guanosine bases of cG **2.34** and cG **2.26** as critical for K^+ transport and selectivity.

(3) In **Section 2.7.4**, a 2:1 K^+:Na^+ extraction selectivity was reported for the (cG **2.34**)$_2$•(H$_2$O)$_n$ dimer (based on both ^{1}H NMR integration and IC measurements). A K^+ > Na^+ transport selectivity was also observed, raising the question of whether ion binding and ion transport is facilitated by the same supramolecular structure. Indeed, ion binding and ion transport selectivities exhibited by ionophores have been shown to reflect one another in some cases.[301] Furthermore, the (cG **2.34**)$_2$•(H$_2$O)$_n$ dimer is likely to span the membrane, satisfying one requirement for synthetic ion channels (see **Sections 1.6** and **1.7**). From a crystal structure that will be discussed in **Chapter 3** (see **Figure 3.8**), the dimer of calix[4]arene 1,3-*alternate* tetramethylamide **2.30** (**Scheme 2.6**, a derivative of calix[4]arene-tetrabutylamide **3.1**) had a length of 25 Å. This length is sufficient to span the hydrocarbon region of an EYPC bilayer.[302] The (cG **2.34**)$_2$•(H$_2$O)$_n$ dimer, bearing guanosine nucleosides in place of the methyl amides of **2.30**, will most likely exceed the 25 Å length of the smaller **2.30**. This being the case, a (cG **2.34**)$_2$•(H$_2$O)$_n$ dimer may serve as the active structure, spanning the membrane and conducting or shuttling ions.

(4) Lastly, water was shown to be an integral component of the (cG **2.34**)$_2$•(H$_2$O)$_n$ dimer. Water is also integral in the structure of many natural and synthetic ion channels (**Chapter 1**), wherein a water-filled pore supported by the channel allows the passage of ions through the hydrophobic membrane. Since the (cG **2.34**)$_2$•(H$_2$O)$_n$ dimer retains a water-filled cavity in CHCl$_3$ (dielectric constant = 5.5), the complex is also expected to

retain its aqueous core in lipid membranes (dielectric constant ≈ 2).[303] The water-filled cavity in (cG **2.34**)$_2$•(H$_2$O)$_n$ may facilitate ion transport across the membrane, providing a polar environment through which cations may pass. Also, the presence of water in the dimer's core alleviates the energy cost for an ion entering the transporter, since a partial solvation shell would be retained.

2.7.15 Conclusions

Nucleoside conjugate cG **2.34** dimerizes in wet CDCl$_3$ to give (cG **2.34**)$_2$•(H$_2$O)$_n$. Water mediates the transformation of a non-specific aggregate into a discrete and functional complex. The (cG **2.34**)$_2$•(H$_2$O)$_n$ dimer is a ditopic receptor capable of extracting alkali halides from aqueous solution into organic solvents. In this receptor, the G-quartet cation binding site is "built" into the complex through self-assembly, and cG **2.34**'s amides serve to bind halide anions. This study underscores water's ability to stabilize a functional noncovalent assembly and provides a rare example of a self-assembled ion pair receptor. In addition, the supramolecular architecture formed from cG **2.34** is tunable, as changing from a halide to the non-coordinating BPh$_4^-$ results in supramolecular polymers. Lastly, cG **2.34** mediates K$^+$-selective transport across EYPC membranes. Although the mechanism and active structure are still unknown, the study of ion pair receptor (cG **2.34**)$_2$•(H$_2$O)$_n$ suggests that this water-containing dimer may serve as the membrane spanning transporter.

In the course of studying the ion transport properties of calix[4]arene-guanosine conjugates, chloride transporter calix[4]arene tetrabutylamide **3.1** was discovered, as discussed in **Section 2.6.2**. **Chapter 3** will focus on the chloride-selective ion channels formed from **3.1** and the chloride transport properties of related secondary amide compounds.

2.7.16. Future Directions.

(1) Certainly, cation transport mediated by cG **2.26** and cG **2.34** deserves further investigation. The promising preliminary results described in **Sections 2.6.2** and **2.7.14** show that these calix[4]arene-guanosine conjugates indeed function as cation-selective transporters, suggesting, at least in part, that the design was correct (see **Section 2.4.4**). The structural insight gained from the study of (cG **2.34**)$_2$•(H$_2$O)$_n$ salt-free and salt-containing complexes provides a basis for structural studies of the active transporter in membranes. For example, circular dichroism has been widely used to gain insight into membrane-bound structures. With the circular dichroism signatures of the (cG **2.34**)$_2$•(H$_2$O)$_n$ complexes in hand, determining the presence of this structure in membranes becomes possible. Also, voltage clamp experiments would determine whether cG **2.26** and cG **2.34** function as ion carriers or ion channels.

(2) Bringing together the data from **Sections 2.7.4** and **2.7.10** leads to the conclusion that (cG **2.34**)$_2$•(H$_2$O)$_n$ binds alkali halide salts as either a contact ion pair or a solvent separated ion pair in the core of the dimer. Although no zwitterionic species were investigated, it seems logical that zwitterionic amino acids might fit nicely into the binding pocket, much like the receptors of de Mendoza and Sessler described in **Section 2.3.2**.[229,230] Since the appended guanosines are chiral, (cG **2.34**)$_2$•(H$_2$O)$_n$ could prove to be an enantioselective host for such chiral guests.

Chapter 3. Chloride Transport by Synthetic Small Molecules

3.1 Introduction.

The initial goal of the research described in this thesis was to develop molecular building blocks that would form ion channels in membranes through self-assembly. This goal has been achieved, as will be described in this chapter. Calix[4]arene tetrabutylamide **3.1**, a ligand discovered in the study of calix[4]arene-guanosine conjugate **2.26** (**Section 2.6.2**), forms chloride-selective ion channels in planar bilayers and in cells. **Section 3.2** briefly discusses applications of synthetic chloride transporters. The structure and function of ion channels formed from calix[4]arene tetrabutylamide **3.1** are then described (**Section 3.3**). In the second part of this chapter, the ion transport properties of linear analogs of **3.1**, oligophenoxyacetamides **3.3-3.8**, are investigated. The rationale for their development is first presented (**Section 3.4**) followed by functional studies of the oligomers (**Section 3.5**), and in particular trimer **3.5**, a more potent chloride transporter than calix[4]arene tetrabutylamide **3.1**.

Sections 3.3 and **3.5** of this chapter have been published separately in the *Journal of the American Chemical Society*.[93,141] The work presented in this chapter was done in a collaboration between Dr. Vladimir Sidorov and myself. Dr. Sidorov conducted many of the experiments that will be discussed, and his work is credited throughout this chapter in the text or in figure captions. My own contributions (the author) are also made clear. The two manuscripts published on this work were prepared by Dr. Sidorov, Prof. Davis and myself. In addition, smaller contributions were made by other researchers and these contributions are credited in individual sections throughout the chapter.

3.2 Applications of Synthetic Chloride Transporters

Identification of compounds that transport chloride across cell membranes has important implications in drug development. Synthetic chloride transporters have already shown potential in the treatment of cystic fibrosis (**Section 1.7**). The peptide C-K$_4$-M2GlyR **1.34** was found to increase Cl$^-$ currents in airway epithelial cells from a human cystic fibrosis patient and N-K$_4$-M2GlyR **1.35** restored secretion of the antioxidant

glutathione.[171,174] Sterol **1.41** was also shown to mediate Cl$^-$ transport across cystic fibrosis cells.[16] These promising leads have opened up a new strategy for the treatment of diseases caused by chloride channel malfunctions. That is, chloride movement across the membrane, along with cellular functions that depend on chloride transport, can be restored by small molecular transporters. In addition to cystic fibrosis, epilepsy and myotonia have been linked to chloride channel defects, and thus represent other diseases that may be alleviated by the restoration of chloride transport.[17]

In addition to chloride transport, compounds that enable H$^+$/Cl$^-$ cotransport also have therapeutic potential. The immunosuppressive and anticancer activities of the prodigiosin family of antibiotics have been attributed to their ability to cotransport H$^+$/Cl$^-$.[304-306] As summarized in **Section 3.1**, the calix[4]arene tetrabutylamide **3.1** and trimer **3.5** do indeed facilitate chloride transport (via a channel mechanism for the case of **3.1**) and H$^+$/Cl$^-$ cotransport. These compounds are potentially valuable leads in drug development for the treatment of cystic fibrosis and cancer.

3.3 Ion Channel Formation from a Calix[4]arene Amide that Binds HCl

3.3.1 Introduction

As described in **Sections 1.6** and **1.7**, both single molecule and self-assembly approaches are used for the design of artificial ion channels. Self-assembly is an attractive approach for making pores within a membrane, as functional structures can arise from simple building blocks. Nature certainly makes spectacular use of self-assembly to form ion channels, as illustrated by the crystal structures of the K$^+$ channel and the ClC chloride channel described in **Sections 1.2.2** and **1.2.3**.[8,9]

While investigating the self-assembly and ion transport properties of calix[4]arene-guanosine conjugate cG **2.26** (**Section 2.6.2**), attention was focused on the secondary amide groups that connect the nucleosides to the calix[4]arene *1,3-alt* scaffold. Compounds **2.30**, **3.1**, **3.2** and **3.3** (**Chart 3.1**) were investigated to determine whether calix[4]arene *1,3-alt* amides might self-assemble in the presence of cations and/or anions. In this section, the results described confirm that calix[4]arene tetrabutylamide **3.1** binds

HCl in solution, forms ion channels in a planar lipid bilayer and in cells, and effectively transports HCl across liposomal membranes by an H^+/Cl^- symport or a Cl^-/OH^- antiport mechanism. Also, solid-state evidence that the analogous calix[4]arene tetramethylamide **2.30** self-assembles in the presence of HCl to form ordered arrays containing chloride-filled and water-filled channels is described. By comparing ion binding and transport properties of calix[4]arene tetrabutylamide **3.1** with those of its structural analogs **2.30** and **3.2**, the compound's hydrophobicity and the amide's substitution pattern are shown to be essential structural factors for mediating chloride transport. The evidence points towards a self-assembled channel being formed by calix[4]arene tetrabutylamide **3.1** in an anion-dependent process.

Chart 3.1

3.1   2.30   3.2   3.3
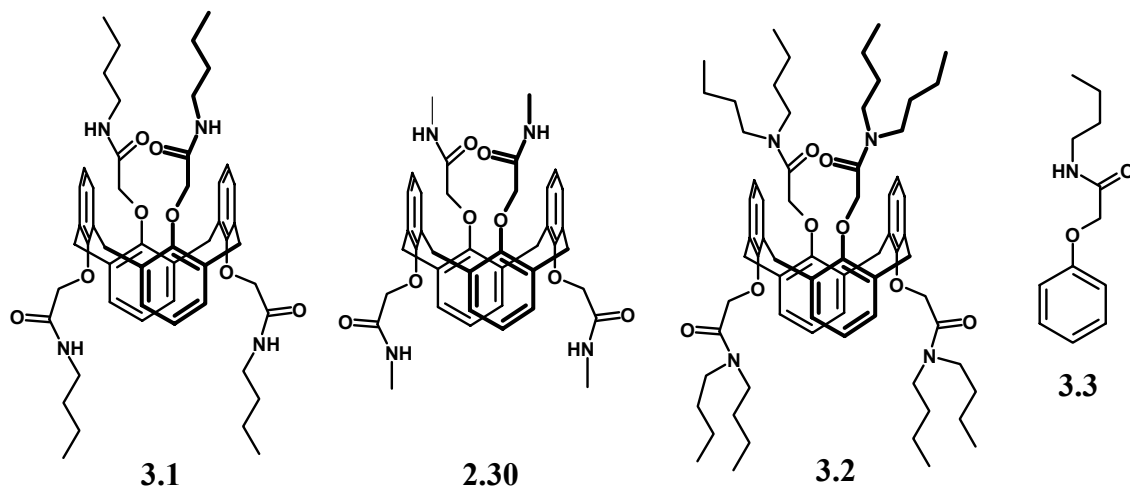
3.3.2 Synthesis of Calix[4]arene tetrabutylamide 3.1 and Control Compounds

Calix[4]arene tetrabutylamide **3.1** and octabutylamide **3.2** were prepared by reaction of tetraacid **2.29** (**Section 2.5.2**) with $SOCl_2$ in benzene to form the acid chloride, followed by coupling with the appropriate amine, as shown in **Scheme 3.1**. Control compound *N*-butyl-2-phenoxyacetamide **3.3** was prepared from 2-phenoxyacetic acid and butylamine as shown in **Scheme 3.2**. Calix[4]arene tetramethylamide **2.30** was prepared

as described in Section **2.5.2** (see **Scheme 2. 6**). Compounds **2.30**, **3.1**, **3.2** and **3.3** were prepared by Dr. Vladimir Sidorov.

Scheme 3.1 Synthesis of calix[4]arene tetrabutylamide **3.1** and octabutylamide **3.2**.
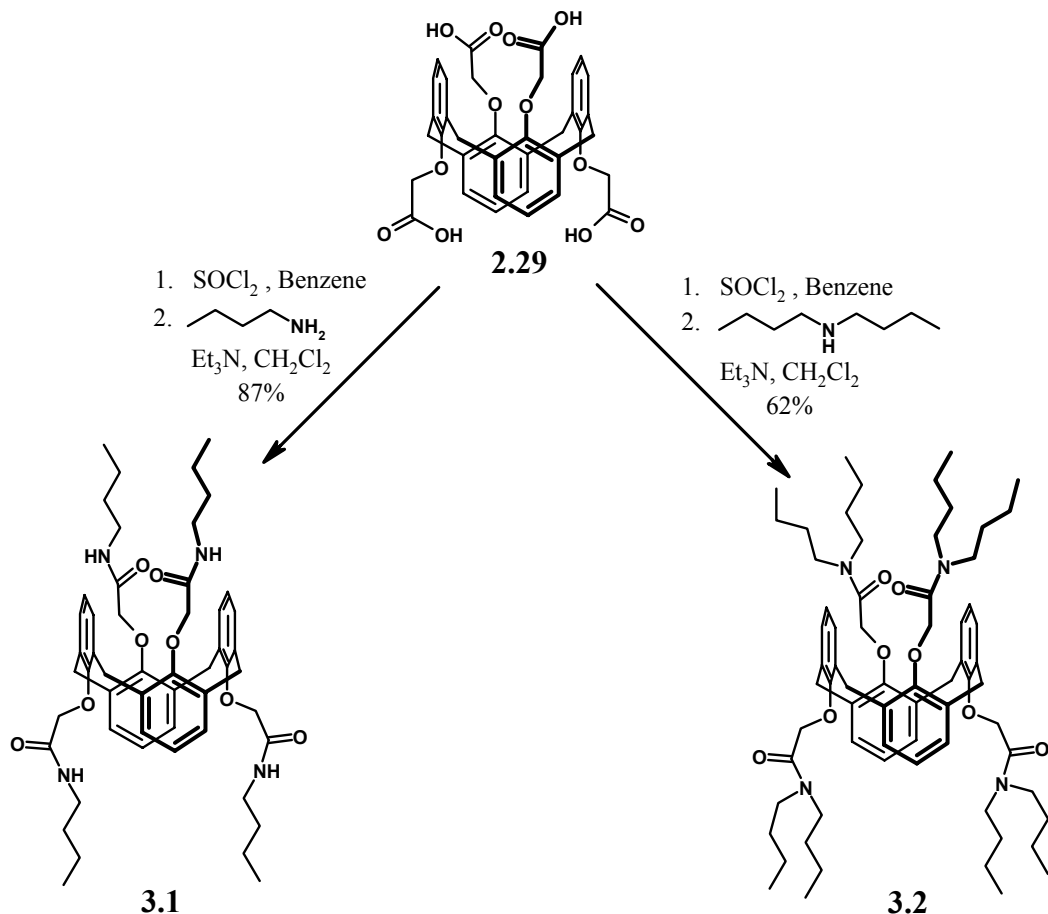
Scheme 3.2 Synthesis of control compound **3.3.**
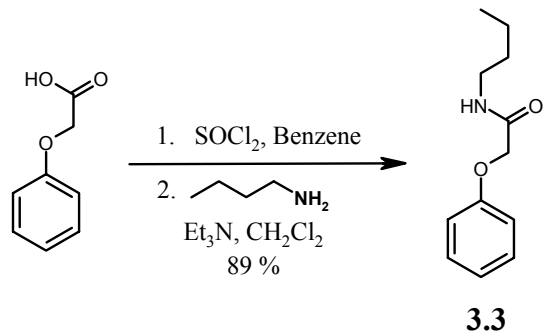
3.3.3 Base Pulse Assays Reveal that Calix[4]arene tetrabutylamide 3.1 Mediates Chloride Transport Across EYPC Membranes

The ability of calix[4]arene tetrabutylamide **3.1** and calix[4]arene tetramethylamide **2.30** to mediate ion flux across a lipid bilayer was studied in base pulse assays (see **Section 1.5.5**). Rapid exchange of intra- and extravesicular electrolytes was observed in the presence of calix[4]arene tetrabutylamide **3.1** at a ligand:lipid ratio of 1:100 (**Figure 3.1A**). These fluorescence assays indicated that ion transport mediated by **3.1** is essentially non-selective towards the cation in buffers containing Na^+, K^+ or Cs^+ (**Figure 3.1A**, **Table 3.1**). As was discussed in **Section 2.6.2**, the only constant in the three transport assays was chloride anion, and **3.1** does indeed mediate Cl^- transport. Further support for this claim will be described throughout this section.

Calix[4]arene tetramethylamide **2.30** showed little transport activity in the presence of extravesicular Na^+, K^+ or Cs^+ chloride solutions at ligand:lipid ratios up to 1:20 (**Figure 3.1B**, **Table 3.1**). The decreased activity of tetramethylamide **2.30** can be attributed to its lower hydrophobicity with respect to tetrabutylamide **3.1**. Reverse-phase HPLC retention times (C-18, 1:1 CH_3CN:0.1 % aqueous TFA, 1 mL/min) were 4.8 min and 54.1 min for **2.30** and **3.1**, respectively. This clearly shows that tetramethylamide **2.30** is significantly more polar than tetrabutylamide **3.1**.[307] The increased polarity of calix[4]arene tetramethylamide **2.30** likely results in poor lipid/water partitioning, and therefore decreased amounts of **2.30** in the membrane.
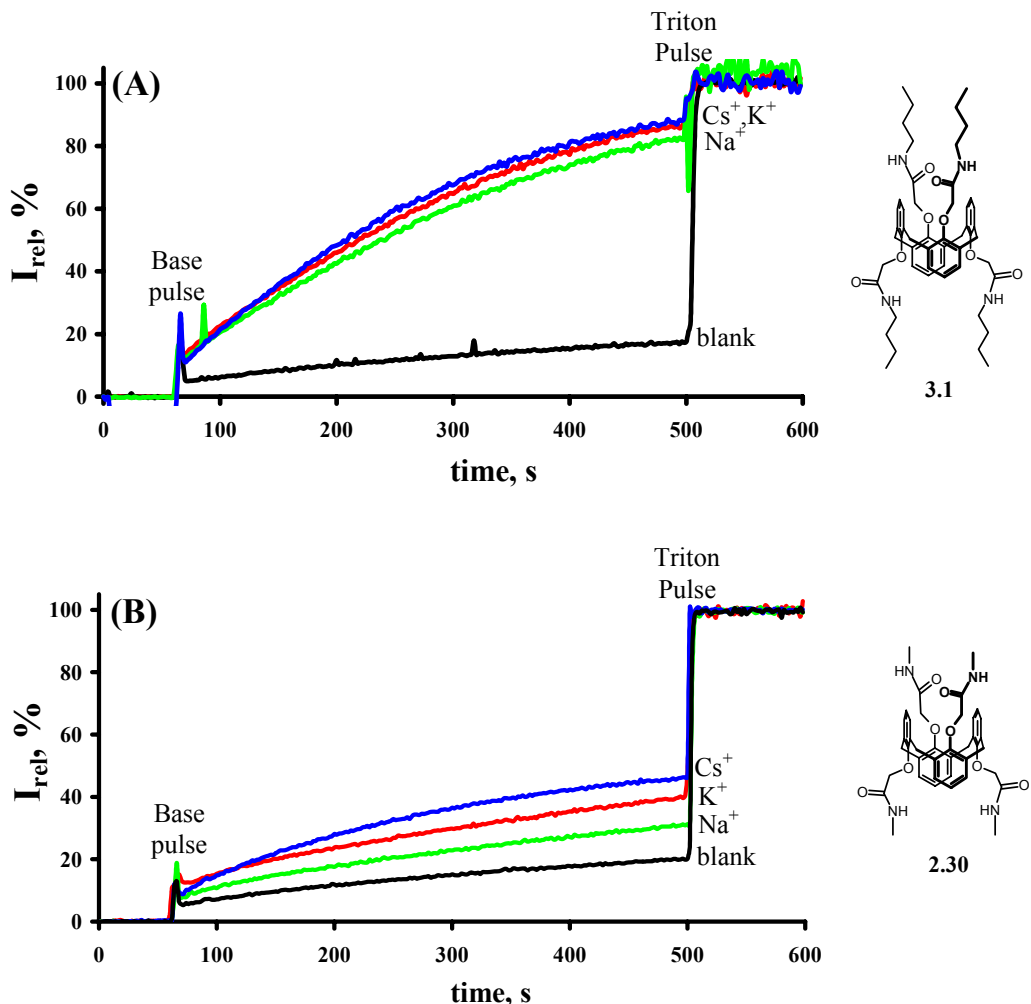
Figure 3.1. Base pulse transport assays with (A) **3.1** and (B) **2.30**. In all experiments, suspensions of EYPC LUVs containing the pH-sensitive dye pyranine in a phosphate buffer were used. The intravesicular solution contained 10 mM sodium phosphate, pH 6.4, 100 mM NaCl and the extravesicular solution contained 10 mM sodium phosphate, pH 6.4, 100 mM MCl (M = Na^+, K^+, Cs^+). Time events: *0 sec:* 20 μl of (A) 0.5 mM **3.1** solution in THF added or (B) 0.5 mM **2.30** in 1:1 THF:MeOH added (final concentration: 5 μM, 1:100 ligand:lipid ratio), *60 sec:* (A,B) 21 μl of 0.5 M NaOH added (Base Pulse), *500 sec:* (A,B) 40 μl of 50 % aqueous Triton X-100 added (Triton Pulse). Extravesicular buffers contained 100 mM NaCl (—), KCl (—), or CsCl (—). Experiments conducted by the author.

Table 3.1. Initial Pseudo-First Order Rate Constants (x 10^{-3} s^{-1}) for Intravesicular/Extravesicular Electrolyte Exchange in the Presence of 5 µM **3.1** or **2.30**.

Ion Transporter	NaCl[a]	KCl[b]	CsCl[c]	Na$_2$SO$_4$[d]
3.1	6.8	6.4	7.7	1.1
2.30	2.5	2.2	4.1	N/A

a NaCl buffer inside, NaCl buffer outside
b NaCl buffer inside, KCl buffer outside
c NaCl buffer inside, CsCl buffer outside
d Na$_2$SO$_4$ buffer inside, Na$_2$SO$_4$ buffer outside

    Secondary amides can interact with both anions and cations, making it entirely reasonable that calix[4]arene tetrabutylamide **3.1** could bind and transport either type of ion. Since the transport activity of calix[4]arene **3.1** was essentially cation-independent (**Figure 3.1A**), the possibility that ion transport mediated by **3.1** might be anion dependent was investigated. Base pulse fluorescence assays were conducted with sodium sulfate-filled LUVs suspended in an isotonic solution. Unlike for chloride-containing solutions, experiments in sulfate buffers revealed that the pH-induced ion flux across the membrane was not mediated by 5-50 µM concentrations of **3.1** (1-10 mol % ligand, **Figure 3.2**). This pronounced Cl$^-$/HSO$_4^-$ transport selectivity (**Table 3.1**, k = 6.8 x 10^{-3} s^{-1} for NaCl-containing buffer, k = 1.1 x 10^{-3} s^{-1} for Na$_2$SO$_4$-containing buffer) implies that calix[4]arene tetrabutylamide **3.1** functions as a Cl$^-$ transporter.
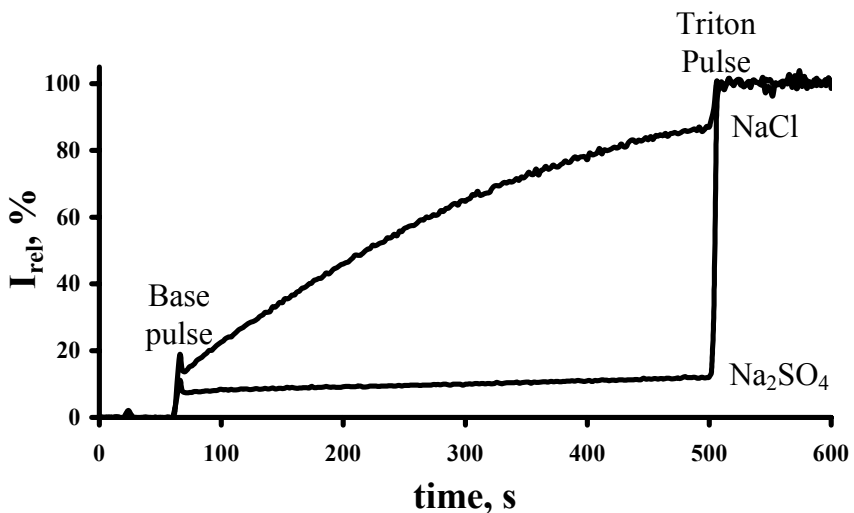
Figure 3.2. Liposome transport assays with **3.1** in liposomal suspensions containing 100 mM NaCl inside and outside (top trace) and 75 mM Na$_2$SO$_4$ inside and outside (bottom trace). Suspensions of EYPC LUVs containing the pH-sensitive dye pyranine in a phosphate buffer were used. Time events: *20 sec:* 20 μl of 0.5 mM **3.1** solution in THF added (final concentration: 5 μM, 1:100 ligand:lipid ratio), *60 sec:* 21 μl of 0.5 M NaOH added (Base Pulse), *500 sec:* 40 μl of 50 % aqueous Triton X-100 added (Triton Pulse). No significant transport in the Na$_2$SO$_4$ buffer was observed even in the presence of 50 μM **3.1** (1:10 ligand:lipid ratio). Experiments conducted by Dr. Vladimir Sidorov.

3.3.4 Pyranine Adsorption to Membranes

The polyanionic dye pyranine is known to adsorb to positively charged vesicles.[77,308] Pyranine also adsorbs to some extent to neutral liposomes such as EYPC, and this issue is addressed here.[185] The fluorescence traces for base pulse assays shown throughout this thesis represent the ratio of deprotonated to protonated forms of the dye (excitation wavelengths at both 460 and 403 nm, see **Section 1.5.5**) and therefore register a response directly proportional to pH.[309] In this way, dye adsorption to the internal surface of the vesicles does not interfere with the pH measurements. The amount of dye adsorbed to the outer surface of EYPC LUVs was estimated by analyzing the immediate fluorescence "burst" response upon addition of base (see, for example, **Figure 3.1A**). This response has never exceeded 15 % of the total fluorescent change observed in the course of

174

experiments. The slower phase of fluorescence increase is due to the rise in intravesicular pH as the ligand transports ions across the EYPC membrane. It is the rate constants of this second phase that are reported in **Tables 2.3**, **3.1** and **3.2** of this thesis. Furthermore, negative controls indicate that there is little fluorescence increase in the absence of an active transporter (see **Figure 3.1A** and **B**, black traces).

The adsorption of pyranine to the membrane can be minimized by incorporation of negatively charged lipids (e.g. phosphatidylglycerol, **Chart 1.3**) into the liposomes. Such liposomes, however, discriminate in their membrane permeability toward different monovalent cations, and therefore may cause misleading results in the transport assays described in **Chapters 2** and **3**.[310]

3.3.5 Calix[4]arene tetrabutylamide 3.1 Does Not Induce Membrane Defects

Calix[4]arene tetrabutylamide **3.1** may transport ions across LUV membranes by inducing membrane defects, by uniport of ions, or via cotransport of ion pairs (H^+/M^+ or OH^-/A^- antiport and H^+/A^- or M^+/OH^- symport mechanisms are possible). The lytic potential of **3.1** was evaluated using a calcein release assay (see **Section 1.5.11**). A suspension of LUVs containing 120 mM calcein showed no fluorescence enhancement upon dilution with an isoosmotic buffer containing **3.1** (5-100 μM, 1-20 mol % ligand). The fluorescence traces (and experimental conditions) were identical to the red and blue traces shown in **Figure 2.42** (**Chapter 2**), where no fluorescence enhancement was observed until the vesicles were lysed with detergent. The absence of dye leakage from the LUVs indicates that **3.1** does not induce membrane defects in liposomes.

3.3.6 ^{1}H NMR Experiments Show that Chloride Transporter 3.1 binds HCl in CDCl$_3$ Solution.

To obtain evidence for Cl$^-$ binding by **3.1**, ^{1}H NMR experiments in CDCl$_3$ were conducted using *n*-Bu$_4$NCl and HCl as Cl$^-$ sources (**Figure 3.3**). Anion receptors usually show chemical shift perturbations upon anion complexation, particularly for amide NH protons that hydrogen bond to the anion.[235,311] Surprisingly, no changes in the ^{1}H NMR

spectrum of the secondary amide **3.1** in CDCl$_3$ were observed upon addition of 1 or 2 equivalents of *n*-Bu$_4$NCl (**Figure 3.3B**). This lack of spectral changes indicates that **3.1** does not bind strongly to the "naked" Cl$^-$ anion, even in this non-polar solvent. Calix[4]arene tetrabutylamide **3.1** does, however, bind HCl in solution. Thus, shaking a CDCl$_3$ solution of **3.1** with aqueous HCl led to complete disappearance of the amide NH proton (H$_e$) and a significant upfield shift of the O-*CH$_2$*-C(O) protons (H$_d$, **Figure 3.3C**). The NMR spectral changes of **3.1** induced by HCl extraction were not simply due to acid treatment, since washing a CDCl$_3$ solution of **3.1** with a H$_2$SO$_4$ solution did not cause any spectral changes (**Figure 3.3D**).
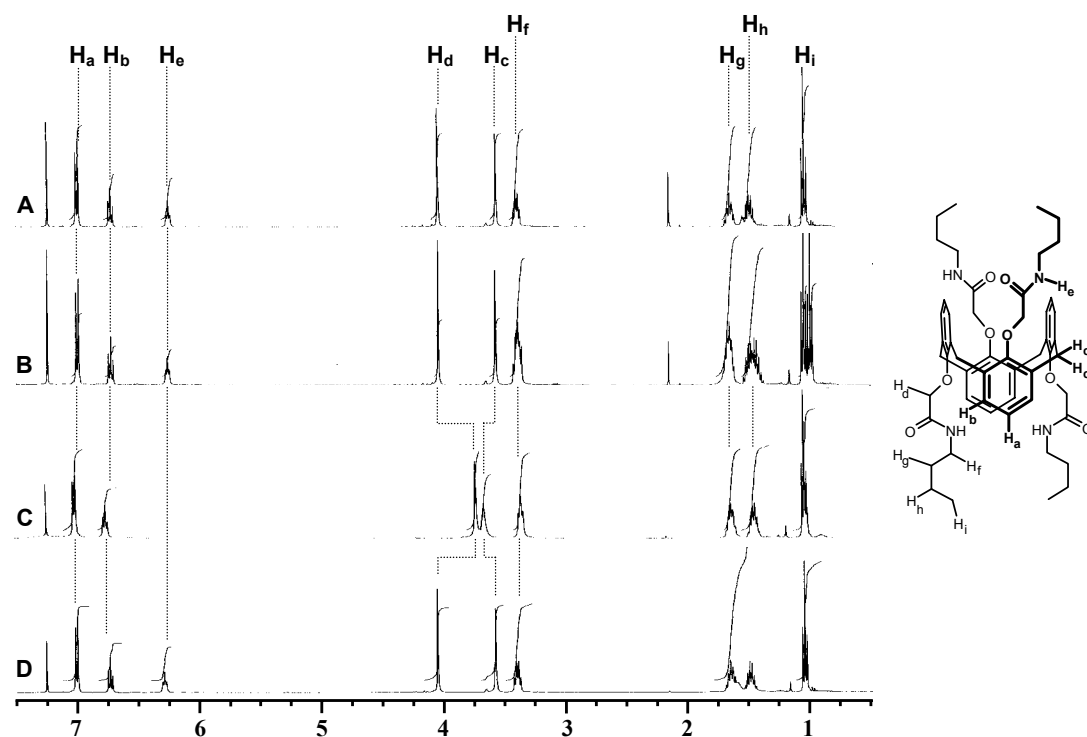
Figure 3.3. ^{1}H NMR spectra of calix[4]arene tetrabutylamide **3.1** in the presence of different species: (A) **3.1** alone in CDCl$_3$ (5 mM); (B) **3.1** with 1 *equiv* of *n*-Bu$_4$NCl in CDCl$_3$; (C) CDCl$_3$ solution of **3.1** after washing with 0.5 M HCl$_{(aq)}$; (D) CDCl$_3$ solution of **3.1** after washing with 0.5 M H$_2$SO$_{4(aq)}$. Experiments conducted by Dr. Vladimir Sidorov.

176

These ^{1}H NMR experiments indicate that calix[4]arene tetrabutylamide **3.1** is a ditopic HCl receptor, since both H$^+$ and Cl$^-$ are needed to induce NMR spectral changes. These NMR data for **3.1** are consistent with the LUV transport results, where efficient ion transport across the membrane was observed in the presence of Cl$^-$ but not HSO$_4^-$. The combined fluorescence and NMR results lead to the conclusion that calix[4]arene tetrabutylamide **3.1** supports ion transport across LUVs in an anion-dependent fashion by either an H$^+$/Cl$^-$ symport or a Cl$^-$/OH$^-$ antiport mechanism.

3.3.7 Calix[4]arene tetrabutylamide 3.1 Mediates Effective H$^+$/Cl$^-$ Transport

With NMR evidence that calix[4]arene tetrabutylamide **3.1** binds HCl in a hydrophobic environment, the possibility that **3.1** could transport HCl across vesicular membranes was investigated. Symport of H$^+$ and Cl$^-$ down the gradient of one of the ions should result in gradient formation for the counterion. Previously, it was shown that a pH gradient across Cl$^-$-filled vesicles in a Cl$^-$ buffer was collapsed by addition of calixarene tetrabutylamide **3.1** (**Figure 3.1A**). The reverse situation was studied by monitoring the intravesicular pH of LUVs experiencing a Cl$^-$ gradient (**Figure 3.4**).
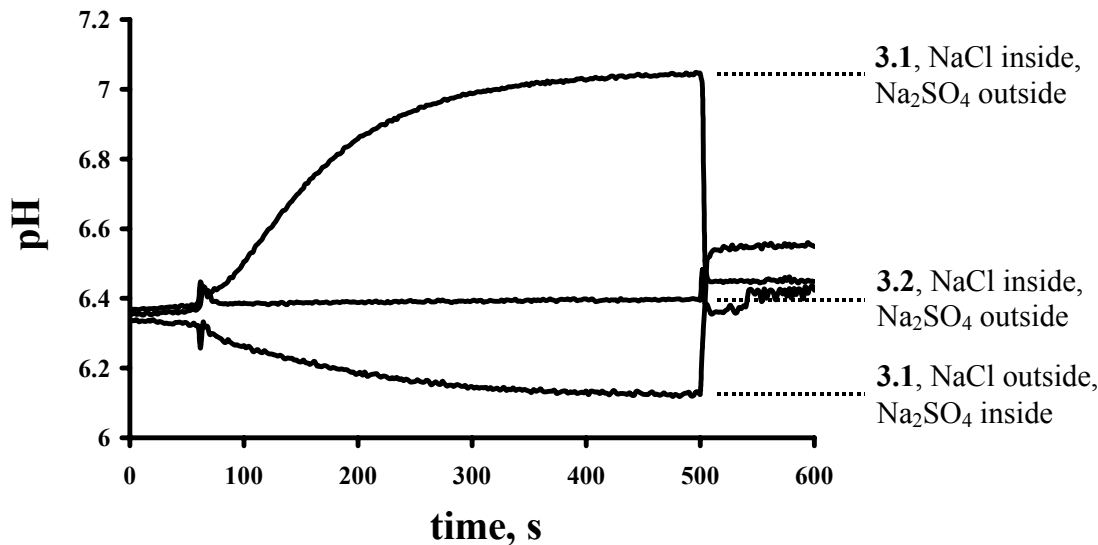
Figure 3.4. Changes of intravesicular pH upon addition of **3.1** or **3.2** to unequally-loaded vesicles. Top trace: addition **3.1** to NaCl-loaded liposomes suspended in a Na_2SO_4 buffer; Middle trace: addition of **3.2** to NaCl-loaded liposomes suspended in a Na_2SO_4 buffer; Bottom trace: addition of **3.1** to Na_2SO_4-loaded liposomes suspended in a NaCl buffer. Final concentration of ligand in all experiments was 5 μM (1:100 ligand:lipid ratio). Time events: *60 sec:* 20 μl of 0.5 M **3.1** or **3.2** solution in THF added, *500 sec:* 40 μl of 50 % Triton X-100 added. Intravesicular pH values were obtained as a function of the ratio of HPTS emission intensities at 510 nm, when excited at 403 and 460 nm, as described in **Section 4.2.2** (see **Figure 4.1**). Experiments conducted by Dr. Vladimir Sidorov.

When a suspension of LUVs filled with saline phosphate buffer (100 mM NaCl, 10 mM sodium phosphate, pH 6.4) containing pyranine diluted with isoosmotic Na_2SO_4 phosphate buffer (75 mM Na_2SO_4, 10 mM sodium phosphate, pH 6.4) was treated with **3.1**, a rapid increase in intravesicular pH was observed (**Figure 3.4**, top trace). The pH gradient reached its maximum ~250 *s* after addition of **3.1** and held constant until the liposomes were lysed with detergent. These results are consistent with an H^+/Cl^- symport or Cl^-/OH^- antiport process. Compound **3.1** moves H^+ along with Cl^- down a chloride

gradient, consequently building a pH gradient across the membrane. Therefore, NaCl-filled vesicles lose Cl$^-$ and H$^+$ upon addition of **3.1** and become more alkaline.

Reversing the intra- and extravesicular buffers resulted in acidification of the intravesicular aqueous compartment. Indeed, when Na$_2$SO$_4$-loaded liposomes suspended in a saline buffer were used, **3.1** mediated effective H$^+$/Cl$^-$ cotransport into the liposomes, down the chloride gradient, causing a decrease in intravesicular pH (**Figure 3.4**, bottom trace). The pH change in these "inversely-loaded" liposomes (-0.3 pH units) was, however, lower than that observed for NaCl-loaded liposomes suspended in a Na$_2$SO$_4$ buffer (+0.6 pH units). This non-symmetrical response in the two experiments may result from several factors. First, the osmotic pressure inside the liposomes is decreasing in the case of NaCl inside (HCl moves out) and increasing when NaCl is outside (HCl moves in), if an H$^+$/Cl$^-$ symport is indeed the mechanism. The extent to which the liposomes can shrink is likely different than the extent to which they can swell. Secondly, calix[4]arene tetrabutylamide **3.1** may undergo Cl$^-$-mediated aggregation when injected into the NaCl buffer, thus preventing the compound from partitioning into the liposome.

3.3.8 The secondary amide NH Group is Essential for HCl Transport Activity of 3.1.

Calix[4]arene octabutylamide **3.2** (**Chart 3.1**) was used as a negative control for tetrabutylamide **3.1**, as the lack of amide NH protons in **3.2** would preclude Cl$^-$ binding. Instead, **3.2** should be a cation ionophore, much like the related tetrakis(diethylcarbamoylmethoxy)-*p*-*tert*-butylcalix[4]arene-*1,3-alt* that coordinates alkali cations in the solid-state and in solution.[312]

To confirm that **3.2** binds Na$^+$, sodium picrate (NaPic) extraction in CDCl$_3$ was monitored by ^{1}H NMR spectroscopy. Complexation of the salt by **3.2** was evident. Two distinct complexes were formed, corresponding to a 1:1 and a 2:1 Na$^+$:**3.2** stoichiometry. The 1:1 complex was generated by adding 1 equivalent of solid sodium picrate to a solution of **3.2** in CDCl$_3$. Binding of this Na$^+$ led to a symmetry loss for **3.2**, indicated by doubling of the ^{1}H NMR signals. Addition of further sodium picrate (up to 10 *equiv*) resulted in a new 2:1 complex. Binding of the second Na$^+$ cation restored the ligand's initial D$_{2d}$ symmetry, as seen by the new single set of NMR signals for this 2:1 complex.

In sharp contrast, no sodium picrate extraction by calix[4]arene tetrabutylamide **3.1** in the presence of up to 10 equivalents of the NaPic was detected by ^{1}H NMR spectroscopy.
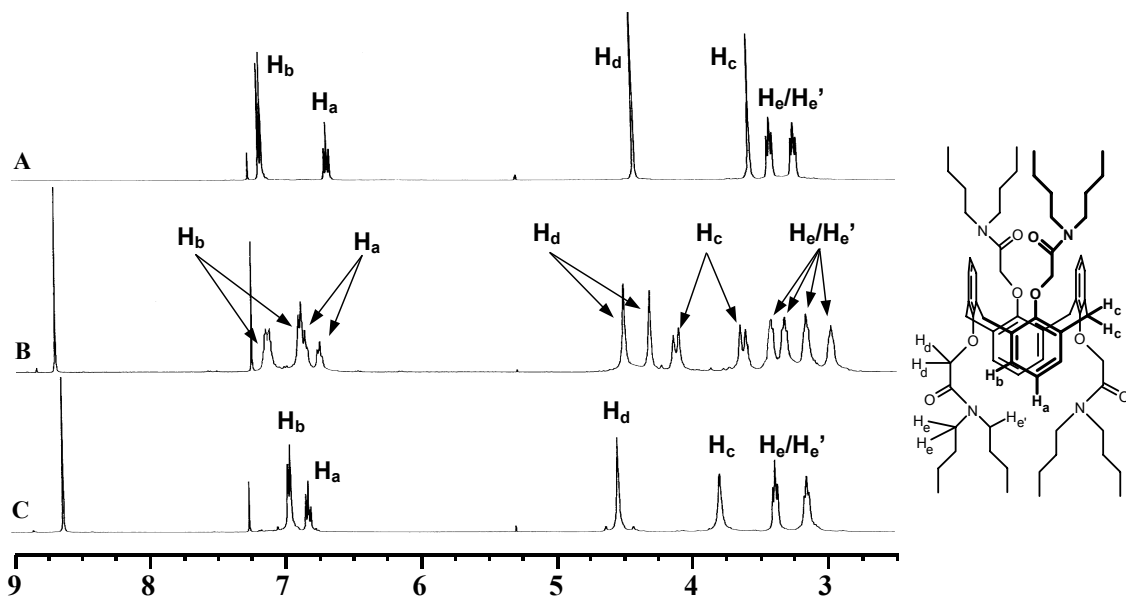
Figure 3.5. ^{1}H NMR spectra of (A) **3.2** in CDCl$_3$ (5 mM), (B) a CDCl$_3$ solution of **3.2** after addition of 1 *equiv* NaPic, and (C) a CDCl$_3$ solution of **3.2** after addition of 2 *equiv* NaPic. No change in spectrum C was observed in the presence of up to 10 *equiv* of solid NaPic. Experiments conducted by Dr. Vladimir Sidorov.

Ion transport assays revealed a high activity for octabutylamide **3.2** in NaCl buffer (**Figure 3.6**, **Table 3.2**). Unlike **3.1**, calix[4]arene octabutylamide **3.2** clearly discriminates between monovalent cations, showing a 3.5-fold drop in rate constant when changing the extravesicular electrolyte from NaCl to CsCl (**Table 3.2**). Fluorescence assays with **3.2** in the presence of Na$_2$SO$_4$-loaded vesicles suspended in isotonic buffer indicated that **3.2** still mediated significant exchange between extra- and intravesicular electrolytes, albeit with a drop in activity (k = 9.1 x 10^{-3} s^{-1}, **Table 3.2**). These data, taken together with the ^{1}H NMR evidence that **3.2** binds Na$^+$ (**Figure 3.5**), strongly suggest that **3.2** functions as a cation transporter, with a preference for Na$^+$ over other alkali metal cations.
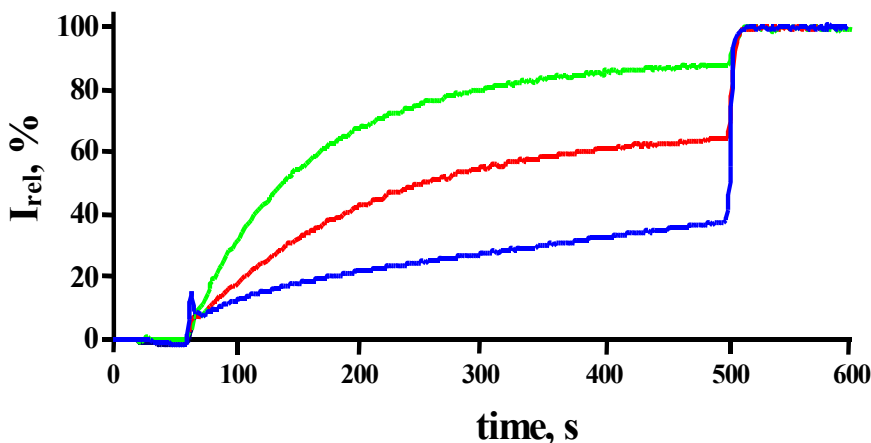
Figure 3.6. Base pulse assays with **3.2**. In all experiments, suspensions of EYPC LUVs containing the pH-sensitive dye pyranine in a phosphate buffer were used. The intravesicular solution contained 10 mM sodium phosphate, pH 6.4, 100 mM NaCl and the extravesicular solution contained 10 mM sodium phosphate, pH 6.4, 100 mM MCl ($M = Na^+, K^+, Cs^+$). Time events: *0 sec:* 20 μl of 0.5 mM **3.2** solution in THF added (final concentration: 5 μM, 1:100 ligand:lipid ratio), *60 sec:* 21 μl of 0.5 M NaOH added (Base Pulse), *500 sec:* 40 μl of 50 % aqueous Triton X-100 added (Triton Pulse). Extravesicular buffers contained 100 mM NaCl (—), KCl (—), or CsCl (—). Experiments conducted by Dr. Vladimir Sidorov.

Table 3.2. Initial Pseudo-First Order Rate Constants ($\times 10^{-3}$ s^{-1}) for Intravesicular/Extravesicular Electrolyte Exchange in the Presence of 5 μM **3.2**. The rate constants for **3.1** (**Table 3.1**) are included for comparison.

| Ion Transporter	NaCl[a]	KCl[b]	CsCl[c]	Na$_2$SO$_4$[d]
3.2	19	12	5.4	9.1
3.1	6.8	6.4	7.7	1.1

a NaCl buffer inside, NaCl buffer outside
b NaCl buffer inside, KCl buffer outside
c NaCl buffer inside, CsCl buffer outside
d Na$_2$SO$_4$ buffer inside, Na$_2$SO$_4$ buffer outside

In marked contrast, calix[4]arene tetrabutylamide **3.1** had shown essentially complete loss of transport activity when the assay buffer was changed from one containing NaCl to one containing Na$_2$SO$_4$ (**Figure 3.2**, **Table 3.1**). Further evidence for different ion transport selectivity provided by calix[4]arene octabutylamide **3.2**, as compared to tetrabutylamide **3.1**, was obtained from an experiment with NaCl-loaded vesicles suspended in isoosmotic Na$_2$SO$_4$ solution. Addition of **3.2** to this vesicular suspension did not result in a pH gradient across the membrane (see **Figure 3.4**, middle trace), whereas addition of **3.1** to the identical system produced a stable pH gradient (**Figure 3.4**, top trace).

3.3.9 Phenoxyacetamide 3.3 as a Control to Probe the Role of the Calix[4]arene Core.

To determine whether chloride transport is an intrinsic property of calix[4]arene **3.1** or a general property of hydrophobic secondary amides, *N*-butyl-2-phenoxyacetamide **3.3** (**Chart 1.1**) was tested in LUV transport assays. Compound **3.3** is a monomeric analog of calix[4]arene **3.1**, bearing the secondary amide that presumably binds Cl⁻, but lacking the calixarene's macrocycle. Base pulse assays, even in the presence of relatively high concentrations of **3.3** (up to 50 μM) showed no ion transport across the LUV membrane. In addition, ^{1}H NMR spectroscopy indicated no HCl binding by **3.3** in CDCl$_3$ (i.e. no loss of the amide NH signal and no significant chemical shift perturbation) under conditions where calix[4]arene **3.1** clearly bound HCl. These control experiments with *N*-butyl-2-phenoxyacetamide **3.3** support the hypothesis that the calixarene's core is critical for the HCl binding and ion transport properties of **3.1**.

As will be discussed in **Section 3.5**, this hypothesis was later proved to be invalid. Oligophenoxyacetamides having two or more phenylene units and bearing secondary butylamides are indeed efficient chloride transporters, with trimer **3.5** (**Chart 3.2**) having the highest activity. The calix[4]arene core is not required for chloride transport.

3.3.10 Calix[4]arene tetramethylamide 2.30 Forms a Channel-like Structure with HCl in the Solid State

After failing to obtain single crystals of tetrabutylamide **3.1** in the presence of HCl, attention was turned to the analogous calix[4]arene tetramethylamide **2.30** (**Chart 3.1**). Whereas **2.30** does not transport ions efficiently across the LUV membrane (**Figure 3.1B**), presumably due to its poor hydrophobicity, its mode of HCl binding should be similar to that for **3.1**. Different protocols afforded two types of **2.30**•HCl crystalline complexes. These structures were solved by Dr. James C. Fettinger. Both solid-state structures show that Cl⁻ anion is hydrogen bonded to the calixarene's amide NH.

Crystals of **2.30**•HCl•3(H_2O), obtained by evaporation of a CH_2Cl_2/THF solution of **2.30** and HCl, have a structure that consists of two-dimensional planar arrays of calixarenes held together by NH···Cl⁻···HN hydrogen bonds in the *x*-direction and by C=O···H-O-H···O=C hydrogen bonds in the *y*-direction (**Figure 3.7**). A side view in the *y*-direction reveals chloride-filled channels, and a side view in the *x*-direction reveals water-filled channels.
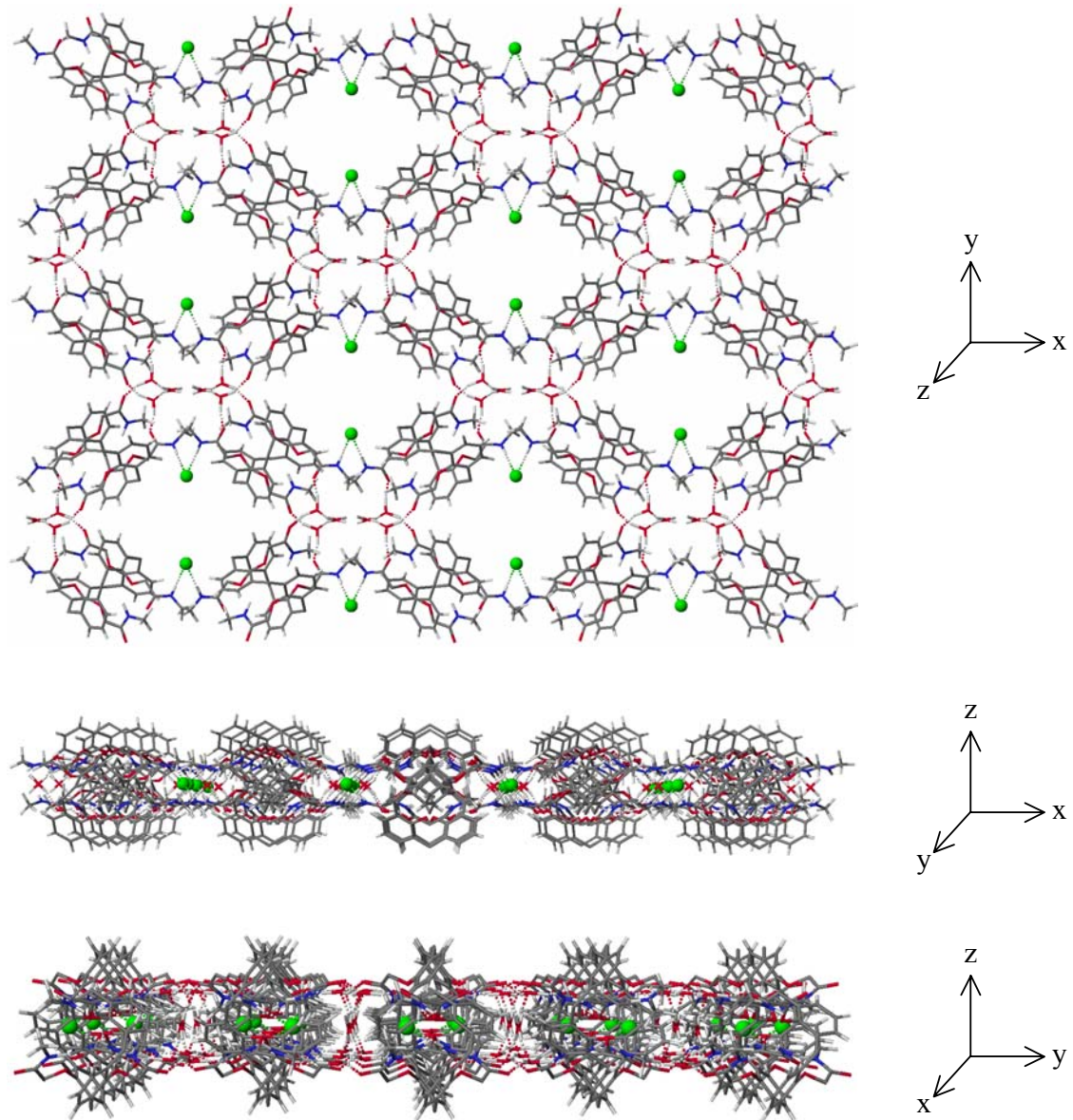
Figure 3.7. Top and side views of the hydrogen-bonded array found in the crystal structure of **2.30**•HCl•3(H$_2$O). The layer continues in the *x* and *y* directions infinitely. The *z*-direction is composed of identical layers held together by crystal packing forces. The Cl$^-$ anions are shown as green spheres. All molecules in the structure are shown in a wire frame representation following the color scheme: gray = carbon, red = oxygen, blue = nitrogen, light gray = hydrogen. Hydrogen bonds between the water molecules (depicted as tetrahedral due to oscillation between two different binding modes) are omitted for clarity. Crystal structure by Dr. James C. Fettinger.

Analysis of a second single crystal, (**2.30**•HCl•H_2O•CH_2Cl_2), grown by layering an aqueous HCl solution over a dichloromethane solution of **2.30**, revealed a structure where two molecules of calixarene **2.30** are linked by oppositely-directed NH···Cl⁻···H-O(H)⁺-H···O=C bridges to give a calixarene dimer (**Figure 3.8**). Each molecule of calixarene **2.30** in **2.30**•HCl•H_2O•CH_2Cl_2 retains a similar geometry as that observed in the structure of **2.30**•HCl•3(H_2O). The main difference in this second structure is that a hydronium cation effectively separates Cl⁻ from the neighboring calixarene molecule.
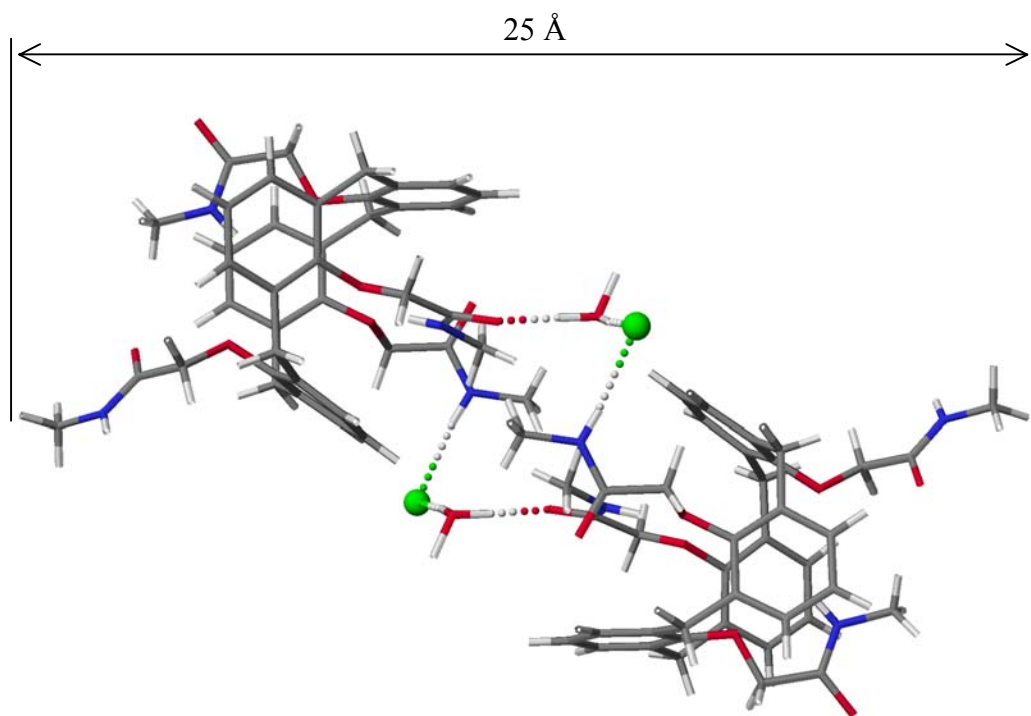
Figure 3.8. Self-assembled dimer observed within the **2.30**•HCl•H_2O•CH_2Cl_2 crystal structure. The CH_2Cl_2 molecules are omitted. The Cl⁻ anions are shown as green spheres. All molecules in the structure are shown in a wire frame representation following the color scheme: gray = carbon, red = oxygen, blue = nitrogen, light gray = hydrogen. Crystal structure by Dr. James C. Fettinger.

Although the global three-dimensional network formed by the two **2.30•HCl** complexes is different, both crystal structures indicate that calixarene **2.30** uses its secondary amide groups to bind HCl. Furthermore, calixarene tetramethylamide **2.30** can definitely self-assemble into extended channel-like structures, held together by hydrogen bonds to bridging Cl$^-$ anions and water molecules.

Looking down the y-axis in **Figure 3.7**, chloride ions in the chloride-filled channels are coordinated by amide NH groups. This is not unlike that observed in the ClC chloride channel selectivity filter, wherein Cl$^-$ ions are coordinated on one side by main chain amide NH groups (see **Section 1.2.3** and **Figure 1.5**).[9] Calix[4]arene tetramethylamide **2.30** also forms water-filled channels in the solid state (**Figure 3.7**, x-direction). Water-filled cavities are intimately involved in ion transport through both the K$^+$ channel and ClC chloride channel pores (see **Sections 1.2.2** and **1.2.3**).[8,9] The pore of the gramicidin A channel is lined with water (**Section 1.3**).[36] Water is also believed to be involved in Na$^+$ transport through the synthetic hydraphile channels (see **Section 1.6** and **Figure 1.18**).[155,157] If calix[4]arene tetrabutylamide **3.1** forms structures akin to that observed in the solid state for **2.30** (**Figure 3.7**), such a water-lined channel through the membrane could provide a pathway for the transport of Cl$^-$ via an ion channel mechanism.

3.3.11 Calix[4]arene tetrabutylamide 3.1 Transports Anions via an Ion Channel Mechanism.

Ligand-mediated ion transport across a lipid bilayer is usually attributed to three mechanisms; defect induction, a carrier process, or channel formation (see **Sections 1.5.1** and **1.5.11**).[63,64,102] Calcein-release experiments showed that **3.1** does not induce membrane defects (**Section 3.3.5**). The Cl$^-$/SO$_4^{2-}$ transport selectivity also suggests that **3.1** acts by a mechanism other than defect induction.

Both carrier and ion channel mechanisms for H$^+$/Cl$^-$ transport are conceivable for a ligand such as calix[4]arene tetrabutylamide **3.1**. A single molecule of **3.1** is certainly too small to span the membrane. The calixarene's *1,3-alt* conformation makes channel-like structures possible, particularly in the presence of a bridging species. The crystal structures of the **2.30•HCl** complexes show calixarene units that are held together by

186

amide···chloride···amide, amide···water···amide and amide···chloride···water···amide hydrogen bonds. If HCl-mediated self-assembly of **3.1** gives similar structures in lipid membranes, then such aggregates could act as ion channels. Even the shortest hydrogen-bonded unit in these structures, a calixarene dimer of ~25 Å (**Figure 3.8**), could conceivably span a bilayer membrane.[302,313] The active gramicidin dimer, an efficient ion channel (see **Section 1.3**), is estimated to be 22 Å in length.[38,39]

Since ion transport supported by **3.1** is not electrically silent, current across the bilayer can be recorded using the voltage clamp technique (see **Section 1.5.3**), a technique that unequivocally distinguishes between channel and carrier mechanisms. Evidence for ion channels formed by calix[4]arene tetrabutylamide **3.1** was obtained from voltage clamp experiments on black lipid membranes (BLMs) (**Figure 3.9**). Voltage clamp experiments and data analyses were done by Robert Mizani in the laboratory of Professor Marco Colombini.
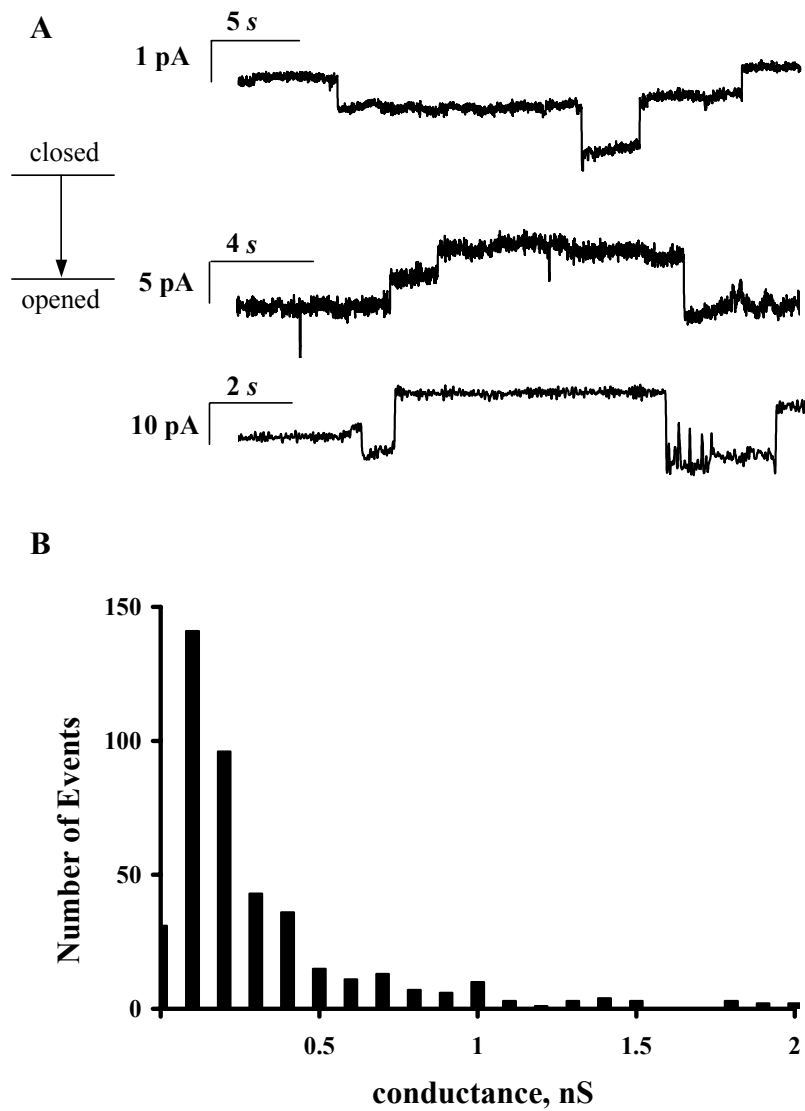
Figure 3.9. (A) Representative current events across a BLM in voltage clamp experiments after application of calix[4]arene tetrabutylamide **3.1** (2.5 μM). The voltage applied was –20 mV for all three recordings. (B) The distribution of conductance ranges observed in voltage clamp experiments with **3.1** acting as an ion channel. Voltage clamp experiments and data analyses were done by Robert Mizani in the laboratory of Professor Marco Colombini.

The voltage clamp assay was conducted using a set-up with two chambers, each filled with an electrolyte solution (1 M KCl, 1 mM MgCl$_2$, 5 mM HEPES, pH 7.0) and divided by a BLM. After voltage was applied across the membrane, a solution of **3.1** was added to one of the chambers. The subsequent current across the membrane was attributed to ion transport mediated by calixarene tetrabutylamide **3.1**, since control experiments with DMSO solvent were negative. Typical current recordings are shown in **Figure 3.9A**. The abrupt changes in current intensity (events) are consistent with an ion channel mechanism. The relatively long-lasting open states, greater than 10 s in some cases, indicate that the channels formed by calixarene tetrabutylamide **3.1** are stable.

Analysis of 480 events gave a distribution of conductance levels (50 pS-2 nS) centered near 100 pS (**Figure 3.9B**). The various conductivity levels are attributed to formation of different self-assembled channel structures (see **Section 1.5.3** and examples in **Sections 1.6** and **1.7**). One explanation for different assemblies formed by **3.1** is competition of calix[4]arene amides with water for Cl$^-$ binding, as revealed in the two different crystal structures for **2.30**•HCl complexes (**Figures 3.7** and **3.8**). While one can only speculate about the structure(s) of the active species, the experiments summarized in **Figure 3.9** clearly indicate that calix[4]arene tetrabutylamide **3.1** can form ion channels.

189

3.3.12 Calix[4]arene tetrabutylamide 3.1 Forms Voltage-dependent Chloride-Specific Channels in HEK-293 Cell Membranes.

Patch-clamp recordings in the whole-cell configuration (see **Section 1.5.2**) revealed that extracellular application of **3.1** to HEK-293 cells (human embryonic kidney cells) caused current across the cell membrane at holding potentials of +120 mV (**Figure 3.10A**). In the range of –120 mV to +80 mV, no response was observed (3 cells out of 15 gave a response at +80 mV, whereas all other cells responded at +120 mV). The channels formed from **3.1** are voltage-dependent, only opening (or forming) at high positive holding potentials.

Importantly, the current was observed only when the cells were suspended in a NaCl buffer. Replacement of this NaCl buffer with isoosmotic sodium glutamate (**Figure 10B**) or Na_2SO_4 buffer (**Figure 10C**) resulted in no current across the membrane at holding potentials between –120 and +120 mV. These results lend further credence to the Cl^--selectivity of ion channels formed by calix[4]arene tetrabutylamide **3.1**. All patch clamp experiments and data analyses were done by Dr. Galya Abdrakhmanova.
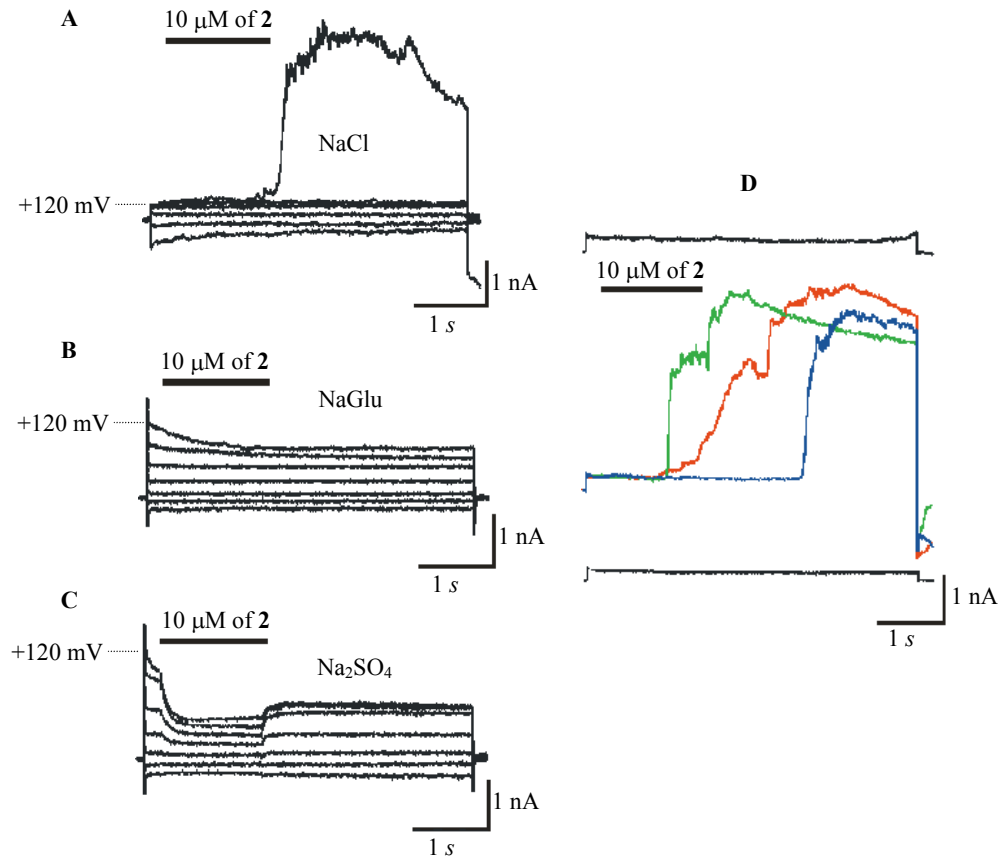
Figure 3.10. Patch clamp recordings in the whole cell configuration (HEK-293 cells). (A) Current across the membrane after application of **3.1** at different voltages. From bottom to top, traces denote currents at -120, -80, -40, 0, +40, +80, +120 mV, respectively, with saline physiological buffer being used. (B) Current across the membrane in a sodium glutamate isoosmotic buffer at different voltages. The potential was varied over a range of −120 through +120 mV, with a 40 mV step. (C) Current across the membrane in a Na_2SO_4 isoosmotic buffer at different voltages. The potential was varied over a range of −120 through +120 mV, with a 40 mV step.(D) Current across the membrane at +120 mV in application/lavage cycles: traces from bottom to top denote: current in absence of **3.1**, current after first application of **3.1** (blue trace), followed by 1.5 min lavage, second application (red trace) and the third application (green trace). Trace on top designates current after lavage without further application of **3.1**. Baselines of the first and the last traces shifted for clarity, saline physiological buffer used. All patch clamp experiments and data analyses were done by Dr. Galya Abdrakhmanova.

191

Calixarene tetrabutylamide **3.1** could be washed out from the cell membrane. After 1.5 minutes of lavage, the current returned to the baseline and no further response at +120 mV was observed without further addition of **3.1**. These data indicate that application of **3.1** did not damage the cell membrane. Subsequent reapplication of **3.1** resulted in a shortening of the delay prior to the response (**Figure 10D**, red trace). A second lavage and application cycle resulted in further decrease in the delay (**Figure 10D**, green trace). One explanation for this phenomenon is that lavage did not completely remove **3.1** from the cell membrane. Instead, inactive aggregates of **3.1** remained. These membrane-retained "seeds" may then accelerate formation of new ion channels upon reapplication of the compound.

3.3.13 Conclusions

Calix[4]arene *1,3-alt* tetrabutylamide **3.1** binds HCl and forms ion channels in lipid bilayer membranes. This is a rare example of a synthetic, non-peptide ion channel showing an anion dependence. The HCl binding and transport activities of **3.1** are attributed to the molecule's overall hydrophobicity and the substitution pattern of the sidechain amide groups. Alteration of these features results in a loss of transport activity (compound **2.30**) or a switch of selectivity from anions to cations (compound **3.2**). Ion transport provided by **3.1** proceeds via either an H^+/Cl^- symport or a Cl^-/OH^- antiport mechanism. Compound **3.1** can regulate H^+ and Cl^- gradients across the membrane, acting as a proton or Cl^- pump. Two crystal structures demonstrate that the calix[4]arene *1,3-alt* tetraamide motif is capable of forming self-assembled channels filled with Cl^- anions and water. Finally, compound **3.1** forms ion channels reversibly in HEK-293 cells that are both Cl^--selective and voltage-dependent.

3.4 Is the Calix[4]arene Core Critical for Chloride Transport? A Clue from Crystal Structures.

As described in **Section 3.3**, calix[4]arene tetrabutylamide **3.1** facilitates H^+/Cl^- transport in liposomes, forms ion channels in planar lipid bilayers and supports electric current in HEK-293 cells. Crystal structures of HCl complexes of calix[4]arene

tetramethylamide **2.30** (**Figures 3.7** and **3.8**) provided a rationale for how Cl$^-$ anions are moved across a membrane by **3.1**. Individual calixarenes are bridged by a network of amide NH···Cl$^-$ and amide NH···H$_2$O hydrogen bonds to give a lattice distinguished by its H$_2$O-filled and Cl$^-$-filled pores.

The structure also revealed that the calixarene macrocycle was not directly involved in HCl complexation. As shown in **Figure 3.11**, one arm from each half of calix[4]arene **2.30** binds Cl$^-$, while the other is folded in towards the calixarene's cavity. It was reasoned that ion transport activity might be maintained, or enhanced, if the calixarene macrocycle was dispensed to produce acyclic analogs that retained the secondary amide groups that are needed for Cl$^-$ binding and self-association.
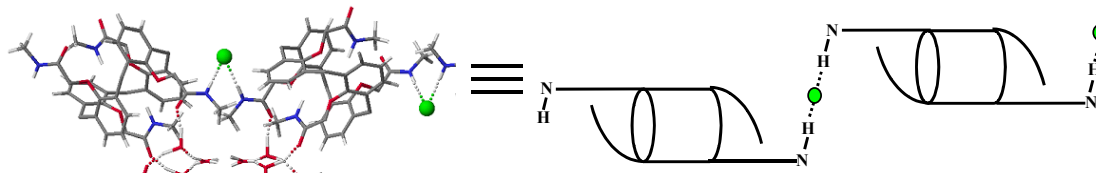
Figure 3.11. Self-assembled dimer observed within the **2.30**•HCl•3(H$_2$O) crystal structure (left, from sheet in **Figure 3.7**) and a representation of the structure showing that only one arm from each half of **2.30** coordinates to Cl$^-$ (green sphere, right). The calix[4]arene cores are depicted with cylinders and the "arms" are depicted with straight lines (binding Cl$^-$) and curved lines (folded in).

3.5 Chloride Transport across Lipid Bilayers and Transmembrane Potential Induction by an Oligophenoxyacetamide.

3.5.1 Introduction

To test the hypothesis stated in **Section 3.4**, a series of compounds was synthesized, ranging from monomer **3.3** to hexamer **3.8** (**Chart 3.2**) and evaluated for their ability to support H$^+$/Cl$^-$ transport across LUVs. In this section, the results described clearly indicate that the trimer **3.5** is the most efficient Cl$^-$ transporter in the series (**Chart 3.2**)

and approximately an order of magnitude more active than calix[4]arene **3.1**. These data conclude that the calix[4]arene core is not critical to the chloride transport function of these secondary amide compounds, i.e. the hypothesis stated in **Section 3.4** was correct. Also, trimer **3.5** has an unprecedented function for a synthetic compound. Due to its high Cl^-/SO_4^{2-} transport selectivity, **3.5** induces a stable potential in liposomes experiencing a transmembrane Cl^-/SO_4^{2-} gradient. These results represent encouraging developments in the search for new classes of synthetic Cl^- transporters.

Chart 3.2

monomer **3.3**   dimer **3.4**   trimer **3.5**

tetramer **3.6**   pentamer **3.7**

hexamer **3.8**
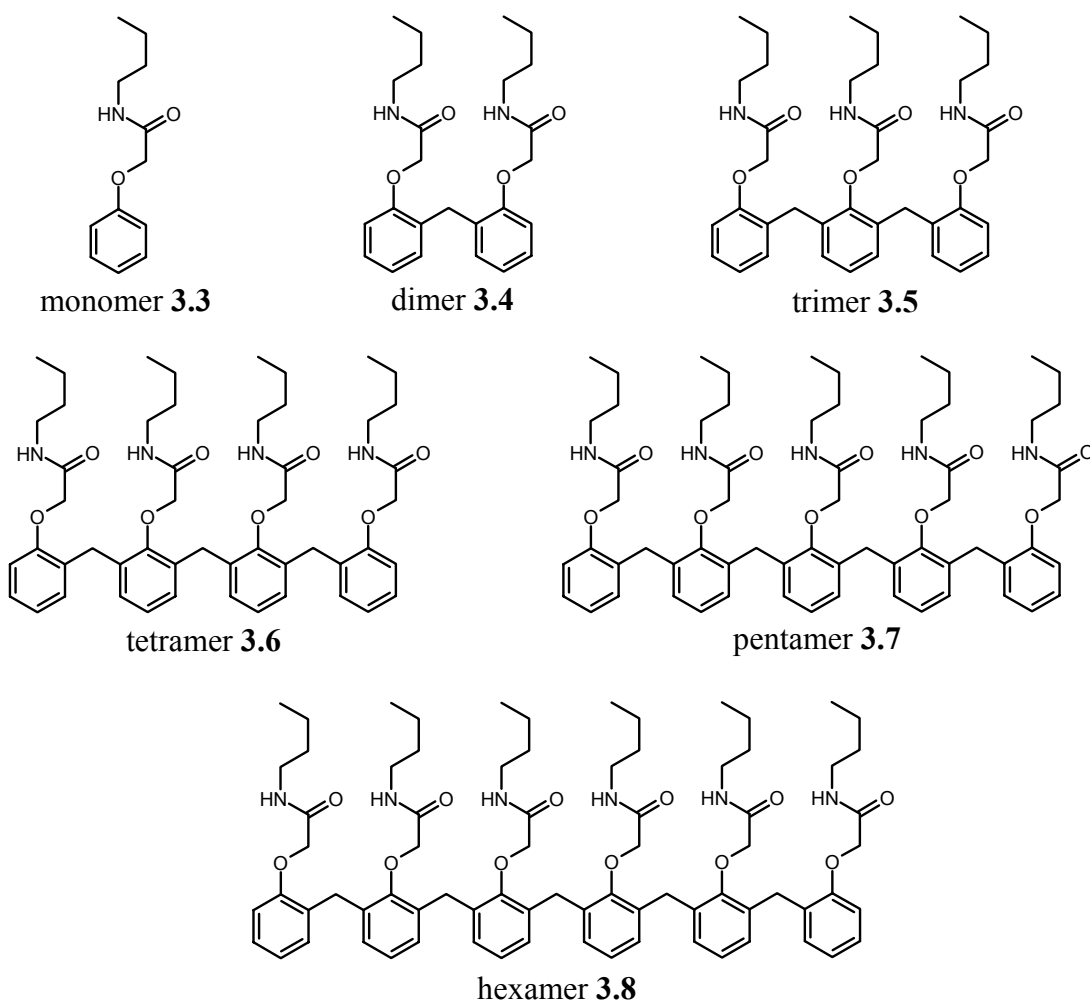
3.5.2 Synthesis of Oligophenoxyacetamides

Oligophenols **3.9-3.13** were prepared according to the procedure of Sone, Ohba and Yamazaki.[314] Oligo-ethyl-phenoxyacetates **3.14-3.18** were synthesized by alkylation of phenols **3.9-3.13** with ethyl bromoacetate (**Scheme 3.3**). Base hydrolysis of **3.14-3.18** afforded oligophenoxyacetic acids **3.19-3.23**. Subsequent reaction of **3.19-3.23** with $SOCl_2$ in benzene, to form the acid chloride, followed by coupling with butylamine yielded oligophenoxyacetamides **3.4-3.8** (**Scheme 3.3**). **Table 3.3** provides yields for the syntheses shown in **Scheme 3.3**. Compounds **3.4-3.7** were prepared by Dr. Vladimir Sidorov with assistance from Simi Adeyeye and hexamer **3.8** was prepared by Jennifer Kuebler. The author's contribution to the synthesis was in the scale-up preparation of trimer **3.5**.

Scheme 3.3 Syntheses of compounds **3.4-3.8** from oligophenols **3.9-3.13**.

	3.9	n = 0		3.14	n = 0

3.9 n = 0
3.10 n = 1
3.11 n = 2
3.12 n = 3
3.13 n = 4

3.14 n = 0
3.15 n = 1
3.16 n = 2
3.17 n = 3
3.18 n = 4

3.19 n = 0
3.20 n = 1
3.21 n = 2
3.22 n = 3
3.23 n = 4

dimer **3.4** n = 0
trimer **3.5** n = 1
tetramer **3.6** n = 2
pentamer **3.7** n = 3
hexamer **3.8** n = 4
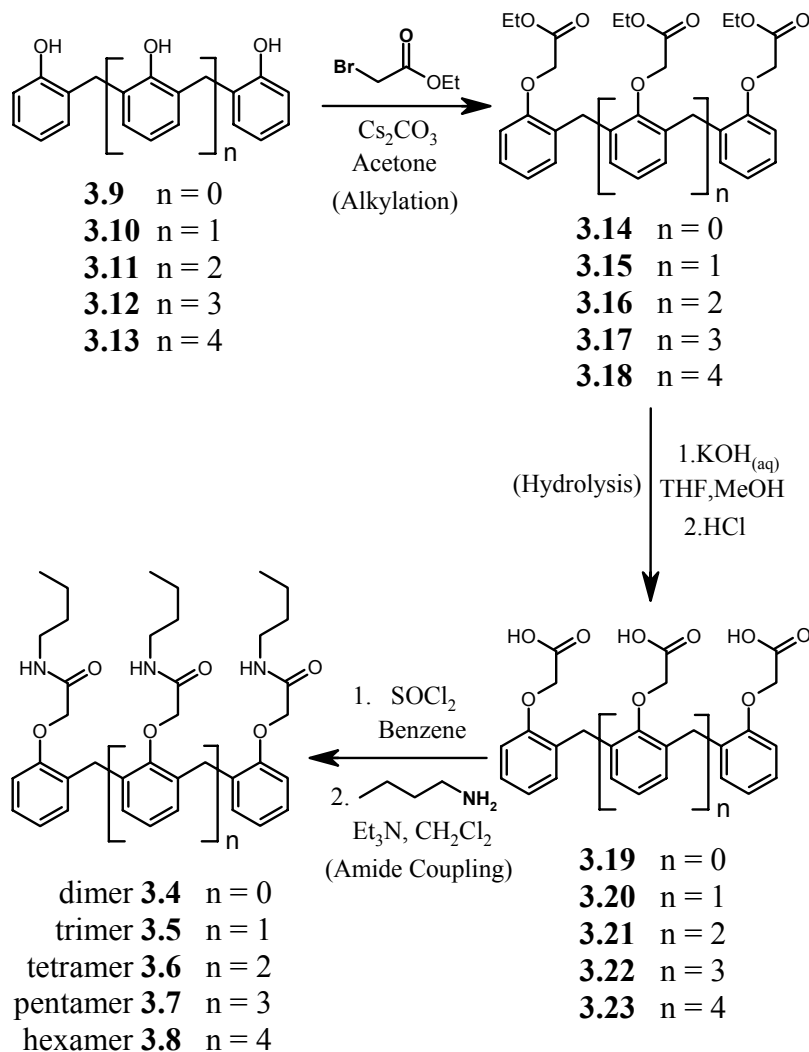
Table 3.3. Yields for the Syntheses of Compounds **3.4-3.8** shown in **Scheme 3.3**.

n	Starting Oligophenol	Alkylation[a] Product / Yield	Hydrolysis[a] Product	Amide Coupling[a] Product / Yield[b]
0	**3.9**	**3.14** / 75 %	**3.19**	**3.4** / 85 % (from **3.14**)
1	**3.10**	**3.15** / 83 %	**3.20**	**3.5** / 89 % (from **3.15**)
2	**3.11**	**3.16** / 77 %	**3.21**	**3.6** / 66 % (from **3.16**)
3	**3.12**	**3.17** / 58 %	**3.22**	**3.7** / 80 % (from **3.17**)
4	**3.13**	**3.18** / 46 %	**3.23**	**3.8** / 68 % (from **3.18**)

a Steps labeled in parentheses in **Scheme 3.3**
b Yields for final oligophenoxyacetamides calculated over three steps from the esters

3.5.3 Trimer 3.5 Identified as the Most Potent Chloride Transporter in the Series

The H^+/Cl^- transport activity of compounds **3.3-3.8** was evaluated *via* the base pulse fluorescent assay (**Figure 3.12**). A significant increase in transport rates with increasing chain length was observed for compounds **3.3**-**3.6**. Monomer **3.3** showed essentially no transport activity, even at 50 μM (1:10 ligand:lipid ratio, **Figure 3.12A**, purple trace). Dimer **3.4** had low transport activity at concentrations below 20 μM (1:25 ligand:lipid ratio, **Figure 12A**, black trace). In sharp contrast, application of trimer **3.5** at concentrations as low as 5 μM (1:100 ligand:lipid ratio, **Figure 12A**, blue trace) resulted in a rapid exchange between extra- and intravesicular electrolytes. Trimer **3.5** was an order of magnitude more active than calix[4]arene tetrabutylamide **3.1** at 5 μM (5.8×10^{-2} s^{-1} *versus* 6.8×10^{-3} s^{-1} established previously for **3.1**, see **Table 3.1**). Further elongation of the oligomer backbone resulted in an activity decrease. Tetramer **3.6** was approximately 6 times less active than trimer **3.5** at 5 μM (1:100 ligand:lipid ratio, **Figure 12A**, red trace), and pentamer **3.7** and hexamer **3.8** demonstrated a further decrease in transport rates (**Figure 3.12A**, green and brown traces, respectively).
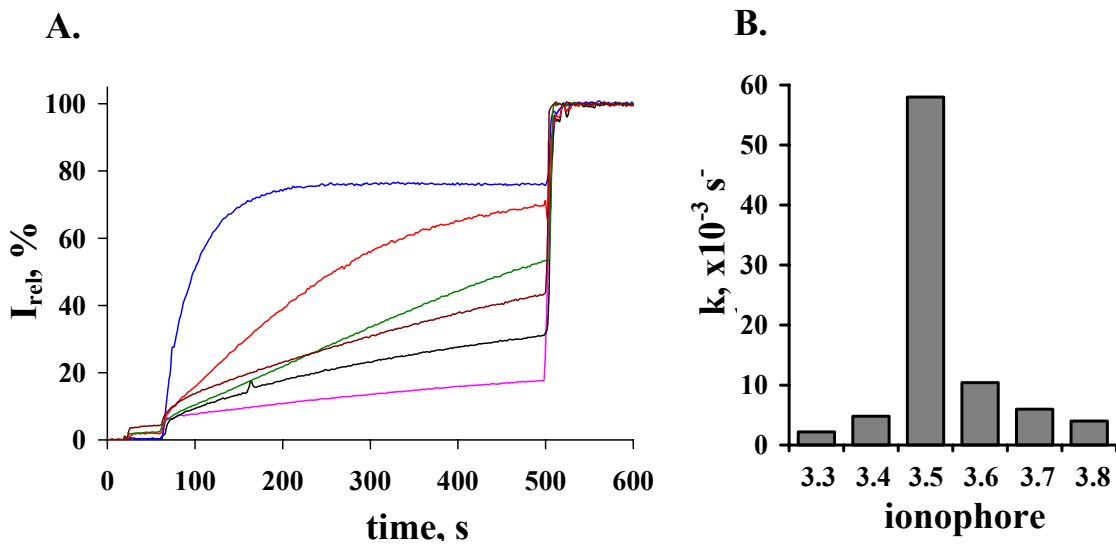
Figure 3.12. (A) Liposome base pulse assays with **3.3-3.8**. Suspension of EYPC LUVs (500 μM of lipid) containing pyranine in a phosphate buffer was used (10 mM sodium phosphate, pH 6.4, 100 mM NaCl inside and outside). Time events: *20 s:* 20 μL of 0.5 mM solution of **3.3-3.8** in DMSO added to give 1:100 ligand:lipid molar ratio, *60 s:* 21 μL of 0.5 M NaOH added, *500 sec:* 40 μL of 50 % Triton X-100 added. Colors in the plot denote application of: — monomer **3.3**, — dimer **3.4**, — trimer **3.5**, — tetramer **3.6**, — pentamer **3.7**, — hexamer **3.8**. (B) Initial pseudo-first order rate constants in the presence of 5 μM of ionophores **3.3** – **3.8** obtained from the base pulse assays shown in A. Experiments conducted by Dr. Vladimir Sidorov.

3.5.4 Rates of Transport Mediated by 3.4-3.8 are Concentration-Dependent

Whereas trimer **3.5** was significantly more active than the other oligomers at all concentrations, the relative transport abilities of compounds **3.3-3.8** varied with concentration, mostly due to the nonlinear increase of activity observed for dimer **3.4** (**Figure 3.13**). This nonlinear increase in transport activity is strong evidence that H^+/Cl^- transport is mediated by a self-associated form of **3.4**. The apparent linear concentration-activity relationship observed for trimer **3.5** suggests that **3.5** is either pre-assembled before membrane insertion or that it acts by a carrier mechanism.
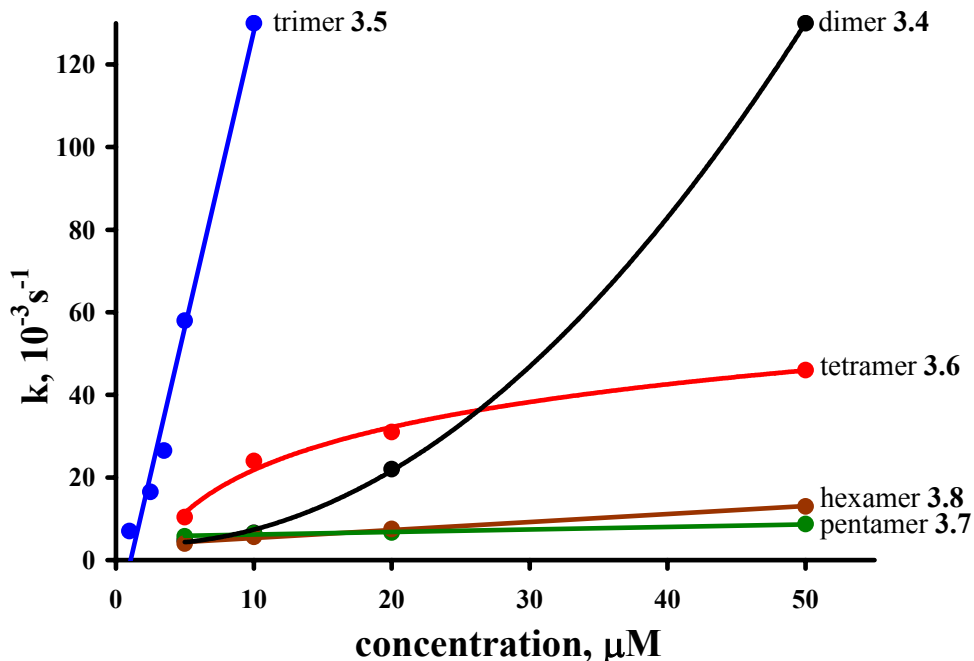
Figure 3.13. Dependence of the initial pseudo-first order rate constants on the concentration of ligand. Each point on the plot represents a base pulse fluorimetric experiment. Color code for traces denotes application of: ▬ dimer **3.4**, ▬ trimer **3.5**, ▬ tetramer **3.6**, ▬ pentamer **3.7**, ▬ hexamer **3.8**. Experiments conducted by Dr. Vladimir Sidorov.

3.5.5 Oligophenoxyacetamides 3.3-3.8 are Chloride-Selective Transporters

Importantly, compounds **3.3-3.8** mediated electrolyte exchange only in the presence of Cl^-. In contrast to the results shown in **Figure 3.12A**, where NaCl extra- and intravesicular buffers were used, no transport activity was detected in LUVs symmetrically loaded with Na_2SO_4, even at ligand concentrations of 50 μM (1:10 ligand:lipid ratio, results similar to those shown in **Figure 3.2** for Cl^-- and SO_4^{2-}-containing buffers). This anion dependent activity is strong evidence that butylamides **3.3-3.8** mediate Cl^- transport across the bilayer.

Direct evidence for Cl^- transport by trimer **3.5** was obtained from ^{35}Cl NMR experiments (**Figure 3.14**). Giant vesicles containing NaCl and $CoCl_2$ were suspended in Co^{2+}-free Na_2SO_4 buffer. The membrane-impermeable Co^{2+} caused a downfield shift and broadening of the ^{35}Cl NMR signal for intravesicular Cl^- (see **Section 1.5.7**).[91] A separate, smaller signal was due to residual extravesicular Cl^- (**Figure 3.14A**). Controls showed no leakage of Cl^- from liposomes even after three days. Addition of trimer **3.5** resulted in an enhancement of the extravesicular Cl^- peak due to outwardly directed Cl^- transport (**Figure 3.14B**). The new intravesicular/extravesicular Cl^- equilibrium in the presence of trimer **3.5** was stable for at least 3 *h*, or until lysis with Triton X-100 released the intravesicular Cl^- to give a single ^{35}Cl NMR resonance (**Figure 3.14C**).
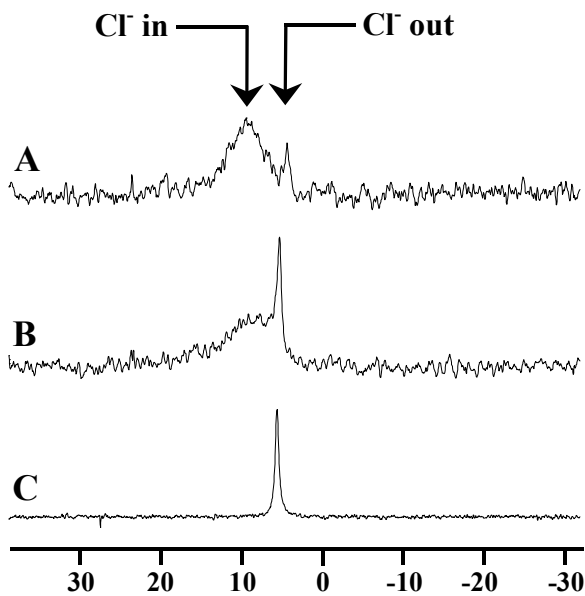
Figure 3.14. ^{35}Cl NMR spectra of a suspension of giant vesicles (88 mM EYPC, 9:1 H$_2$O:D$_2$O, 100 mM NaCl, 10 mM CoCl$_2$,10 mM sodium phosphate, pH 5.4) suspended in 75 mM Na$_2$SO$_4$ Co^{2+}-free buffer (9:1 H$_2$O:D$_2$O, sodium phosphate, pH 6.4). Spectra correspond to (A) giant vesicles in the absence of **3.5**, (B) giant vesicles 1 *h* after application of **3.5** in DMSO (1:100 ligand:lipid ratio) and (C) vesicles after lysis with Triton X-100. Experiments conducted by the author.

3.5.6 Oligophenoxyacetamides 3.3-3.8 Mediate Effective H$^+$/Cl$^-$ Transport

The combined pH-stat and ^{35}Cl NMR data indicate that the acyclic trimer **3.5**, like its predecessor calix[4]arene tetrabutylamide **3.1** (see **Section 3.3.7**), co-transports H$^+$/Cl$^-$. Addition of **3.3-3.8** to a suspension of NaCl-loaded liposomes in Na$_2$SO$_4$ buffer resulted in alkalinization of the vesicular aqueous compartment due to effective H$^+$/Cl$^-$ co-transport down the chloride gradient (**Figure 3.15A**). The highest activity in the series of acyclic oligomers **3.3-3.8**, in terms of the time required to establish equilibrium, was again demonstrated by trimer **3.5**. The overall activity trend was: trimer **3.5** >> tetramer **3.6** ~ calixarene **3.1** > dimer **3.4** > pentamer **3.7** ~ hexamer **3.8**. As expected, reversed loading of liposomes (Na$_2$SO$_4$-loaded liposomes in NaCl buffer) resulted in acidification

201

of the vesicular compartment upon application of trimer **3.5** (**Figure 3.15B**, bottom trace).
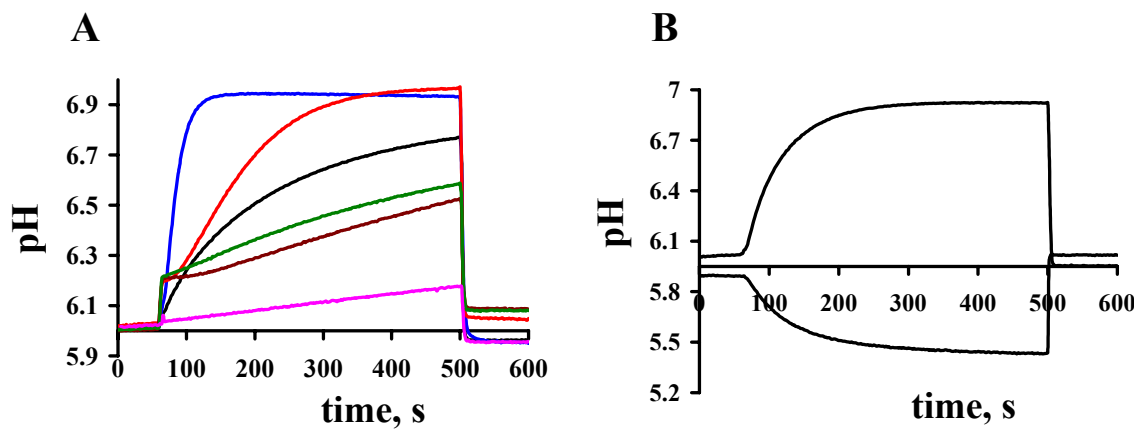
Figure 3.15. (A) Alkalinization of the vesicular aqueous compartment upon application of **3.3**-**3.8** to a suspension of NaCl-containing vesicles in isoosmolar Na_2SO_4 buffer. Concentration of **3.3**-**3.8** in the vesicular suspension was 20 μM, or 4:100 ligand:lipid ratio. Color code for traces denotes application of: ▬ dimer **3.4**, ▬ trimer **3.5**, ▬ tetramer **3.6**, ▬ pentamer **3.7**, ▬ hexamer **3.8**. (B) Alkalinization (upper trace) and acidification (lower trace) of the vesicular aqueous compartment upon injection of **3.5** (final concentration: 5 μM, 1:100 ligand:lipid ratio) to a suspension of NaCl-containing vesicles in isoosmolar Na_2SO_4 buffer (upper trace) and to a suspension of Na_2SO_4-containing vesicles in isoosmolar NaCl buffer (lower trace). Liposomes were lysed with Triton X-100 at the end of each experiment. Experiments conducted by Dr. Vladimir Sidorov.

3.5.7 ^{1}H NMR Experiments Suggest that Trimer 3.5 Does Not Bind HCl in CDCl$_3$ Solution.

Calix[4]arene tetrabutylamide **3.1** was shown to bind HCl in CDCl$_3$ (**Section 3.3.6**). In contrast, ^{1}H NMR experiments indicate that trimer **3.5** does not bind HCl under the same conditions. Washing a CDCl$_3$ solution of trimer **3.5** with 0.5 M, 1 M, 6 M or 12 M HCl$_{(aq)}$ results in no observable changes in the ^{1}H NMR spectrum. That trimer **3.5** does

not bind HCl may provide one explanation why trimer **3.5** transports Cl⁻ at a higher rate than calix[4]arene tetrabutylamide **3.1**. As described in **Sections 1.2.2** and **1.2.3** for the K⁺ and ClC chloride channels, strong binding and high transport rates do not necessarily go hand-in-hand.[8,9] If trimer **3.5** can indeed recognize Cl⁻, or H⁺/Cl⁻ pairs, but the interactions between **3.5** and the ions are weak, this may account for the observed increase in transport rate over the HCl-binding calix[4]arene tetrabutylamide **3.1**.

3.5.8 Potential Induction by Trimer 3.5 Across LUVs Experiencing a Transmembrane Chloride Gradient.

Although trimer **3.5** transports both Cl⁻ and H⁺ into sulfate-loaded liposomes suspended in a chloride buffer, Cl⁻ is transported faster than H⁺, and therefore the overall process is not electrically silent. Monitoring the transmembrane potential using the potential-sensitive dye safranin O (see **Section 1.5.10**) revealed the formation of stable negative charge inside liposomes (75 mM Na_2SO_4 inside, 100 mM NaCl outside, safranin O outside) within 2 *min* of applying trimer **3.5** (1:100 ligand:lipid ratio, **Figure 3.16**, red trace). The magnitude of the transmembrane potential induced by **3.5** under an inwardly directed Cl⁻ gradient is comparable to that generated by 0.12 mol % valinomycin (see **Section 1.5.10**, 1:833 ligand: lipid ratio) in liposomes with an outwardly directed K⁺ gradient (**Figure 3.16**, blue trace, 100 mM KCl inside, 100 mM NaCl outside). The lower two traces in **Figure 3.16** verify that trimer **3.5** and valinomycin are functionally orthogonal. In other words, trimer **3.5** creates a transmembrane potential under conditions where valinomycin cannot create a potential (**Figure 3.16**, green trace) and *vice versa* (**Figure 3.16**, black trace).

To our knowledge, trimer **3.5** is the first synthetic compound reported to induce a stable potential in LUVs due to a transmembrane anionic gradient. Maintenance of this membrane potential and the stable transmembrane Cl⁻ equilibrium demonstrated by ³⁵Cl NMR (**Figure 3.14**) indicate that trimer **3.5** does not induce membrane defects.
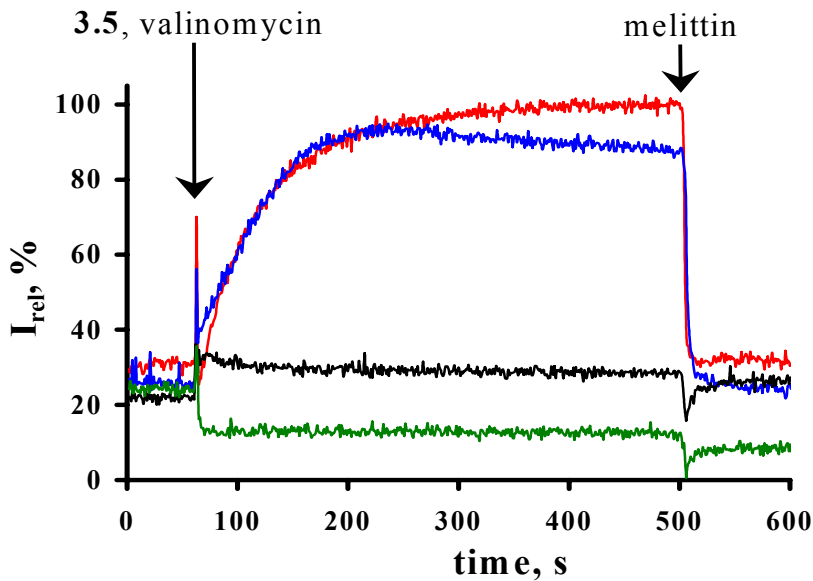
Figure 3.16. Liposome potential fluorescent assays. Suspensions of EYPC LUVs were used (10 mM sodium phosphate, pH 6.4, 100 mM KCl or 75 mM Na_2SO_4 inside and 100 mM NaCl, 60 nM potential-sensitive dye safranin O, ex 521 nm, em 580 nm, outside). Color code for traces denotes the formation of potential in: — KCl vesicles upon application of valinomycin, — Na_2SO_4 vesicles upon application of trimer **3.5**, — KCl vesicles upon application of trimer **3.5**, — Na_2SO_4 vesicles upon application of valinomycin. Potentials were quenched at the end of each experiment by injecting 20 μL of a 1 mM aqueous solution of the defect-inducing peptide melittin. Experiments conducted by Dr. Vladimir Sidorov.

3.5.9 Conclusions

Trimer **3.5** was identified as the most potent chloride transporter from the series of oligophenoxyacetamides **3.3-3.8**. Also, **3.5** transports Cl⁻ an order of magnitude faster than calix[4]arene tetrabutylamide **3.1**, proving that the calix[4]arene core is not essential for chloride transport function. The mechanism by which these linear oligomers transport ions is yet to be determined. Trimer **3.5** has demonstrated the unprecedented ability to generate a potential in LUVs due to a transmembrane anion gradient. Lastly, trimer **3.5** exhibits high activity at low μM concentrations, has a low molecular weight and can be obtained by a simple preparation, making this compound a potential drug lead for the treatment of cystic fibrosis and cancer (see **Section 3.2**).

3.6 Future Directions

(1) Elucidation of the transport mechanism and active structure of trimer **3.5** is the next step, based on research presented in this chapter. Planar bilayer voltage clamp experiments would determine whether or not trimer **3.5** forms ion channels in membranes and if a single active structure or multiple active structures are at work. If channels are formed, voltage dependence can also be determined. Insight into the transport mechanism (carrier or channel) can also be obtained by comparing transport rates in EYPC and DPPC liposomes, as described in **Section 1.6.2**.[131]

The obvious question is: what is special about trimer **3.5** that makes this compound substantially more active then dimer **3.4** and tetramer **3.6**? One potentially critical factor is the lipid:water partitioning, i.e. the hydrophobicity. As discussed in **Section 3.5.4** and shown in **Figure 3.13**, the activity of dimer **3.4** increases nonlinearly with concentration. Determining the relative hydrophobicity between dimer **3.4** and trimer **3.5**, along with both the investigation of more polar and of more hydrophobic derivatives of dimer **3.4** will give insight into the effects of hydrophobicity on ion transport activity. The polarity can be increased or decreased simply by shortening or lengthening the amides' alkyl chains, respectively.

(2) As described in **Section 1.7**, peptide C-K$_4$-M2GlyR **1.34** and sterol **1.41** demonstrated the ability to mediate chloride transport across cystic fibrosis airway epithelial cells.[16,170] This function makes these compounds potential drugs for cystic fibrosis treatment. The chloride channel-forming calix[4]arene tetrabutylamide **3.1** and chloride transporter trimer **3.5** have similar potential, and should be tested on cystic fibrosis cell lines.

The anticancer activity of **3.1** and **3.5** should also be investigated, since the ability **3.1** and **3.5** to cotransport H$^+$/Cl$^-$ resembles the H$^+$/Cl$^-$ transport facilitated by anticancer agents of the prodigiosin family of antibiotics (see **Section 3.2**).[304-306]

Lastly, ion transporters have potential as bactericidal agents, as demonstrated by the hydraphile channels and D,L-α-cyclic peptides (**Section 1.6.2**).[15,162] The ability of calix[4]arene tetrabutylamide **3.1** and trimer **3.5** to inhibit or kill *Escherichia coli* and Gram-positive and Gram-negative bacteria should be assessed.

Chapter 4. Experimental and References

4.1 General Experimental

The ^{1}H NMR spectra were recorded on a Bruker DRX-400 or Bruker Avance 400 operating at 400.13 MHz, or on a Bruker DRX-500 operating at 500.13 MHz. Chemical shifts are reported in ppm relative to the residual protonated solvent peak. The ^{13}C NMR spectra were recorded on a Bruker DRX-400 instrument operating at 100.61 MHz and chemical shift values are reported in ppm relative to the solvent peak. All NMR spectra were recorded at 20-25 °C (room temperature) unless otherwise specified. Two-dimensional ^{1}H-^{1}H COSY (^{1}H-^{1}H three-bond coupling), ^{1}H-^{1}H NOESY (^{1}H-^{1}H through-space magnetization transfer) and ^{1}H-^{13}C HMQC (^{1}H-^{13}C one-bond coupling) experiments were run using previously published standard protocols.[282] Fast Atom Bombardment (FAB) mass spectra were recorded on a JEOL SX-102A magnetic sector mass spectrometer. Electrospray (ESI) mass spectra were recorded from MeOH solutions on a Finnigan LCQ mass spectrometer by direct infusion. The samples were ionized by nanoelectrospray and detected in the positive ion mode. All fluorimetric experiments were carried out on an SLM Aminco® (Aminco Bowman® Series 2) Luminescence Spectrometer. Vapor pressure osmometry (VPO) was performed on a Wescor 5520, Vapro^{TM} instrument. The pH of solutions was monitored with an Orion pH-meter, model 420A, with a Ag/AgCl pH-sensitive electrode. High-pressure extrusion was performed on an Avanti^{TM} mini-extruder with a 0.1 μm polycarbonate membrane (unless otherwise specified). Circular dichroism spectra were recorded on an Applied Photophysics 180 PiStar instrument at 25 °C in a cylindrical 0.1 mm path length quartz cuvette. X-ray crystallographic data were collected on a Bruker SMART1000 single crystal CCD-diffractometer. Elemental analyses were performed by Schwarzkopf Microanalytical Laboratories, Woodside, NY. Isothermal titration calorimetry (ITC) was performed on an Omega isothermal titration calorimeter. Chromatography was performed using 60-200 mesh silica purchased from Baker. Thin layer chromatography was performed on Kieselgel 60 F254 and Uniplate^{TM} Silica Gel GF silica-coated glass plates and visualized by UV and I$_2$. Dueterated solvents were purchased from Cambridge Isotope Laboratories.

All chemicals and solvents were purchased from Sigma, Fluka, Aldrich or Acros. Egg yolk L-α-phosphatidyl choline (EYPC) was purchased from Avanti Polar Lipids and stored as a 1.0 g/mL solution in EtOH at –40 °C.

4.2 Chapter 2 Experimental

4.2.1 Synthesis

5,11,17,23-Tetrakis(butoxymethyl)-25,26,27,28-tetrahydroxycalix[4]arene 2.38. A solution of *p*-H-calix[4]arene (7.10 g, 16.7 mmol), paraformaldehyde (10.52 g, 351.0 mmol), glacial HOAc (112 mL), conc. H_3PO_4 (119 mL), and conc. HCl (126 mL) in dioxane (500 mL) was stirred at 80 °C for 12 h.[265] The mixture was concentrated to 300 mL, poured into an ice/water mixture (500 mL) and extracted with $CHCl_3$ (2 x 70 mL). The combined organic layers were washed with H_2O (100 mL), dried over Na_2SO_4 and the solvent was evaporated under reduced pressure to give crude *p*-chloromethyl-calix[4]arene **2.37** (10.64 g) as a light brown solid. Na (21.3 g, 926 mmol) was washed with hexanes (to remove kerosene) and dissolved in BuOH (500 mL) to generate NaOBu *in situ*. A suspension of crude compound **2.37** (10.64 g) in BuOH (100 mL) was added to the NaOBu solution and the mixture was stirred for 10 h at room temperature under a nitrogen atmosphere. The mixture was acidified with conc. HCl (75 mL) to give a clear brown solution and an insoluble white precipitate. The solution was decanted into a separatory funnel, diluted with $CHCl_3$ (600 mL), washed with H_2O (2 x 500 mL), and the solvent was evaporated under reduced pressure. Coevaporation with $CHCl_3$ (2 x 500 mL) followed by drying under high vacuum was necessary to remove all BuOH to afford calixarene **2.38** (7.0 g, 53 % over two steps) as a light brown solid. ^1H NMR (400 MHz, $CDCl_3$): δ 10.12 (s, 4 H, OH), 6.99 (s, 8 H, ArH), 4.25 (s, 8 H, Ar-*CH₂*-OBu), 4.22 (d, 4 H, J = 13.3 Hz, CH₂-bridge), 3.50 (d, 4 H, J = 13.3 Hz, CH₂-bridge), 3.37 (t, 8 H, J = 6.5 Hz, O*CH₂*CH₂CH₂CH₃), 1.59-1.49 (m, 8 H, OCH₂*CH₂*CH₂CH₃), 1.41-1.30 (m, 8 H, OCH₂CH₂*CH₂*CH₃), 0.90 (t, 12 H, J = 7.3 Hz, OCH₂CH₂CH₂*CH₃*); ^{13}C NMR (100 MHz,

CDCl$_3$): δ 148.2, 132.3, 128.4, 128.0, 72.3, 70.0, 31.8, 31.7, 19.4, 13.9; HRMS (FAB) [M+H]$^+$ calcd for C$_{28}$H$_{55}$N$_5$O$_5$Si$_3$ 626.3589, found 626.3567.

5,11,17,23-Tetrakis(butoxymethyl)-25,26,27,28-tetra-(ethoxycarbonylmethoxy) calix[4]arene 1,3-*alternate* 2.39. Calixarene **2.38** (6.50 g, 8.46 mmol) was dissolved in acetone (250 mL). Cs$_2$CO$_3$ (13.8 g, 42.3 mmol) and ethyl bromoacetate (4.7 mL, 42.3 mmol) were added and the resulting suspension was stirred at reflux under a nitrogen atmosphere for 24 h. The solvent was evaporated under reduced pressure. The remaining solid was taken into CH$_2$Cl$_2$ (300 mL), washed with H$_2$O (2 x 300 mL), concentrated, and purified by flash chromatography (1 % MeOH in CH$_2$Cl$_2$) to give calixarene **2.39** (4.33 g, 46 %) as a clear light brown oil. ^{1}H NMR (400 MHz, CDCl$_3$): δ 7.07 (s, 8 H, ArH), 4.29 (s, 8 H, Ar-*CH$_2$*-OBu), 4.23 (q, 8 H, J = 7.0 Hz, O*CH$_2$*CH$_3$), 4.00 (s, 8 H, CH$_2$), 3.75 (s, 8 H, CH$_2$), 3.42 (t, 8 H, J = 6.6 Hz, O*CH$_2$*CH$_2$CH$_2$CH$_3$), 1.62-1.54 (m, 8 H, OCH$_2$*CH$_2$*CH$_2$CH$_3$), 1.44-1.33 (m, 8 H, OCH$_2$CH$_2$*CH$_2$*CH$_3$), 1.32 (t, 12 H, J = 7.0 Hz, OCH$_2$*CH$_3$*), 0.92 (t, 12 H, J = 7.5 Hz, OCH$_2$CH$_2$CH$_2$*CH$_3$*); ^{13}C NMR (100 MHz, CDCl$_3$): δ 169.3, 155.1, 133.2, 132.6, 130.3, 72.7, 70.1, 69.4, 60.7, 35.9, 31.9, 19.4, 14.2, 14.0; HRMS (FAB) [M+Cs]$^+$ calcd for C$_{64}$H$_{88}$O$_{16}$Cs 1245.5127, found 1245.5179.

5,11,17,23-Tetrakis(butoxymethyl)-25,26,27,28-tetra-(hydroxycarbonylmethoxy) calix[4]arene 1,3-*alternate* 2.40. A solution of calixarene **2.39** (3.43 g, 3.10 mmol) and 45 wt % KOH$_{(aq)}$ (10.0 mL, 117 mmol) in MeOH (30 mL) and THF (30 mL) was stirred at room temperature for 2 h. The solvent was evaporated under reduced pressure and the remaining solid was taken into H$_2$O (75 mL). The aqueous solution was acidified to pH 1 with 6 N HCl, extracted with CH$_2$Cl$_2$ (2 x 50 mL), and the combined organic layers were dried over Na$_2$SO$_4$ and the solvent evaporated under reduced pressure to give calixarene **2.40** (3.0 g, 97 %) as a light brown solid. ^{1}H NMR (400 MHz, CDCl$_3$): δ 7.07 (s, 8 H, ArH), 4.34 (s, 8 H, CH$_2$), 4.09 (s, 8 H, CH$_2$), 3.88 (s, 8 H, CH$_2$), 3.49 (t, 8 H, J = 6.5 Hz, O*CH$_2$*CH$_2$CH$_2$CH$_3$), 1.65-1.52 (m, 8 H, OCH$_2$*CH$_2$*CH$_2$CH$_3$), 1.43-1.30 (m, 8 H, OCH$_2$CH$_2$*CH$_2$*CH$_3$), 0.92 (t, 12 H, J = 7.3 Hz, OCH$_2$CH$_2$CH$_2$*CH$_3$*); ^{13}C NMR (100 MHz,

CDCl$_3$): δ 168.4, 152.9, 135.7, 133.3, 129.2, 72.0, 70.9, 67.1, 37.3, 31.6, 19.3, 13.9; HRMS (FAB) [M+Cs]$^+$ calcd for C$_{56}$H$_{72}$O$_{16}$Cs 1133.3875, found 1133.3827.

5,11,17,23-Tetrakis(butoxymethyl)-25,26,27,28-tetra-(chlorocarbonylmethoxy) calix[4]arene 1,3-*alternate* 2.41). A solution of calixarene **2.40** (3.00 g, 3.00 mmol) and SOCl$_2$ (7.44 mL, 102 mmol) in benzene (30 mL) was stirred at reflux under a nitrogen atmosphere for 2 h. The solvent was evaporated under reduced pressure and the remaining solid was coevaporated with benzene (2 x 30 mL) to remove residual SOCl$_2$ to give calixarene **2.41** (3.00 g, 93 %) as a brownish solid. IR (neat) 1812, 1465, 1512, 1101, 937 cm^{-1}; ^{1}H NMR (400 MHz, CDCl$_3$): δ 7.10 (s, 8 H, ArH), 4.36 (s, 8 H, CH$_2$), 3.96 (s, 8 H, CH$_2$), 3.94 (s, 8 H, CH$_2$), 3.47 (t, 8 H, J = 6.8 Hz, OC*H$_2$*CH$_2$CH$_2$CH$_3$), 1.65-1.56 (m, 8 H, OCH$_2$*CH$_2$*CH$_2$CH$_3$), 1.45-1.35 (m, 8 H, OCH$_2$CH$_2$*CH$_2$*CH$_3$), 0.93 (t, 12 H, J = 7.5 Hz, OCH$_2$CH$_2$CH$_2$*CH$_3$*).

2',3',5'-*O*-tri-*tert*-butyldimethylsilylguanosine 2.42. Guanosine **2.42** was prepared following the procedure of Li and Miller[266] and recrystallized from MeOH to give a white solid in 80% yield. ^{1}H NMR (400 MHz, DMSO-d$_6$): δ 10.61 (s, 1 H, NH1), 7.88 (s, 1 H, H8), 6.45 (bs, 2 H, NH$_2$), 5.74 (d, 1 H, J = 7.2 Hz, H1'), 4.57 (dd, 1 H, J = 7.2, 4.4 Hz, H2'), 4.15 (d, 1 H, J = 4.4 Hz, H3'), 3.97-3.91 (m, 1 H, H4'), 3.84 (dd, 1 H, J = 11.1, 5.5 Hz, H5'), 3.70 (dd, 1 H, J = 11.1, 3.6 Hz, H5"), 0.89 (s, 18 H, *t*-Bu-Si), 0.72 (s, 9 H, *t*-Bu-Si), 0.10 (s, 3 H, CH$_3$-Si), 0.08 (s, 9 H, CH$_3$-Si), -0.09 (s, 3 H, CH$_3$-Si), -0.29 (s, 3 H, CH$_3$-Si); ^{13}C NMR (100 MHz, DMSO-d$_6$): δ 156.7, 153.8, 151.6, 134.9, 116.5, 85.7, 85.2, 75.2, 72.8, 62.9, 25.8, 25.7, 25.5, 18.0, 17.8, 17.5, -4.7, -4.8, -5.5, -5.8; HRMS (FAB) [M+H]$^+$ calcd for C$_{28}$H$_{56}$N$_5$O$_5$Si$_3$ 626.3589, found 626.3567.

2',3'-*O*-di-*tert*-butyldimethylsilylguanosine 2.43. Guanosine **2.42** (10.0 g, 16.0 mmol)) was dissolved in nitromethane (140 mL). A solution of ZnBr$_2$ in aqueous nitromethane (140 mL, 49 g ZnBr$_2$ in 350 mL nitromethane and 3.5 mL H$_2$O) was added, and the mixture stirred for 4 d at room temperature.[267] The reaction mixture was poured into 2 M NH$_4$OAc (1 L), extracted with CH$_2$Cl$_2$ (700 mL), washed with H$_2$O (700 mL), dried over

Na$_2$SO$_4$ and the solvent was evaporated under reduced pressure. Crystallization from MeOH:CHCl$_3$ gave guanosine **2.43** (6.54 g, 80 %) as a white solid. ^{1}H NMR (400 MHz, DMSO-d$_6$): δ 10.61 (s, 1 H, NH1), 7.96 (s, 1 H, H8), 6.42 (bs, 2 H, NH$_2$), 5.71 (d, 1 H, J = 7.2 Hz, H1'), 5.21 (t, 1 H, J = 5.6 Hz, OH), 4.67 (dd, 1 H, J = 7.2, 4.4 Hz, H2'), 4.21 (d, 1 H, J = 4.4 Hz, H3'), 3.93-3.88 (m, 1 H, H4'), 3.69-3.60 (m, 1 H, H5'), 3.58-3.50 (m, 1H, H5"), 0.90 (s, 9 H, *t*-Bu-Si), 0.72 (s, 9 H, *t*-Bu-Si), 0.10 (s, 3 H, CH$_3$-Si), 0.09 (s, 3 H, CH$_3$-Si). -0.10 (s, 3 H, CH$_3$-Si), -0.32 (s, 3 H, CH$_3$-Si); ^{13}C NMR (100 MHz, DMSO-d$_6$): δ 156.7, 153.7, 151.4, 135.7, 116.7, 86.7, 85.7, 75.0, 73.1, 61.3, 25.7, 25.5, 17.8, 17.6, -4.7, -4.8, -5.0, -5.5; HRMS (FAB) [M+H]$^+$ calcd for C$_{22}$H$_{42}$N$_5$O$_5$Si$_2$ 512.2725, found 512.2737.

2',3'-*O*-di-*tert*-butyldimethylsilyl-2-*N,N*-dimethylaminomethyleneguanosine 2.44. To a solution of guanosine **2.43** (6.54 g, 12.8 mmol) in DMF (50 mL) was added DMF-dimethylacetal (5.10 mL, 38.4mmol) and the solution was stirred at room temperature under nitrogen for 20 h. The reaction mixture was poured into H$_2$O (100 mL), extracted with EtOAc (200 mL), washed with H$_2$O (2 x 100 mL), dried over Na$_2$SO$_4$ and the solvent was evaporated under reduced pressure to give guanosine **2.44** (6.75 g, 93 %) as a white solid. ^{1}H NMR (400 MHz, DMSO-d$_6$): δ 11.41 (s, 1 H, NH1), 8.46 (s, 1 H, N=*CH*-N(CH$_3$)$_2$), 8.10 (s, 1 H, H8), 5.78 (d, 1 H, J = 6.0 Hz, H1'), 5.21 (t, 1 H, J = 5.6 Hz, OH), 4.70 (dd, 1 H, J = 6.0, 4.8 Hz, H2'), 4.31-4.27 (m, 1 H, H3'), 3.95-3.90 (m, 1 H, H4'), 3.76-3.67 (m, 1 H, H5'), 3.63-3.54 (m, 1H, H5"), 3.11 (s, 3 H, N=CH-N(*CH$_3$*)$_2$), 3.02 (s, 3 H, N=CH-N(*CH$_3$*)$_2$), 0.90 (s, 9 H, *t*-Bu-Si), 0.74 (s, 9 H, *t*-Bu-Si), 0.11 (s, 3 H, CH$_3$-Si), 0.09 (s, 3 H, CH$_3$-Si). -0.09 (s, 3 H, CH$_3$-Si), -0.30 (s, 3 H, CH$_3$-Si); ^{13}C NMR (100 MHz, DMSO-d$_6$): δ 157.8, 157.5, 157.3, 149.7, 137.5, 120.2, 87.1, 86.0, 74.6, 72.3, 60.9, 40.7, 34.6, 25.7, 25.5, 17.8, 17.6, -4.6, -4.8, -5.5; HRMS (FAB) [M+H]$^+$ calcd for C$_{25}$H$_{47}$N$_6$O$_5$Si$_2$ 567.3147, found 567.3144.

5'-phthalimido-5'-deoxy-2',3'-*O*-di-*tert*-butyldimethylsilyl-2-*N,N*-dimethyl-aminomethyleneguanosine 2.45. A stirred solution of guanosine **2.44** (6.64 g, 11.7 mmol), Ph$_3$P (3.69 g, 14.1 mmol) and phthalimide (2.07 g, 14.1 mmol) in THF (175 mL)

was cooled to 0 °C under a nitrogen atmosphere. DEAD (2.72 mL, 14.1 mmol) was added dropwise over 1 min and the solution was allowed to warm to room temperature and stirred for 21 h. The solvent was evaporated under reduced pressure and the remaining oil was taken into EtOAc (200 mL), washed with 0.1 N NaOH (2 x 100 mL), 0.1 N HCl (100 mL), saturated $NaCl_{(aq)}$ (100 mL), and dried over Na_2SO_4. After solvent evaporation, the oil was purified by flash chromatography (3 % MeOH in CH_2Cl_2) to give crude guanosine **2.45** (contained $Ph_3P=O$), which was carried on without further purification. An analytical sample was obtained from the column. ^1H NMR (400 MHz, DMSO-d_6): δ 11.42 (bs, 1 H, NH1), 8.54 (s, 1 H, N=*CH*-N(CH$_3$)$_2$), 8.10 (s, 1 H, H8), 7.95-7.89 (m, 2 H, phthalimide-ArH), 7.88-7.82 (m, 2 H, phthalimide-ArH), 5.80 (d, 1 H, J = 7.5 Hz, H1'), 5.39 (dd, 1 H, J = 7.5, 4.3 Hz, H2'), 4.19-4.08 (m, 3 H, H3', H4', H5'), 3.89-3.78 (m, 1 H, H5"), 3.06 (s, 3 H, N=CH-N(*CH$_3$*)$_2$), 3.01 (s, 3 H, N=CH-N(*CH$_3$*)$_2$), 0.79 (s, 9 H, *t*-Bu-Si), 0.71 (s, 9 H, *t*-Bu-Si), -0.04 (s, 3 H, CH$_3$-Si), -0.10 (s, 6 H, CH$_3$-Si). -0.33 (s, 3 H, CH$_3$-Si); ^{13}C NMR (100 MHz, DMSO-d_6): δ 168.1, 157.6, 157.5, 157.1, 149.8, 138.9, 135.0, 131.3, 123.4, 120.8, 87.4, 82.5, 73.5, 72.2, 40.7, 34.8, 25.6, 25.5, 17.8, 17.6, -4.8, -5.1, -5.5; HRMS (FAB) [M+H]$^+$ calcd for $C_{33}H_{50}N_7O_6Si_2$ 696.3361, found 696.3334.

5'-phthalimido-5'-deoxy-2',3'-*O*-di-*tert*-butyldimethylsilylguanosine 2.46. Crude guanosine **2.45** was dissolved in EtOH (240 mL), $ZnCl_2$ (8.00 g, 58.5 mmol) was added and the suspension was stirred at reflux for 16 h. The solvent was evaporated under reduced pressure, and the remaining oil was taken into CH_2Cl_2 (500 mL), washed with H_2O (2 x 250 mL) and dried over Na_2SO_4. After solvent evaporation, the solid was purified by flash chromatography (3-5 % MeOH in CH_2Cl_2) to give guanosine **2.46** (5.1 g, 69 % over 2 steps) as a yellowish solid. ^1H NMR (400 MHz, DMSO-d_6): δ 10.65 (s, 1 H, NH1), 8.04 (s, 1 H, H8), 7.93-7.88 (m, 2 H, phthalimide-ArH), 7.87-7.82 (m, 2 H, phthalimide-ArH), 6.43 (bs, 2 H, NH$_2$), 5.72 (d, 1 H, J = 8.0 Hz, H1'), 4.93 (dd, 1 H, J = 8.0, 4.5 Hz, H2'), 4.23 (d, 1 H, J = 4.5 Hz, H3'), 4.16-4.04 (m, 2 H, H4', H5'), 3.95-3.85 (m, 1 H, H5"), 0.80 (s, 9 H, *t*-Bu-Si), 0.71 (s, 9 H, *t*-Bu-Si), 0.01 (s, 3 H, CH$_3$-Si), -0.04 (s, 3 H, CH$_3$-Si), -0.06 (s, 3 H, CH$_3$-Si), -0.32 (s, 3 H, CH$_3$-Si); ^{13}C NMR (100 MHz,

DMSO-d$_6$): δ 168.0, 156.8, 153.7, 151.6, 136.3, 134.9, 131.3, 123.4, 116.9, 98.0, 85.7, 83.1, 73.7, 73.6, 25.6, 17.8, 17.6, -4.7, -5.1, -5.6; HRMS (FAB) [M+H]$^+$ calcd for C$_{30}$H$_{45}$N$_6$O$_6$Si$_2$ 641.2940, found 641.2927.

5'-amino-5'-deoxy-2',3'-O-di-*tert*-butyldimethylsilylguanosine 2.47. A solution of guanosine **2.46** (4.56 g, 7.12 mmol) and H$_2$NNH$_2$ (2.23 mL, 71.2 mmol) in EtOH (150 mL) was stirred at reflux for 2.5 h. Upon cooling to room temperature, a white solid precipitated out of solution and was collected by filtration (700 mg). The filtrate was evaporated under reduced pressure and the remaining white solid was triturated with ether and collected (1.60 g). Combining the solids gave guanosine **2.47** (2.30 g, 64 %) as a white solid. Note: guanosine **2.47** was contaminated with phthalhydrazide. The reported yield was calculated by subtracting the mass of phthalhydrazide, determined by NMR integration. Phthalhydrazide does not affect the final coupling to calixarene **2.41** and is removed in the final purification of cG **2.34**. An analytical sample of guanosine **2.47** was obtained by crystallization from EtOH. ^{1}H NMR (400 MHz, DMSO-d$_6$): δ 7.98 (s, 1 H, H8), 6.56 (bs, 2 H, C2-NH$_2$), 5.69 (d, 1 H, J = 7.5 Hz, H1'), 4.76 (dd, 1 H, J = 7.5, 4.8 Hz, H2'), 4.24 (d, 1 H, J = 4.8 Hz, H3'), 3.89 (t, 1 H, J = 5.3 Hz, H4'), 2.92-2.82 (m, 2 H, H5', H5"), 0.89 (s, 9 H, *t*-Bu-Si), 0.70 (s, 9 H, *t*-Bu-Si), 0.10 (s, 3 H, CH$_3$-Si), 0.08 (s, 3 H, CH$_3$-Si), -0.10 (s, 3 H, CH$_3$-Si), -0.36 (s, 3 H, CH$_3$-Si); ^{13}C NMR (100 MHz, DMSO-d$_6$): δ 156.9, 153.8, 151.4, 136.4, 117.0, 86.9, 86.1, 74.1, 73.1, 43.1, 25.8, 25.5, 17.8, 17.5, -4.6, -4.7, -5.6; HRMS (FAB) [M+H]$^+$ calcd for C$_{22}$H$_{43}$N$_6$O$_4$Si$_2$ 511.2884, found 511.2882.

2',3',5'-O-tri-*tert*-butyldimethylsilyladenosine 2.51. Adenosine **2.51** was prepared following the procedure of Li and Miller[266] and purified by flash chromatography (2-10 % MeOH in CH$_2$Cl$_2$) to give a white solid in 89 % yield. ^{1}H NMR (400 MHz, DMSO-d$_6$): δ 8.32 (s, 1 H, H2), 8.12 (s, 1 H, H8), 7.31 (bs, 2 H, NH$_2$), 5.91 (d, 1 H, J = 6.5 Hz, H1'), 4.89 (dd, 1 H, J = 6.5, 4.5 Hz, H2'), 4.30 (dd, 1 H, J = 4.5, 1.5 Hz, H3'), 4.04-3.95 (m, 2 H, H4', H5'), 3.72 (dd, 1 H, J = 13.8, 6.8 Hz, H5"), 0.91 (s, 9 H, *t*-Bu-Si), 0.88 (s, 9

H, *t*-Bu-Si), 0.70 (s, 9 H, *t*-Bu-Si), 0.12 (s, 3 H, CH$_3$-Si), 0.10 (s, 3 H, CH$_3$-Si), 0.07 (s, 6 H, CH$_3$-Si), -0.12 (s, 3 H, CH$_3$-Si), -0.37 (s, 3 H, *t*-Bu-Si); ^{13}C NMR (100 MHz, DMSO-d$_6$): δ 156.1, 152.5, 149.4, 139.5, 119.2, 86.8, 85.2, 74.2, 72.3, 62.5, 25.8, 25.7, 25.4, 18.0, 17.8, 17.5, -4.7, -4.8, -4.9, -5.5, -5.6; HRMS (FAB) [M+H]$^+$ calcd for C$_{28}$H$_{56}$N$_5$O$_4$Si$_3$ 610.3640, found 610.3662.

2',3'-*O*-di-*tert*-butyldimethylsilyladenosine 2.52. Adenosine **2.51** (3.95 g, 6.48 mmol) was dissolved in nitromethane (56 mL), a solution of ZnBr$_2$ in aqueous nitromethane (56 mL, 49 g ZnBr$_2$ in 350 mL nitromethane and 3.5 mL H$_2$O) was added, and the mixture was stirred for 4 d at room temperature.[267] The reaction mixture was poured into 1 M NH$_4$OAc (400 mL), extracted with CH$_2$Cl$_2$ (400 mL), washed with H$_2$O (400 mL), dried over Na$_2$SO$_4$ and the solvent was evaporated under reduced pressure. Crystallization from MeOH:CHCl$_3$ gave adenosine **2.52** (2.75 g, 86 %) as a white solid. ^{1}H NMR (400 MHz, DMSO-d$_6$): δ 8.39 (s, 1 H, H2), 8.13 (s, 1 H, H8), 7.39 (bs, 2 H, NH$_2$), 5.89 (d, 1 H, J = 7.3 Hz, H1'), 5.73 (dd, 1 H, J = 8.0, 4.0 Hz, OH), 4.89 (dd, 1 H, J = 7.3, 4.5 Hz, H2'), 4.28 (dd, 1 H, J = 4.5, 0.8 Hz, H3'), 4.00-3.95 (m, 1 H, H4'), 3.72 (dt, 1 H, J = 12.3, 4.0 Hz, H5'), 3.62-3.52 (m, 1 H, H5''), 0.91 (s, 9 H, *t*-Bu-Si), 0.69 (s, 9 H, *t*-Bu-Si), 0.11 (s, 3 H, CH$_3$-Si), 0.10 (s, 3 H, CH$_3$-Si), -0.16 (s, 3 H, CH$_3$-Si), -0.48 (s, 3 H, CH$_3$-Si); ^{13}C NMR (100 MHz, DMSO-d$_6$): δ 156.3, 152.4, 149.0, 140.4, 119.6, 87.7, 87.3, 74.2, 73.2, 61.3, 25.8, 25.5, 17.9, 17.6, -4.6, -4.7, -4.8, -5.7; HRMS (FAB) [M+H]$^+$ calcd for C$_{22}$H$_{42}$N$_5$O$_4$Si$_2$ 496.2775, found 496.2780.

2',3'-*O*-di-*tert*-butyldimethylsilyl-6-*N*,*N*-dimethylaminomethyleneadenosine 2.53. To a solution of adenosine **2.52** (2.58 g, 5.21 mmol) in DMF (25 mL) was added DMF-dimethylacetal (2.10 mL, 15.6 mmol) and the solution was stirred at room temperature under nitrogen atmosphere for 20 h. The reaction mixture was poured into H$_2$O (50 mL), extracted with EtOAc (75 mL), washed with H$_2$O (2 x 50 mL), dried over Na$_2$SO$_4$ and the solvent was evaporated under reduced pressure to give adenosine **2.53** (2.81 g, 98 %) as a white solid. ^{1}H NMR (400 MHz, DMSO-d$_6$): δ 8.92 (s, 1 H, N=*CH*-N(CH$_3$)$_2$), 8.52 (s, 1

214

H, H2), 8.41 (s, 1 H, H8), 5.95 (d, 1 H, J = 7.0 Hz, H1'), 5.55 (dd, 1 H, J = 7.3, 4.5 Hz, OH), 4.90 (dd, 1 H, J = 7.0, 4.5 Hz, H2'), 4.30 (dd, 1 H, J = 4.5, 1.0 Hz, H3'), 4.00-3.96 (m, 1 H, H4'), 3.74 (dt, 1 H, J = 12.3, 4.5 Hz, H5'), 3.63-3.54 (m, 1 H, H5''), 3.19 (s, 3 H, N=CH-N(CH₃)₂), 3.13 (s, 3 H, N=CH-N(CH₃)₂), 0.91 (s, 9 H, *t*-Bu-Si), 0.68 (s, 9 H, *t*-Bu-Si), 0.12 (s, 3 H, CH₃-Si), 0.10 (s, 3 H, CH₃-Si), -0.16 (s, 3 H, CH₃-Si), -0.49 (s, 3 H, CH₃-Si); ¹³C NMR (100 MHz, DMSO-d₆): δ 159.4, 158.2, 151.8, 151.1, 141.9, 126.1, 87.5, 87.1, 74.3, 73.0, 61.4, 40.8, 34.7, 25.8, 25.5, 17.9, 17.5, -4.6, -4.7, -4.8, -5.6; HRMS (FAB) [M+H]⁺ calcd for C₂₅H₄₇N₆O₄Si₂ 551.3198, found 551.3201.

5'-phthalimido-5'-deoxy-2',3'-*O*-di-*tert*-butyldimethylsilyl-6-*N,N*-dimethyl-aminomethyleneadenosine 2.54. A stirred solution of adenosine **2.53** (2.72 g, 4.94 mmol), Ph₃P (1.55 g, 5.93 mmol) and phthalimide (0.870 g, 5.93 mmol) in THF (80 mL) was cooled to 0 °C under a nitrogen atmosphere. DEAD (0.93 mL, 5.93 mmol) was added dropwise over 1 min and the solution was allowed to warm to room temperature and stirred for 21 h. The solvent was evaporated under reduced pressure and the remaining oil was taken into EtOAc (100 mL), washed with 0.1 N NaOH (2 x 50 mL), 0.1 N HCl (50 mL), saturated NaCl(aq) (50 mL), and dried over Na₂SO₄. After solvent evaporation, the oil was dissolved in hot MeOH, and the product crystallized upon standing overnight to give adenosine **2.54** (2.62 g, 78 %) as a white solid. ¹H NMR (400 MHz, DMSO-d₆): δ 8.91 (s, 1 H, N=*CH*-N(CH₃)₂), 8.59 (s, 1 H, H2), 8.25 (s, 1 H, H8), 7.91-7.82 (m, 4 H, phthalimide-ArH), 5.97 (d, 1 H, J = 7.5 Hz, H1'), 5.23 (dd, 1 H, J = 7.5, 4.3 Hz, H2'), 4.32 (d, 1 H, J = 4.3 Hz, H3'), 4.19-4.11 (m, 2 H, H4', H5'), 3.92 (dd, 1 H, J = 17.1, 9.3 Hz, H5''), 3.19 (s, 3 H, N=CH-N(CH₃)₂), 3.13 (s, 3 H, N=CH-N(CH₃)₂), 0.83 (s, 9 H, *t*-Bu-Si), 0.65 (s, 9 H, *t*-Bu-Si), 0.02 (s, 3 H, CH₃-Si), -0.02 (s, 3 H, CH₃-Si), -0.12 (s, 3 H, CH₃-Si), -0.49 (s, 3 H, CH₃-Si); ¹³C NMR (100 MHz, DMSO-d₆): δ 168.1, 159.3, 158.1, 151.9, 151.6, 142.4, 134.9, 131.5, 126.0, 123.4, 86.8, 83.3, 73.5, 72.9, 40.8, 34.7, 25.6, 25.5, 17.9, 17.5, -4.7, -5.0, -5.6; HRMS (FAB) [M+H]⁺ calcd for C₃₃H₅₀N₇O₅Si₂ 680.3412, found 680.3435.

5'-phthalimido-5'-deoxy-2',3'-*O*-di-*tert*-butyldimethylsilyladenosine 2.55. Adenosine **2.54** (2.51 g, 3.78 mmol) was dissolved in EtOH (75 mL), $ZnCl_2$ (1.55 g, 11.3 mmol) was added and the suspension was stirred at reflux for 1 h. The reaction mixture was poured into H_2O (250 mL) and extracted with CH_2Cl_2 (3 x 125 mL). The combined organic layers were washed with saturated $NaCl_{(aq)}$ (100 mL), dried over Na_2SO_4 and the solvent was evaporated under reduced pressure to give adenosine **2.55** (2.30 g, 97 %) as a white solid. ^1H NMR (400 MHz, DMSO-d_6): δ 8.47 (s, 1 H, H2), 7.98 (s, 1 H, H8), 7.92-7.81 (m, 4 H, phthalimide-ArH), 7.30 (bs, 2 H, NH_2), 5.91 (d, 1 H, J = 7.5 Hz, H1'), 5.22 (dd, 1 H, J = 7.5, 4.5 Hz, H2'), 4.31 (d, 1 H, J = 4.5 Hz, H3'), 4.19-4.10 (m, 2 H, H4', H5'), 3.94-3.85 (m, 1 H, H5"), 0.82 (s, 9 H, *t*-Bu-Si), 0.66 (s, 9 H, *t*-Bu-Si), 0.02 (s, 3 H, CH_3-Si), -0.03 (s, 3 H, CH_3-Si), -0.11 (s, 3 H, CH_3-Si), -0.45 (s, 3 H, CH_3-Si); ^{13}C NMR (100 MHz, DMSO-d_6): δ 168.1, 156.1, 152.6, 149.5, 140.6, 134.8, 131.5, 123.3, 119.4, 86.8, 83.1, 73.5, 72.9, 25.6, 25.5, 17.8, 17.5, -4.7, -4.8, -5.0, -5.6; HRMS (FAB) $[M+H]^+$ calcd for $C_{30}H_{45}N_6O_5Si_2$ 625.2990, found 625.3023.

5'-amino-5'-deoxy-2',3'-*O*-di-*tert*-butyldimethylsilyladenosine 2.56. A solution of adenosine **2.55** (2.08 g, 3.41 mmol) and H_2NNH_2 (1.20 mL, 38.3 mmol) in EtOH (60 mL) was stirred at reflux for 2.5 h. The solvent was evaporated under reduced pressure and the remaining solid was triturated with CH_3CN to give adenosine **2.56** (880 mg, 52 %) as an off-white solid. An analytical sample was obtained by crystallization from CH_3CN/hexanes. ^1H NMR (400 MHz, DMSO-d_6): δ 8.41 (s, 1 H, H2), 8.12 (s, 1 H, H8), 7.28 (bs, 2 H, C6-NH_2), 5.85 (d, 1 H, J = 7.3 Hz, H1'), 4.97 (dd, 1 H, J = 7.3, 4.5 Hz, H2'), 4.31 (dd, 1 H, J = 4.5, 1.0 Hz, H3'), 3.92-3.86 (m, 1 H, H4'), 2.86 (dd, 1 H, J = 13.6, 5.3 Hz, H5'), 2.78 (dd, 1 H, J = 13.6, 5.0 Hz, H5"), 2.09 (bs, 2 H, C5'-NH_2), 0.91 (s, 9 H, *t*-Bu-Si), 0.67 (s, 9 H, *t*-Bu-Si), 0.12 (s, 3 H, CH_3-Si), 0.10 (s, 3 H, CH_3-Si), -0.13 (s, 3 H, CH_3-Si), -0.48 (s, 3 H, CH_3-Si); ^{13}C NMR (100 MHz, DMSO-d_6): δ 156.1, 152.5, 149.4, 140.6, 119.5, 87.8, 87.1, 73.6, 72.9, 43.6, 25.8, 25.5, 17.8, 17.5, -4.6, -4.7, -5.7; HRMS (FAB) $[M+H]^+$ calcd for $C_{22}H_{43}N_6O_3Si_2$ 495.2935, found 495.2902.

Calix[4]arene-guanosine cG 2.34. To a solution of calixarene **2.41** (977 mg, 0.911 mmol) and guanosine **2.47** (2.79 g, 5.47 mmol) in CH_2Cl_2 (150 mL) under nitrogen atmosphere was added Et_3N (2.50 mL, 18.2 mmol) and the mixture was stirred at room temperature for 24 h. The solvent was evaporated under reduced pressure followed by purification by flash chromatography (5 % MeOH in CH_2Cl_2) to give cG **2.34** (1.34 g, 49 %) as a white solid. ^1H NMR (400 MHz, DMSO-d_6, 50 ^{o}C): δ 10.52 (s, 4 H, N1H), 7.95 (s, 4 H, H8), 7.93 (bs, 4 H, 5'-Amide NH), 7.00 (s, 4 H, Calix-ArH), 6.93 (s, 4 H, Calix-ArH), 6.06 (bs, 8 H, C2-NH_2), 5.75 (d, 4 H, J = 7.2 Hz, H1'), 4.76 (dd, 4 H, J = 7.2, 4.6 Hz, H2'), 4.26 (d, 4 H, J = 4.6 Hz, H3'), 4.14 (d, 4 H, J = 11.6 Hz, C(O)-CH_2-O), 4.09 (d, 4 H, J = 11.6 Hz, C(O)-CH_2-O), 3.99 (t, 4 H, J = 5.9 Hz, H4'), 3.71 (app d, 8 H, J = 7.0 Hz, CH_2-bridge), 3.67-3.57 (m, 4 H, H5'), 3.55-3.41 (m, 12 H, H5" + Ar-CH_2-O), 3.24 (t, 8 H, J = 6.6 Hz, OCH_2CH$_2$CH$_2$CH$_3$), 1.49-1.37 (m, 8 H, OCH$_2$$CH_2CH_2CH_3$), 1.32-1.19 (m, 8 H, OCH$_2$CH$_2$$CH_2CH_3$), 0.91 (s, 36 H, t-Bu-Si), 0.82 (t, 12 H, J = 7.4 Hz, OCH$_2$CH$_2$CH$_2$$CH_3$), 0.75 (s, 36 H, t-Bu-Si), 0.11 (s, 12 H, CH$_3$-Si), 0.09 (s, 12 H, CH$_3$-Si), -0.07 (s, 12 H, CH$_3$-Si), -0.27 (s, 12 H, CH$_3$-Si); ^{13}C NMR (100 MHz, DMSO-d_6, 22 ^{o}C): δ 168.8, 156.7, 154.9, 153.5, 151.4, 136.5, 134.0, 133.5, 133.1, 130.2, 130.0, 117.1, 85.9, 84.6, 74.0, 73.8, 71.7, 70.6, 69.1, 31.2, 25.8, 25.7, 25.5, 18.9, 17.9, 17.7, 17.5, 13.8, -4.8, -5.6; MS (ESI) $[(M+2H)/2]^{2+}$ calcd for $C_{144}H_{234}N_{24}O_{28}Si_8$ 1486.8, found 1486.8. Anal. calcd for $C_{144}H_{232}N_{24}O_{28}Si_8$: C, 58.19; H, 7.87, found: C, 58.05; H, 7.99.

Calix[4]arene-adenosine cA 2.35. To a suspension of calixarene **2.41** (254 mg, 0.237 mmol) and adenosine **2.56** (680 mg, 1.42 mmol) in CH_2Cl_2 (20 mL) under nitrogen atmosphere was added Et_3N (0.66 mL, 4.7 mmol) and the mixture was stirred at room temperature for 24 h. The solvent was evaporated under reduced pressure followed by purification by flash chromatography (3 % MeOH in CH_2Cl_2) to give cA **2.35** (280 mg, 41 %) as a white solid. ^1H NMR (400 MHz, DMSO-d_6, 50 ^{o}C): δ 8.36 (s, 4 H, H2), 8.09 (s, 4 H, H8), 7.72 (t, 4 H, J = 5.7 Hz, 5'-Amide NH), 7.06 (bs, 8 H, C6-NH_2), 7.01 (s, 4 H, Calix-ArH), 6.94 (s, 4 H, Calix-ArH), 5.90 (d, 4 H, J = 6.8 Hz, H1'), 5.05 (dd, 4 H, J = 6.8, 4.6 Hz, H2'), 4.37 (d, 4 H, J = 4.6 Hz, H3'), 4.17 (d, 4 H, J = 11.6 Hz, C(O)-CH_2-O), 4.12 (d, 4 H, J = 11.6 Hz, C(O)-CH_2-O), 4.01 (t, 4 H, J = 5.9 Hz, H4'), 3.78-3.64 (m, 12

H, H5' + CH$_2$-bridge), 3.55-3.35 (m, 12 H, H5" + Ar-CH$_2$-O), 3.25 (t, 8 H, J = 6.6 Hz, OCH$_2$CH$_2$CH$_2$CH$_3$), 1.48-1.37 (m, 8 H, OCH$_2$CH$_2$CH$_2$CH$_3$), 1.31-1.19 (m, 8 H, OCH$_2$CH$_2$CH$_2$CH$_3$), 0.90 (s, 36 H, t-Bu-Si), 0.81 (t, 12 H, J = 7.4 Hz, OCH$_2$CH$_2$CH$_2$CH$_3$), 0.70 (s, 36 H, t-Bu-Si), 0.09 (s, 12 H, CH$_3$-Si), 0.07 (s, 12 H, CH$_3$-Si), -0.12 (s, 12 H, CH$_3$-Si), -0.41 (s, 12 H, CH$_3$-Si); ^{13}C NMR (100 MHz, DMSO-d$_6$, 22 ^{o}C): δ 168.8, 156.1, 154.9, 152.4, 149.3, 140.7, 133.8, 133.5, 132.7, 130.2, 130.1, 119.7, 87.1, 84.7, 73.7, 73.2, 71.8, 70.6, 69.0, 31.3, 25.7, 25.6, 25.5, 18.9, 17.7, 17.5, 13.8, 0.2, -4.8, -5.7; HRMS (FAB) [M+Cs]$^+$ calcd for C$_{144}$H$_{232}$N$_{24}$O$_{24}$Si$_8$Cs 3038.4880, found 3038.4922.

4-butoxymethyl-2,6-dimethylphenol 2.58. A solution of 2,6-dimethylphenol (1.00 g, 8.18 mmol), paraformaldehyde (2.45 g, 81.8 mmol), glacial HOAc (8 mL), conc. H$_3$PO$_4$ (8.5 mL), and conc. HCl (9.0 mL) in dioxane (85 mL) was stirred at 80 ^{o}C for 24 h.[265] The orange solution was diluted with an ice/water mixture (60 mL) and extracted with CHCl$_3$ (2 x 70 mL). The combined organic layers were dried over Na$_2$SO$_4$ and the solvent evaporated under reduced pressure to give crude 4-chloromethyl-2,6-dimethylphenol **2.57** as an orange syrup. Compound **2.57** was dissolved in BuOH (75 mL), K$_2$CO$_3$ (5.66 g, 40.9 mmol) was added, and the suspension was stirred at 80 ^{o}C under a nitrogen atmosphere for 2 d. The mixture was filtered to remove K$_2$CO$_3$ and the filtrate was diluted with CHCl$_3$ (500 mL), washed with H$_2$O (2 x 500 mL), and concentrated to give a reddish-brown syrup. Purification by flash chromatography (CH$_2$Cl$_2$) afforded 4-butoxymethyl-2,6-dimethylphenol **2.58** (0.560 g, 33 % over 2 steps) as a white solid. ^{1}H NMR (400 MHz, CDCl$_3$): δ 6.96 (s, 2H, ArH), 4.36 (s, 2 H, Ar-CH$_2$-O), 3.45 (t, 2 H, J = 6.6 Hz, OCH$_2$CH$_2$CH$_2$CH$_3$), 2.24 (s, 6 H, Ar-CH$_3$), 1.64-1.55 (m, 2 H, OCH$_2$CH$_2$CH$_2$CH$_3$), 1.44-1.34 (m, 2 H, OCH$_2$CH$_2$CH$_2$CH$_3$), 0.92 (t, 3 H, J = 7.5 Hz, OCH$_2$CH$_2$CH$_2$CH$_3$); ^{13}C NMR (100 MHz, CDCl$_3$): δ 133.4, 128.8, 128.4, 122.8, 72.7, 70.0, 31.8, 19.4, 15.9, 13.9.

Ethyl-(4-butoxymethyl-2,6-dimethyl)-phenoxyacetate 2.59. Compound **2.58** (0.560 g, 2.69 mmol) was dissolved in acetone (80 mL). Cs$_2$CO$_3$ (4.38 g, 13.5 mmol) and ethyl

bromoacetate (0.45 mL, 4.0 mmol) were added and the resulting suspension was stirred at reflux under a nitrogen atmosphere for 24 h. The solvent was evaporated under reduced pressure. The remaining oil was taken into CH_2Cl_2 (50 mL), washed with H_2O (2 x 50 mL), concentrated, and purified by flash chromatography (CH_2Cl_2) to give compound **2.59** (0.35 g, 48 %) as a clear oil. ^{1}H NMR (400 MHz, CDCl$_3$): δ 6.98 (s, 2H, ArH), 4.38 (s, 2 H, CH$_2$), 4.37 (s, 2 H, CH$_2$), 4.30 (q, 2 H, J = 7.1 Hz, O*CH$_2$*CH$_3$) 3.47 (t, 2 H, J = 6.6 Hz, O*CH$_2$*CH$_2$CH$_2$CH$_3$), 2.29 (s, 6 H, Ar-CH$_3$), 1.64-1.55 (m, 2 H, OCH$_2$*CH$_2$*CH$_2$CH$_3$), 1.45-1.35 (m, 2 H, OCH$_2$CH$_2$*CH$_2$*CH$_3$), 1.33 (t, 3 H, J = 7.1 Hz, OCH$_2$*CH$_3$*), 0.92 (t, 3 H, J = 7.5 Hz, OCH$_2$CH$_2$CH$_2$*CH$_3$*); ^{13}C NMR (100 MHz, CDCl$_3$): δ 169.1, 154.7, 134.5, 130.6, 128.5, 72.6, 70.4, 69.1, 61.2, 31.8, 19.4, 16.3, 14.2, 13.9; HRMS (FAB) M$^+$ calcd for C$_{17}$H$_{26}$O$_4$ 294.1831, found 294.1823.

(4-butoxymethyl-2,6-dimethylphenoxy)-acetic acid 2.60. A solution of compound **2.59** (0.350 g, 1.19 mmol) and 45 wt % KOH$_{(aq)}$ (7.0 mL, 82 mmol) in MeOH (21 mL) and THF (21 mL) was stirred at room temperature for 2 h. The solvent was evaporated under reduced pressure and the remaining solid was taken into H_2O (70 mL). The aqueous solution was acidified to pH 1 with 6 N HCl, extracted with CH_2Cl_2 (2 x 50 mL), the combined organic layers were dried over Na$_2$SO$_4$ and the solvent was evaporated under reduced pressure to give compound **2.60** (0.318 g, 100 %) as a brownish solid. ^{1}H NMR (400 MHz, CDCl$_3$): δ 7.00 (s, 2 H, ArH), 4.41 (s, 2 H, CH$_2$), 4.38 (s, 2 H, CH$_2$), 3.46 (t, 2 H, J = 6.5 Hz, O*CH$_2$*CH$_2$CH$_2$CH$_3$), 2.27 (s, 6 H, Ar-CH$_3$), 1.65-1.54 (m, 2 H, OCH$_2$*CH$_2$*CH$_2$CH$_3$), 1.45-1.34 (m, 2 H, OCH$_2$CH$_2$*CH$_2$*CH$_3$), 0.92 (t, 3 H, J = 7.3 Hz, OCH$_2$CH$_2$CH$_2$*CH$_3$*); ^{13}C NMR (100 MHz, CDCl$_3$): δ 153.8, 135.0, 130.4, 128.5, 77.2, 72.4, 70.4, 68.6, 31.8, 19.3, 16.2, 13.9; HRMS (FAB) M$^+$ calcd for C$_{15}$H$_{22}$O$_4$ 266.1518, found 266.1516.

5'-(2-(4-butoxymethyl-2,6-dimethylphenoxy)-ethoxycarbonylamino)-2',3'-*O*-di-*tert*-butyldimethylsilylguanosine G 2.36. A solution of compound **2.60** (0.318 g, 1.19 mmol) and SOCl$_2$ (0.85 mL) in benzene (15 mL) was stirred at reflux under a nitrogen atmosphere for 2 h. The solvent was evaporated under reduced pressure and the

remaining brownish solid was coevaporated with benzene (2 x 20 mL) to give (4-butoxymethyl-2,6-dimethylphenoxy)-acetyl chloride **2.61** (0.372 g, IR showed no acid O-H stretch and a single C=O stretch at 1816 cm^{-1}). A suspension of compound **2.61** (0.372 g, 1.31 mmol), guanosine **2.47** (0.800 g, 1.57 mmol) and Et$_3$N (0.91 mL, 6.5 mmol) in CH$_2$Cl$_2$ (20 mL) was stirred at room temperature under a nitrogen atmosphere for 24 h. The solvent was evaporated under reduced pressure and the remaining solid was purified by flash chromatography to afford G **2.36** (0.65 g, 66 %) as a white solid. ^{1}H NMR (400 MHz, DMSO-d$_6$): δ 10.67 (s, 1 H, N1H), 8.51 (t, 1 H, J = 6.0 Hz, amide NH), 8.05 (s, 1 H, H8), 6.96 (s, 2 H, ArH), 6.45 (bs, 2 H, NH$_2$), 5.72 (d, 1 H, J = 7.8 Hz, H1'), 4.79 (dd, 1 H, J = 7.8, 4.3 Hz, H2'), 4.33 (d, 1 H, J = 4.3 Hz, H3'), 4.31 (s, 2H, CH$_2$). 4.18 (s, 2H, CH$_2$), 3.99 (dd, 1 H, J = 8.0, 6.0 Hz, H4'), 3.69-3.56 (m, 1 H, H5'), 3.49-3.39 (m, 1 H, H5"), 3.38 (t, 2H, J = 6.5 Hz, O*CH$_2$*CH$_2$CH$_2$CH$_3$), 2.20 (s, 6 H, Ar-CH$_3$), 1.54-1.44 (m, 2 H, OCH$_2$*CH$_2$*CH$_2$CH$_3$), 1.37-1.26 (m, 2 H, OCH$_2$CH$_2$*CH$_2$*CH$_3$), 0.90 (s, 9 H, *t*-Bu-Si), 0.86 (t, 3 H, J = 7.3 Hz, OCH$_2$CH$_2$CH$_2$*CH$_3$*), 0.71 (s, 9 H, *t*-Bu-Si), 0.11 (s, 3 H, CH$_3$-Si), 0.10 (s, 3 H, CH$_3$-Si), -0.08 (s, 3 H, CH$_3$-Si), -0.34 (s, 3 H, CH$_3$-Si); ^{13}C NMR (100 MHz, DMSO-d6): d 168.3, 156.6, 153.6, 153.5, 151.5, 136.3, 134.5, 130.1, 130.0, 128.1, 116.8, 85.6, 84.4, 73.8, 73.5, 71.5, 70.4, 69.3, 31.3, 25.7, 25.5, 18.9, 17.8, 17.5, 15.8, 13.8, -4.7, -4.8, -5.7; HRMS (FAB) [M+H]$^+$ calcd for C$_{37}$H$_{63}$N$_6$O$_7$Si$_2$ 759.4297, found 759.4312. Anal. calcd for C$_{37}$H$_{62}$N$_6$O$_7$Si$_2$: C, 58.54; H, 8.23, found: C, 58.35; H, 8.48.

25,26,27,28-tetra-(hydroxycarbonylmethoxy)calix[4]arene 1,3-*alternate* 2.29. The tetraester **2.28** (25,26,27,28-tetra-(ethoxycarbonylmethoxy)calix[4]arene 1,3-*alternate*) (98 mg, 0.13 mmol)^{257} was dissolved in a solution of 3 mL of MeOH and 5 mL of THF. A 45 wt % KOH$_{(aq)}$ solution (1 mL) was then added dropwise. The reaction mixture was stirred overnight at room temperature under a nitrogen atmosphere. The organic solvents were removed under reduced pressure at 70 ^{o}C, and the remaining aqueous solution was acidified to pH 1 by addition of 4 N HCl and allowed to stand at 0 ^{o}C for 6 h. The resulting precipitate (tetraacid **2.29**) was collected by filtration, washed with water and dried under high vacuum at 80 ^{o}C. The aqueous filtrate was extracted with CH$_2$Cl$_2$, and the solvent was evaporated under reduced pressure affording additional tetraacid **2.29**.

The resulting solids were combined and dried under vacuum to afford tetraacid **2.29** (65 mg, 78 %) as a white solid. ^{1}H NMR (500 MHz, DMSO-d$_6$): δ 12.21 (br s, 4 H, C(O)-OH), 7.07 (d, 8 H, J = 7.5 Hz, Ar-H), 6.62 (t, 4 H, J = 7.5 Hz, Ar-H), 4.03 (s, 8 H, CH$_2$), 3.77 (s, 8 H, CH$_2$).

Calix[4]arene-guanosine 2.26. To a solution of tetraacid **2.29** (35 mg, 0.053 mmol) and 5'-amino-5'-deoxy-2',3'-*O*-isopropylideneguanosine **2.27** (87 mg, 0.27 mmol)[258] in DMF (10 mL) at 0 °C was added EDCI (100 mg, 0.52 mmol). The reaction mixture was stirred for 20 min at 0 °C, DMAP (15 mg, 0.79 mmol) was added, and the resulting reaction mixture was stirred at room temperature for 18 h. The solvent was evaporated under reduced pressure at 50 °C and the remaining oil was triturated with MeOH. The resulting white precipitate was isolated by centrifugation and washed twice with MeOH. Purification by preparative TLC on microcrystalline cellulose plates (H$_2$O:CH$_3$CN 24:76) afforded calix[4]arene-guanosine **2.26** (55 mg, 55 %) as a white solid. ^{1}H NMR (500 MHz, DMSO-d$_6$): δ 10.71 (br s, 4 H, N1H), 7.90 (s, 4 H, H8), 7.07 (bs, 4 H, C(O)-NH), 6.97 (d, 4 H, J = 7.5 Hz, Ar-H), 6.92 (d, 4 H, J = 7.5 Hz, Ar-H), 6.58 (t, 4 H, J = 7.5 Hz), 6.51 (br s, 8 H, NH$_2$), 5.95 (d, 4 H, J = 2.0 Hz, H1'), 5.18 (dd, 4 H, J = 7.9, 2.0 Hz, H2'), 5.04-5.00 (m, 4 H, H3'), 4.17-4.14 (m, 4 H, H4'), 3.78 (s, 8 H, Ar-*CH$_2$*-Ar), 3.74-3.49 (m, 8 H, H5', H5''), 3.25-3.15 (m, 8 H, CH$_2$), 1.47 (s, 12 H, CH$_3$), 1.28 (s, 12 H, CH$_3$). MS (FAB) [M+H]$^+$ calcd for C$_{88}$H$_{97}$N$_{24}$O$_{24}$ 1873.7, found 1873.8.

25,26,27,28-tetra-(chlorocarbonylmethoxy)calix[4]arene 1,3-*alternate* 2.31. To a suspension of tetraacid **2.29** (48 mg, 0.073 mmol) in benzene (3 mL) was added SOCl$_2$ (1.0 mL, 14 mmol). The reaction mixture was stirred at reflux for 2.5 h, cooled to room temperature, and the solvent was evaporated under reduced pressure. Residual SOCl$_2$ was removed by co-evaporation with benzene (5 mL) to give tetraacid chloride **2.31** (50 mg , 94 %), which was used immediately without further purification. ^{1}H NMR (400 MHz, CDCl$_3$): δ 7.17 (d, 8 H, J = 7.5 Hz, Ar-H), 6.95 (t, 4 H, J = 7.5 Hz, Ar-H), 4.02 (s, 8 H, CH$_2$), 3.98 (s, 8 H, CH$_2$).

221

Calix[4]arene tetramethylamide 1,3-*alternate* 2.30. Aqueous CH_3NH_2 (40 wt % solution, 100 ml) was boiled to release CH_3NH_2 gas. The gas was passed through two water traps, containing solid NaOH, and bubbled through a solution of **2.29** (38 mg, 0.052 mmol) in CH_2Cl_2 (10 mL). After 2.5 hours at room temperature, the solution was concentrated and the residue was submitted to preparative TLC (silica gel, 10 % MeOH in $CHCl_3$) to give calix[4]arene tetramethylamide 1,3-*alternate* **2.30** (22 mg, 60 %) as a white solid. ^1H NMR ($CDCl_3$): δ 7.04 (d, 8 H, J=7.5 Hz, Ar-H), 6.84 (t, 4 H, J=7.5 Hz, Ar-H), 5.79 (q, 4 H, J = 4.8 Hz, C(O)-*NH*-CH_3), 4.07 (s, 8 H, CH_2), 3.70 (s, 8 H, CH_2), 2.88 (d, 12 H, J = 4.8 Hz, C(O)-NH-*CH_3*).

4.2.2 Experimental Details

Transmission Electron Microscopy (TEM). TEM images were taken by Mahnaz El-Kouedi at Georgetown University. TEM characterization was performed using a JEOL 1200 EX Transmission Electron Microscope. Imaging was performed on copper mesh grids that were dipped into aqueous suspensions of (cG **2.26**•Na^+)$_n$•(BPh_4^-)$_n$. Samples were imaged on 200 Cu mesh formvar-coated grids (EM Sciences). A uranyl acetate stain was used to enhance contrast.

Complex Formation from cG 2.34. Typically, a suspension of cG **2.34** (3.0 mg) in $CDCl_3$ (1 mL) was stirred with either H_2O or a 1.0 M aqueous salt solution (1 mL) for 12 h. The organic layer was separated, centrifuged to remove residual water (and salt), and analyzed.

^{23}Na NMR Measurements. ^{23}Na NMR spectra were recorded on a Bruker DRX-500 operating at 132.29 MHz and are reported in ppm relative to 25 mM NaCl in D_2O at 0 ppm (external standard). A 5 mm broad band probe was used. For all experiments, 95,000 transients were collected and a 90° pulse of 7.7 µs, acquisition time of 619 ms with a 1 s delay between pulses, and a sweep width of 13.2 kHz were used. The sample concentrations were 20 mM in cG **2.34**, cA **2.35** and G **2.36**.

Salt Back-Extractions Measured by Ion Chromatography (IC). Ion chromatographs were run on a Dionex DX-120 Ion Chromatograph. Eluents were 4.8 mM Na_2CO_3/0.6 mM $NaHCO_3$ for anions and 20 mM methylsulfonic acid for cations. Ion concentrations are reported relative to a 1.0 mM standard for each ion. In all experiments, 1.2 mL of 2 mM L (L = cG **2.34**, cA **2.35**, G **2.36**) in CD_2Cl_2 was stirred with 1 mL of 1 M salt (salts were NaCl, NaBr, KCl, KBr, and 1:1:1:1 Na:K:Cl:Br) for 12 h. The aqueous salt solutions were removed and the organic layers were centrifuged to remove residual water and salt. Millipore H_2O (1 mL) was layered over the CD_2Cl_2 solution (1 mL) containing the ligand (and salt, if extracted) and the biphasic mixture was stirred for 12 h to effect back-extraction of the salt into H_2O. Salt concentrations in the aqueous layer were measured by IC. Importantly, stirring the already back-extracted organic layers with Millipore H_2O for an additional 12 h resulted in no further back-extraction, i.e. all salt was removed during the first back-extraction.

Pulsed Field Gradient (PFG) NMR. The necessary hardware set-up and the software protocols for all PFG-NMR experiments were prepared by Dr. Yiu-Fai Lam. Diffusion experiments were recorded on a Bruker Avance400 NMR spectrometer with a 5 mm broad band inverse probe in Shigemi tubes (Shigemi, Inc., Allison Park, PA) at 26 $^{\circ}$C using the pulse sequence developed by Tanner[315] with an added homo-spoil gradient (Bruker pulse sequence "stegp1s, v. 1.1.2.2"). The gradient strength was calibrated using water at 25 $^{\circ}$C and temperature was calibrated with a methanol sample. The pulsed gradients were incremented from 1.7 to 30.0 gauss/cm in 18 steps with a duration (δ) of 2 ms and 32 transients were collected with a pulse delay of 6 s in all cases. The pulsed gradient separation (Δ) was 200 ms for experiments in $CDCl_3$ and 800 ms for experiments in DMSO-d_6. The sample height was maintained at 8 mm to minimize the effects of convection. Measurements of the (cG **2.34**)$_2$•NaCl•(H_2O)$_n$/cA **2.35** mixture in $CDCl_3$ and cG **2.34**/cA **2.35** mixture in DMSO-d_6 were repeated 16 times and 8 times, respectively, and the diffusion coefficients reported are the mean ± standard deviation of all experiments. Sample concentrations were 6.7-6.8 mM in cG **2.34** and cA **2.35**.

According to the Pulsed Gradient Spin Echo technique, the ratio between the echo intensity in the presence (I) and absence (I_o) of a pulsed gradient is given by: $\ln(I/I_o) = -\gamma^2 g^2 \delta^2 (\Delta-\delta/3)D_s$ (**Equation 2.1**), where γ is the gyromagnetic ratio, g is the pulsed gradient strength (gauss/cm), δ and Δ are the duration and separation of the two gradient pulses, respectively, and D_s is the diffusion coefficient.[270] All spectra were processed using XWINNMR 3.0 (Bruker) and data analyses were accomplished using the t1/t2 routine. Diffusion coefficients were obtained by fitting H1' peak volumes to a single exponential decay (**Equation 2.1**) using the program Simfit (Bruker).

Energy Dispersive X-ray (EDX) Analysis. EDX was performed with an AMRAY 1820K scanning electron microscope with an acceleration potential of 20 kV. The sample was prepared by washing a solution of (cG **2.34**)$_2$•(H$_2$O)$_n$ (2 mM in cG **2.34**) in CHCl$_3$ with 1.0 M NaBPh$_{4(aq)}$. The resulting biphasic suspension, containing the (cG **2.34**•Na$^+$)$_n$•(BPh$_4^-$)$_n$ polymer precipitate, was centrifuged and the liquids were drawn off. The solid precipitate was purified by centrifugation with and removal of CHCl$_3$ (3x) and water (3x) followed by drying under high vacuum for 18 h. The data are the average and standard deviation of three runs at different spots on the sample.

Preparation of EYPC HPTS-containing LUVs. Egg yolk L-α-phosphatidyl choline (EYPC, 62.5 mg, 82 μmol) was dissolved in a CHCl$_3$/MeOH mixture, the solution was evaporated under reduced pressure and the resulting thin film was dried under high vacuum for 2.5 h. The lipid film was hydrated in 1.35 mL of phosphate buffer (10 mM Na$_n$H$_{3-n}$PO$_4$, n = 1,2, pH = 6.4, 75-100 mM M$_n$X, M = Na$^+$, K$^+$, Cs$^+$, X = Cl$^-$, SO$_4^{2-}$) containing 10 μM HPTS (pyranine, 8-hydroxypyrene-1,3,6-trisulfonic acid trisodium salt) for 40 min, over which time the suspension was submitted to 5 freeze-thaw cycles. The large multilamellar liposome suspension (1 mL) was submitted to high pressure extrusion at room temperature (21 passes through a 0.1 μm polycarbonate membrane). The suspension of LUVs obtained was separated from extravesicular dye by size exclusion chromatography (SEC) (stationary phase: Sephadex G-10, mobile phase:

phosphate buffer) and diluted by the same phosphate buffer to give a stock solution with the lipid concentration at 11 mM (assuming 100% inclusion).

Preparation of EYPC Calcein-containing LUVs. Calcein (224.1 mg, 0.36 mmol) was suspended in 3 mL of phosphate buffer (10 mM $Na_nH_{3-n}PO_4$, n = 1,2, pH 6.4). The pH of the solution was adjusted to 6.4 by addition of 7.8 M NaOH-containing phosphate buffer, at which point all calcein was dissolved to give a 120 mM solution. The osmolality of the extravesicular buffer was adjusted to equal that of the calcein-containing solution with 2 M NaCl (monitored by VPO). A thin film was prepared from 62.5 mg of EYPC (82 μM) as described in "Preparation of EYPC HPTS-containing LUVs" above. The lipid film was hydrated in 1.35 mL of the120 mM calcein buffer for 40 min, over which time the suspension was submitted to 5 freeze-thaw cycles. The multilamellar liposome suspension (1 mL) was submitted to high-pressure extrusion at room temperature (21 passes through a 0.1 μm polycarbonate membrane). Calcein-containing LUVs were separated from extravesicular dye by SEC (stationary phase: Sephadex G-25, mobile phase: extravesicular isoosmolar NaCl buffer) and diluted with the same NaCl phosphate buffer to give a stock solution with the lipid concentration at 11 mM (assuming 100% inclusion).

Base Pulse Assays. Typically, 100 μL of HPTS-loaded EYPC LUVs (11 mM stock solution) was suspended in 1.90 mL of the corresponding buffer and placed into a fluorimetric cell. The emission of HPTS at 510 nm was monitored with excitation wavelengths at 403 and 460 nm simultaneously. During the experiment, 20 μL of 0 - 10 mM solution of the compound of interest was injected (through an injection port), followed by injection of 21 μL of 0.5 M aqueous NaOH. Addition of the NaOH resulted in a pH increase of unity in the extravesicular buffer. Maximal possible changes in dye emission were obtained at the end of each experiment upon lysis of liposomes by injection of detergent (40 μL of 50 % aqueous Triton X100). The final transport trace was obtained as a ratio of the emission intensities monitored at 460 and 403 nm and normalized to 100% of transport.

Determination of Pseudo-First Order Transport Rate Constants. Pseudo-first order rate constants were assessed as slopes of the plot of $\ln([H^+_{ins}]-[H^+_{out}])$ *versus* time, where $[H^+_{ins}]$ and $[H^+_{out}]$ are the actual intravesicular and extravesicular proton concentrations, respectively. $[H^+_{out}]$ was assumed to remain constant over the course of the experiment, while $[H^+_{ins}]$ values were calculated for each point from HPTS emission intensities according to the calibration equation $pH = 1.1684 \cdot \log(I_0/I_1)+6.9807$ (**Figure 4.1**). The absolute values of rate constants varied depending on the age of the vesicular solution (never exceeding three days) and the actual stock solution of liposomes used. The ratios between absolute values of rate constants obtained within the same time, however, were not altered significantly.
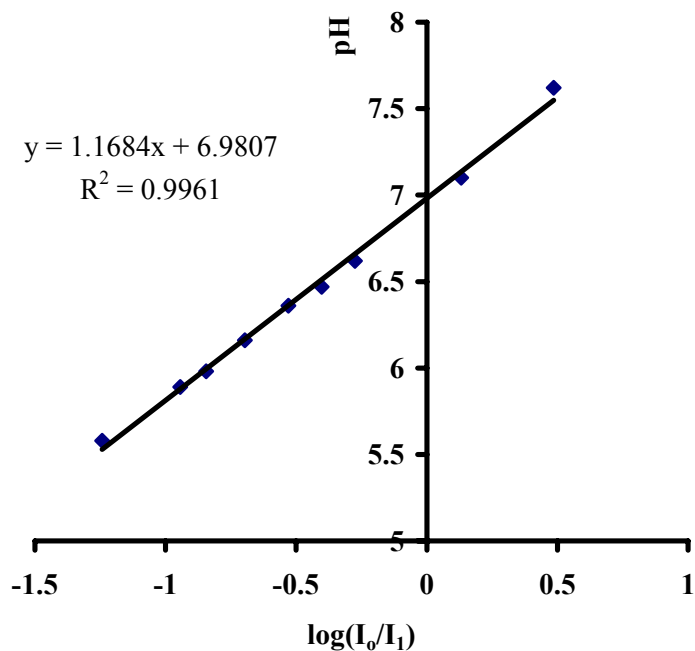
Figure 4.1. Calibration plot relating the HPTS emission intensity to the pH of the solution. Intravesicular pH values were obtained as a function of the ratio of HPTS emission intensities at 510 nm, when excited at 460 and 403 nm. The calibration was performed by measuring the HPTS emission intensities and the pH values of a 470 pM HPTS solution in 10 mM phosphate buffer containing 100 mM NaCl (pH was varied in the range of 5.6 through 7.6 by addition of 0.5 M NaOH or 0.5 M HCl). The calibration equation obtained (pH = $1.1684 \cdot \log(I_o/I_1) + 6.9807$, where I_o is the emission intensity with excitation at 460 nm and I_1 is emission intensity with excitation at 403 nm) was applied to convert the emission intensities into actual pH values.

Calcein Release Assays. Calcein-loaded EYPC LUVs (100 μL of the 11 mM stock solution) were suspended in 1.90 mL of isoosmotic NaCl buffer and submitted to fluorescence analysis. Calcein emission was monitored at 520 nm with excitation at 490 nm. During the experiment, 20 μL of a 500 μM – 10 mM solution of the compound of interest was injected, and the maximal possible changes in dye emission were obtained at the end of each experiment by lysis of liposomes by injection of detergent (40 μL of 50 % aqueous Triton X100).

4.3 Chapter 3 Experimental

4.3.1 Synthesis

Calix[4]arene tetramethylamide 2.30. Prepared as described in **Section 4.2.1**.

Calix[4]arene tetrabutylamide 3.1. 25,26,27,28-tetra-(hydroxycarbonylmethoxy) calix[4]arene 1,3-*alternate* **2.29** (700 mg, 1.07 mmol) was suspended in 30 mL of benzene and $SOCl_2$ (2.0 mL, 27 mmol) was added. The mixture was stirred at reflux for 2.5 h, the solvent was evaporated under reduced pressure and residual $SOCl_2$ was removed by coevaporation with benzene. The acid chloride **2.31** obtained was reacted without further purification. Acid chloride **2.31** was dissolved in 30 mL of CH_2Cl_2, and Et_3N (3.0 mL, 22 mmol) and $BuNH_2$ (3.0 mL, 30 mmol) were added. The reaction mixture was stirred overnight at room temperature, poured into a separatory funnel, washed with H_2O and 0.1 N $HCl_{(aq)}$ and purified by column chromatography (4 % MeOH in CH_2Cl_2) to afford calix[4]arene tetrabutylamide **3.1** (814 mg, 87 %) as a white solid. ^1H NMR (400 MHz, $CDCl_3$): δ 7.00 (d, 8 H, J = 7.5 Hz, Ar-H), 6.73 (t, 4 H, J = 7.5 Hz, Ar-H), 6.26 (t, 4 H, J = 6.2 Hz, C(O)-NH), 4.05 (s, 8 H, Ar-O-CH_2-C(O)), 3.58 (s, 8 H, Ar-CH_2-Ar), 3.41(app q, 8 H, J = 7.0 Hz, NH-CH_2-CH_2-CH_2-CH_3), 1.66 (app p, 8 H, J = 7.5 Hz, NH-CH_2-CH_2-CH_2-CH_3), 1.54 (app h, 8 H, J = 7.5 Hz, NH-CH_2-CH_2-CH_2-CH_3), 1.06 (t, 12 H, J = 7.5 Hz, NH-CH_2-CH_2-CH_2-CH_3); ^{13}C NMR (100 MHz, $CDCl_3$): δ 167.7, 154.2, 133.9, 131.2, 122.1, 70.1, 38.8, 36.2, 32.5, 20.2, 13.8; MS (FAB) $[M+H]^+$ calcd for $C_{52}H_{69}N_4O_8$ 877.5, found 877.5.

Calix[4]arene octabutylamide 3.2. Tetrakis(carboxy-methoxy)-*p*-H-calix[4]arene **2.29** (423 mg, 0.650 mmol) was activated with thionyl chloride as described for compound **3.1**. The acid chloride obtained (**2.31**) was dissolved in 30 mL of CH_2Cl_2, and Et_3N (2.0 mL, 14 mmol) and $BuNH_2$ (3.0 mL, 18 mmol) were added. The reaction mixture was stirred overnight at room temperature, poured into a separatory funnel, washed with H_2O and 0.1 N $HCl_{(aq)}$ and purified by column chromatography (6 % MeOH in CH_2Cl_2) to give **3.2** contaminated with the **3.2**•Na^+ complex. Final purification was achieved by

repeated washing with deionized water to give calix[4]arene octabutylamide **3.2** (443 mg, 62 %) as a white solid. ^{1}H NMR (400 MHz, CDCl$_3$): δ 7.16 (d, 8 H, J = 8.1 Hz, Ar-H), 6.67 (t, 4 H, J = 7.7 Hz, Ar-H), 4.41 (s, 8 H, Ar-O-*CH$_2$*-C(O)), 3.56 (s, 8 H, Ar-*CH$_2$*-Ar), 3.41 (t, 8 H, J = 7.7 Hz, N-(*CH$_2$*-CH$_2$-CH$_2$-CH$_3$)$_2$), 3.23 (t, 8 H, J = 7.7 Hz, N-(*CH$_2$*-CH$_2$-CH$_2$-CH$_3$)$_2$), 1.63-1.52 (m, 16 H, N-(CH$_2$-*CH$_2$*-CH$_2$-CH$_3$)$_2$), 1.40-1.27 (m, 16 H, N-(CH$_2$-CH$_2$-*CH$_2$*-CH$_3$)$_2$), 0.95 (t, 12 H, J = 7.3 Hz, N-(CH$_2$-CH$_2$-CH$_2$-*CH$_3$*)$_2$), 0.92 (t, 12 H, J = 7.3 Hz, N-(CH$_2$-CH$_2$-CH$_2$-*CH$_3$*)$_2$); ^{13}C NMR (100 MHz, CDCl$_3$): δ 167.6, 155.4, 133.3, 129.5, 123.0, 71.7, 47.0, 45.5, 33.6, 31.2, 29.6, 20.2, 20.0, 13.9, 13.7; MS (FAB) [M+H]$^+$ calcd for C$_{68}$H$_{101}$N$_4$O$_8$ 1101.7, found 1101.7.

N-butyl-2-phenoxyacetamide 3.3. Phenoxyacetic acid (2.0 g, 13.2 mmol) was activated with SOCl$_2$ (3.0 mL in 50 mL of benzene, 41 mmol) by the same procedure as described for compound **3.1**. The phenoxyacetyl chloride was reacted without purification. The total amount obtained was dissolved in 30 mL of CH$_2$Cl$_2$ and Et$_3$N (3.0 mL, 22 mmol) and BuNH$_2$ (3.0 mL, 30 mmol) were added. The reaction mixture was stirred overnight at room temperature, the solvent was evaporated under reduced pressure, and the resulting oil was dried under high vacuum. Purification by column chromatography (2 % MeOH in CH$_2$Cl$_2$) afforded *N*-butyl-2-phenoxyacetamide **3.3** (2.43 g, 89 %) as a white crystalline solid. ^{1}H NMR (400 MHz, CDCl$_3$): δ 7.32 (t, 2 H, J = 7.6 Hz, Ar-H), 7.02 (t, 1 H, J = 7.2 Hz, Ar-H), 6.91 (d, 2 H, J = 8.0 Hz, Ar-H), 6.57 (br s, 1 H, C(O)-NH), 4.48 (s, 2 H, Ar-O-*CH$_2$*-C(O)), 3.34 (q, 2 H, J = 6.8 Hz, NH-*CH$_2$*-CH$_2$-CH$_2$-CH$_3$), 1.50 (p, 2 H, J = 7.2 Hz, NH-CH$_2$-*CH$_2$*-CH$_2$-CH$_3$), 1.33 (h, 2 H, J = 7.2 Hz, NH-CH$_2$-CH$_2$-*CH$_2$*-CH$_3$), 0.91 (t, 3 H, J = 7.2 Hz, NH-CH$_2$-CH$_2$-CH$_2$-*CH$_3$*); ^{13}C NMR (100 MHz, CDCl$_3$): δ 168.0, 157.1, 129.7, 122.0, 114.5, 67.3, 38.6, 31.5, 19.9, 13.6.; MS (FAB) [M]$^+$ calcd for C$_{12}$H$_{17}$NO$_2$ 207.1, found 207.3.

Bis-(ethyl phenoxyacetate) 3.14. Diphenol **3.9** (382 mg, 1.91mmol),[314] ethyl bromoacetate (0.87 g, 5.2 mmol) and Cs$_2$CO$_3$ (1.24 g, 3.82 mmol) were suspended in 50 mL of acetone and stirred at reflux overnight. The reaction mixture was cooled to room temperature and the solvent was evaporated under reduced pressure. The residual solid

was taken into $CHCl_3$, the organic layer was washed with H_2O and 0.1 N $HCl_{(aq)}$, separated, and the solvent was removed under reduced pressure. Purification by column chromatography (CH_2Cl_2) afforded bis-(ethyl phenoxyacetate) **3.14** (537 mg, 75 %). ^{1}H NMR (400 MHz, DMSO-d$_6$): δ 7.15-7.10 (m, 4 H, Ar-H), 6.86-6.83 (m, 4 H, Ar-H), 4.78 (s, 4 H, Ar-O-*CH$_2$*-CO), 4.17 (q, 4 H, J = 7.1 Hz, Ar-O-CH$_2$-CO-*CH$_2$*-CH$_3$), 3.96 (s, 2 H, Ar-*CH$_2$*-Ar), 1.21 (t, 6H, J = 7.1 Hz, Ar-O-CH$_2$-CO-CH$_2$-*CH$_3$*); ^{13}C NMR (100 MHz, DMSO-d$_6$): δ 169.3, 155.9, 130.8, 129.1, 127.6, 121.4, 112.0, 65.4, 61.0, 29.6, 14.5; MS (FAB) [M+H]$^+$ calcd for $C_{21}H_{25}O_6$ 373.2, found 373.1.

Diphenoxyacetic acid 3.19. Bis-(ethyl phenoxyacetate) **3.14** (476 mg, 1.28 mmol) was dissolved in 3 mL MeOH and 5 mL THF and 1 mL of 45 wt % $KOH_{(aq)}$ was added dropwise. The reaction mixture was stirred overnight at room temperature, evaporated to dryness, dissolved in 10 mL of water and acidified to pH 1 with 6 N HCl. The precipitate formed was collected by filtration and washed with water. The aqueous layer was extracted with chloroform (4x), the organic layer separated and the solvent removed under reduced pressure. The solid formed was recombined with the filtrate and dried for 3 h under high vacuum to give diphenoxyacetic acid **3.19** (434 mg, 100 %). ^{1}H NMR (400 MHz, DMSO-d$_6$): δ 7.12-7.06 (m, 4 H, Ar-H), 6.82-6.78 (m, 4 H, Ar-H), 4.56 (s, 4 H, Ar-O-*CH$_2$*-CO), 3.95 (s, 2 H, Ar-*CH$_2$*-Ar); ^{13}C NMR (100 MHz, DMSO-d$_6$): δ 170.8, 156.4, 130.7, 129.2, 127.4, 120.9, 112.1, 66.1, 29.5; MS (FAB) [M+H]$^+$ calcd for $C_{17}H_{17}O_6$ 317.1, found 317.1.

Bis-(*N*-butyl-2-phenoxyacetamide) 3.4. Diphenoxyacetic acid **3.19** (418 mg, 1.32 mmol) was suspended in benzene (25 mL), and $SOCl_2$ (2.0 mL, 27 mmol) was added. The reaction mixture was stirred at reflux for 2.5 hours. Over the course of the reaction, the turbid suspension changed into a yellow transparent solution. The reaction mixture was cooled to room temperature, the solvent and excess $SOCl_2$ was removed under reduced pressure, and the remaining traces $SOCl_2$ were removed by co-evaporation with benzene. Diphenoxyacetyl chloride was reacted without further purification. The total amount obtained was dissolved in 25 mL of CH_2Cl_2 and Et$_3$N (556 µL, 4.0 mmol) and

BuNH$_2$ (650 μL, 6.6 mmol) were added. The reaction mixture was stirred overnight at room temperature, the solvent was removed under reduced pressure, and the resulting oil was dried under high vacuum. The oil was dissolved in CHCl$_3$ and the organic layer was washed with H$_2$O, separated, dried over sodium sulfate, and the solvent removed under reduced pressure. Purification by column chromatography (1 % MeOH in CH$_2$Cl$_2$) afforded bis-(N-butyl-2-phenoxyacetamide) **3.4** (448 mg, 80 %) as a white solid. ^{1}H NMR (400 MHz, DMSO-d$_6$): δ 7.62 (t, 2 H, J = 6.0 Hz, C(O)-NH), 7.16 (dt, 2 H, J = 1.6 Hz, 7.8 Hz, Ar-H), 7.03 (dd, 2 H, J = 1.2 Hz, 7.6 Hz, Ar-H), 6.90-6.85 (m, 4 H, Ar-H), 4.45 (s, 4 H, Ar-O-*CH$_2$*-C(O)), 4.04 (s, 2 H, Ar-*CH$_2$*-Ar), 3.08 (app q, 4 H, J = 6.8 Hz, NH-*CH$_2$*-CH$_2$-CH$_2$-CH$_3$), 1.35 (p, 4 H, J = 7.2 Hz, NH-CH$_2$-*CH$_2$*-CH$_2$-CH$_3$), 1.21 (h, 4 H, J = 7.2 Hz, NH-CH$_2$-CH$_2$-*CH$_2$*-CH$_3$), 0.83 (t, 6 H, J = 7.2 Hz, NH-CH$_2$-CH$_2$-CH$_2$-*CH$_3$*); ^{13}C NMR (100 MHz, DMSO-d$_6$): δ 167.8, 156.0, 130.6, 129.2, 127.7, 121.5, 112.3, 67.7, 38.4, 31.6, 30.0, 19.9, 14.1; MS (FAB) [M+H]$^+$ calcd for C$_{25}$H$_{35}$N$_2$O$_4$ 426.3, found 427.3.

Tris-(ethyl phenoxyacetate) 3.15. Triphenol **3.10** (53 mg, 0.17mmol),[314] ethyl bromoacetate (117 mg, 0.70 mmol) and Cs$_2$CO$_3$ (166 mg, 0.51 mmol) were suspended in 25 mL of acetone, and stirred at reflux overnight. The reaction mixture was cooled to room temperature and the solvent was evaporated under reduced pressure. The residual solid was taken into CHCl$_3$, the organic layer was washed with H$_2$O and 0.1 N HCl$_{(aq)}$, separated, and the solvent was removed under reduced pressure. Purification by column chromatography (CH$_2$Cl$_2$) afforded tris-(ethyl phenoxyacetate) **3.15** (68 mg, 83 %). ^{1}H NMR (400 MHz, CDCl$_3$): δ 7.15-6.72 (m, 11 H, Ar-H), 4.60 (s, 4 H, Ar-O-*CH$_2$*-C(O)), 4.39 (s, 2 H, Ar-O-*CH$_2$*-C(O)), 4.25-4.18 (m, 6 H, C(O)-*CH$_2$*-CH$_3$), 4.12 (s, 4 H, Ar-*CH$_2$*-Ar), 1.25 (app t, 9 H, J = 7.2 Hz, C(O)-CH$_2$-*CH$_3$*); ^{13}C NMR (100 MHz, CDCl$_3$): δ 169.1, 169.0, 155.9, 155.0, 133.6, 131.0, 129.7, 129.0, 127.3, 124.5, 121.6, 111.4, 70.1, 65.7, 61.2, 61.0, 29.7, 14.1; MS (FAB) [M+H]$^+$ calcd for C$_{32}$H$_{37}$O$_9$ 565.2, found 565.2.

Triphenoxyacetic acid 3.20. Tris-(ethyl phenoxyacetate) **3.15** (59 mg, 0.104 mmol) was dissolved in 3 mL MeOH and 5 mL THF and 1 mL of 45 wt % KOH$_{(aq)}$ was added dropwise. The reaction mixture was stirred overnight at room temperature, evaporated to

dryness, dissolved in 2 mL of water and acidified to pH 1 with 6 N HCl. The precipitate formed was collected by filtration and washed with water. The aqueous layer was extracted with chloroform (4x), the organic layer separated and the solvent removed under reduced pressure. The solid formed was recombined with the filtrate and dried for 6 h under high vacuum to give triphenoxyacetic acid **3.20** (57 mg, 100 %). ^{1}H NMR (400 MHz, acetone-d$_6$): δ 7.2-6.85 (m, 11 H, Ar-H), 4.70 (s, 4 H, Ar-O-*CH$_2$*-C(O)), 4.49 (s, 2 H, Ar-O-*CH$_2$*-C(O)), 4.13 (s, 4 H, Ar-*CH$_2$*-Ar); ^{13}C NMR (100 MHz, acetone-d$_6$): δ 170.4, 156.8, 155.8, 134.7, 131.5, 130.4, 129.7, 128.1, 125.1, 122.0, 117.7, 112.5, 70.4, 65.6, 30.1.

Tris-(*N*-butyl-2-phenoxyacetamide) 3.5. Triphenoxyacetic acid **3.20** (48 mg, 0.10 mmol) was activated with SOCl$_2$ (1.0 mL in 3 mL of benzene, 14 mmol) by the same procedure as described for compound **3.4**. The triphenoxyacetyl chloride was reacted without purification. The total amount obtained was dissolved in 10 mL of CH$_2$Cl$_2$, and Et$_3$N (125 μL, 0.90 mmol) and BuNH$_2$ (150 μL, 1.5 mmol) were added. The reaction mixture was stirred overnight at room temperature, the solvent was removed under reduced pressure, and the resulting oil was dried under high vacuum. The oil was dissolved in CHCl$_3$ and the organic layer was washed with H$_2$O, separated, dried over sodium sulfate, and the solvent removed under reduced pressure. Purification by column chromatography (2 % MeOH in CH$_2$Cl$_2$) afforded tris-(*N*-butyl-2-phenoxyacetamide) **3.5** (51 mg, 79 %) as a white crystalline solid. ^{1}H NMR (400 MHz, DMSO-d$_6$): δ 7.99 (t, 1 H, J = 5.6 Hz, C(O)-NH), 7.66 (t, 2 H, J = 5.6 Hz, C(O)- NH), 7.18 (dt, 2 H, J = 8.0, 1.6 Hz, Ar-H), 7.04 (dd, 2 H, J = 8.0, 1.6 Hz, Ar-H), 6.96-6.87 (m, 7 H, Ar-H), 4.43 (s, 4 H, Ar-O-*CH$_2$*-C(O)), 4.19 (s, 2 H, Ar-O-*CH$_2$*-C(O)), 4.06 (s, 4 H, Ar-*CH$_2$*-Ar), 3.13-3.05 (m, 6 H, NH-*CH$_2$*-CH$_2$-CH$_2$-CH$_3$), 1.43-1.31 (m, 6 H, NH-CH$_2$-*CH$_2$*-CH$_2$-CH$_3$), 1.28-1.16 (m, 6 H, NH-CH$_2$-CH$_2$-*CH$_2$*-CH$_3$), 0.82 (app t, 9 H, J = 7.6 Hz, NH-CH$_2$-CH$_2$-CH$_2$-*CH$_3$*); ^{13}C NMR (100 MHz, DMSO-d$_6$): δ 167.3, 155.4, 154.4, 133.4, 130.3, 128.8, 128.5, 127.5, 124.3, 121.0, 111.8, 38.0, 31.2, 29.3, 19.5, 13.6; MS (FAB) [M+H]$^+$ calcd for C$_{38}$H$_{52}$N$_3$O$_6$ 646.4, found 646.4.

Tetrakis-(ethyl phenoxyacetate) 3.16. Tetraphenol **3.11** (571 mg, 1.38 mmol),[314] ethyl bromoacetate (1.38 g, 8.30 mmol) and Cs_2CO_3 (1.80 g, 5.50 mmol) were suspended in 25 mL of acetone and stirred at reflux overnight. The reaction mixture was cooled to room temperature and the solvent was evaporated under reduced pressure. The residual solid was taken into $CHCl_3$, the organic layer was washed with H_2O and 0.1 N $HCl_{(aq)}$, separated, and the solvent was evaporated under reduced pressure. Purification by column chromatography (1:2 EtOAc:hexanes) afforded tetrakis-(ethyl phenoxyacetate) **3.16** (800 mg, 77 %). ^{1}H NMR (400 MHz, DMSO-d_6): δ 7.16 (dt, 2 H, J = 8.0, 1.6 Hz, Ar-H), 7.06 (dd, 2 H, J = 8.0, 1.6 Hz, Ar-H), 6.97-6.83 (m, 10 H, Ar-H), 4.77 (s, 4H, Ar-O-*CH₂*-C(O)), 4.43 (s, 4 H, Ar-O-*CH₂*-C(O)), 4.17-4.08 (m, 8 H, C(O)-*CH₂*-CH₃), 4.05 (s, 2H, Ar-*CH₂*-Ar), 4.00 (s, 4 H, Ar-*CH₂*-Ar), 1.20-1.14 (m, 12 H, C(O)-CH₂-*CH₃*); ^{13}C NMR (100 MHz, DMSO-d_6): δ 169.2, 169.0, 155.8, 155.1, 134.0, 130.9, 129.2, 129.0, 127.9, 124.4, 121.5, 112.2, 70.1, 65.3, 61.0, 61.0, 29.5, 14.4, 14.4; MS (FAB) [M+H]$^+$ calcd for $C_{43}H_{49}O_{12}$ 757.3, found 757.2.

Tetraphenoxyacetic acid 3.21. Tetrakis-(ethyl phenoxyacetate) **3.16** (765 mg, 1.01 mmol) was dissolved in 3 mL MeOH and 5 mL THF and 1 mL of 45 wt % $KOH_{(aq)}$ was added dropwise. The reaction mixture was stirred overnight at room temperature, evaporated to dryness, dissolved in 10 mL of water and acidified to pH 1 with 6 N HCl. The precipitate formed was collected by filtration and washed with water. The aqueous layer was extracted with chloroform (4x), the organic layer separated and the solvent removed under reduced pressure. The solid formed was recombined with the filtrate and dried for 4 h under high vacuum to give tetraphenoxyacetic acid **3.21** (677 mg, 100 %). ^{1}H NMR (400 MHz, DMSO-d_6): δ 13.80 (s, 4 H, C(O)-OH), 7.55 (dt, 2 H, J = 7.8, 1.6 Hz, Ar-H), 7.44 (dd, 2 H, J = 7.8, 1.6 Hz, Ar-H), 7.32-7.17 (m, 10 H, Ar-H), 4.86 (s, 4 H, Ar-O-*CH₂*-C(O)), 4.51 (s, 4 H, Ar-O-*CH₂*-C(O)), 4.20 (s, 2 H, Ar-*CH₂*-Ar), 4.13 (s, 4 H, Ar-*CH₂*-Ar); ^{13}C NMR (100 MHz, DMSO-d_6): δ 170.3, 170.1, 155.6, 154.8, 133.6, 130.4, 128.8, 128.6, 127.4, 124.4, 120.9, 111.7, 69.7, 64.8, 29.1, 29.0; MS (FAB) [M+H]$^+$ calcd for $C_{35}H_{33}O_{12}$ 645.2, found 645.0.

Tetrakis-(*N*-butyl-2-phenoxyacetamide) 3.6. Tetraphenoxyacetic acid **3.21** (649 mg, 1.05 mmol) was activated with $SOCl_2$ (5.0 mL in 15 mL of benzene, 69 mmol) by the same procedure as described for compound **3.4**. The tetraphenoxyacetyl chloride was reacted without purification. The total amount obtained was dissolved in 25 mL of CH_2Cl_2 and Et_3N (3.4 mL, 24 mmol) and $BuNH_2$ (4.1 mL, 41 mmol) were added. The reaction mixture was stirred overnight at room temperature, the solvent was removed under reduced pressure, and the resulting oil was dried under high vacuum. The oil was dissolved in $CHCl_3$ and the organic layer was washed with H_2O, separated, dried over sodium sulfate, and the solvent removed under reduced pressure. Purification by column chromatography (2 % MeOH in CH_2Cl_2) afforded tetrakis-(*N*-butyl-2-phenoxyacetamide) **3.6** (577 mg, 64 %) as an off-white solid. ^{1}H NMR (400 MHz, DMSO-d_6): δ 7.98 (t, 2 H, J = 5.8 Hz, C(O)-NH), 7.68 (t, 2 H, J = 5.8 Hz, C(O)-NH), 7.18 (dt, 2 H, J = 7.6, 1.2 Hz, Ar-H), 7.03 (dd, 2 H, J = 7.6, 1.2 Hz, Ar-H), 6.98-6.84 (m, 10 H, Ar-H), 4.43 (s, 4 H, Ar-O-*CH$_2$*-C(O)), 4.14 (s, 4 H, Ar-O-*CH$_2$*-C(O)), 4.08 (s, 2 H, Ar-*CH$_2$*-Ar), 4.05 (s, 4 H, Ar-*CH$_2$*-Ar), 3.12-3.05 (m, 8 H, NH-*CH$_2$*-CH$_2$-CH$_2$-CH$_3$), 1.39-1.33 (m, 8 H, NH-CH$_2$-*CH$_2$*-CH$_2$-CH$_3$), 1.25-1.17 (m, 8 H, NH-CH$_2$-CH$_2$-*CH$_2$*-CH$_3$), 0.82 (t, 12 H, J = 7.4 Hz, NH-CH$_2$-CH$_2$-CH$_2$-*CH$_3$*); ^{13}C NMR (100 MHz, DMSO-d_6): δ 167.3, 155.4, 154.4, 133.5, 133.4, 130.2, 128.7, 127.5, 124.4, 121.1, 111.8, 71.8, 67.1, 37.9, 31.2, 31.1, 29.3, 19.5, 19.5, 13.6; MS (FAB) [M+H]$^+$ calcd for $C_{51}H_{69}N_4O_8$ 865.5, found 865.4.

Pentakis-(ethyl phenoxyacetate) 3.17. Pentaphenol **3.12** (508 mg, 0.98 mmol),[314] ethyl bromoacetate (1.23 g, 7.40 mmol) and Cs_2CO_3 (1.6 g, 4.9 mmol) were suspended in 25 mL of acetone, and stirred at reflux overnight. The reaction mixture was cooled to room temperature and the solvent was evaporated under reduced pressure. The residual solid was taken into $CHCl_3$, the organic layer was washed with H_2O and 0.1 N $HCl_{(aq)}$, separated, and the solvent was evaporated under reduced pressure. Purification by column chromatography (1:2 EtOAc:hexanes) afforded pentakis-(ethyl phenoxyacetate) **3.17 (**540 mg, 58 %). ^{1}H NMR (400 MHz, DMSO-d_6): δ 7.16 (dt, 2 H, J = 7.8, 1.6 Hz, Ar-H), 7.06 (dd, 2 H, J = 7.8, 1.6 Hz, Ar-H), 7.00-6.82 (m, 13 H, Ar-H), 4.77 (s, 4 H, Ar-O-*CH$_2$*-C(O)), 4.43 (s, 4 H, Ar-O-*CH$_2$*-C(O)), 4.40 (s, 2 H, Ar-O-*CH$_2$*-C(O)), 4.17-4.08

(m, 10 H, C(O)-*CH$_2$*-CH$_3$), 4.06 (s, 4 H, Ar-*CH$_2$*-Ar), 4.01 (s, 4 H, Ar-*CH$_2$*-Ar), 1.20-1.13 (m, 15 H, C(O)-CH$_2$-*CH$_3$*); ^{13}C NMR (100 MHz, DMSO-d$_6$): δ 169.2, 169.0, 155.8, 155.3, 155.1, 155.1, 134.0, 134.0, 133.9, 130.9, 129.2, 129.0, 127.9, 125.0, 124.9, 121.5, 112.2, 70.1, 65.3, 61.0, 61.0, 29.7, 29.5, 14.4, 14.4; MS (FAB) [M+H]$^+$ calcd for C$_{54}$H$_{61}$O$_{15}$ 949.4, found 949.1.

Pentaphenoxyacetic acid 3.22. Pentakis-(ethyl phenoxyacetate) **3.17** (515 mg, 0.54 mmol) was dissolved in 3 mL MeOH and 5 mL THF and 1 mL of 45 wt % KOH$_{(aq)}$ was added dropwise. The reaction mixture was stirred overnight at room temperature, evaporated to dryness, dissolved in 10 mL of water and acidified to pH 1 with 6 N HCl. The acidic aqueous solution was evaporated to dryness by co-evaporation with acetone. The solid residue was triturated with acetone, the precipitate removed by filtration, and the filtrate was evaporated to dryness to give pentaphenoxyacetic acid **3.22** (509 mg, 100 %) as a white solid. ^{1}H NMR (400 MHz, DMSO-d$_6$): δ 12.92 (s, 5 H, C(O)-OH), 7.16 (dt, 2 H, J = 7.8, 1.6 Hz, Ar-H), 7.07 (dd, 2 H, J = 7.8, 1.6 Hz, Ar-H), 6.96-6.80 (m, 13 H, Ar-H), 4.67 (s, 4 H, Ar-O-*CH$_2$*-C(O)), 4.36 (s, 4 H, Ar-O-*CH$_2$*-C(O)), 4.34 (s, 2 H, Ar-O-*CH$_2$*-C(O)), 4.08 (s, 4 H, Ar-*CH$_2$*-Ar), 4.01 (s, 4 H, Ar-*CH$_2$*-Ar); MS (FAB) [M+H]$^+$ calcd for C$_{44}$H$_{41}$O$_{15}$ 809.2, found 809.0.

Pentakis-(*N*-butyl-2-phenoxyacetamide) 3.7. Pentaphenoxyacetic acid **3.22** (515 mg, 0.64 mmol) was activated with SOCl$_2$ (3.0 mL in 10 mL of benzene, 41 mmol) by the same procedure as described for compound **3.4**. The pentaphenoxyacetyl chloride was reacted without purification. The total amount obtained was dissolved in 25 mL of CH$_2$Cl$_2$ and Et$_3$N (3.0 mL, 22 mmol) and BuNH$_2$ (3.0 mL, 30 mmol) were added. The reaction mixture was stirred overnight at room temperature, the solvent was removed under reduced pressure, and the resulting oil was dried under high vacuum. The oil was dissolved in CHCl$_3$ and the organic layer was washed with H$_2$O, separated, dried over sodium sulfate, and the solvent removed under reduced pressure. Purification by column chromatography (3 % MeOH in CH$_2$Cl$_2$) afforded pentakis-(*N*-butyl-2-phenoxyacetamide) **3.7** (480 mg, 69 %) as a yellowish solid. ^{1}H NMR (400 MHz,

235

DMSO-d$_6$): δ 7.97-7.95 (m, 3 H, C(O)-NH), 7.66 (t, 2 H, J = 5.6 Hz, C(O)-NH), 7.18 (app t, 2 H, J = 7.8 Hz, Ar-H), 7.03 (app d, 2 H, J = 7.2 Hz, Ar-H), 6.99-6.84 (m, 13 H, Ar-H), 4.43 (s, 4 H, Ar-O-*CH$_2$*-C(O)), 4.14 (s, 4 H, Ar-O-*CH$_2$*-C(O)), 4.11 (s, 2 H, Ar-O-*CH$_2$*-C(O)), 4.08 (s, 4 H, Ar-*CH$_2$*-Ar), 4.05 (s, 4 H, Ar-*CH$_2$*-Ar), 3.12-3.05 (m, 10 H, NH-*CH$_2$*-CH$_2$-CH$_2$-CH$_3$), 1.41-1.31 (m, 10 H, NH-CH$_2$-*CH$_2$*-CH$_2$-CH$_3$), 1.27-1.17 (m, 10 H, NH-CH$_2$-CH$_2$-*CH$_2$*-CH$_3$), 0.83-0.80 (m, 15 H, NH-CH$_2$-CH$_2$-CH$_2$-*CH$_3$*); ^{13}C NMR (100 MHz, DMSO-d$_6$): δ 167.8, 167.8, 167.7, 155.9, 154.9, 154.8, 134.0, 133.9, 133.9, 130.7, 129.3, 129.2, 129.2, 129.0, 128.0, 124.9, 121.5, 112.3, 72.2, 72.1, 67.6, 31.6, 31.6, 29.7, 29.5, 19.9, 19.9, 14.1; MS (FAB) [M+H]$^+$ calcd for C$_{64}$H$_{86}$N$_5$O$_{10}$ 1084.6, found 1084.3.

Hexakis-(ethyl phenoxyacetate) 3.18. Hexaphenol **3.13** (253 mg, 0.41 mmol),[314] ethyl bromoacetate (0.616 g, 3.70 mmol) and Cs$_2$CO$_3$ (0.802 g, 2.50 mmol) were suspended in 40 mL of acetone, and stirred at reflux overnight. The reaction mixture was cooled to room temperature and the solvent was evaporated under reduced pressure. The residual solid was taken into CHCl$_3$, the organic layer was washed with H$_2$O and 0.1 N HCl$_{(aq)}$, separated, and the solvent was evaporated under reduced pressure. Purification by column chromatography (1:2 EtOAc:hexanes) afforded hexakis-(ethyl phenoxyacetate) **3.18** (211 mg, 46 %). ^{1}H NMR (400 MHz, CDCl$_3$): δ 7.15 (dt, 2 H, J = 7.9, 1.6 Hz, Ar-H), 7.08 (dd, 2 H, J = 7.9, 1.6 Hz, Ar-H), 6.98-6.84 (m, 16 H, Ar-H), 4.6 (s, 4 H, Ar-O-*CH$_2$*-C(O)), 4.37 (s, 4 H, Ar-O-*CH$_2$*-C(O)), 4.34 (s, 4 H, Ar-O-*CH$_2$*-C(O)), 4.24-4.07 (m, 22 H, C(O)-*CH$_2$*-CH$_3$ and Ar-*CH$_2$*-Ar), 1.27-1.13 (m, 18 H, C(O)-CH$_2$-*CH$_3$*); MS (FAB) [M+Na]$^+$ calcd for C$_{65}$H$_{72}$O$_{18}$Na 1163.5, found 1163.0.

Hexaphenoxyacetic acid 3.23. Hexakis-(ethyl phenoxyacetate) **3.18** (202 mg, 0.18 mmol) was dissolved in 3 mL MeOH and 5 mL THF and 1 mL of 45 wt % KOH$_{(aq)}$ was added dropwise. The reaction mixture was stirred overnight at room temperature under nitrogen, evaporated to dryness, dissolved in 5 mL of water and acidified to pH 1 with 6 N HCl. The acidic aqueous solution was evaporated to dryness by co-evaporation with acetone. The solid residue was triturated with acetone, the precipitate removed by filtration, and the filtrate was evaporated to dryness to give hexaphenoxyacetic acid **3.23**

(201 mg, 100 %). ^{1}H NMR (400 MHz, DMSO-d$_6$): δ 12.86 (s, 6 H, C(O)-OH), 7.13 (dt, 2 H, J = 7.9, 1.6 Hz, Ar-H), 7.03 (dd, 2 H, J = 7.9, 1.6 Hz, Ar-H), 6.96-6.79 (m, 16 H, Ar-H), 4.65 (s, 4 H, Ar-O-*CH$_2$*-C(O)), 4.33 (s, 4 H, Ar-O-*CH$_2$*-C(O)), 4.32 (s, 4 H, Ar-O-*CH$_2$*-C(O)), 4.06 (br s, 6 H, Ar-*CH$_2$*-Ar), 3.98 (s, 4 H, Ar-*CH$_2$*-Ar).

Hexakis-(*N*-butyl-2-phenoxyacetamide) 3.8. Hexaphenoxyacetic acid **3.23** (201 mg, 0.20 mmol) was activated with SOCl$_2$ (1.9 mL in 10 mL of benzene, 26 mmol) by the same procedure as described for compound **3.4**. The hexaphenoxyacetyl chloride was reacted without purification. The total amount obtained was dissolved in 10 mL of CH$_2$Cl$_2$ and Et$_3$N (0.5 mL, 3.6 mmol) and BuNH$_2$ (0.5 mL, 5.5 mmol) were added. The reaction mixture was stirred overnight at room temperature, the solvent was removed under reduced pressure, and the resulting oil was dried under high vacuum. The oil was dissolved in CHCl$_3$ and the organic layer was washed with H$_2$O, separated, dried over sodium sulfate, and the solvent removed under reduced pressure. Purification by column chromatography (3 % MeOH in CH$_2$Cl$_2$) afforded hexakis-(*N*-butyl-2-phenoxyacetamide) **3.8** (160 mg, 60 %) as an orangish solid. ^{1}H NMR (400 MHz, DMSO-d$_6$): δ 7.97-7.93 (m, 4 H, C(O)-NH), 7.65 (t, 2 H, J = 6.0 Hz, C(O)-NH), 7.16 (dt, 2 H, J = 7.9, 1.6 Hz, Ar-H), 7.03 (dd, 2 H, J = 7.9, 1.6 Hz, Ar-H), 7.00-6.84 (m, 16 H, Ar-H), 4.43 (s, 4 H, Ar-O-*CH$_2$*-C(O)), 4.13 (s, 4 H, Ar-O-*CH$_2$*-C(O)), 4.10 (s, 4 H, Ar-O-*CH$_2$*-C(O)), 4.07 (s, 6 H, Ar-*CH$_2$*-Ar), 4.04 (s, 4 H, Ar-*CH$_2$*-Ar), 3.12-3.04 (m, 12 H, NH-*CH$_2$*-CH$_2$-CH$_2$-CH$_3$), 1.41-1.31 (m, 12 H, NH-CH$_2$-*CH$_2$*-CH$_2$-CH$_3$), 1.27-1.17 (m, 12 H, NH-CH$_2$-CH$_2$-*CH$_2$*-CH$_3$), 0.83-0.79 (m, 18 H, NH-CH$_2$-CH$_2$-CH$_2$-*CH$_3$*); ^{13}C NMR (100 MHz, DMSO-d$_6$): δ 167.3, 167.2, 155.4, 154.4, 133.5, 133.4, 130.2, 128.8, 128.7, 128.6, 127.5, 124.5, 124.4, 121.0, 111.8, 71.8, 71.7, 67.1, 37.9, 31.1, 29.3, 29.1, 19.5, 19.4, 13.6; MS (FAB) [M+H]$^+$ calcd for C$_{77}$H$_{103}$N$_6$O$_{12}$ 1303.8, found 1303.4.

4.3.2 Experimental Details

2.30•HCl Crystals. Crystal structures were solved by Dr. James C. Fettinger. (A) Calix[4]arene tetramethylamide **2.30** (15 mg) was dissolved in 1.5 mL of a THF:12 M HCl mixture (95:5). The solution was slowly evaporated to give an oily precipitate that was then redissolved in 2 mL of CH_2Cl_2. Slow evaporation afforded crystals of the **2.30**•HCl•3(H_2O) complex. (B) Calix[4]arene tetramethylamide **2.30** (15 mg) was dissolved in 2 mL of CH_2Cl_2, and 1 mL of 6 M aqueous HCl was layered over the organic solution. Immediate formation of a white emulsion in the organic layer occurred. Crystals of **2.30**•HCl•H_2O•CH_2Cl_2 formed at the aqueous-organic interface after several days. **Table 4.1** shows crystal data and structure refinement parameters for the two crystal structures. For detailed crystallographic data, see structure reports for UM747 (**2.30**•HCl•3(H_2O)) and UM753 (**2.30**•HCl•H_2O•CH_2Cl_2) at the Department of Chemistry and Biochemistry, University of Maryland, College Park, MD 20742.

Table 4.1. Crystal data and structure refinement for **2.30**•HCl•3(H_2O) and **2.30**•HCl•H_2O•CH_2Cl_2 complexes.

	2.30•HCl•3(H₂O)	**2.30•HCl•H₂O•CH₂Cl₂**
empirical formula	$C_{40}H_{50}ClN_4O_{11}$	$C_{41}H_{48}Cl_3N_4O_9$
formula weight	798.29	847.18
temperature	193(2) K	193(2) K
crystal system	orthorhombic	monoclinic
space group	*Fddd*	P2(1)/*n*
unit cell dimensions	a = 20.9026(7) Å, α= 90°	a = 10.1237(3) Å, α= 90°
	b = 26.5756(9) Å, β= 90°	b = 22.7400(7) Å, β= 97.07°
	c = 27.7713(10) Å, γ = 90°	c = 17.7902(6) Å, γ = 90°
volume	15426.9(9) Å^3	4064.4(2) Å^3
Z	16	4
density (calculated)	1.375 Mg/ m^3	1.384 Mg/m^3
absorption coefficient	0.166 mm^{-1}	0.286 mm^{-1}
data/restraints/parameters	3404 / 3 / 326	7147 / 0 / 723
goodness-of-fit on F_2	1.060	1.092
final *R* indices [$I > 2\sigma(I)$]	R1 = 0.0617, wR2 = 0.1785	R1 = 0.0431, wR2 = 0.1117
R indices (all data)	R1 = 0.0851, wR2 = 0.1958	R1 = 0.0570, wR2 = 0.1196

EYPC HPTS-Containing LUVs. Prepared as described in **Section 4.2.2**.

EYPC Calcein-Containing LUVs. Prepared as described in **Section 4.2.2**.

Unequally-loaded vesicular suspensions (intra- and extravesicular buffers are different). The osmolality of the extravesicular buffer was adjusted by addition of a 1 M solution of the appropriate salt in the phosphate buffer (monitored by VPO). The pH of the extravesicular buffer was adjusted to that of the intravesicular buffer by addition of 1 M HCl or 1 M NaOH solution (monitored by a pH-meter).

Base Pulse Assays. Conducted as described in **Section 4.2.2**.

Calcein-release assay. Conducted as described in **Section 4.2.2**.

Analysis of pH changes in liposomes experiencing a Cl⁻ gradient. (A) Outwardly directed gradient of Cl⁻: HPTS-loaded vesicles (100 μL of the 11 mM stock solution), filled with a saline phosphate buffer (10 mM sodium phosphate, pH 6.4, 100 mM NaCl) were suspended in 1.90 mL of an isoosmotic sulfate phosphate buffer (10 mM sodium phosphate, pH 6.4, 75 mM Na_2SO_4) and placed into a fluorimetric cell. The fluorimetric assays were conducted as described under "Base Pulse Assays" in **Section 4.2.2**, with the exception that no base pulse (0.5 NaOH) was added in these experiments. Intravesicular pH values were obtained as a function of the ratio of HPTS emission intensities using the calibration equation pH = $1.1684 \cdot \log(I_o/I_1) + 6.9807$, where I_o is the emission intensity with excitation at 460 nm and I_1 is emission intensity with excitation at 403 nm, as described in **Section 4.2.2** and shown in **Figure 4.1**. (B) Inwardly directed gradient of Cl⁻: HPTS-loaded vesicles (100 μL of the stock solution), filled with a sulfate phosphate buffer (10 mM sodium phosphate, pH 6.4, ~75 mM Na_2SO_4) were suspended in 1.90 mL of an isoosmotic saline phosphate buffer (10 mM sodium phosphate, pH 6.4, 100 mM NaCl) and placed into a fluorimetric cell. Further analysis was conducted as described for the case of an outwardly directed gradient of Cl⁻.

Voltage clamp experiments. Voltage clamp experiments and data analyses were done by Robert Mizani in the laboratory of Professor Marco Colombini. Bilayer membranes were made from monolayers of diphytanoylphospatidyl choline (DPhPC) by the method of Montal and Mueller.[316] Recordings were made under voltage clamp conditions using calomel electrodes with saturated KCl bridges. Solutions consisted of 1 M KCl, 1 mM $MgCl_2$, 5 mM HEPES, pH 7.0. The voltage was applied from the trans side. Once calix[4]arene tetrabutylamide **3.1** was incorporated into the lipid (by addition to the cis side), the current through the membrane was recorded using both a chart recorder and directly digitized storing as a computer file. The conductance values were calculated by dividing the current by the applied voltage. The events were grouped into conductance ranges of equal magnitude for the purpose of showing the distribution of recorded conductances.

Patch clamp experiments. Patch clamp experiments and data analyses were done by Dr. Galya Abdrakhmanova. HEK-293 cells, plated in 100-mm dishes containing 10 mL of the growth media, were maintained at 37 °C with 5% CO_2 in the incubator. Growth medium for HEK-293 cells was minimum essential medium supplemented with 10% fetal bovine serum, 100 U/mL penicillin and 100 μg/mL streptomycin. Electrophysiological recordings were performed in the whole-cell configuration of the patch clamp technique using a DAGAN 8900 amplifier (Dagan Corp., Minneapolis, MN). The patch electrodes, pulled from borosilicate glass capillaries, had a resistance of 3-4 MΩ when filled with internal solution containing (in mM): CsCl, 110; tetraethylammonium chloride, 20; MgATP, 5; EGTA, 14; HEPES, 20 and titrated to pH 7.4 with CsOH. Approximately 90% of electrode resistance was compensated electronically, so that effective series resistance was less than 1 MΩ. HEK cells were used for experiments 2 to 4 days after plating the cells on the coverslips. Generation of the voltage clamp protocols and acquisition of data were carried out using PCLAMP software (Axon Instruments, Inc., Burlingame, CA). Sampling frequency was 0.5-2.0 kHz and current signals were filtered at 10 kHz before digitization and storage. All experiments were performed at room temperature (23-25 °C). Cells selected for

recordings had a capacitance of 25-35 pF. Cells plated on plastic coverslips (15mm round thermanox, Nunc, Inc., Napierville, IL) were transferred to an experimental chamber mounted on the stage of an inverted microscope (Diaphot, Nikon, Nagano, Japan) and were bathed in a solution containing (in mM): NaCl, 137; $CaCl_2$, 2; KCl, 5.4; HEPES, 10; glucose, 10; $MgCl_2$, 1 (pH 7.4 adjusted with NaOH). The experimental chamber was constantly perfused at a rate of approximately 1mL/min with a control bathing solution. In solutions buffered on the cell under recording KCl was omitted and in some experiments NaCl was replaced by isoosmotic amounts of Na_2SO_4 or Na glutamate. Servo-controlled miniature solenoid valves were used for rapid switching between control and test solutions (delay in solution change was < 20ms). Calix[4]arene tetrabutylamide **3.1** was dissolved in DMSO, and DMSO was added in an equal amount to the control and test solutions.

Analysis of the Electrostatic Potential on the Surface of Liposomes. LUVs (100 μL of 11 mM stock solution) containing a phosphate buffer with either 100 mM KCl or 75 mM Na_2SO_4 inside were suspended in 1.90 mL of 100 mM NaCl buffer containing 60 nM safranin (a potential-sensitive dye). Safranin emission was monitored at 580 nm with excitation at 521 nm. During the course of the experiment, 20 μL of a 0-0.12 mM DMSO solution of valinomycin or 0-2 mM of **3.3-3.8** DMSO solution was added. Experiments were completed by injection of 20 μL of a 1 mM aqueous solution of the defect-inducing peptide melittin.[317]

Liposome Preparation for ^{35}Cl NMR Assays. Egg yolk L-α-phosphatidylcholine (1.0 mg/mL EYPC ethanol solution, 250 μL, 329 μmol) was dissolved in a $CHCl_3$/MeOH mixture, the solution was evaporated under reduced pressure and the resulting thin film was dried under high vacuum for 2.5 h. The lipid film was hydrated in 1.0 mL of phosphate buffer (9:1 H_2O:D_2O, 10 mM sodium phosphate, pH = 5.4, 100 mM NaCl) containing 10 mM $CoCl_2$ (^{35}Cl shift reagent) for 40 min. During hydration, the suspension was submitted to 5 freeze-thaw cycles. The giant liposome suspension (1 mL) was submitted to high-pressure extrusion at room temperature (41 passes through a 5.0

241

μm polycarbonate membrane). The giant vesicle suspension was partially separated from extravesicular $CoCl_2$ by size exclusion chromatography (SEC) (stationary phase: Sephadex G-25, mobile phase: 9:1 H_2O:D_2O, 10 mM sodium phosphate, pH = 6.4, 75 mM Na_2SO_4) to give 12 mL of the giant vesicle suspension (NaCl/$CoCl_2$ inside, Na_2SO_4 outside). The suspension was concentrated to approximately 1.5 mL by centrifugation at 14,000 rpm for 30 sec followed by removal of the non-vesicle containing buffer (this step further decreased the extravesicular $CoCl_2$ concentration). The 1.5 mL suspension was diluted to 3 mL with the Na_2SO_4 buffer (9:1 H_2O:D_2O, 10 mM sodium phosphate, pH = 6.4, 75 mM Na_2SO_4) to give a suspension that was 88 mM in EYPC (assuming 100% of lipid was incorporated into liposomes and estimating 20% was lost in purification/concentration). This suspension was used directly in ^{35}Cl NMR transport assays.

Chloride Transport Monitored by ^{35}Cl NMR. All ^{35}Cl NMR spectra were recorded on a Bruker DRX500 instrument operating at 49.00 MHz for the ^{35}Cl resonance and chemical shift values are reported in ppm relative to 25 mM NaCl in D_2O at 0 ppm (external standard). A 5 mm broad band probe was used. A 90° pulse width (22 μs), acquisition time of 200 ms with no delay between pulses, and a sweep width of 8.2 kHz were used in all experiments. The number of transients ranged from 3,000 to 20,000. For each run, 400 μL of the giant vesicle suspension was placed in a 5 mm NMR tube and the instrument was locked on D_2O.

REFERENCES

(1)   Rolf, I. P. *Rolfing: The Integration of Human Structures*; Dennis-Landman: Santa Monica, 1977.

(2)   Philp, D.; Stoddart, J. F. "Self-Assembly in Natural and Unnatural Systems" *Angew. Chem.-Int. Ed. Engl.* **1996**, *35*, 1155-1196.

(3)   Fiammengo, R.; Crego-Calama, M.; Reinhoudt, D. N. "Synthetic Self-Assembled Models with Biomimetic Functions" *Curr. Opin. Chem. Biol.* **2001**, *5*, 660-673.

(4)   Hille, B. *Ion Channels of Excitable Membranes*; 3rd ed.; Sinauer Associates, Inc.: Sunderland, 2001.

(5)   Hepler, P. K.; Vidali, L.; Cheung, A. Y. "Polarized Cell Growth in Higher Plants" *Annu. Rev. Cell Dev. Biol.* **2001**, *17*, 159-187.

(6)   Lange, K. "Regulation of Cell Volume via Microvillar Ion Channels" *J. Cell. Physiol.* **2000**, *185*, 21-35.

(7)   Caplan, M. J. "Ion Pumps in Epithelial Cells: Sorting, Stabilization, and Polarity" *Am. J. Physiol.* **1997**, *35*, G1304-G1313.

(8)   Doyle, D. A.; Cabral, J. M.; Pfuetzner, R. A.; Kuo, A. L.; Gulbis, J. M.; Cohen, S. L.; Chait, B. T.; MacKinnon, R. "The Structure of the Potassium Channel: Molecular Basis of K^+ Conduction and Selectivity" *Science* **1998**, *280*, 69-77.

(9)   Dutzler, R.; Campbell, E. B.; Cadene, M.; Chait, B. T.; MacKinnon, R. "X-Ray Structure of a ClC Chloride Channel at 3.0 Å Reveals the Molecular Basis of Anion Selectivity" *Nature* **2002**, *415*, 287-294.

(10) Theil, E. C.; Raymond, K. N. in *Bioinorganic Chemistry*; Bertini, I., Gray, H. B., Lippard, S. J., Valentine, J. S., Eds.; University Science Books: Sausalito, 1994, pp 1-35.

(11) Rivas, J. C. M.; Schwalbe, H.; Lippard, S. J. "Interchain Hydrogen-Bonding Interactions May Facilitate Translocation of K^+ Ions across the Potassium Channel Selectivity Filter, as Suggested by Synthetic Modeling Chemistry" *Proc. Natl. Acad. Sci. U. S. A.* **2001**, *98*, 9478-9483.

(12) Reddy, G. L.; Iwamoto, T.; Tomich, J. M.; Montal, M. "Synthetic Peptides and 4-Helix Bundle Proteins as Model Systems for the Pore-Forming Structure of Channel Proteins .2. Transmembrane Segment M2 of the Brain Glycine Receptor is a Plausible Candidate for the Pore-Lining Structure" *J. Biol. Chem.* **1993**, *268*, 14608-14615.

(13) Oblatt-Montal, M.; Reddy, G. L.; Iwamoto, T.; Tomich, J. M.; Montal, M. "Identification of an Ion Channel-Forming Motif in the Primary Structure of CFTR, the Cystic-Fibrosis Chloride Channel" *Proc. Natl. Acad. Sci. U. S. A.* **1994**, *91*, 1495-1499.

(14) Winum, J.-Y.; Matile, S. "Rigid Push-Pull Oligo(*p*-Phenylene) Rods: Depolarization of Bilayer Membranes with Negative Membrane Potential" *J. Am. Chem. Soc.* **1999**, *121*, 7961-7962.

(15) Fernandez-Lopez, S.; Kim, H. S.; Choi, E. C.; Delgado, M.; Granja, J. R.; Khasanov, A.; Kraehenbuehl, K.; Long, G.; Weinberger, D. A.; Wilcoxen, K. M.; Ghadiri, M. R. "Antibacterial Agents Based on the Cyclic D,L-Alpha-Peptide Architecture" *Nature* **2001**, *412*, 452-455.

(16) Jiang, C. W.; Lee, E. R.; Lane, M. B.; Xiao, Y. F.; Harris, D. J.; Cheng, S. H. "Partial Correction of Defective Cl⁻ Secretion in Cystic Fibrosis Epithelial Cells by an Analog of Squalamine" *Am. J. Physiol.* **2001**, *281*, L1164-L1172.

(17) Hubner, C. A.; Jentsch, T. J. "Ion Channel Diseases" *Hum. Mol. Genet.* **2002**, *11*, 2435-2445.

(18) Ashcroft, F. M. *Ion Channels and Disease*; Academic Press: San Diego, 2000.

(19) Felix, R. "Channelopathies: Ion Channel Defects Linked to Heritable Clinical Disorders" *J. Med. Genet.* **2000**, *37*, 729-740.

(20) Sakmann, B.; Neher, E. *Single-Channel Recording*; 2nd ed.; Plenum Press: New York, 1995.

(21) Henderson, R.; Baldwin, J. M.; Ceska, T. A.; Zemlin, F.; Beckmann, E.; Downing, K. H. "Model for the Structure of Bacteriorhodopsin Based on High-Resolution Electron Cryomicroscopy" *J. Mol. Biol.* **1990**, *213*, 899-929.

(22) Mindell, J. A.; Maduke, M.; Miller, C.; Grigorieff, N. "Projection Structure of a ClC-Type Chloride Channel at 6.5 Angstrom Resolution" *Nature* **2001**, *409*, 219-223.

(23) Heginbotham, L.; Abramson, T.; Mackinnon, R. "A Functional Connection between the Pores of Distantly Related Ion Channels as Revealed by Mutant K$^+$ Channels" *Science* **1992**, *258*, 1152-1155.

(24) Heginbotham, L.; Lu, Z.; Abramson, T.; Mackinnon, R. "Mutations in the K$^+$ Channel Signature Sequence" *Biophys. J.* **1994**, *66*, 1061-1067.

(25) Yellen, G.; Jurman, M. E.; Abramson, T.; Mackinnon, R. "Mutations Affecting Internal TEA Blockade Identify the Probable Pore-Forming Region of a K$^+$ Channel" *Science* **1991**, *251*, 939-942.

(26) Sali, D.; Bycroft, M.; Fersht, A. R. "Stabilization of Protein Structure by Interaction of Alpha-Helix Dipole with a Charged Side-Chain" *Nature* **1988**, *335*, 740-743.

(27) Jiang, Y. X.; Lee, A.; Chen, J. Y.; Cadene, M.; Chait, B. T.; MacKinnon, R. "Crystal Structure and Mechanism of a Calcium-Gated Potassium Channel" *Nature* **2002**, *417*, 515-522.

(28) Jiang, Y. X.; Lee, A.; Chen, J. Y.; Ruta, V.; Cadene, M.; Chait, B. T.; MacKinnon, R. "X-Ray Structure of a Voltage-Dependent K$^+$ Channel" *Nature* **2003**, *423*, 33-41.

(29) Maduke, M.; Miller, C.; Mindell, J. A. "A Decade of ClC Chloride Channels: Structure, Mechanism, and Many Unsettled Questions" *Annu. Rev. Biophys. Biomolec. Struct.* **2000**, *29*, 411-438.

(30) Steinmeyer, K.; Lorenz, C.; Pusch, M.; Koch, M. C.; Jentsch, T. J. "Multimeric Structure of ClC-1 Chloride Channel Revealed by Mutations in Dominant Myotonia-Congenita (Thomsen)" *Embo J.* **1994**, *13*, 737-743.

(31) Dutzler, R.; Campbell, E. B.; MacKinnon, R. "Gating the Selectivity Filter in ClC Chloride Channels" *Science* **2003**, *300*, 108-112.

(32) Adam, D. "Protein Chemists Favour Automatic Answers" *Nature* **2002**, *415*, 822-822.

(33) MacKinnon, R. "Nothing Automatic About Ion-Channel Structures" *Nature* **2002**, *416*, 261-262.

(34) Hille, B. "Ionic Channels in Nerve Membranes" *Prog. Biophys. Mol. Biol.* **1970**, *21*, 1-32.

(35) Armstrong, C. M. "Interaction of Tetraethylammonium Ion Derivatives with Potassium Channels of Giant Axons" *J. Gen. Physiol.* **1971**, *58*, 413-437.

(36) Woolley, G. A.; Wallace, B. A. "Model Ion Channels - Gramicidin and Alamethicin" *J. Membr. Biol.* **1992**, *129*, 109-136.

(37) Bamberg, E.; Apell, H. J.; Alpes, H. "Structure of Gramicidin A Channel - Discrimination between Pi- L,D and Beta-Helix by Electrical Measurements with Lipid Bilayer Membranes" *Proc. Natl. Acad. Sci. U. S. A.* **1977**, *74*, 2402-2406.

(38) Ketchem, R. R.; Hu, W.; Cross, T. A. "High-Resolution Conformation of Gramicidin-A in a Lipid Bilayer by Solid-State NMR" *Science* **1993**, *261*, 1457-1460.

(39) Goulian, M.; Mesquita, O. N.; Fygenson, D. K.; Nielsen, C.; Andersen, O. S.; Libchaber, A. "Gramicidin Channel Kinetics under Tension" *Biophys. J.* **1998**, *74*, 328-337.

(40) Bamberg, E.; Janko, K. "Action of a Carbon-Sub-Oxide Dimerized Gramicidin A on Lipid Bilayer Membranes" *Biochim. Biophys. Acta* **1977**, *465*, 486-499.

(41) Stankovic, C. J.; Heinemann, S. H.; Delfino, J. M.; Sigworth, F. J.; Schreiber, S. L. "Transmembrane Channels Based on Tartaric Acid Gramicidin-a Hybrids" *Science* **1989**, *244*, 813-817.

(42) Hladky, S. B.; Haydon, D. A. "Ion Transfer across Lipid Membranes in Presence of Gramicidin-A .1. Studies of Unit Conductance Channel" *Biochim. Biophys. Acta* **1972**, *274*, 294-312.

(43) Myers, V. B.; Haydon, D. A. "Ion Transfer across Lipid Membranes in Presence of Gramicidin-A .2. Ion Selectivity" *Biochim. Biophys. Acta* **1972**, *274*, 313-322.

(44) Duclohier, H.; Wroblewski, H. "Voltage-Dependent Pore Formation and Antimicrobial Activity by Alamethicin and Analogues" *J. Membr. Biol.* **2001**, *184*, 1-12.

(45) Mueller, P.; Rudin, D. O. "Action Potentials Induced in Biomolecular Lipid Membranes" *Nature* **1968**, *217*, 713-719.

(46) Fox, R. O.; Richards, F. M. "A Voltage-Gated Ion Channel Model Inferred from the Crystal Structure of Alamethicin at 1.5-Å Resolution" *Nature* **1982**, *300*, 325-330.

(47) Hall, J. E.; Vodyanoy, I.; Balasubramanian, T. M.; Marshall, G. R. "Alamethicin - a Rich Model for Channel Behavior" *Biophys. J.* **1984**, *45*, 233-247.

(48) Sansom, M. S. P. "The Biophysics of Peptide Models of Ion Channels" *Prog. Biophys. Mol. Biol.* **1991**, *55*, 139-235.

(49) Boheim, G. "Statistical Analysis of Alamethicin Channels in Black Lipid-Membranes" *J. Membr. Biol.* **1974**, *19*, 277-303.

(50) Haberman, E. "Bee Wasp Venoms" *Science* **1972**, *177*, 314-322.

(51) Dempsey, C. E. "The Actions of Melittin on Membranes" *Biochim. Biophys. Acta* **1990**, *1031*, 143-161.

(52) Bechinger, B. "Structure and Functions of Channel-Forming Peptides: Magainins, Cecropins, Melittin and Alamethicin" *J. Membr. Biol.* **1997**, *156*, 197-211.

(53) Terwilliger, T. C.; Eisenberg, D. "The Structure of Melittin .1. Structure Determination and Partial Refinement" *J. Biol. Chem.* **1982**, *257*, 6010-6015.

(54) Terwilliger, T. C.; Eisenberg, D. "The Structure of Melittin .2. Interpretation of the Structure" *J. Biol. Chem.* **1982**, *257*, 6016-6022.

(55) Tosteson, M. T.; Tosteson, D. C. "The Sting - Melittin Forms Channels in Lipid Bilayers" *Biophys. J.* **1981**, *36*, 109-116.

(56) Kempf, C.; Klausner, R. D.; Weinstein, J. N.; Vanrenswoude, J.; Pincus, M.; Blumenthal, R. "Voltage-Dependent Trans-Bilayer Orientation of Melittin" *J. Biol. Chem.* **1982**, *257*, 2469-2476.

(57) Terwilliger, T. C.; Weissman, L.; Eisenberg, D. "The Structure of Melittin in the Form-I Crystals and its Implication for Melittin's Lytic and Surface Activities" *Biophys. J.* **1982**, *37*, 353-361.

(58) Karle, I. L.; Flippenanderson, J. L.; Agarwalla, S.; Balaram, P. "Crystal Structure of Leu1 Zervamicin, a Membrane Ion Channel Peptide - Implications for Gating Mechanisms" *Proc. Natl. Acad. Sci. U. S. A.* **1991**, *88*, 5307-5311.

(59)   Chugh, J. K.; Bruckner, H.; Wallace, B. A. "Model for a Helical Bundle Channel Based on the High-Resolution Crystal Structure of Trichotoxin_A50E" *Biochemistry* **2002**, *41*, 12934-12941.

(60)   Shai, Y.; Bach, D.; Yanovsky, A. "Channel Formation Properties of Synthetic Pardaxin and Analogs" *J. Biol. Chem.* **1990**, *265*, 20202-20209.

(61)   Kagan, B. L.; Hirakura, Y.; Azimov, R.; Azimova, R.; Lin, M. C. "The Channel Hypothesis of Alzheimer's Disease: Current Status" *Peptides* **2002**, *23*, 1311-1315.

(62)   Kagan, B. L.; Hirakura, Y.; Azimov, R.; Azimova, R. "The Channel Hypothesis of Huntington's Disease" *Brain Res. Bull.* **2001**, *56*, 281-284.

(63)   Gokel, G. W.; Murillo, O. "Synthetic Organic Chemical Models for Transmembrane Channels" *Acc. Chem. Res.* **1996**, *29*, 425-432.

(64)   Kobuke, Y. in *Advances in Supramolecular Chemistry*; Gokel, G. W., Ed.; JAI Press Inc.: Greenwich, 1997; Vol. 4, pp 163-210.

(65)   Hille, B.; Armstrong, C. M.; MacKinnon, R. "Ion Channels: From Idea to Reality" *Nat. Med.* **1999**, *5*, 1105-1109.

(66)   Neher, E. "Ion Channels for Communication between and within Cells (Nobel Lecture)" *Angew. Chem.-Int. Edit. Engl.* **1992**, *31*, 824-829.

(67)   Sakmann, B. "Elementary Steps in Synaptic Transmission Revealed by Currents through Single Ion Channels (Nobel Lecture)" *Angew. Chem.-Int. Edit. Engl.* **1992**, *31*, 830-841.

(68)   Hanke, W.; Schlue, W.-R. *Planar Lipid Bilayers*; Academic Press: London, 1993.

(69)   McIntyre, J. C.; Sleight, R. G. "Fluorescence Assay for Phospholipid Membrane Asymmetry" *Biochemistry* **1991**, *30*, 11819-11827.

(70)   Woodle, M. C.; Papahadjopoulos, D. "Liposome Preparation and Size Characterization" *Methods Enzymol.* **1989**, *171*, 193-217.

(71)   Huang, C. H. "Studies on Phosphatidylcholine Vesicles. Formation and Physical Characteristics" *Biochemistry* **1969**, *8*, 344-352.

(72) Moscho, A.; Orwar, O.; Chiu, D. T.; Modi, B. P.; Zare, R. N. "Rapid Preparation of Giant Unilamellar Vesicles" *Proc. Natl. Acad. Sci. U. S. A.* **1996**, *93*, 11443-11447.

(73) Barenholz, Y.; Gibbes, D.; Litman, B. J.; Goll, J.; Thompson, T. E.; Carlson, F. D. "Simple Method for Preparation of Homogeneous Phospholipid Vesicles" *Biochemistry* **1977**, *16*, 2806-2810.

(74) Zumbuehl, O.; Weder, H. G. "Liposomes of Controllable Size in the Range of 40 to 180 nm by Defined Dialysis of Lipid-Detergent Mixed Micelles" *Biochim. Biophys. Acta* **1981**, *640*, 252-262.

(75) Szoka, F.; Papahadjopoulos, D. "Procedure for Preparation of Liposomes with Large Internal Aqueous Space and High Capture by Reverse-Phase Evaporation" *Proc. Natl. Acad. Sci. U. S. A.* **1978**, *75*, 4194-4198.

(76) Olson, F.; Hunt, C. A.; Szoka, F. C.; Vail, W. J.; Papahadjopoulos, D. "Preparation of Liposomes of Defined Size Distribution by Extrusion through Polycarbonate Membranes" *Biochim. Biophys. Acta* **1979**, *557*, 9-23.

(77) Kano, K.; Fendler, J. H. "Pyranine as a Sensitive pH Probe for Liposome Interiors and Surfaces - pH Gradients across Phospholipid Vesicles" *Biochim. Biophys. Acta* **1978**, *509*, 289-299.

(78) Sakai, N.; Brennan, K. C.; Weiss, L. A.; Matile, S. "Toward Biomimetic Ion Channels Formed by Rigid-Rod Molecules: Length-Dependent Ion-Transport Activity of Substituted Oligo(*p*- Phenylene)s" *J. Am. Chem. Soc.* **1997**, *119*, 8726-8727.

(79) Weiss, L. A.; Sakai, N.; Ghebremariam, B.; Ni, C. Y.; Matile, S. "Rigid Rod-Shaped Polyols: Functional Nonpeptide Models for Transmembrane Proton Channels" *J. Am. Chem. Soc.* **1997**, *119*, 12142-12149.

(80) Tedesco, M. M.; Ghebremariam, B.; Sakai, N.; Matile, S. "Modeling the Selectivity of Potassium Channels with Synthetic, Ligand-Assembled Pi Slides" *Angew. Chem.-Int. Edit.* **1999**, *38*, 540-543.

(81) Fyles, T. M.; James, T. D.; Kaye, K. C. "Activities and Modes of Action of Artificial Ion-Channel Mimics" *J. Am. Chem. Soc.* **1993**, *115*, 12315-12321.

(82) Benz, R.; McLaughlin, S. "The Molecular Mechanism of Action of the Proton Ionophore FCCP (Carbonylcyanide Para-Trifluoromethoxyphenylhydrazone)" *Biophys. J.* **1983**, *41*, 381-398.

(83) Gupta, R. K.; Gupta, P. "Direct Observation of Resolved Resonances from Intra-Cellular and Extracellular Na-23 Ions in NMR-Studies of Intact-Cells and Tissues Using Dysprosium(III) Tripolyphosphate as Paramagnetic Shift-Reagent" *J. Magn. Reson.* **1982**, *47*, 344-350.

(84) Chu, W. J.; Elgavish, G. A. "Gadolinium and Dysprosium Chelates of DTPA-Amide-Dextran: Synthesis, H-1 NMR Relaxivity, and Induced Na-23 NMR Shift" *NMR Biomed.* **1995**, *8*, 159-163.

(85) Jelicks, L. A.; Gupta, R. K. "Observation of Intracellular Sodium Ions by Double-Quantum-Filtered Na-23 NMR with Paramagnetic Quenching of Extracellular Coherence by Gadolinium Tripolyphosphate" *J. Magn. Reson.* **1989**, *83*, 146-151.

(86) Stadler, E.; Dedek, P.; Yamashita, K.; Regen, S. L. "Amphotericin-B Mimics - a Sterol-Based Ionophore" *J. Am. Chem. Soc.* **1994**, *116*, 6677-6682.

(87) Pregel, M. J.; Jullien, L.; Lehn, J. M. "Towards Artificial Ion Channels - Transport of Alkali-Metal Ions across Liposomal Membranes by Bouquet Molecules" *Angew. Chem.-Int. Edit. Engl.* **1992**, *31*, 1637-1640.

(88) Pregel, M. J.; Jullien, L.; Canceill, J.; Lacombe, L.; Lehn, J. M. "Channel-Type Molecular-Structures .4. Transmembrane Transport of Alkali-Metal Ions by Bouquet Molecules" *J. Chem. Soc.-Perkin Trans. 2* **1995**, 417-426.

(89) Murillo, O.; Watanabe, S.; Nakano, A.; Gokel, G. W. "Synthetic Models for Transmembrane Channels - Structural Variations That Alter Cation Flux" *J. Am. Chem. Soc.* **1995**, *117*, 7665-7679.

(90) Shungu, D. C.; Briggs, R. W. "Application of 1D and 2D Na-23 Magnetization-Transfer NMR to the Study of Ionophore-Mediated Transmembrane Cation-Transport" *J. Magn. Reson.* **1988**, *77*, 491-503.

(91) Shachar-Hill, Y.; Shulman, R. G. "Co^{2+} as a Shift-Reagent for ^{35}Cl NMR of Chloride with Vesicles and Cells" *Biochemistry* **1992**, *31*, 6272-6278.

(92) Koulov, A. V.; Mahoney, J. M.; Smith, B. D. "Facilitated Transport of Sodium or Potassium Chloride across Vesicle Membranes Using a Ditopic Salt-Binding Macrobicycle" *Org. Biomol. Chem.* **2003**, *1*, 27-29.

(93) Sidorov, V.; Kotch, F. W.; Kuebler, J. L.; Lam, Y.-F.; Davis, J. T. "Chloride Transport across Lipid Bilayers and Transmembrane Potential Induction by an Oligophenoxyacetamide" *J. Am. Chem. Soc.* **2003**, *125*, 2840-2841.

(94) Riddell, F. G.; Arumugam, S.; Patel, A. "Chloride Transport through Model Biological Membranes Studied by Cl-35 NMR" *Chem. Commun.* **1990**, 74-76.

(95) Biwersi, J.; Tulk, B.; Verkman, A. S. "Long-Wavelength Chloride-Sensitive Fluorescent Indicators" *Anal. Biochem.* **1994**, *219*, 139-143.

(96) Minta, A.; Tsien, R. Y. "Fluorescent Indicators for Cytosolic Sodium" *J. Biol. Chem.* **1989**, *264*, 19449-19457.

(97) Schlesinger, P. H.; Ferdani, R.; Liu, J.; Pajewska, J.; Pajewski, R.; Saito, M.; Shabany, H.; Gokel, G. W. "SCMTR: A Chloride-Selective, Membrane-Anchored Peptide Channel That Exhibits Voltage Gating" *J. Am. Chem. Soc.* **2002**, *124*, 1848-1849.

(98) Schlesinger, P. H.; Ferdani, R.; Pajewski, R.; Pajewska, J.; Gokel, G. W. "A Hydrocarbon Anchored Peptide That Forms a Chloride-Selective Channel in Liposomes" *Chem. Commun.* **2002**, 840-841.

(99) Woolley, G. A.; Kapral, M. K.; Deber, C. M. "Potential-Sensitive Membrane Association of a Fluorescent Dye" *FEBS Lett.* **1987**, *224*, 337-342.

(100) Woolley, G. A.; Deber, C. M. "A Lipid Vesicle System for Probing Voltage-Dependent Peptide Lipid Interactions - Application to Alamethicin Channel Formation" *Biopolymers* **1989**, *28*, 267-272.

(101) Easwaran, K. R. K. "Interaction between Valinomycin and Metal-Ions" *Met. Ions Biol. Syst.* **1985**, *19*, 109-137.

(102) Bell, T. W. "Carriers and Channels: Current Progress and Future Prospects" *Curr. Opin. Chem. Biol.* **1998**, *2*, 711-716.

(103) Allen, T. M.; Cleland, L. G. "Serum-Induced Leakage of Liposome Contents" *Biochim. Biophys. Acta* **1980**, *597*, 418-426.

(104) New, R. C. C. in *Liposomes: A Practical Approach*; IRL Press: Oxford, 1990, pp 131-134.

(105) Rex, S. "Pore Formation Induced by the Peptide Melittin in Different Lipid Vesicle Membranes" *Biophys. Chem.* **1996**, *58*, 75-85.

(106) Baumeister, B.; Sakai, N.; Matile, S. "Giant Artificial Ion Channels Formed by Self-Assembled, Cationic Rigid-Rod Beta-Barrels" *Angew. Chem.-Int. Edit.* **2000**, *39*, 1955-1958.

(107) Schlesinger, P. H.; Djedovic, N. K.; Ferdani, R.; Pajewska, J.; Pajewski, R.; Gokel, G. W. "Anchor Chain Length Alters the Apparent Mechanism of Chloride Channel Function in SCMTR Derivatives" *Chem. Commun.* **2003**, 308-309.

(108) Lear, J. D.; Wasserman, Z. R.; DeGrado, W. F. "Synthetic Amphiphilic Peptide Models for Protein Ion Channels" *Science* **1988**, *240*, 1177-1181.

(109) Tabushi, I.; Kuroda, Y.; Yokota, K. "A,B,D,F-Tetrasubstituted β-Cyclodextrin as Artificial Channel Compound" *Tetrahedron Lett.* **1982**, *23*, 4601-4604.

(110) Kobuke, Y.; Ueda, K.; Sokabe, M. "Artificial Non-Peptide Single Ion Channels" *J. Am. Chem. Soc.* **1992**, *114*, 7618-7622.

(111) Gokel, G. W.; Mukhopadhyay, A. "Synthetic Models of Cation-Conducting Channels" *Chem. Soc. Rev.* **2001**, *30*, 274-286.

(112) Fyles, T. M. "Bilayer Membranes and Transporter Models" *Curr. Opin. Chem. Biol.* **1997**, *1*, 497-505.

(113) Boon, J. M.; Smith, B. D. "Synthetic Membrane Transporters" *Curr. Opin. Chem. Biol.* **2002**, *6*, 749-756.

(114) Kobuke, Y.; Ueda, K.; Sokabe, M. "Totally Synthetic Voltage Dependent Ion Channel" *Chem. Lett.* **1995**, 435-436.

(115) Kobuke, Y.; Morita, K. "Artificial Ion Channels of Amphiphilic Ion Pairs Composed of Oligoether-Ammonium and Hydrophobic Carboxylate or Phosphates" *Inorg. Chim. Acta* **1998**, *283*, 167-174.

(116) Kobuke, Y.; Ohgoshi, A. "Supramolecular Ion Channel Containing *Trans*-Azobenzene for Photocontrol of Ionic Fluxes" *Colloids and Surfaces A* **2000**, *169*, 187-197.

(117) Tanaka, Y.; Kobuke, Y.; Sokabe, M. "A Nonpeptidic Ion-Channel with K^+ Selectivity" *Angew. Chem.-Int. Edit. Engl.* **1995**, *34*, 693-694.

(118) Kobuke, Y.; Nagatani, T. "A Supramolecular Ion Channel Based on Amphiphilic Cholic Acid Derivatives" *Chem. Lett.* **2000**, 298-299.

(119) Kobuke, Y.; Nagatani, T. "Transmembrane Ion Channels Constructed of Cholic Acid Derivatives" *J. Org. Chem.* **2001**, *66*, 5094-5101.

(120) Goto, C.; Yamamura, M.; Satake, A.; Kobuke, Y. "Artificial Ion Channels Showing Rectified Current Behavior" *J. Am. Chem. Soc.* **2001**, *123*, 12152-12159.

(121) Yoshino, N.; Satake, A.; Kobuke, Y. "An Artificial Ion Channel Formed by a Macrocyclic Resorcin[4]arene with Amphiphilic Cholic Acid Ether Groups" *Angew. Chem.-Int. Ed.* **2001**, *40*, 457-459.

(122) Ghadiri, M. R.; Granja, J. R.; Milligan, R. A.; McRee, D. E.; Khazanovich, N. "Self-Assembling Organic Nanotubes Based on a Cyclic Peptide Architecture" *Nature* **1993**, *366*, 324-327.

(123) Ghadiri, M. R.; Granja, J. R.; Buehler, L. K. "Artificial Transmembrane Ion Channels from Self-Assembling Peptide Nanotubes" *Nature* **1994**, *369*, 301-304.

(124) Kim, H. S.; Hartgerink, J. D.; Ghadiri, M. R. "Oriented Self-Assembly of Cyclic Peptide Nanotubes in Lipid Membranes" *J. Am. Chem. Soc.* **1998**, *120*, 4417-4424.

(125) Clark, T. D.; Buehler, L. K.; Ghadiri, M. R. "Self-Assembling Cyclic Beta(3)-Peptide Nanotubes as Artificial Transmembrane Ion Channels" *J. Am. Chem. Soc.* **1998**, *120*, 651-656.

(126) Hartgerink, J. D.; Clark, T. D.; Ghadiri, M. R. "Peptide Nanotubes and Beyond" *Chem.-Eur. J.* **1998**, *4*, 1367-1372.

(127) Bong, D. T.; Clark, T. D.; Granja, J. R.; Ghadiri, M. R. "Self-Assembling Organic Nanotubes" *Angew. Chem.-Int. Ed.* **2001**, *40*, 988-1011.

(128) Medoff, G.; Brajtburg, J.; Kobayashi, G. S.; Bolard, J. "Anti-Fungal Agents Useful in Therapy of Systemic Fungal Infections" *Annu. Rev. Pharmacol. Toxicol.* **1983**, *23*, 303-330.

(129) Gennis, R. B. *Biomembranes: Molecular Structure and Function*; Springer-Verlag: New York, 1989.

(130) Cotero, B. V.; Rebolledo-Antunez, S.; Ortega-Blake, I. "On the Role of Sterol in the Formation of the Amphotericin B Channel" *Biochim. Biophys. Acta-Biomembr.* **1998**, *1375*, 43-51.

(131) Krasne, S.; Eisenman, G.; Szabo, G. "Freezing and Melting of Lipid Bilayers and Mode of Action of Nonaction, Valinomycin, and Gramicidin" *Science* **1971**, *174*, 412-415.

(132) Sadownik, A.; Deng, G.; Janout, V.; Regen, S. L. "Rapid Construction of a Squalamine Mimic" *J. Am. Chem. Soc.* **1995**, *117*, 6138-6139.

(133) Stone, R. "Deja Vu Guides the Way to New Antimicrobial Steroid" *Science* **1993**, *259*, 1125.

(134) Otto, S.; Osifchin, M.; Regen, S. L. "Modular Control over the Selectivity of Self-Assembling and Membrane-Spanning Ion Conductors" *J. Am. Chem. Soc.* **1999**, *121*, 7276-7277.

(135) Otto, S.; Osifchin, M.; Regen, S. L. "Squeezing a Synthetic Ionophore and Mechanistic Insight out of a Lipid Bilayer" *J. Am. Chem. Soc.* **1999**, *121*, 10440-10441.

(136) DiGiorgio, A. F.; Otto, S.; Bandyopadhyay, P.; Regen, S. L. "Ion Conductors That Favor Passive Transport in Ergesterol-Rich over Cholesterol-Rich Phospholipid Membranes" *J. Am. Chem. Soc.* **2000**, *122*, 11029-11030.

(137) Bandyopadhyay, P.; Janout, V.; Zhang, L.-H.; Regen, S. L. "Ion Conductors Derived from Cholic Acid and Spermine: Importance of Facial Hydrophobicity on Na$^+$ Transport and Membrane Selectivity" *J. Am. Chem. Soc.* **2001**, *123*, 7691-7696.

(138) Bandyopadhyay, P.; Bandyopadhyay, P.; Regen, S. L. "Ion Conductors Derived from Biogenic Amines, Bile Acids, and Amino Acids" *Bioconjugate Chem.* **2002**, *13*, 1314-1318.

(139) Bandyopadhyay, P.; Bandyopadhyay, P.; Regen, S. L. "An Ion Conductor That Recognizes Osmotically-Stressed Phospholipid Bilayers" *J. Am. Chem. Soc.* **2002**, *124*, 11254-11255.

(140) Sakai, N.; Ni, C. Y.; Bezrukov, S. M.; Matile, S. "Voltage-Dependent Ion Channel Formation by Rigid Rod-Shaped Polyols in Planar Lipid Bilayers" *Bioorg. Med. Chem. Lett.* **1998**, *8*, 2743-2746.

(141) Sidorov, V.; Kotch, F. W.; Abdrakhmanova, G.; Mizani, R.; Fettinger, J. C.; Davis, J. T. "Ion Channel Formation from a Calix[4]arene Amide That Binds HCl" *J. Am. Chem. Soc.* **2002**, *124*, 2267-2278.

(142) Sakai, N.; Majumdar, N.; Matile, S. "Self-Assembled Rigid-Rod Ionophores" *J. Am. Chem. Soc.* **1999**, *121*, 4294-4295.

(143) Sakai, N.; Gerard, D.; Matile, S. "Electrostatics of Cell Membrane Recognition: Structure and Activity of Neutral and Cationic Rigid Push-Pull Rods in Isoelectric, Anionic, and Polarized Lipid Bilayer Membranes" *J. Am. Chem. Soc.* **2001**, *123*, 2517-2524.

(144) Cross, G. G.; Fyles, T. M.; James, T. D.; Zojaji, M. "Design and Synthesis of Artificial Ion Channels" *Synlett* **1993**, 449-460.

(145) Fyles, T. M.; James, T. D.; Pryhitka, A.; Zojaji, M. "Assembly of Ion Channel Mimics from a Modular Construction Set" *J. Org. Chem.* **1993**, *58*, 7456-7468.

(146) Behr, J. P.; Kirch, M.; Lehn, J. M. "Carrier-Mediated Transport through Bulk Liquid Membranes - Dependence of Transport Rates and Selectivity on Carrier Properties in a Diffusion-Limited Process" *J. Am. Chem. Soc.* **1985**, *107*, 241-246.

(147) Fyles, T. M.; Loock, D.; van Straaten-Nijenhuis, W. F.; Zhou, X. "Pores Formed by Bis-Macrocyclic Bola-Amphiphiles in Vesicle and Planar Bilayer Membranes" *J. Org. Chem.* **1996**, *61*, 8866-8874.

(148) Fyles, T. M.; Loock, D.; Zhou, X. "Ion Channels Based on Bis-Macrocyclic Bolaamphiphiles: Effects of Hydrophobic Substitutions" *Can. J. Chem.* **1998**, *76*, 1015-1026.

(149) Fyles, T. M.; Hu, C. W.; Knoy, R. "Transmembrane Ion Conductance by an Acyclic Bolaamphiphile" *Org. Lett.* **2001**, *3*, 1335-1337.

(150) Fyles, T. M.; Loock, D.; Zhou, X. "A Voltage-Gated Ion Channel Based on a Bis-Macrocyclic Bolaamphiphile" *J. Am. Chem. Soc.* **1998**, *120*, 2997-3003.

(151) Fyles, T. M.; Knoy, R.; Mullen, K.; Sieffert, M. "Membrane Activity of Isophthalic Acid Derivatives: Ion Channel Formation by a Low Molecular Weight Compound" *Langmuir* **2001**, *17*, 6669-6674.

(152) Cameron, L. M.; Fyles, T. M.; Hu, C. W. "Synthesis and Membrane Activity of a Bis(Metacyclophane)Bolaamphiphile" *J. Org. Chem.* **2002**, *67*, 1548-1553.

(153) Eggers, P. K.; Fyles, T. M.; Mitchell, K. D. D.; Sutherland, T. "Ion Channels from Linear and Branched Bola-Amphiphiles" *J. Org. Chem.* **2003**, *68*, 1050-1058.

(154) Gokel, G. W. "Hydraphiles: Design, Synthesis and Analysis of a Family of Synthetic, Cation-Conducting Channels" *Chem. Commun.* **2000**, 1-9.

(155) Murillo, O.; Suzuki, I.; Abel, E.; Murray, C. L.; Meadows, E. S.; Jin, T.; Gokel, G. W. "Synthetic Transmembrane Channels: Functional Characterization Using Solubility Calculations, Transport Studies, and Substituent Effects" *J. Am. Chem. Soc.* **1997**, *119*, 5540-5549.

(156) Abel, E.; Maguire, G. E. M.; Meadows, E. S.; Murillo, O.; Jin, T.; Gokel, G. W. "Planar Bilayer Conductance and Fluorescence Studies Confirm the Function and Location of a Synthetic, Sodium-Ion-Conducting Channel in a Phospholipid Bilayer Membrane" *J. Am. Chem. Soc.* **1997**, *119*, 9061-9062.

(157) Meadows, E. S.; Barbour, L. J.; Fronczek, F. R.; Evans, C. M.; Watkins, S. F.; Gokel, G. W. "Channel-Like Structures Formed from Extended Networks of 4,13-Diaza-18-Crown-6 Complexes" *Inorg. Chim. Acta* **2000**, *300*, 333-338.

(158) Meadows, E. S.; Abel-Santos, E.; Frankel, D. C.; Gokel, G. W. "The Presence of Cholestanyl Substituents in Hydraphile Channels Inhibits Cation Transport in the Phospholipid Bilayer" *Tetrahedron Lett.* **2000**, *41*, 1871-1875.

(159) Murray, C. L.; Gokel, G. W. "Cation Flux Dependence on Carbon Chain Length in Hydraphile Channels as Assessed by Dynamic Na-23 NMR Methods in Phospholipid Bilayers" *Chem. Commun.* **1998**, 2477-2478.

(160) Shabany, H.; Gokel, G. W. "Enhancement of Cation Transport in Synthetic Hydraphile Channels Having Covalently-Linked Headgroups" **2000**, 2373-2374.

(161) Hall, C. D.; Kirkovits, G. J.; Hall, A. C. "Towards a Redox-Active Artificial Ion Channel" *Chem. Commun.* **1999**, 1897-1898.

(162) Leevy, W. M.; Donato, G. M.; Ferdani, R.; Goldman, W. E.; Schlesinger, P. H.; Gokel, G. W. "Synthetic Hydraphile Channels of Appropriate Length Kill *Escherichia coli*" *J. Am. Chem. Soc.* **2002**, *124*, 9022-9023.

(163) de Mendoza, J.; Cuevas, F.; Prados, P.; Meadows, E. S.; Gokel, G. W. "A Synthetic Cation-Transporting Calix[4]arene Derivative Active in Phospholipid Bilayers" *Angew. Chem.-Int. Ed.* **1998**, *37*, 1534-1537.

(164) Voyer, N.; Robitaille, M. "A Novel Functional Artificial Ion Channel" *J. Am. Chem. Soc.* **1995**, *117*, 6599-6600.

(165) Meillon, J. C.; Voyer, N. "A Synthetic Transmembrane Channel Active in Lipid Bilayers" *Angew. Chem.-Int. Edit. Engl.* **1997**, *36*, 967-969.

(166) Biron, E.; Voyer, N.; Meillon, J.-C.; Cormier, M.-E.; Auger, M. "Conformational and Orientation Studies of Artificial Ion Channels Incorporated into Lipid Bilayers" *Biopolymers* **2001**, *55*, 364-372.

(167) Rajendra, S.; Lynch, J. W.; Schofield, P. R. "The Glycine Receptor" *Pharmacol. Ther.* **1997**, *73*, 121-146.

(168) Grenningloh, G.; Rienitz, A.; Schmitt, B.; Methfessel, C.; Zensen, M.; Beyreuther, K.; Gundelfinger, E. D.; Betz, H. "The Strychnine-Binding Subunit of the Glycine Receptor Shows Homology with Nicotinic Acetylcholine-Receptors" *Nature* **1987**, *328*, 215-220.

(169) Langosch, D.; Becker, C. M.; Betz, H. "The Inhibitory Glycine Receptor - a Ligand-Gated Chloride Channel of the Central-Nervous-System" *Eur. J. Biochem.* **1990**, *194*, 1-8.

(170) Wallace, D. P.; Tomich, J. M.; Iwamoto, T.; Henderson, K.; Grantham, J. J.; Sullivan, L. P. "A Synthetic Peptide Derived from Glycine-Gated Cl⁻ Channel Induces Transepithelial Cl⁻ and Fluid Secretion" *Am. J. Physiol.* **1997**, *41*, C1672-C1679.

(171) Mitchell, K. E.; Iwamoto, T.; Tomich, J.; Freeman, L. C. "A Synthetic Peptide Based on a Glycine-Gated Chloride Channel Induces a Novel Chloride Conductance in Isolated Epithelial Cells" *Biochim. Biophys. Acta-Biomembr.* **2000**, *1466*, 47-60.

(172) Ashcroft, F. M. in *Ion Channels and Disease*; Academic Press: San Diego, 2000, pp 211-229.

(173) Broughman, J. R.; Mitchell, K. E.; Sedlacek, R. L.; Iwamoto, T.; Tomich, J. M.; Schultz, B. D. "NH$_2$-Terminal Modification of a Channel-Forming Peptide Increases Capacity for Epithelial Anion Secretion" *Am. J. Physiol.* **2001**, *280*, C451-C458.

(174) Gao, L.; Broughman, J. R.; Iwamoto, T.; Tomich, J. M.; Venglarik, C. J.; Forman, H. J. "Synthetic Chloride Channel Restores Glutathione Secretion in Cystic Fibrosis Airway Epithelia" *Am. J. Physiol.* **2001**, *281*, L24-L30.

(175) Gao, L.; Kim, K. J.; Yankaskas, J. R.; Forman, H. J. "Abnormal Glutathione Transport in Cystic Fibrosis Airway Epithelia" *Am. J. Physiol.* **1999**, *277*, L113-L118.

(176) Broughman, J. R.; Shank, L. P.; Takeguchi, W.; Schultz, B. D.; Iwamoto, T.; Mitchell, K. E.; Tomich, J. M. "Distinct Structural Elements That Direct Solution Aggregation and Membrane Assembly in the Channel-Forming Peptide M2GlyR" *Biochemistry* **2002**, *41*, 7350-7358.

(177) Sheppard, D. N.; Rich, D. P.; Ostedgaard, L. S.; Gregory, R. J.; Smith, A. E.; Welsh, M. J. "Mutations in CFTR Associated with Mild-Disease-Form Cl$^-$ Channels with Altered Pore Properties" *Nature* **1993**, *362*, 160-164.

(178) You, S. C.; Peng, S. Y.; Lien, L.; Breed, J.; Sansom, M. S. P.; Woolley, G. A. "Engineering Stabilized Ion Channels: Covalent Dimers of Alamethicin" *Biochemistry* **1996**, *35*, 6225-6232.

(179) Starostin, A. V.; Butan, R.; Borisenko, V.; James, D. A.; Wenschuh, H.; Sansom, M. S. P.; Woolley, G. A. "An Anion-Selective Analogue of the Channel-Forming Peptide Alamethicin" *Biochemistry* **1999**, *38*, 6144-6150.

(180) Tieleman, D. P.; Borisenko, V.; Sansom, M. S. P.; Woolley, G. A. "Understanding pH-Dependent Selectivity of Alamethicin K18 Channels by Computer Simulation" *Biophys. J.* **2003**, *84*, 1464-1469.

(181) Fahlke, C.; Yu, H. T.; Beck, C. L.; Rhodes, T. H.; George, A. L. "Pore-Forming Segments in Voltage-Gated Chloride Channels" *Nature* **1997**, *390*, 529-532.

(182) Corringer, P. J.; Bertrand, S.; Galzi, J. L.; Devillers-Thiery, A.; Changeux, J. P.; Bertrand, D. "Mutational Analysis of the Charge Selectivity Filter of the Alpha 7 Nicotinic Acetylcholine Receptor" *Neuron* **1999**, *22*, 831-843.

(183) Schlesinger, P. H.; Ferdani, R.; Pajewska, J.; Pajewski, R.; Gokel, G. W. "Replacing Proline at the Apex of Heptapeptide-Based Chloride Ion Transporters Alters Their Properties and Their Ionophoretic Efficacy" *New J. Chem.* **2003**, *27*, 60-67.

(184) Deng, G.; Dewa, T.; Regen, S. L. "A Synthetic Ionophore That Recognizes Negatively Charged Phospholipid Membranes" *J. Am. Chem. Soc.* **1996**, *118*, 8975-8976.

(185) Merritt, M.; Lanier, M.; Deng, G.; Regen, S. L. "Sterol-Polyamine Conjugates as Synthetic Ionophores" *J. Am. Chem. Soc.* **1998**, *120*, 8494-8501.

(186) Sakai, N.; Sorde, N.; Das, G.; Perrottet, P.; Gerard, D.; Matile, S. "Synthetic Multifunctional Pores: Deletion and Inversion of Anion/Cation Selectivity Using pM and pH" *Org. Biomol. Chem.* **2003**, *1*, 1226-1231.

(187) Sakai, N.; Matile, S. "Recognition of Polarized Lipid Bilayers by *p*-Oligophenyl Ion Channels: From Push-Pull Rods to Push-Pull Barrels" *J. Am. Chem. Soc.* **2002**, *124*, 1184-1185.

(188) Sakai, N.; Houdebert, D.; Matile, S. "Voltage-Dependent Formation of Anion Channels by Synthetic Rigid-Rod Push-Pull Beta-Barrels" *Chem.-Eur. J.* **2003**, *9*, 223-232.

(189) Sidorov, V.; Kotch, F. W.; El-Khouedi, M.; Davis, J. T. "Toward Artificial Ion Channels: Self-Assembled Nanotubes from Calix[4]arene-Guanosine Conjugates" *Chem. Commun.* **2000**, 2369-2370.

(190) Kotch, F. W.; Sidorov, V.; Lam, Y.-F.; Kayser, K. J.; Li, H.; Kaucher, M.; Davis, J. T. "Water-Mediated Association Provides an Ion Pair Receptor" *J. Am. Chem. Soc.* **2003**, accepted.

(191) Westhof, E. *Water and Biological Macromolecules*; CRC Press: Boca Raton, 1993.

(192) Bloomfield, V. A.; Crothers, D. M.; Tinoco, I. J. *Nucleic Acids: Structures, Properties, and Functions*; University Science Books: Sausalito, 2000.

(193) Mattos, C. "Protein-Water Interactions in a Dynamic World" *Trends Biochem. Sci.* **2002**, *27*, 203-208.

(194) Rupley, J. A.; Careri, G. "Protein Hydration and Function" *Adv. Protein Chem.* **1991**, *41*, 37-172.

(195) Bryant, R. G. "The Dynamics of Water-Protein Interactions" *Annu. Rev. Biophys. Biomolec. Struct.* **1996**, *25*, 29-53.

(196) Kuhn, L. A.; Siani, M. A.; Pique, M. E.; Fisher, C. L.; Getzoff, E. D.; Tainer, J. A. "The Interdependence of Protein Surface-Topography and Bound Water Molecules Revealed by Surface Accessibility and Fractal Density Measures" *J. Mol. Biol.* **1992**, *228*, 13-22.

(197) Colombo, M. F.; Rau, D. C.; Parsegian, V. A. "Protein Solvation in Allosteric Regulation - a Water Effect on Hemoglobin" *Science* **1992**, *256*, 655-659.

(198) Bhat, T. N.; Bentley, G. A.; Boulot, G.; Greene, M. I.; Tello, D.; Dallacqua, W.; Souchon, H.; Schwarz, F. P.; Mariuzza, R. A.; Poljak, R. J. "Bound Water Molecules and Conformational Stabilization Help Mediate an Antigen-Antibody Association" *Proc. Natl. Acad. Sci. U. S. A.* **1994**, *91*, 1089-1093.

(199) Robinson, C. R.; Sligar, S. G. "Molecular Recognition Mediated by Bound Water - a Mechanism for Star Activity of the Restriction-Endonuclease Eco Ri" *J. Mol. Biol.* **1993**, *234*, 302-306.

(200) Zaks, A.; Klibanov, A. M. "The Effect of Water on Enzyme Action in Organic Media" *J. Biol. Chem.* **1988**, *263*, 8017-8021.

(201) Westhof, E. "Water - an Integral Part of Nucleic Acid Structure" **1988**, *17*, 125-144.

(202) Texter, J. "Nucleic Acid-Water Interactions" *Prog. Biophys. Mol. Biol.* **1978**, *33*, 83-97.

(203) Kubinec, M. G.; Wemmer, D. E. "NMR Evidence for DNA Bound Water in Solution" *J. Am. Chem. Soc.* **1992**, *114*, 8739-8740.

(204) Lan, T.; McLaughlin, L. W. "Minor Groove Hydration is Critical to the Stabilization of DNA Duplexes" *J. Am. Chem. Soc.* **2000**, *122*, 6512-6513.

(205) Spink, C. H.; Chaires, J. B. "Effects of Hydration, Ion Release, and Excluded Volume on the Melting of Triplex and Duplex DNA" *Biochemistry* **1999**, *38*, 496-508.

(206) Haider, S.; Parkinson, G. N.; Neidle, S. "Crystal Structure of the Potassium Form of an Oxytricha Nova G-Quadruplex" *J. Mol. Biol.* **2002**, *320*, 189-200.

(207) Hud, N. V.; Polak, M. "DNA-Cation Interactions: The Major and Minor Grooves Are Flexible Ionophores" *Curr. Opin. Struct. Biol.* **2001**, *11*, 293-301.

(208) MacGillivray, L. R.; Atwood, J. L. "A Chiral Spherical Molecular Assembly Held Together by 60 Hydrogen Bonds" *Nature* **1997**, *389*, 469-472.

(209) Shivanyuk, A.; Rebek, J., Jr. "Reversible Encapsulation by Self-Assembling Resorcinarene Subunits" *Proc. Natl. Acad. Sci. U. S. A.* **2001**, *98*, 7662-7665.

(210) Shivanyuk, A.; Rebek, J., Jr. "Reversible Encapsulation of Multiple, Neutral Guests in Hexameric Resorcinarene Hosts" *Chem. Commun.* **2001**, 2424-2425.

(211) Avram, L.; Cohen, Y. "Spontaneous Formation of Hexameric Resorcinarene Capsule in Chloroform Solution as Detected by Diffusion NMR" *J. Am. Chem. Soc.* **2002**, *124*, 15148-15149.

(212) Avram, L.; Cohen, Y. "The Role of Water Molecules in a Resorcinarene Capsule as Probed by NMR Diffusion Measurements" *Org. Lett.* **2002**, *4*, 4365-4368.

(213) Shivanyuk, A.; Rebek, J., Jr. "Assembly of Resorcinarene Capsules in Wet Solvents" *J. Am. Chem. Soc.* **2003**, *125*, 3432-3233.

(214) Philip, I. E.; Kaifer, A. E. "Electrochemically Driven Formation of a Molecular Capsule around the Ferrocenium Ion" **2002**, *124*, 12678-12679.

(215) Murayama, K.; Aoki, K. "Resorcin[4]arene Dimer Linked by Eight Water Molecules and Incorporating a Tetraethylammonium Ion: Guest-Driven Capsule Formation via Cation-Pi Interactions" *Chem. Commun.* **1998**, 607-608.

(216) Shivanyuk, A.; Rissanen, K.; Kolehmainen, E. "Encapsulation of Et_3N^+-H Center Dot Center Dot Center Dot OH2 in a Hydrogen-Bonded Resorcarene Capsule" *Chem. Commun.* **2000**, 1107-1108.

(217) Shivanyuk, A.; Rebek, J., Jr. "Hydrogen-Bonded Capsules in Polar, Protic Solvents" *Chem. Commun.* **2001**, 2374-2375.

(218) Habata, Y.; Takeshita, M.; Fukuda, Y.; Akabori, S.; Bradshaw, J. S. "Pseudo-Crown Ether-Like Structure by Hydrogen-Bonded Dimerization: A Water Complex with Bis(2'-Hydroxyethyl)-2,6-Pyridinedicarboxylate in Solid, Solution, and Gas Phases" *J. Heterocycl. Chem.* **2001**, *38*, 1323-1327.

(219) Arena, G.; Casnati, A.; Mirone, L.; Sciotto, D.; Ungaro, R. "A New Water-Soluble Calix[4]arene Ditopic Receptor Rigidified by Microsolvation: Acid-Base and Inclusion Properties" *Tetrahedron Lett.* **1997**, *38*, 1999-2002.

(220) Far, A. R.; Shivanyuk, A.; Rebek, J., Jr. "Water-Stabilized Cavitands" *J. Am. Chem. Soc.* **2002**, *124*, 2854-2855.

(221) Perez, C.; Espinola, G.; Foces-Foces, C.; Nunez-Coello, P.; Carrasco, H.; Martin, J. D. "A Synthetic Hydroxy Acid That Shows Tubular-Shaped Structure in Solid-State and Ionophoric Activity in Phospholipid Bilayers" *Org. Lett.* **2000**, *2*, 1185-1188.

(222) Carrasco, H.; Foces-Foces, C.; Perez, C.; Rodriguez, M. L.; Martin, J. D. "Tubular Hydrogen-Bonded Networks Sustained by Water Molecules" *J. Am. Chem. Soc.* **2001**, *123*, 11970-11981.

(223) Hong, B. H.; Lee, J. Y.; Lee, C. W.; Kim, J. C.; Bae, S. C.; Kim, K. S. "Self-Assembled Arrays of Organic Nanotubes with Infinitely Long One-Dimensional H-Bond Chains" *J. Am. Chem. Soc.* **2001**, *123*, 10748-10749.

(224) Schmidtchen, F. P. "Tetazac: A Novel Artificial Receptor for Binding Ω-Amino Carboxylates" *J. Org. Chem.* **1986**, *51*, 5161-5168.

(225) Pedersen, C. J. "Cyclic Polyethers and Their Complexes with Metal Salts" *J. Am. Chem. Soc.* **1967**, *89*, 7017-7036.

(226) Izatt, R. M.; Pawlak, K.; Bradshaw, J. S.; Bruening, R. L. "Thermodynamic and Kinetic Data for Macrocycle Interaction with Cations, Anions, and Neutral Molecules" *Chem. Rev.* **1995**, *95*, 2529-2586.

(227) Beer, P. D.; Gale, P. A. "Anion Recognition and Sensing: The State of the Art and Future Perspectives" *Angew. Chem.-Int. Edit.* **2001**, *40*, 487-516.

(228) Kirkovits, G. J.; Shriver, J. A.; Gale, P. A.; Sessler, J. L. "Synthetic Ditopic Receptors" *J. Incl. Phenom. Macrocycl. Chem.* **2001**, *41*, 69-75.

(229) Galan, A.; Andreu, D.; Echavarren, A. M.; Prados, P.; de Mendoza, J. "A Receptor for the Enantioselective Recognition of Phenylalanine and Tryptophan under Neutral Conditions" *J. Am. Chem. Soc.* **1992**, *114*, 1511-1512.

(230) Sessler, J. L.; Andrievsky, A. "Efficient Transport of Aromatic Amino Acids by Sapphyrin-Lasalocid Conjugates" *Chem.-Eur. J.* **1998**, *4*, 159-167.

(231) Smith, P. J.; Reddington, M. V.; Wilcox, C. S. "Ion-Pair Binding by a Urea in Chloroform Solution" *Tetrahedron Lett.* **1992**, *33*, 6085-6088.

(232) Smith, P. J.; Kim, E. I.; Wilcox, C. S. "Substrate-Specific Catalysis by Ion-Pairs" *Angew. Chem.-Int. Edit. Engl.* **1993**, *32*, 1648-1650.

(233) Reetz, M. T.; Niemeyer, C. M.; Harms, K. "Crown Ethers with a Lewis Acidic Center - a New Class of Heterotopic Host Molecules" *Angew. Chem.-Int. Edit.* **1991**, *30*, 1472-1474.

(234) Reetz, M. T.; Johnson, B. M.; Harms, K. "A Novel Receptor for Ditopic Binding of Alkali-Metal Halides" *Tetrahedron. Lett.* **1994**, *35*, 2525-2528.

(235) Deetz, M. J.; Shang, M.; Smith, B. D. "A Macrobicyclic Receptor with Versatile Recognition Properties: Simultaneous Binding of an Ion Pair and Selective Complexation of Dimethylsulfoxide" *J. Am. Chem. Soc.* **2000**, *122*, 6201-6207.

(236) Mahoney, J. M.; Beatty, A. M.; Smith, B. D. "Selective Recognition of an Alkali Halide Contact Ion-Pair" *J. Am. Chem. Soc.* **2001**, *123*, 5847-5848.

(237) Rudkevich, D. M.; Stauthamer, W.; Verboom, W.; Engbersen, J. F. J.; Harkema, S.; Reinhoudt, D. N. "UO$_2$-Salens - Neutral Receptors for Anions with a High Selectivity for Dihydrogen Phosphate" *J. Am. Chem. Soc.* **1992**, *114*, 9671-9673.

(238) Tsukube, H. in *Cation Binding by Macrocycles*; Inoue, Y., Gokel, G. W., Eds.; M. Dekker: New York, 1990, p 503.

(239) Rudkevich, D. M.; Brzozka, Z.; Palys, M.; Visser, H. C.; Verboom, W.; Reinhoudt, D. N. "A Difunctional Receptor for the Simultaneous Complexation of Anions and Cations - Recognition of KH$_2$PO$_4$" *Angew. Chem.-Int. Edit. Engl.* **1994**, *33*, 467-468.

(240) Rudkevich, D. M.; Mercerchalmers, J. D.; Verboom, W.; Ungaro, R.; Dejong, F.; Reinhoudt, D. N. "Bifunctional Recognition - Simultaneous Transport of Cations and Anions through a Supported Liquid Membrane" *J. Am. Chem. Soc.* **1995**, *117*, 6124-6125.

(241) Nishizawa, S.; Shigemori, K.; Teramae, N. "A Thiourea-Functionalized Benzo-15-Crown-5 for Cooperative Binding of Sodium Ions and Anions" *Chem. Lett.* **1999**, 1185-1186.

(242) Scheerder, J.; van Duynhoven, J. P. M.; Engbersen, J. F. J.; Reinhoudt, D. N. "Solubilization of NaX Salts in Chloroform by Bifunctional Receptors" *Angew. Chem.-Int. Edit. Engl.* **1996**, *35*, 1090-1093.

263

(243) Beer, P. D.; Dent, S. W. "Potassium Cation Induced Switch in Anion Selectivity Exhibited by Heteroditopic Ruthenium(II) and Rhenium(I) Bipyridyl Bis(Benzo-15-Crown-5) Ion Pair Receptors" *Chem. Commun.* **1998**, 825-826.

(244) Reetz, M. T. In *Comprehensive Supramolecular Chemistry*; Atwood, J. L., Davies, J. E. D., MacNicol, D. D., Vogtle, F., Gokel, G. W., Eds.; Pergamon: Oxford, 1996; Vol. 2, pp 553-562.

(245) Antonisse, M. M. G.; Reinhoudt, D. N. "Neutral Anion Receptors: Design and Application" *Chem. Commun.* **1998**, 443-448.

(246) Schall, O. F.; Gokel, G. W. "Molecular Boxes Derived from Crown-Ethers and Nucleotide Bases - Probes for Hoogsteen vs Watson-Crick H-Bonding and Other Base-Base Interactions in Self-Assembly Processes" *J. Am. Chem. Soc.* **1994**, *116*, 6089-6100.

(247) Schwabacher, A. W.; Lee, J. H.; Lei, H. Y. "Self-Assembly of a Hydrophobic Binding Site" *J. Am. Chem. Soc.* **1992**, *114*, 7597-7598.

(248) Lee, J. H.; Schwabacher, A. W. "Ditopic Binding by a Self-Assembled Receptor - Metal in a Structural and Functional Role" *J. Am. Chem. Soc.* **1994**, *116*, 8382-8383.

(249) Shi, X.; Fettinger, J. C.; Davis, J. T. "Ion-Pair Recognition by Nucleoside Self-Assembly: Guanosine Hexadecamers Bind Cations and Anions" *Angew. Chem.-Int. Edit.* **2001**, *40*, 2827-2831.

(250) Piotrowski, H.; Severin, K. "A Self-Assembled, Redox-Responsive Receptor for the Selective Extraction of LiCl from Water" *Proc. Natl. Acad. Sci. U. S. A.* **2002**, *99*, 4997-5000.

(251) Forman, S. L.; Fettinger, J. C.; Pieraccini, S.; Gottarelli, G.; Davis, J. T. "Toward Artificial Ion Channels: A Lipophilic G-Quadruplex" *J. Am. Chem. Soc.* **2000**, *122*, 4060-4067.

(252) Guschlbauer, W.; Chantot, J. F.; Thiele, D. "4-Stranded Nucleic-Acid Structures 25 Years Later - from Guanosine Gels to Telomer DNA" *J. Biomol. Struct. Dyn.* **1990**, *8*, 491-511.

(253) Kotch, F. W.; Fettinger, J. C.; Davis, J. T. "A Lead-Filled G-Quadruplex: Insight into the G-Quartet's Selectivity for Pb^{2+} over K^+" *Org. Lett.* **2000**, *2*, 3277-3280.

(254) Shi, X. D.; Fettinger, J. C.; Davis, J. T. "Homochiral G-Quadruplexes with Ba^{2+} but not with K$^+$: The Cation Programs Enantiomeric Self-Recognition" *J. Am. Chem. Soc.* **2001**, *123*, 6738-6739.

(255) Jaunky, W.; Hosseini, M. W.; Planeix, J. M.; De Cian, A.; Kyritsakas, N.; Fischer, J. "Molecular Braids: Quintuple Helical Hydrogen Bonded Molecular Network" *Chem. Commun.* **1999**, 2313-2314.

(256) Kleina, C.; Graf, E.; Hosseini, M. W.; De Cian, A.; Fischer, J. "Metallatubulane: Synthesis and Structural Analysis of an Infinite Tubular Coordination Network Formed by the Self-Assembly of a Tetracyanocyclophane and Silver Cations" *Chem. Commun.* **2000**, 239-240.

(257) Iwamoto, K.; Shinkai, S. "Syntheses and Ion Selectivity of All Conformational Isomers of Tetrakis((Ethoxycarbonyl)Methoxy)Calix[4]arene" *J. Org. Chem.* **1992**, *57*, 7066-7073.

(258) Stout, M. G.; Robins, M. J.; Olsen, R. K.; Robins, R. K. "Purine Nucleosides .25. Synthesis of Certain Derivatives of 5'-Amino-5'-Deoxy- and 5'-Amino-2',5'-Dideoxy-Beta-D-Ribofuranosylpurines as Purine Nucleotide Analogs" *J. Med. Chem.* **1969**, *12*, 658-662.

(259) Oosawa, F.; Asakura, S. *Thermodynamics of the Polymerization of Protein*; Academic Press: New York, 1975.

(260) ten Cate, A. T.; Sijbesma, R. P. "Coils, Rods and Rings in Hydrogen-Bonded Supramolecular Polymers" *Macromol. Rapid Commun.* **2002**, *23*, 1094-1112.

(261) Brunsveld, L.; Folmer, B. J. B.; Meijer, E. W.; Sijbesma, R. P. "Supramolecular Polymers" *Chem. Rev.* **2001**, *101*, 4071-4097.

(262) Moore, J. S. "Supramolecular Polymers" *Curr. Opin. Colloid Interface Sci.* **1999**, *4*, 108-116.

(263) Pinnavaia, T. J.; Marshall, C. L.; Mettler, C. M.; Fisk, C. I.; Miles, H. T.; Becker, E. D. "Alkali-Metal Ion Specificity in Solution Ordering of a Nucleotide, 5'-Guanosine Monophosphate" *J. Am. Chem. Soc.* **1978**, *100*, 3625-3627.

(264) Patel, P. K.; Koti, A. S. R.; Hosur, R. V. "NMR Studies on Truncated Sequences of Human Telomeric DNA: Observation of a Novel A-Tetrad" *Nucleic Acids Res.* **1999**, *27*, 3836-3843.

(265) Huang, Z. T.; Wang, G. Q.; Yang, L. M.; Lou, Y. X. "The Selective Chloromethylation of 25,27-Dihydroxy-26,28- Dimethoxycalix[4]arene and Nucleophilic-Substitution Therefrom" *Synth. Commun.* **1995**, *25*, 1109-1118.

(266) Li, H.; Miller, M. J. "Syntheses of 5 '-Deoxy-5 '-N-Hydroxylaminopyrimidine and Purine Nucleosides: Building Blocks for Novel Antisense Oligonucleosides with Hydroxamate Linkages" *J. Org. Chem.* **1999**, *64*, 9289-9293.

(267) Seela, F.; Ott, J.; Potter, B. V. L. "Oxygen Chiral Phosphate in Uridylyl(3'-5')Adenosine by Oxidation of a Phosphite Intermediate - Synthesis and Absolute-Configuration" *J. Am. Chem. Soc.* **1983**, *105*, 5879-5886.

(268) Chien, T. C.; Chen, C. S.; Yeh, J. Y.; Wang, K. C.; Chern, J. W. "Nucleosides .7. Synthesis of N-Triphenylphosphoranylidene Nucleosides by Mitsunobu Reaction - a Novel Protecting Group for Primary Amines of Nucleosides" *Tetrahedron Lett.* **1995**, *36*, 7881-7884.

(269) Marcus, Y. "Thermodynamics of Solvation of Ions .5. Gibbs Free-Energy of Hydration at 298.15-K" *J. Chem. Soc.-Faraday Trans.* **1991**, *87*, 2995-2999.

(270) Stejskal, E. O.; Tanner, J. E. "Spin Diffusion Measurements - Spin Echoes in Presence of a Time-Dependent Field Gradient" *J. Chem. Phys.* **1965**, *42*, 288-292.

(271) Johnson, C. S. "Diffusion Ordered Nuclear Magnetic Resonance Spectroscopy: Principles and Applications" *Prog. Nucl. Magn. Reson. Spectrosc.* **1999**, *34*, 203-256.

(272) Altieri, A. S.; Hinton, D. P.; Byrd, R. A. "Association of Biomolecular Systems via Pulsed-Field Gradient NMR Self-Diffusion Measurements" *J. Am. Chem. Soc.* **1995**, *117*, 7566-7567.

(273) Krishnan, V. V. "Determination of Oligomeric State of Proteins in Solution from Pulsed-Field Gradient Self-Diffusion Coefficient Measurements. A Comparison of Experimental, Theoretical, and Hard-Sphere Approximated Values" *J. Magn. Reson.* **1997**, *124*, 468-473.

(274) Timmerman, P.; Weidmann, J. L.; Jolliffe, K. A.; Prins, L. J.; Reinhoudt, D. N.; Shinkai, S.; Frish, L.; Cohen, Y. "NMR Diffusion Spectroscopy for the Characterization of Multicomponent Hydrogen-Bonded Assemblies in Solution" *J. Chem. Soc.-Perkin Trans. 2* **2000**, 2077-2089.

(275) Avram, L.; Cohen, Y. "Effect of a Cationic Guest on the Characteristics of the Molecular Capsule of Resorcinarene: A Diffusion NMR Study" *Org. Lett.* **2003**, *5*, 1099-1102.

(276) Otto, W. H.; Keefe, M. H.; Splan, K. E.; Hupp, J. T.; Larive, C. K. "Analysis of Molecular Square Size and Purity via Pulsed-Field Gradient NMR Spectroscopy" *Inorg. Chem.* **2002**, *41*, 6172-6174.

(277) Wills, P. R.; Georgalis, Y. "Concentration-Dependence of the Diffusion Coefficient of a Dimerizing Protein - Bovine Pancreatic Trypsin-Inhibitor" *J. Phys. Chem.* **1981**, *85*, 3978-3984.

(278) de la Torre, J. G.; Bloomfield, V. A. "Hydrodynamic Properties of Complex, Rigid, Biological Macromolecules - Theory and Applications" *Q. Rev. Biophys.* **1981**, *14*, 81-139.

(279) Chang, X. Q.; Keller, D.; O'Donoghue, S. I.; Led, J. J. "NMR Studies of the Aggregation of Glucagon-Like Peptide-1: Formation of a Symmetric Helical Dimer" *FEBS Lett.* **2002**, *515*, 165-170.

(280) ten Cate, A. T.; Dankers, P. Y. W.; Kooijman, H.; Speck, A. L.; Sijbesma, R. P.; Meijer, E. W. "Enantioselective Cyclization of Racemic Supramolecular Polymers" *J. Am. Chem. Soc.* **2003**, *125*, 6860-6861.

(281) Lo, M. C.; Helm, J. S.; Sarngadharan, G.; Pelczer, I.; Walker, S. "A New Structure for the Substrate-Binding Antibiotic Ramoplanin" *J. Am. Chem. Soc.* **2001**, *123*, 8640-8641.

(282) Marlow, A. L.; Mezzina, E.; Spada, G. P.; Masiero, S.; Davis, J. T.; Gottarelli, G. "Cation-Templated Self-Assembly of a Lipophilic Deoxyguanosine: Solution Structure of a K^+-dG(8) Octamer" *J. Org. Chem.* **1999**, *64*, 5116-5123.

(283) Sessler, J. L.; Sathiosatham, M.; Doerr, K.; Lynch, V.; Abboud, K. A. "A G-Quartet Formed in the Absence of a Templating Metal Cation: A New 8-(N,N-Dimethylaniline)Guanosine Derivative" *Angew. Chem.-Int. Edit.* **2000**, *39*, 1300-1303.

(284) Sheu, C.; Kang, P.; Khan, S.; Foote, C. S. "Low-Temperature Photosensitized Oxidation of a Guanosine Derivative and Formation of an Imidazole Ring-Opened Product" *J. Am. Chem. Soc.* **2002**, *124*, 3905-3913.

267

(285) Gottarelli, G.; Masiero, S.; Mezzina, E.; Spada, G. P.; Mariani, P.; Recanatini, M. "The Self-Assembly of a Lipophilic Deoxyguanosine Derivative and the Formation of a Liquid-Crystalline Phase in Hydrocarbon Solvents" *Helv. Chim. Acta* **1998**, *81*, 2078-2092.

(286) Araki, K.; Abe, M.; Ishizaki, A.; Ohya, T. "Multiple Hydrogen-Bonding Network - a Novel Mode of Self-Recognition in a Layered Crystalline-Structure of a Guanosine Derivative" *Chem. Lett.* **1995**, 359-360.

(287) Gellert, M.; Lipsett, M. N.; Davies, D. R. "Helix Formation by Guanylic Acid" *Proc. Natl. Acad. Sci. U. S. A.* **1962**, *48*, 2013-2018.

(288) Elbasyouny, A.; Brugge, H. J.; Vondeuten, K.; Dickel, M.; Knochel, A.; Koch, K. U.; Kopf, J.; Melzer, D.; Rudolph, G. "Host Guest Complexes of 18-Crown-6 with Neutral Molecules Possessing the Structure Element OH_2, NH_2, CH_2" *J. Am. Chem. Soc.* **1983,** *105*, 6568-6577.

(289) Watson, W. H.; Galloy, J.; Grossie, D. A.; Vogtle, F.; Muller, W. M. "Host-Guest Complex Chemistry - Structures of 18-Crown-6 and Diaza-18-Crown-6 with Neutral Molecules" *J. Org. Chem.* **1984**, *49*, 347-353.

(290) Grootenhuis, P. D. J.; Uiterwijk, J.; Reinhoudt, D. N.; Vanstaveren, C. J.; Sudholter, E. J. R.; Bos, M.; Vaneerden, J.; Klooster, W. T.; Kruise, L.; Harkema, S. "Complexes of Macrocyclic Polyethers and Neutral Guest Molecules - a Systematic Approach to the Complexation of Water Molecules by 2,6-Pyridinium Crown Ethers" *J. Am. Chem. Soc.* **1986**, *108*, 780-788.

(291) Young, V. G.; Sykes, A. G. "Absence of Hydronium Ion Formation in a Ternary Crown Ether Mineral Acid Water Complex: X-Ray Crystal Structure of 1,8-Oxybis(Ethyleneoxyethyleneoxy)Anthracene-9,10-Dione.HNO_3.$3H_2O$" *Inorg. Chem.* **1998**, *37*, 376-378.

(292) Otting, G. "NMR Studies of Water Bound to Biological Molecules" *Prog. Nucl. Magn. Reson. Spectrosc.* **1997**, *31*, 259-285.

(293) Bagno, A.; Campulla, M.; Pirana, M.; Scorrano, G.; Stiz, S. "Preferential Solvation of Organic Species in Binary Solvent Mixtures Probed by Intermolecular H-1 NOESY NMR Spectroscopy" *Chem.-Eur. J.* **1999**, *5*, 1291-1300.

(294) Angulo, M.; Hawat, C.; Hofmann, H. J.; Berger, S. "Site-Specific Solvation Determined by Intermolecular Nuclear Overhauser Effect-Measurements and Molecular Dynamics" *Org. Biomol. Chem.* **2003**, *1*, 1049-1052.

(295) Arimura, T.; Kawabata, H.; Matsuda, T.; Muramatsu, T.; Satoh, H.; Fujio, K.; Manabe, O.; Shinkai, S. "New Water-Soluble Host Calixarenes Bearing Chiral Substituents" *J. Org. Chem.* **1991**, *56*, 301-306.

(296) Ikeda, A.; Nagasaki, T.; Shinkai, S. "Conformational Analysis of Calix[n]arenes with Chiral Substituents by Using Circular-Dichroism" *J. Phys. Org. Chem.* **1992**, *5*, 699-710.

(297) Castellano, R. K.; Nuckolls, C.; Rebek, J., Jr. "Transfer of Chiral Information through Molecular Assembly" *J. Am. Chem. Soc.* **1999**, *121*, 11156-11163.

(298) Gottarelli, G.; Masiero, S.; Spada, G. P. "The Use of CD Spectroscopy for the Study of the Self-Assembly of Guanine Derivatives" *Enantiomer* **1998**, *3*, 429-436.

(299) Russ, J. C. *Fundamentals of Energy Dispersive X-Ray Analysis*; Butterworths: London, 1984.

(300) Budka, J.; Lhotak, P.; Michlova, V.; Stibor, I. "Urea Derivatives of Calix[4]arene 1,3-alternate: An Anion Receptor with Profound Negative Allosteric Effect" *Tetrahedron Lett.* **2001**, *42*, 1583-1586.

(301) Koulov, A. V.; Lambert, T. N.; Shukla, R.; Jain, M.; Boon, J. M.; Smith, B. D.; Li, H.; Sheppard, D. N.; Joos, J.-B.; Clare, J. P.; Davis, A. P. "Chloride Transport Across Vesicle and Cell Membranes by Steroid-Based Receptors" *Angew. Chem. Int. Ed.* **2003**, *42*, 4931-4933.

(302) Lewis, B. A.; Engelman, D. M. "Lipid Bilayer Thickness Varies Linearly with Acyl Chain-Length in Fluid Phosphatidylcholine Vesicles" *J. Mol. Biol.* **1983**, *166*, 211-217.

(303) Dilger, J. P.; McLaughlin, S. G. A.; McIntosh, T. J.; Simon, S. A. "Dielectric-Constant of Phospholipid-Bilayers and the Permeability of Membranes to Ions" *Science* **1979**, *206*, 1196-1198.

(304) Sato, T.; Konno, H.; Tanaka, Y.; Kataoka, T.; Nagai, K.; Wasserman, H. H.; Ohkuma, S. "Prodigiosins as a New Group of H^+/Cl^- Symporters That Uncouple Proton Translocators" *J. Biol. Chem.* **1998**, *273*, 21455-21462.

(305) Melvin, M. S.; Tomlinson, J. T.; Park, G.; Day, C. S.; Saluta, G. R.; Kucera, G. L.; Manderville, R. A. "Influence of the A-Ring on the Proton Affinity and Anticancer Properties of the Prodigiosins" *Chem. Res. Toxicol.* **2002**, *15*, 734-741.

(306) Tanigaki, K.; Sato, T.; Tanaka, Y.; Ochi, T.; Nishikawa, A.; Nagai, K.; Kawashima, H.; Ohkuma, S. "BE-18591 as a New H^+/Cl^- Symport Ionophore That Inhibits Immunoproliferation and Gastritis" *FEBS Lett.* **2002**, *524*, 37-42.

(307) Kaliszan, R. in *Quantitative Structure-Chromatographic Retention Relationships*; John Wiley & Sons: New York, 1987, pp 232-267.

(308) Clement, N. R.; Gould, J. M. "Pyranine (8-Hydroxy-1,3,6-Pyrenetrisulfonate) as a Probe of Internal Aqueous Hydrogen-Ion Concentration in Phospholipid Vesicles" *Biochemistry* **1981**, *20*, 1534-1538.

(309) Venema, K.; Gibrat, R.; Grouzis, J. P.; Grignon, C. "Quantitative Measurement of Cationic Fluxes, Selectivity and Membrane-Potential Using Liposomes Multilabelled with Fluorescent Probes" *Biochim. Biophys. Acta* **1993**, *1146*, 87-96.

(310) Papahadjopoulos, D. "Na^+-K^+ Discrimination by Pure Phospholipid Membranes" *Biochim. Biophys. Acta* **1971**, *241*, 254-259.

(311) Kavallieratos, K.; Bertao, C. M.; Crabtree, R. H. "Hydrogen Bonding in Anion Recognition: A Family of Versatile, Nonpreorganized Neutral and Acyclic Receptors" *J. Org. Chem.* **1999**, *64*, 1675-1683.

(312) Beer, P. D.; Drew, M. G. B.; Gale, P. A.; Leeson, P. B.; Ogden, M. I. "Structures of Potassium Encapsulated within the 1,3-alternate Conformation of Calix[4]arenes" *J. Chem. Soc.-Dalton Trans.* **1994**, 3479-3485.

(313) Caffrey, M.; Feigenson, G. W. "Fluorescence Quenching in Model Membranes .3. Relationship between Calcium Adenosine-Triphosphatase Enzyme Activity and the Affinity of the Protein for Phosphatidylcholines with Different Acyl Chain Characteristics" *Biochemistry* **1981**, *20*, 1949-1961.

(314) Sone, T.; Ohba, Y.; Yamazaki, H. "Inclusion Properties of Acyclic Para-Substituted Phenol-Formaldehyde Oligomers" *Bull. Chem. Soc. Jpn.* **1989**, *62*, 1111-1116.

(315) Tanner, J. E. "Use of Stimulated Echo in NMR-Diffusion Studies" *J. Chem. Phys.* **1970**, *52*, 2523-2526.

(316) Montal, M.; Mueller, P. "Formation of Bimolecular Membranes from Lipid Monolayers and a Study of Their Electrical Properties" *Proc. Natl. Acad. Sci. U. S. A.* **1972**, *69*, 3561-3566.

(317) Hider, R. C.; Khader, F.; Tatham, A. S. "Lytic Activity of Monomeric and Oligomeric Melittin" *Biochim. Biophys. Acta* **1983**, *728*, 206-214.